Numerical evaluation of stability methods for rubble mound breakwater toes

March 2015

S.P.K. Verpoorten

Hydraulic Engineering
Civil Engineering and Geosciences

TU Delft Delft University of Technology

Van Oord
Marine ingenuity

Numerical evaluation of stability methods for rubble mound breakwater toes

by

Senne Paul Katrien Verpoorten

Master's thesis
in partial fulfilment of the requirements for the degree of

Master of Science
in Civil Engineering

Delft University of Technology
faculty of Civil Engineering and Geosciences
department of Hydraulic Engineering

presented publicly on Thursday the 12th of March 2015 at 14:00

Master's thesis committee	Prof.dr.ir. W.S.J. Uijttewaal	Delft University of Technology
	Dr. B. Zanuttigh	Delft University of Technology and Università di Bologna
	Ir. H.J. Verhagen	Delft University of Technology
	Ir. W.J. Ockeloen	Van Oord Nederland bv
Digital version	Available at http://repository.tudelft.nl/	
Cover	'Winter Storms' at Porthcawl, UK. Photo courtesy of Nick Russill.	

TU Delft Delft University of Technology

Van Oord
Marine ingenuity

Abstract

Seaports are often protected against waves and currents by rubble mound breakwaters. At the interface between outer breakwater slope and seabed a toe structure is often build, which provides stability to the outer slope. The toe consists of a relatively small heap of rock. Since 1977 dedicated studies are made to the stability of these rock elements under wave attack. A large number of stability methods is available, but prediction accuracy is low and validity ranges are too small for use in practice. Clarity on applicability of these methods is desired by designers.

In Baart (2008) a new approach towards toe stability is defended. The 'decoupled model approach' determines stability with a two-step model. In the first step local hydraulic conditions right above the toe bed are calculated. The second step uses these conditions in a general formula for stone motion to predict motion. In this thesis the decoupled model approach is implemented and tested by means of the computational fluid dynamics model IH-2VOF. Prediction capacity of existing toe stability methods is reviewed against numerical results. The approach predicts motion rather than an amount of damage. To achieve this, critical values for stability and damage were imposed where necessary.

The IH-2VOF model was reviewed first. Convergence tests gave recommendations for the computational grid layout. During testing it was found that position of the partially standing wave, produced by breakwater reflection under regular waves, is of major importance when reviewing different tests. It was discovered also that turbulence modelling in IH-2VOF did not function properly. The Nammuni-Krohn (2009) cases were modelled and numerical results were compared with physical measurements by Nammuni-Krohn. Little correspondence was found, likely caused by differences between numerical and physical model. High sensitivity to stone properties (diameter, porosity and Forchheimer coefficients) was encountered. Analytical solutions for flow velocity either over- or underestimated the numerical results.

Work by Peters (2014a) increased confidence in the utility of IH-2VOF for breakwater modelling. Under the assumption that turbulence is not of large importance, the Ebbens (2009) cases were modelled. By literature study the formulae by Izbash (1930), Rance and Warren (1968), Dessens (2004), Steenstra (2014) and Peters (2014b) were selected to predict stone motion. Calibration of these formulae was necessary; Rance and Warren (1968) and Peters (2014b) produced most reliable results. They probably do not need any calibration, making them more universally applicable. Prediction of motion by toe stability methods and decoupled model approach were compared. The formulae by Van der Meer (1991), Gerding (1993) and Van der Meer (1998) give good agreement when validity limits are respected. If neglected, prediction capacity did not decrease much. Van Gent and Van der Werf (2014) and Muttray et al. (2014) then perform good as well. Low sensitivity to the critical values for stability and damage was found.

The decoupled model approach is considered to be appropriate to determine toe stability. The results in this study should on the other hand not be used for design purposes as long as some fundamental problems are not solved. The incorrect turbulence calculation, high sensitivity to stone properties and velocity measurement difficulties of the motion formulae are the main issues which should be investigated in further research.

Preface

This thesis completes the Master's programme Hydraulic Engineering of the faculty of Civil Engineering at Delft University of Technology. Research is conducted in cooperation with Dutch contractor Van Oord Nederland bv, and is part of the Nevlock collaboration programme. The 'Dutch-Flemish research centre for coastal structures' (Nevlock) is a cooperation between Dutch and Flemish universities and marine contractors. Its target is to combine knowledge and experience into new research towards better coastal development. This study is intended to create more insight in breakwater toe stability.

Eight months of work poured in a report of about 170 pages. An accomplishment which would not have been possible without support of many people.

Thesis work was conducted at Van Oord's office in Rotterdam. I would like to thank Greg Smith and Wouter Ockeloen for giving me this opportunity. It provided the link with real engineering work — that what academic research after all is intended for.

With their constructive feedback, my thesis committee supported in reaching the level of detail necessary in this research. The defects in IH-2VOF would not have been discovered without their interest in functioning of the model. Many thanks go to Barbara Zanuttigh for helping me understand reflection behaviour and modelling; to Jeroen van den Bos for setting up IH-2VOF; to Ruben Peters for the enjoyable weeks we worked together on testing IH-2VOF; and to Markus Muttray for the motivating conversation we had in summer and for the combined dataset on toe stability experiments. A special word of gratitude goes to Kevin Geboers, who assisted in running 400 simulations on TU Delft computers. The brave computers in room 0.20 and 1.97 carried out their tasks diligently.

Of course this report would not have been produced without the unconditional support and encouragements of my parents, friends and colleagues. They made last year the most enjoyable of all years of education.
Please do not cease making every day an interesting one.

Senne Verpoorten

Rotterdam, February 2015

Contents

1

Introduction

1.1. Background

The topic of research is the stability of rubble mound breakwaters toes. Rubble mound breakwaters are structures which consist of several layers of loose rock or (often concrete) units, forming together a barrier for waves and currents near harbours and beaches, see figure 1.1. The toe berm is located at the border between foreshore slope and breakwater slope, see figure 1.2. It has several functions, e.g. to inhibit the armour layer material from sliding off, and to provide the required counter weight for the outer slope's macro stability. A toe structure must not be confounded with a berm. The latter has often much larger dimensions and is intended to reduce wave attack, although in shallow water the difference between a toe and a berm can get indistinguishable.

Figure 1.1: Breakwater structure at Dubai Maritime City

Since 1977 dedicated studies to toe stability have been made, resulting in a large number of design formulae and methods (see appendix A and B). Accuracy is low and the validity range of the input parameters is very limited (Muttray, 2013). In design of a certain new breakwater, Van Oord calculated that for only 30% of breakwater stretch the commonly used formulae by Gerding (1993) and Van der Meer (1998) are valid. Van Oord and the other members of Nevlock are thus interested in a design formula which is both accurate and usable in practice.

In the past decade efforts have been made to filter out such a formula. Unfortunately this resulted quite often in a new formula which in its turn does not fit all research data. In 2008 a new and more fundamental approach is presented in Baart (2008) which gives promising results. In this research it will be attempted to couple a numerical approach to Baart's method.

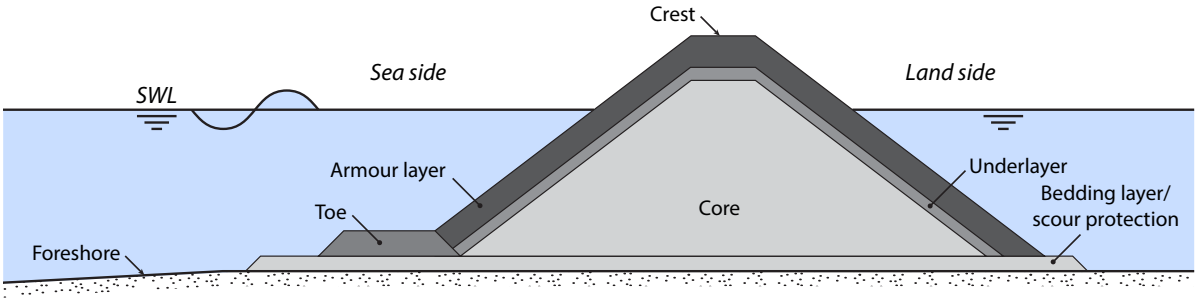

Figure 1.2: Principle sketch of a rubble mound breakwater

During the course of this research Ruben Peters, graduate student at Delft University of Technology, has also conducted research on toe stability. For his Master's thesis he tried to model motion of individual stones, by carrying out flume experiments. To his work often reference will be made and some parts are elaborated together.

In the following sections a detailed description of the problem at hand will be made, based on literature study, after which the research questions are formulated. A proposal for the research methodology is then given, i.e. how will the research questions be answered. The chapter ends with an overview of the report structure.

1.2. Review of literature

To get grip on the subject of breakwater toe stability, a review of literature is required. This will give insight in the problems at hand, but also in which efforts have already been made – it is useless to reinvestigate approaches which proved to be inappropriate. Since we are interested in a design stability formula (i.e. under which condition is the toe stable), no study will be made to design formulae for toe dimensions (i.e. how high and wide must the toe be to fulfil its supporting function). Only research on breakwaters with toes consisting of rock will be investigated.

In the Master's thesis of Baart (2008) a very extensive literature study has been made for research on toe stability up to 2008. Therefore only the headlines of research before 2008 will be given. For research after 2008 a more thorough review will be made. After stipulating the headlines of each research report in section 1.2.1, a comparison is made in section 1.2.2 for some aspects of research. It is already worth mentioning that in appendix A a diagram of historical research is given. In appendix B an overview of formulae and methods in literature is presented, together with all definitions of damage, advised design damage levels and a table with the different datasets and stability methods. Figure 1.3 show how some of the governing parameters are defined.

Before starting the review, it is useful to discuss some common terminology.

Stability method Since stability is not always calculated with a single formula, it is chosen to speak of a stability *method* rather than a stability *formula*. This way the term also incorporates the more extensive calculation methods, like for instance the method by Baart (2008).

Stability number Most stability methods work with a classical stability formula, which gives an expression for the stability number $H_s/\Delta D_{n50}$ for structures built up of rubble under wave attack. In some research this stability number is written as N_s as a shorthand version, so $N_s \equiv \frac{H_s}{\Delta \cdot D_{n50}}$. The stability number implies that higher values of N_s allow for smaller or lighter stones under the same wave attack.

Definition of damage Together with stability a damage parameter is often included in the stability method to give the engineer the possibility of tuning his design. By changing the damage parameter and thus allowing

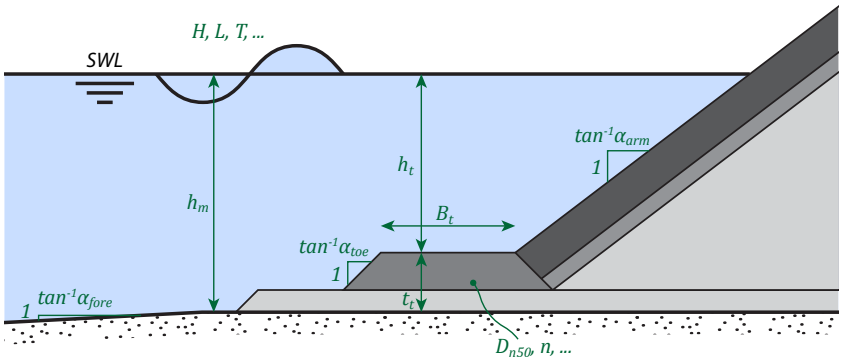

Figure 1.3: Important parameters in toe stability

a certain amount of damage, the stability number changes accordingly. The definition of damage and its quantitative representation is subject of debate, as will be shown in the review of literature. In appendix B an overview of existing damage parameters is given.

Depth conditions Since wave breaking conditions change with water depth (Holthuijsen, 2007, §7.6), most stability methods are given either for shallow or deep water conditions. In research on toe stability one speaks of 'shallow water' or 'depth limited' conditions when wave height is approaching mean water depth ($H_s/h_m \leqslant 0.5$ according to e.g. Baart (2008)). This definition differs from the classical definition, as will be shown later on in this chapter.

1.2.1. Review per author

Van der Meer (1991) Literature study starts in 1991, when Van der Meer presented a stability formula in the Rock Manual by CIRIA et al. (1991). Van der Meer carried out scale tests in a flume with shallow water conditions. He fitted a design curve, based on relative water depth h_t/h_m only. The formula is given in the form of a classical stability equation. No damage parameter is included, so the design curve does not allow for optimization of the structure dimensions.

Gerding (1993), Van der Meer et al. (1995) Gerding did extensive research on toe stability in his Master's thesis. He performed a large number of scale tests in a flume. Gerding presented a new definition of damage in his stability formula. The amount of damage was defined as the number of stones removed from a strip of the toe structure (see also appendix B). Three damage levels were defined. After curve fitting he presented two design formulae, one with H_s and one with $H_{2\%}$. In 1995 Van der Meer presented the knowledge gained in a paper, in which the formula with $H_{2\%}$ was rejected as it "did not decease the existing scatter". The formula with H_s has been incorporated in the new Rock Manual by CIRIA et al. (2007) as equation 5.187.

The formulae use the damage parameter and water depth at the toe as input. From Gerding's test data it appeared that wave steepness and toe width is not of influence. This conclusion is however made on a very limited number of test cases: for the steepness the conclusion is drawn based on only two test results per situation.

The paper of Van der Meer mentioned that the design curve is not ideal since the stability number can become zero. This does not allow for some natural minimal displacement beneath a threshold value of motion (see §4.3.1 in Baart (2008)).

Burcharth and Z. Liu (1995) Burcharth and Liu did some toe stability analysis in the context of the Rubble Mound Breakwater Failure Mode-project. Based on some flume experiments they presented a formula which allows for the design of toe structures made of concrete cubes. A small deviation can be present in this research since rock is modelled here.

Docters van Leeuwen (1996) In the Master's thesis of Docters van Leeuwen an assumption made by Gerding was verified. She examined the influence of stone density (incorporated in the relative stone density Δ) on stability. It appears that this influence is modelled correctly by Gerding. She discovered that the influence of the mean water depth h_m cannot be neglected. The formula of Gerding is indeed correct for his range of h_m-values, but outside this range h_m should be somehow accounted for in the stability formula. Docters van Leeuwen did not propose a new formula.

Docters van Leeuwen was the first to investigate, to a very limited extent, the relation between flow velocity and stability of stones. She calculated a wave-induced orbital flow velocity at the toe surface by using linear wave theory. This again proves the need to incorporate h_m in the formula. Subsequently the threshold of motion was investigated by means of the criterion of Rance and Warren (1968). It appeared that this method works quite well. With this investigation she made a start in a more fundamental approach of toe stability, namely by decoupling the direct relation between wave action and damage by means of the flow velocity at the toe surface.

Van der Meer (1998) Experience pointed out that use of the formula by Gerding (1993) could produce unrealistic results – Van der Meer already made this consideration in his publication of 1995. He published a new formula based on the work by Gerding. Now a minimal stability is provided by using an offset. The validity range did not change, however.

This formula has also been incorporated in the new Rock Manual by CIRIA et al. (2007), as equation 5.188. Still a limit of $h_m/H_s < 2.0$ ($\gamma > 0.5$) is imposed, meaning that the formula is only valid for relatively shallow water.

Sayao (2007) Formulae up to now did not take the foreshore steepness and the wave steepness into account. Sayao performed dimensional analysis on new experimental data from 2005. He fitted a new design formula which gives a value for N_s and which takes foreshore slope, relative water depth and the Iribarren number as input. No configurable damage parameter is thus available. In further research it is proven that foreshore slope and wave steepness (or wave length) indeed influence stability. Unfortunately his formula produced quite some scatter for the test results, so no research has been appended directly to Sayao's work. The formula is conservative, since it models a condition with nearly no damage.

At this point the literature study by Baart ends, so a more extensive literature study will be given for the remaining recent studies.

Baart (2008)

The subject of Stephan Baart's Master's thesis has its origin in the work and recommendations by Docters van Leeuwen (1996). Stability methods up to now were empirically fitted stability formulae, which take information on the hydraulic parameters and toe dimensions as input, and the stability number N_s as output. This is quite a big step since there are a lot of processes involved in moving a stone. Baart made an extensive analysis of the formulae by Gerding (1993) and Van der Meer (1998), from which followed that there are quite some flaws and uncertainties remaining.

Baart proposed a new concept for the assessment of breakwater toe stability. His hypotheses, assumptions and model will be cited here, as they are so clearly stated and so important for the new line of research:

> "A new hypothesis is formulated to describe toe rock stability. Important propositions are:
>
> a. There is a critical value for the load on toe rocks (threshold of movement), instead of a power relation between damage and stability.
> b. The stability problem should be regarded for local conditions at the top surface of the toe bund.
>
> Two invalidated assumptions are made:
>
> a. The combination of down rush and porous outflow of water is normative for toe rock stability. This assumption follows from the theoretical view on the physical process and from suggestions in literature.
> b. Flow, turbulence and accelerations can be represented by one characteristic parameter, namely the velocity amplitude of local oscillatory flow.

> The concept for this study's model is based on two steps:
> Step 1: Assessment of the amplitude of local water velocity at the toe bund. This is calculated by summation of the contributions of the incoming wave and down rush, taking a phase difference into account.
> Step 2: Description of the critical velocity for a toe rock. The Rance/Warren stability criterion is used with a theoretical adaptation, which accounts for the effect of porous outflow.
>
> Coupling these two steps implies that a rock will move if the occurring velocity exceeds the critical velocity."
>
> *(Cited from Baart (2008), page v-vi)*

Baart thus proposed a two step model with flow velocity at the toe surface as intermediate result. He was able to verify his hypotheses for the datasets from flume tests by Gerding (1993), from tests by the US Army Corps of Engineers in 1987, and from tests during the first research project on berm breakwaters MAST I in 1992. The dataset of Docters van Leeuwen however did not give the expected results.

Baart derived flow velocity analytically by using down rush energy, a long wave approximation, a reflection model and porous flow via a head gradient. This leaves room for improvement, as situations with complex breakwater geometries or components make an analytical expression difficult or even impossible. After calculating flow velocity he used the stability criterion by Rance and Warren (1968), which determines whether stones in a horizontal bed will displace under oscillatory flow. Baart adapted the criterion to incorporate porous flow. He also tested an adapted Izbash-criterion, but this did not give better results. Although Baart used analytical expressions and an empirically determined stability criterion, still his method gives better results in terms of accuracy of stability prediction compared with empirically derived formulae.

Baart also investigated a different description of damage, normalized by toe width. This is a next step in percentual damage description. Unfortunately it seemed not to give any improvement in accuracy. Next he proposed new limits for N_{od} which mark the threshold of motion rather than an acceptable amount of damage. The first is of course less subjective than the latter and thus preferable.

Ebbens (2009)

The limited validity range of the formulae by Gerding (1993) and Van der Meer (1998) was of concern: their formulae were not yet experimentally validated for very shallow water. Furthermore the change of hydraulic conditions when waves break in front of the breakwater, and not on the armour layer or toe structure, were not investigated thoroughly. For this Ebbens varied the foreshore slope in new flume experiments, like in Sayao (2007). He defined very shallow water conditions to have $h_m/H_s < 2.0$ ($\gamma > 0.5$). Wave breaking results in a strong increase in turbulence, attacking the toe structure even more than under deep water conditions. To incorporate wave steepness and foreshore slope, Ebbens used the Iribarren number:

$$\xi_{0p} = \frac{\tan \alpha_{fore}}{\sqrt{H_s/L_{0p}}}$$

His first effort was to validate the formula by Van der Meer (1998) in the region for $h_t/h_m < 0.4$. For this he simulated the experiments by Gerding with extended range in relative water depth. He concluded that the formula by Van der Meer (1998) is more correct than the one by Gerding (1993). This only held for experiments in which foreshore steepness had not been changed.

His second research aspect was the influence of foreshore slope and wave steepness, from which the latter has a remarkable history in research (see section 1.2.2). His test results clearly show a decrease of damage with increasing wave steepness and with decreasing foreshore steepness. This holds for very shallow water. He included this effect in a new stability formula. It takes the Iribarren parameter (thus wave steepness and foreshore steepness) and a new damage parameter as input. Ebbens proposed a percentual damage parameter which scales the number of fully removed stones with toe stone porosity and volume. Toe dimensions are thus included in the damage parameter.

Nammuni-Krohn (2009)

In 2009 Julia Nammuni-Krohn performed an additional Master's thesis, or minor research project, in her Master's programme. She tried to find experimental proof for some aspects of Baart's study in 2008. By means of flume experiments she measured wave-induced flow velocity at breakwater toes.

In her experiments she used Acoustic Doppler Velocimeters (ADVs) and wave gauges to measure the necessary phenomena. With Fourier curve fitting a formula for maximum flow velocity near the toe was obtained. Down rush seemed to form an additional component next to regular orbital velocities, as was expected by Baart. Unfortunately she did not have enough time to analyse irregular wave results, so her formula is only verified for regular waves. Besides, a lot of scatter was encountered.

Although she could not fully verify Baart's analytical expressions, her work can be seen as a next step in the line of research by Docters van Leeuwen and Baart.

Baart et al. (2010)

Work from Baart (2008), Ebbens (2009) and Nammuni-Krohn (2009) has been put together in this paper. First the work by Ebbens is presented. Secondly the new approach investigated by Baart is discussed, after which the validation by Nammuni-Krohn is given. Here it is clearly stated that Baart overestimated the flow velocity with his analytical expressions, though it seems to be a constant deviation. The trends described by Baart's method are thus correct.

In 2008 Baart could not explain why the dataset of Docters van Leeuwen performed badly against his formulae. Work by Ebbens had shown that foreshore steepness is of importance. A correction factor is thus proposed, which scales the orbital flow velocity to the foreshore steepness. With this correction the dataset of Docters van Leeuwen also fit the prediction method by Baart.

Muttray (2013)

In the work by Muttray it is attempted to give a new fundamental approach towards toe stability. The approach also defines a critical flow velocity at which toe rock will start moving, which agrees with the hypothesis by Baart (2008). The intermediate steps in derivation again use a lot of curve fitting. The formula presented is thus nearly as empirical as the work by Gerding, Van der Meer and others, even though the background is more fundamental. Muttray already acknowledged this by the comments he made in his paper.

Muttray started with an extensive review of existing toe stability formulae, together with their bias (difference between measured and calculated damage) and scatter (standard deviation with compensation for bias). It must be remarked that this bias is not a very interesting tool, since it only presents how good a researcher is able to fit a curve to his own data and not how this curve would perform against data from others. Muttray concluded his review by two points: firstly it appeared that the water depth above the toe h_t is most governing in determining toe stability. Secondly he gave his concern that data points for higher waves are lacking.

For the stability analysis Muttray started with fundamental work by Izbash: stones will move "when a critical flow velocity v_{cr} is reached." The formula for this v_{cr} is reduced for deep lying surfaces, where wave-induced flow velocities will be lower. Finally the formula is transformed into a calculation of $N_{s,cr}$, i.e. a critical stability number which defines the threshold of motion. This coincides with the work in Baart (2008) in the sense that they both define a threshold of motion, although Muttray does this by a simple linear approach and curve fitting instead of an analytical approach. At this point indeed Muttray started with curve fitting to give values for the coefficients in $N_{s,cr}$. Fitting is done based on datasets generated by Markle (1989), Gerding and Ebbens.

Next, Muttray tried to couple the critical stability number $N_{s,cr}$ with the amount of damage N_{od}. Again, this is done by curve fitting. First he considered a linear function which has it offset at $N_s = N_{s,cr}$, which is analogous to Baart (2008). Then he changed his mind:

> "However, for practical applications it may be convenient to have a damage function that includes the range of marginal damage (i.e., if $N_s/N_{s,cr} < 1$) and provides a slightly conservative estimate of the damage numbers around the start of the damage. Approximating the damage progression by a cubic function [...] has been proposed by Baart et al. (2010) and appears thus more favourable from a practical point of view."
>
> *(Cited from Muttray (2013), page 60)*

Muttray proposed the following relation, derived by curve fitting:

$$\sqrt[3]{N_{od}} = \frac{N_s}{N_{s,cr}}$$

and joined it with the formula for $N_{s,cr}$. The result was a new stability formula in the classical representation. Next he wrote the following consideration:

> "It should be noted that a cubic approach [...] does not necessarily provide a more meaningful description of the physics involved in the toe damage progression than a linear or a polynomial approach."
>
> *(Cited from Muttray (2013), page 60)*

Some additional analysis of old datasets was made. According to Muttray, Ebbens made a mistake in measuring wave heights. Muttray plotted a corrected stability value against foreshore steepness, from which he concluded that there is no influence of steepness on toe damage. Also toe berm geometry has been investigated for which he also stated that it does not influence stability. Both analyses showed however very large scatter, so he concluded that "toe berm damage is apparently to some extent a random process that cannot be described in explicit detail by a deterministic approach."

Finally Muttray proposed a new percentual description for damage, based on toe dimensions, which is more suited for use in practice.

Arets (2013)

Bachelor student Kees Arets investigated the use of numerical wave flume model IH-2VOF to simulate flow velocities near the toe. The model might be used as an alternative for flume experiments, since it is able to calculate water levels, pressure and flow velocities at arbitrary points. Arets tried to simulate the experiments by Nammuni-Krohn (2009). Model set-up took unfortunately a large amount of time, so not much time was left to make an extensive comparison. However, some trials showed agreement with the results of Nammuni-Krohn. Only regular waves have been modelled.

His work is very interesting since he suspects that the IH-2VOF model is indeed suited to simulate toe stability experiments. Experiments can thus be done with a computer instead of a physical flume, although calibration might still be needed. This way the line of research started by Baart (2008) can be continued.

The model took quite a long time to run on a normal desktop computer, so for extensive simulations use of a cluster computing system[1] might be required. Arets advised to make the numerical flume as short as possible, since this does not influence accuracy but reduces computation time.

Van Gent and Van der Werf (2014)

In 2014 Marcel van Gent and Ivo van der Werf published a paper with the results of their contribution to toe stability. They were interested in the effect of the geometry on its stability. In previous research not much attention was paid to toe height or width, or it was considered as not influencing stability. Result of new flume experiments is a new stability formula, although it is presented as a calculation for N_{od} instead of N_s.

After reviewing existing literature the experimental set-up is presented. Two methods of counting damage were investigated. The N_{od} value was calculated for stones which had been displaced "over a distance of more than one stone diameter." This was compared with a graphical method, in which stereo photography combined with a conversion formula gave a relation between S (eroded area scaled with stone diameter) and N_{od}. This appeared to work quite well.

Analysis of variation in toe dimensions demonstrated that damage increases for higher and wider toes. The first is result of reduced water depth above the toe, which is confirmed in earlier formulae where $h_t \propto N_{od}^{-1}$ for constant N_s. Next to toe geometry the influence of wave steepness was reinvestigated. It confirmed the conclusion in Ebbens (2009), namely that higher wave steepness reduces damage.

For derivation of a new stability method, Van Gent and Van der Meer followed partially the approach with a characteristic flow velocity at the toe. Previous research by Van Gent had proven that an approach with linear wave theory is sufficiently accurate in predicting velocities. They confirmed this hypothesis by analysing Nammuni-Krohn's experiments with irregular waves:

> "[It shows] that the calculated characteristic velocity [...] does not deviate much from the 2%-exceedance value of the maximum velocity per wave. [...] the calculated characteristic velocity may be suitable for estimates of rock toe stability."
>
> *(Cited from Van Gent and Van der Werf (2014), page 171)*

[1] A cluster computing system consists of several linked computers which together form a powerful system. Computation speed is heavily increased by executing tasks in parallel.

After curve fitting the new stability method is presented and tested against other datasets. Scatter is largely reduced within its validity range.

Finally a new approach for damage allowance is given. Instead of working with percentual damage, they proposed to scale the acceptable N_{od}-value with a factor based on toe width. Wider toes then allow for more damage.

Muttray et al. (2014)

At the 34th International Conference on Coastal Engineering (ICCE) in 2014, Muttray changed his view on toe stability drastically. He expressed his concerns on the classical approach in which curve fitting on dimensionless parameters is used (see §1.2.2). In a conversation with Muttray on July 16, 2014, we discussed his criticism and his presentation. He advises to use the approach with a critical flow velocity as proposed by Baart.

Muttray composed a dataset from the research by Gerding (1993), Docters van Leeuwen (1996), Ebbens (2009) and Van Gent and Van der Werf (2014). The formulae by Van der Meer (1998), Muttray (2013) and Van Gent and Van der Werf (2014) were tested on their predictive capacity on this dataset. Stability was often predicted rather well, but the damage number N_{od} had a lot of scatter. Accuracy was improved when applying the formulae on their originating dataset only. Muttray writes:

> "It appears from the above that the most recent [...] and the most accepted [...] toe stability formulae suffer from a lack of accuracy and general validity. [...] This lack of general validity is considered as the main shortcoming of the three toe stability formulae [...]"
>
> *(Cited from Muttray et al. (2014), page 5-6)*

Muttray suspects that interdependencies between parameters, in particular the relation between H_s and h_t, may result in incorrect representation of these parameters in the stability formulae. The dataset proves his hypothesis.

A new toe stability formula is developed by a step-by-step approach. This approach starts with a very simple case and is consecutively extended with more parameters. The final formula predicts the stability N_s as a function of wave length, foreshore slope, toe berm slope, damage number N_{od} and water depth above the toe. It corresponds to Hudson-approaches for armour layer stability. Muttray concludes with a warning that the formula is not intended for design purposes, as many assumptions in the derivation could not be proven. It may be used however "as a benchmark for toe berm testing and design."

1.2.2. Review per aspect

Approach for toe stability

From the review above it appears that there exist two common approaches towards assessing toe stability (see also appendix A). The first is an empirical approach by conducting physical experiments. It will be called the *empirical curve fitting approach*. For the parameters varied in the experiments dimensional analysis is done to create dimensionless parameter combinations. They are put into one or more formulae which are subsequently fitted to the experimental data. Fitting is done either by statistical analysis or, in more ancient research, just 'by the eye'. Physical background is often not included in the formula, although the trends are reviewed against this background. E.g. in the formula by Gerding (1993) the water depth h_t is first fitted to match the data; only afterwards in §5.6 he gives an explanation why this could be correct.

In the diagram in appendix A all research in the left hand box follows more or less this approach. Only Docters van Leeuwen (1996), who adds a small part on characteristic velocities, and Muttray (2013), who tries to use a fundamental background but eventually ends up with a lot of curve fitting, try to follow a more fundamental approach.

The second approach is the approach initiated by Docters van Leeuwen (1996) and extensively investigated by Baart (2008). It will be called the *decoupled model approach*. In this approach one attempts to decouple the relation between boundary conditions (hydraulic and structural) and a damage parameter, by means of a characteristic velocity. All researchers agree upon the definition of this characteristic velocity as being the flow velocity right above the toe structure. This velocity can be result of many physical processes. Baart composes it from orbital wave pattern, downrush on the armour slope, porous head gradient and wave reflection. The next step is to use a stability criterion to check whether stones will start to move.

In appendix A this approach can be found in the right hand box. In some way the work in Muttray (2013) also belongs to this part since a critical flow velocity and a critical stability number is defined.

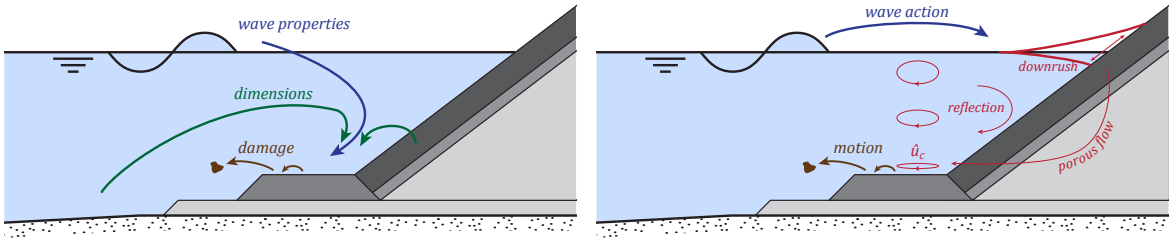

Figure 1.4: Principle sketches of the *empirical curve fitting approach* (left) and the *decoupled model approach* (right)

Van Gent and Van der Werf (2014) end up in a combination of the two approaches. They incorporate a flow velocity amplitude in their method which is based on linear wave theory. On the other hand they use curve fitting to let their method match the experimental data. A drawback of their method is that the flow velocity can only be calculated for rather deep water with waves breaking on the breakwater.

Van Oord, Delft University of Technology, Delta Marine Consultants (BAM Infraconsult) and Deltares agree upon the choice of the *decoupled model approach* as the most promising line of research. The research in this report is thus in line with this approach.

Benefits are the following:

- The approach has more physical background as it models the intermediate processes, so it is fundamentally more correct.
- Other influences on flow velocity, for instance currents or oblique wave impact, can easily be incorporated as an additional term or factor.
- Flow velocity is expected to be determinable using numerical models. A physical flume will then probably only be required to calibrate such a model.
- If flow velocity can be calculated numerically, complex geometries and wave patterns can be investigated. This would be nearly impossible with analytical descriptions.
- It is easier to incorporate further research, e.g. modelling of turbulence.

Known drawbacks are the following:

- At this point in research only the threshold of motion can be modelled accurately, since stability criteria by e.g. Izbash or Rance and Warren do not give a description of damage development. In research by Baart no approximation of N_{od} was given; in research by Muttray and Van Gent and Van der Werf curve fitting was used. Damage development is a time-dependent and complex process, which has not been investigated yet.
- It takes more effort to use the decoupled model approach as more input parameters and more calculations are required. Accuracy can thus go down since more parameters, like for instance porosity, have to be determined or measured, inherently imposing measurement and estimation errors.

Influence of wave steepness

As mentioned during review of the work by Ebbens, the influence of wave steepness has a remarkable history in research results. According to Ebbens (2009) Gravesen and Sørensen (1977) stated that higher wave steepness induced *more* damage. Gerding (1993) however concluded that wave steepness does not influence damage. It must be mentioned that this conclusion was drawn based on only two data points per situation. Docters van Leeuwen (1996) could not prove anything on steepness due to a lack of data points on this topic.

Sayao (2007) reinvestigated the influence of the wave steepness. Both Sayao and Ebbens conclude that higher wave steepness induce *less* damage, so the contrary of Gravesen and Sørensen. Muttray (2013) rejects

the influence by correcting a mistake in the measured wave heights by Ebbens. Van Gent and Van der Werf (2014) finally reconfirm the conclusion of Sayao and Ebbens.

Since steepness is defined as wave height over wave length ($s \equiv H/L$, Holthuijsen (2007); Schiereck and Verhagen (2012)), lower steepness means longer waves for the same wave height, which results in more wave energy transport (Holthuijsen, 2007, §5.5). Longer waves can thus induce more damage to a structure, so the observations by Sayao, Ebbens and Van Gent and Van der Werf seem to be physically correct.

In short we have:

$s \propto N_{od}$ Gravesen and Sørensen

$s \nsim N_{od}$ Gerding, Van der Meer, Muttray (2013)

$s \propto N_{od}^{-1}$ Sayao, Ebbens, Van Gent and Van der Werf, Muttray (2014)

Description of damage

Several authors defined a method to describe toe structure damage (see appendix B). All of these formulae make use of the number of displaced stones at the toe, but counting techniques and the way of relating them to the toe structure dimensions give large variations in results. Already in the definition of N, the number of displaced or removed stones, counting methods do not agree: one will count a stone when it has been removed completely from the toe edge (e.g. in Gerding (1993), Baart (2008)), the other when the stone has displaced over more than one stone diameter (Van Gent and Van der Werf, 2014).

Subsequently the N-value is related to the toe structure dimensions, to make it comparable for different layouts. In this way a standardized definition for the amount of damage is available. Two methods are typical: the first is to give the average loss per strip with a width of one stone, the second to give percentual damage. Examples of the first can be found in Gerding (1993) and Docters van Leeuwen (1996), where N_{od} is defined. This definition is again prone to interpretation: Gerding weighs against the number of strips, while Docters van Leeuwen weighs against the mean number of stones per strip. Also in percentual descriptions opinions vary. Baart (2008) uses toe length and width, Ebbens (2009) uses volume and porosity and Muttray (2013) uses toe height, toe width and porosity. Design values proposed by the authors change accordingly with their damage definitions.

Van Gent and Van der Werf (2014) propose a factor by which the design values for N_{od} by Gerding should be multiplied to account for toe dimensions, but when we rewrite this definition, we get in fact a modified Baart-definition:

$$
\begin{aligned}
N_{od} &\leqslant N_{acceptable} \cdot f_B \\
\frac{N}{L/D_{n50}} &\leqslant N_{acceptable} \cdot \sqrt{\frac{B_t}{3D_{n50}}} \\
\frac{N}{\frac{L}{D_{n50}}\sqrt{\frac{B_t}{3D_{n50}}}} &\leqslant N_{acceptable} \\
\text{Baart: } \frac{N}{\frac{L}{D_{n50}} \cdot \frac{B_t}{D_{n50}}} &= N_{odB}
\end{aligned}
$$

From the above we can conclude that there is nearly no consensus in the exact (practical) description of damage. Also on the weighing principle (per strip or percentual) researchers do not agree. Baart even writes: “Eventually the description of damage has proven not to be that important altogether. In any way N_{odB} is not better than N_{od} (for Gerding’s data set).” (Baart, 2008, p. 129). This creates a major problem in comparing and using experimental data. Mostly the counting method imposes a big problem; if only there would be photographs left, one could recount the displacements in a uniform fashion. It will also be difficult to adopt the decoupled model approach to damage description since damage development is a time-dependent process. This was already stated as a drawback of the approach.

Definition of shallow water

A final aspect to consider is the definition of shallow water. In Ebbens (2009) toe damage development has been investigated for very shallow water, which seems to be quite different from deep water. This means it is important to consider the change in hydraulic conditions (mostly wave breaking) when comparing different stability methods and experimental data.

Two influences can be seen: relative wave height and relative depth. The first is the relation between wave height and water depth, which is known as the breaker index $\gamma \equiv H/h$ (Holthuijsen, 2007; Schiereck and Verhagen, 2012). Depending on this value, wave breaking occurs at or in front of the breakwater; the higher the value, the shallower the hydraulic conditions, which results in more seawards breaking. When this occurs water motion becomes highly turbulent which results in more toe damage (Ebbens, 2009). The second influence, relative depth, is known as the relation between the water depth above the toe and in front of the toe, h_t/h_m. A lower value will result in less damage, since the toe then becomes small in relation to water depth, thus imposing less hindrance to the wave (Gerding, 1993).

In literature on toe stability shallow water is often described with the breaker index γ, by giving validity limits for this parameter (Baart, 2008; Ebbens, 2009; Muttray, 2013; Van Gent and Van der Werf, 2014). The relative depth h_t/h_m is included in the stability formula. According to Gerding (1993) on page 17, the formula by Van der Meer in 1991 is given for *depth limited – shallow* – situations, i.e. $\gamma \approx 0.5$. In Gerding (1993) it is simply stated that 'a depth limited situation was present'; from his experiment data it appears that indeed $\gamma \approx 0.5$. Docters van Leeuwen states that using $H_{2\%}$ instead of H_s is better for shallow water situations. Baart assumes surging waves in transitional water depth for his analytical derivation of $\hat{u}_c$. In Ebbens (2009) research is done for *very shallow water*, i.e. $\gamma > 0.5$.

A final remark: in classic literature on waves (e.g. Holthuijsen (2007)) shallow or deep water is mostly determined by the relation between water depth and wave *length* (h/L or kd).

1.3. Problem definition, target of research, scope

1.3.1. Problem definition

In the literature study of section 1.2 the historical efforts in clarifying breakwater toe stability have been reviewed. There appear to be the following ways to determine stability formulae:

- Physical model tests – most commonly used
- Analytical approaches – tried by Baart (2008) and Muttray (2013), but inflexible
- 'Real-world' breakwaters – no data available, infeasible to measure
- Numerical model tests – not yet investigated thoroughly

Physical model tests are up to now most often used to fit a design method. An analytical description would be academically interesting, but it is often based on assumptions and simplifications. When it comes to complex situations it could become impossible to solve. Common problems with the empirical and analytical stability methods are:

- There are too many methods. Which one should be used? Which approach is best?
- Experimental data show a lot of scatter, so accuracy of the methods is low.
- The validity range of the methods is small, or there exist large simplifications and assumptions.
- Each method performs well on data used for fitting, but not on data from other experiments.
- Researchers do not agree upon the definition of damage. What kind of damage number should be used or is the threshold of motion more interesting?
- Fitted formulae often lack physical background for dimensionless parameters. Influence of e.g. foreshore steepness or wave length is not always included, although research by others has proven that they do influence stability.

It is clear that empirical and pure analytical stability methods impose a lot of problems and considerations. A better approach for toe stability would be useful.

1.3.2. TARGET OF RESEARCH

Main goal of this research is to reduce the problems described above. Researchers and companies agree upon the fact that numerical methods could solve some problems in toe stability research. These methods are more flexible than pure analytical approaches and they still have an analytical background. Nowadays computational power required is widely available.

A numerical method will likely provide a practical tool to assess toe stability, however, it is not yet sure whether it will be possible to produce a single design formula. On the other hand it is clear that the decoupled model approach proposed by Baart (2008) is the best way to continue research. This is confirmed by conversations with ir. Henk Jan Verhagen (Delft University of Technology), ir. Greg Smith (Van Oord), Markus Muttray PhD (Delta Marine Consultants) and dr.ir. Marcel van Gent (Deltares).

The target of research is thus as follows:

> *To give advice on which method is most useful in determining breakwater toe stability, by evaluation of existing stability methods with a numerical flume and the decoupled model approach.*

1.3.3. RESEARCH QUESTIONS

Two steps will be required to reach the target of research. They are defined in the following main research questions:

1. *Can the IH-2VOF model be used to simulate physical flume experiments on breakwater toe stability?*
2. *Which existing method on breakwater toe stability gives, using the decoupled model approach and based on calculations with a VOF model, best results for prediction of the threshold of motion?*

To be able to answer these questions, some sub-questions must be answered:

a. *Which are criteria on which VOF models should be evaluated in light of the target of research?*
b. *Which formula or method is best to determine whether toe stones will start to displace under influence of the hydraulic load?*
c. *How can stability prediction by toe stability methods be transformed into a threshold of motion?*
d. *Which are criteria on which toe stability methods should be evaluated in light of the target of research?*

1.3.4. SCOPE OF RESEARCH

In the research questions some terms have been used, for which it is useful to give a clarification and a limitation in scope:

Useful Performing best against the evaluation criteria.

Breakwater toe Toe structure of a breakwater, constructed as a berm of loose rock supporting the armour layer. Toes consisting of concrete elements, embedded toes or vertical breakwaters are thus not investigated.

Existing methods In this study it is certainly not intended to create or fit a new stability formula. This would require too much time and Van Oord is not interested in yet another inaccurate or incomplete stability method.

Numerical flume The IH-2VOF model is a 2D model. 3D effects will not be calculated, which imposes no problem as most historical experiments are performed in flumes too. It must be stressed that no physical experiments will be conducted. Existing experimental data will be used for comparison instead.

Decoupled model approach This method is described on page 8, in which a characteristic flow velocity at or near the toe is calculated.

Threshold of motion Instead of predicting damage, which from literature study appeared to be quite difficult to model, a threshold of motion shall be calculated. This threshold is the point at which hydraulic load will displace stones.

Hydraulic load The IH-2VOF model calculates water levels, flow velocities and pressures at the points of interest. In addition turbulence can be incorporated to some extent.

1.4. STRATEGY

Strategy will describe how research questions will be answered. This will be done with help of the diagram in figure 1.5 on the next page.

Research questions show two phases in research. During the *first phase* it will be tried to simulate the flume experiments by Nammuni-Krohn (2009) with the IH-2VOF model. Flow velocities from these experiments will be compared with values computed by the model. The IH-2VOF model can then be evaluated with the criteria from sub-question a.

The *second phase* can then start. Additional model runs will be done to simulate experiments by Ebbens (2009). Stability methods will be evaluated based on the threshold of motion. Software will produce velocities, which can be translated into a threshold of motion using the formula from sub-question b. The stability methods should then be compared with this threshold. This is done by putting a critical value for N_{od} or $N_{\%}$, based on how damage was defined and counted in the original research. Stability methods, with a fixed value for N, can subsequently be transformed in a formula for the threshold of motion, e.g. motion if $f(H_s, \Delta, ...) \leqslant 1$. Experimental and numerical thresholds of motion can then be compared, which forms basis for evaluation of stability methods. From this an advice on stability methods will be given.

1.5. REPORT STRUCTURE AND DATASETS

This report will start with a description of the decoupled model approach in chapter 2. Datasets available are reviewed. Then the report is split up in two parts representing the two phases above. In the first phase the IH-2VOF model is set up, configurations are explored and convergence tests are done to find optimal settings, all of which can be found in chapter 3. Next the dataset by Nammuni-Krohn (2009) is modelled with IH-2VOF and the results are reviewed in chapter 4. An answer to the first research question is then obtained. In the second phase the existing toe stability methods are reviewed with help of the decoupled model approach. This is done in chapter 5. Research will finally be concluded with chapter 6.

The appendices contain among others listings of formulae, datasets and model configurations. A logbook of the IH-2VOF model and some information on running cases in batches is also provided.

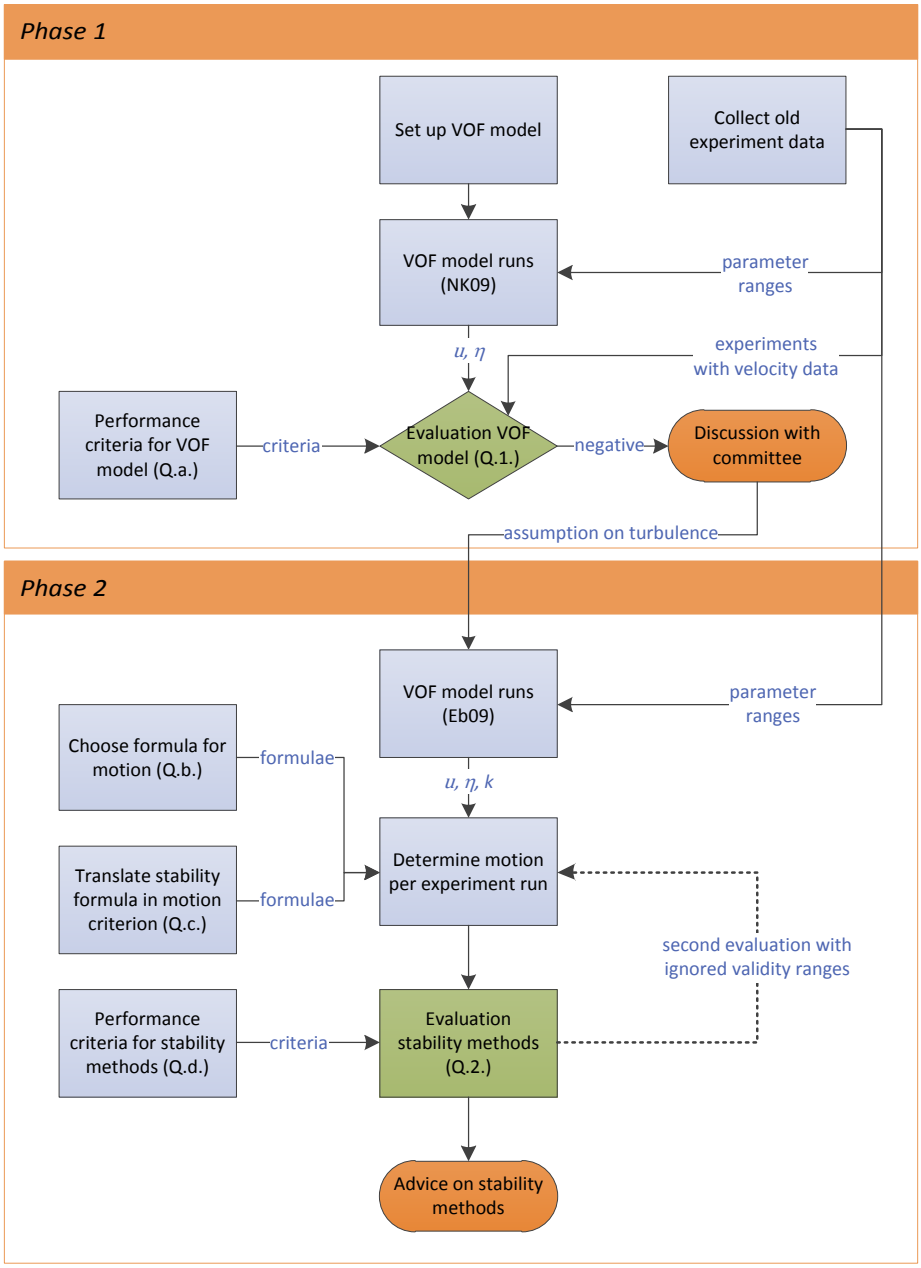

Figure 1.5: Research strategy diagram

2

Implementation of the decoupled model approach

2.1. Description of the decoupled model approach

The decoupled model approach is the new approach towards toe stability, as proposed by Docters van Leeuwen (1996) and Baart (2008). Difference with the empirical curve fitting approach was already described in section 1.2.2. In the decoupled model approach hydraulic conditions above the toe act as a link between wave-induced flow and stone stability, see figure 2.1. In Baart (2008) it was proposed that horizontal flow velocity above the bed should be taken as the characteristic measure. Other measures like e.g. pressures or accelerations might also be of importance.

The IH-2VOF model will be used to obtain local hydraulic conditions above the toe. A yet to be chosen formula for stone motion should translate these conditions into stone motion prediction. This prediction will be compared with the prediction by toe stability methods.

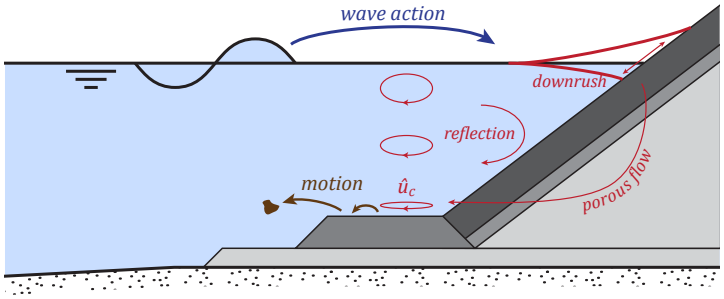

Figure 2.1: Principle sketch of the decoupled model approach

The following terms will be used frequently and require a definition to avoid confusion:

Stability method A single or multiple formulae together which determine whether a breakwater toe structure is stable under the prevailing wave climate (§1.2).

Motion formula A formula which gives information on stone stability in general situations.

Stability number The dimensionless $N_s = H_s/\Delta D_{n50}$ value for breakwater stone stability (§1.2).

Damage parameter Parameters in stability methods expressing the amount of damage. Typical examples are N_{od} and $N_{\%}$. Note that exact definition of damage may vary per method.

Stability parameter The typical dimensionless parameter Ψ in motion formulae. It is often related to transport parameter Φ.

2.2. Formulae for the threshold of motion

2.2.1. Introduction to stone stability

This section gives a short overview of the existing motion formulae and their advantages and limitations. A small-scale literature study has been performed towards stone stability. Criteria on which motion formulae are evaluated will be formed and applied on the formulae available. It is beyond the scope of this research to try to improve or adapt these formulae to the current situation[1]. They will be used "as is" for engineering purposes. The section concludes with an overview of the required output from the numerical model, i.e. the output from step one of the DMA. Literature study initiated with the work by Hofland (2005), Hoan (2008) and Steenstra (2014). Their work focused on stability of stones attacked by non-uniform flow. The theses contain extensive literature studies, to which reference is made for a complete and detailed overview.

Stone stability is the interaction between fluid flow and movement of the stone. The flow results in all kinds of forces on the stones (Steenstra, 2014, §2.2) which might be sufficient to let the stone move. The amount of movement, i.e. whether the stone will only be rocking or whether it will really move, is up to now only predictable by empirical relationships. This is partially caused by the complex mutual interaction between stone movement and fluid flow, and partially by the stochastical character of the process. Stones do not possess a well-defined, simple shape and also turbulence – an important component of the stone forces – is random in nature. They can both be described statistically (Schiereck and Verhagen, 2012, §2.2).

2.2.2. Threshold of motion

In figure 2.3 in Hoan (2008) a diagram presents the different approaches in general stone stability. They are characterized by whether they are deterministic or probabilistic, and whether they define a threshold criterion or an amount of transport. Older motion formulae are deterministic methods defining a threshold of motion, e.g. formulae by Shields (1936) and Rance and Warren (1968). The threshold works with a critical value of the hydraulic conditions at which a 'considerable' amount of movement is noticed. If stability could be expressed in e.g. parameter X then the threshold is defined by a critical value X_c so that when $X \geqslant X_c$ there would be stone movement. In e.g. Schiereck and Verhagen (2012, §3.2.2) and Steenstra (2014, §2.3.2) it is described that this condition is prone to the (subjective) interpretation of the researcher. This makes it a difficult parameter to use in research as it is hard to compare between experiments, despite efforts made to make the condition more defined. On the other hand a threshold of motion is an easy to understand condition, which is important for engineering and communication practices.

More recent work follows the deterministic road towards transport formulae, to avoid subjectivity as far as possible. Most motion formulae are presented using the dimensionless stability parameter Ψ and the dimensionless transport parameter Φ. The first gives a ratio between load and resistance, the second is a measure for the amount of stone movement. They are related to each other by a transport formula $\Phi = f(\Psi)$. This relation also holds for non-uniform flow, see Steenstra (2014, §2.3.2). In design practices one could pose a limit to the amount of transport allowed, say Φ_c, and verify whether the calculated Φ stays below this value. In fact this is similar to the principle of a threshold of motion: the designer puts a subjective limit to the amount of allowed stone displacement. The difference is that the designer can choose to let some displacement take place, which is interesting for e.g. temporary structures. The similarity to damage number N_{od} is also described in Schiereck and Verhagen (2012, p. 55): *"The choice of Ψ_c depends on the amount of transport that is acceptable, hence Ψ_c can also be regarded as a damage number."*

As already described in section 1.4 this research will use the threshold of motion concept. Can it be defended to use this concept when it is such a subjective criterion? In the work by Baart (2008) it was proven that a threshold of motion is a workable method for toe stability. Graphs in chapter 5 in Dessens (2004) confirm this behaviour. For engineering practices it is an understandable and practical measure to work with. Designers and contractor clients often choose for a conservative value for the damage number, which corresponds to the subjective levels "hardly any damage" or "insignificant damage", see appendix B. This corresponds to a design for the threshold of motion. It is not the most economical choice, but from a political point of view

[1] In e.g. Baart (2008) the formula by Rance and Warren (1968) was adapted to account for porous flow.

a logical choice. A third reason to use the threshold concept is the fact that in historical experiments damage was recorded in different and incomparable ways. The amount of displaced stones is not reported in such detail that they could be reassessed with a uniform parameter.

Finally it must be stated that the more recent motion formulae can be translated to a threshold criterion by imposing a critical value of Φ and/or Ψ. By this they can be used in this research. This adds however subjectivity to the formulae. This subjectivity is also visible in the defined damage levels for N_{od}: mostly a transition range is given.

2.2.3. REQUIREMENTS FOR MOTION FORMULAE

The formulae for motion need to fulfil some requirements imposed by the research approach, the dataset and the modelling possibilities of the IH-2VOF model. The formulae will subsequently be reviewed against these requirements and the best formulae will be chosen.

Formula for non-uniform flow Uniform flow can be defined as flow in which there are no changes of flow velocity in the direction of the flow. The acceleration in space[1] is thus zero. In case of breakwater toes, waves and loose stone elements will form a flow which is certainly not uniform. Acceleration and deceleration of the fluid produce additional pressure differences and generate turbulence, see e.g. Hofland (2005, §2.4, 2.5) or Steenstra (2014, §2.1, 2.2). The motion formula should thus be intended for non-uniform flow. This is a strict requirement.

Applicability for RANS-models The IH-2VOF model solves the Reynolds-averaged Navier-Stokes (RANS) equations, see chapter 3. The output of the model is therefore limited to discrete velocities, pressures, water levels and, if implemented, values of turbulence intensity. The parameters of motion formulae should therefore be given in, or derived from, the model output. This is a strict requirement.

Focus on coarse material Breakwater toes are constructed of stones which are large relative to the toe dimensions; a toe is often only a couple of stones wide and high. The definition of stones or coarse material is therefore open to discussion: what can be regarded as sand or gravel in a real-life breakwater could be regarded as large rock in scale models. Hence this is not a strict requirement. The most important thing to verify is whether the research focuses on non-cohesive, loose grains.

Availability of a threshold of motion criterion A motion formula which is intended for defining the threshold of motion is easy to use, even though it is a subjective criterion. Transport parameter Φ however can be converted to such a criterion with a subjective limit. If research would present such a limit, this would be practical. In other cases a limit has to be chosen. This requirement is thus not strict.

A final comment should be made regarding turbulence modelling. It will be proven in section 3.5 that the current version of the IH-2VOF model is not able to model turbulence in a correct way. Use of a motion formula which has the value of turbulence intensity k as input variable is therefore possible, but the outcome could be of little use. A formula which uses a bulk coefficient, including turbulence effects, is then a better option, although it is scientifically less correct.

2.2.4. REVIEW OF MOTION FORMULAE

The motion formulae hereafter are found in work by Baart (2008), Hofland (2005), Hoan (2008) and Steenstra (2014). The background of each formula will be discussed very briefly; for more detail reference is made to the original works or the literature study in the theses cited. Each formula will be presented in its original form. The subscripts to stability parameters Ψ is kept to these in the work by Steenstra (2014).

Izbash, as presented in Schiereck and Verhagen (2012) The approach by Izbash in 1930 was based on a force balance on single stones: when a certain equilibrium condition is passed the stone will start to move. It makes use of a characteristic velocity near the stone, which was not defined in more detail. The definition

[1] Note the difference with *stationary* flow, in which acceleration in *time* is zero.

of the stone diameter is not known exactly either. Even though the formula is very old, it is often used as reference in research on stone stability. The formula reads:

$$u_c = 1.2\sqrt{2\Delta g d} \tag{Izb30}$$

in which:

u_c Critical velocity [m/s]

Δ Relative density [-]

d Stone diameter [m]

Shields (1936) Shields derived a stability parameter for granular beds under uniform flow. It is based on local shear stress as load and stone weight as resistance. For situations with non-uniform flow an influence factor K_v is defined. The factor is derived empirically and available for a limited number of situations only, see Schiereck and Verhagen (2012, §3.4). Shields also defined a critical value of Ψ by means of a diagram, see e.g. figure 3-2 in Schiereck and Verhagen (2012). The motion formula can be given in many forms, but here the one with the bed shear stress is presented:

$$\Psi_S = \frac{\tau_b}{(\rho_s - \rho_w) g d} \tag{Shi36}$$

in which:

Ψ_S Shields stability parameter [-]

τ_b Bed shear stress [N/m^2]

d Stone diameter [m]

Rance and Warren (1968) The work by Rance and Warren focused on finding a threshold of motion of coarse material under oscillatory flow. The experiment results were originally presented in a diagram. In Schiereck and Fontijn (1996) a formula for motion was fitted to the diagram data. In Baart (2008) the formula was used and adapted to incorporate the head gradient due to porous flow in the breakwater toe. Both formulae respectively read:

$$\hat{u}_{bc}^{2.5} = 2.15^{-1}\sqrt{T}(\Delta g)^{1.5} D_{n50} \tag{Ran68a}$$

$$\hat{u}_{bc}^{2.5} = 0.46\sqrt{T}\left((\Delta - C_{PF} i) g\right)^{1.5} D_{n50} \tag{Ran68b}$$

in which:

$\hat{u}_{bc}$ Critical horizontal orbital flow velocity above the bed [m/s]

T Wave period [s]

D_{n50} Median nominal stone diameter [m]

C_{PF} Coefficient for porous flow, fitted to a value of 0.4 [-]

i Head gradient over the toe due to porous flow [-]

Sleath (1978) Sleath extended the work by Shields to oscillatory flow, which is useful for wave loads. The Shields parameter Ψ_S is kept, though a second line in the diagram for the threshold of motion is added. The diagram is presented in figure 8-6 in Schiereck and Verhagen (2012).

Jongeling et al. (2003) The research by Jongeling et al. developed a method which couples stability of granular materials to numerical RANS-models. The effect of turbulence is added with the k-ε model. The formula uses a depth-averaged velocity and a critical stability value is provided. With depth-averaging Jongeling

et al. break with the principle of a certain characteristic velocity near the stone. In Hoan (2008) the formula has been critically reviewed and tested, which resulted in a new value for α. The Jongeling formula reads:

$$\Psi_{WL} = \frac{\left\langle \left(u + \alpha \sqrt{k} \right)^2 \right\rangle_d}{\Delta g D_{n50}} \tag{Jon03}$$

in which:

- u Horizontal flow velocity at each depth level [m/s]
- α Empirical turbulence magnification factor, Hoan (2008) fitted a value of 6.0 (originally 3.5) [-]
- k Turbulence intensity [m^2/s^2]
- $\langle \ldots \rangle_d$ Spatial average over a height d above the bed
- d Water layer thickness which is important for stability, $d = 5D_{n50} + 0.2h$ [m]
- h Water level above the bed [m]

A critical value for the stability was given as $\Psi_{WL,c} = 8$.

Dessens (2004) Dessens did research to accelerating flow. He fitted a motion formula which is based on the local acceleration and velocity. The flow was accelerating so the influence of turbulence is low. The acceleration is measured in space. No clear definition of the averaging process is given and it is questionable whether for toe stability the averaging must be performed over the full water column. The coefficients contain the influence of turbulence and are fitted based on a threshold of motion. The final formula reads:

$$\Psi_{MS} = \frac{\frac{1}{2} C_B u^2 + C_M d a}{\Delta g d} \tag{Des04}$$

in which:

- Ψ_{MS} Dessens stability parameter [-]
- C_B Bulk coefficient for drag and turbulence, fitted to a value of 0.10 [-]
- u Horizontal (depth-averaged) flow velocity [m/s]
- C_M Inertia coefficient, fitted to a value of 3.92 [-]
- d Stone diameter; in Dessens (2004, §3.9) it can be found that it is probably the D_{n50}-value [m]
- a Horizontal (depth-averaged) flow acceleration in space, $a = \bar{u} \frac{\partial \bar{u}}{\partial x}$ [m/s^2]

The critical value of $\Psi_{MS,c} = 0.3$ was found during fitting, see figure 5.19 in Dessens (2004).

Hofland (2005) In the PhD thesis by Hofland a thorough study was made towards mechanisms governing stone stability. The effects of turbulence are investigated to a large extent. An important aspect of his formula is the implementation of a mixing layer between laminar flow and a turbulent eddy. An other important aspect is that the method was developed for use with a RANS-model, like the formula by Jongeling et al. (2003). In Hoan (2008) the value for α was reviewed and fitted to a new value. In the conclusions of his thesis Hofland mentions that the model "is not suited for waves". The Hofland formula reads:

$$\Psi_{Lm} = \frac{\max \left[\left\langle \bar{u} + \alpha \sqrt{k} \right\rangle_{L_m} \frac{L_m}{y} \right]^2}{\Delta g d} \tag{Hof05}$$

in which:

Ψ_{L_m}	Hofland stability parameter [-]
$\bar{u}$	Time-averaged horizontal flow velocity at each depth level [m/s]
α	Empirical turbulence magnification factor, Hoan (2008) fitted a value of 3.0 (originally 6.0) [-]
k	Turbulence intensity [m^2/s^2]
$\langle \ldots \rangle_{L_m}$	Spatial moving average filter over the region $y \pm L_m/2$
$\max[\ldots]^2$	Spatial maximum over the water column h. Note that $\max[x^2] = (\max[x])^2$.
L_m	Bahkmetev mixing length, $L_m = \kappa \cdot y \sqrt{1 - y/h}$ [m]
y	Measurement level above the bed; $y = 0$ at the theoretical bed level [m]
d	Stone diameter; from §4.5.1 and §4.5.2 in Hofland (2005) it can be assumed that it is probably the D_{n50}-value [m]
κ	Von Kármán constant, $\kappa = 0.41$ [-]
h	Water level above the bed [m]

The discrete calculation method is as follows: at every y one takes the average of $\bar{u} + \alpha\sqrt{k}$ over the region $y \pm L_m/2$ in which also L_m is determined by y. Each average is multiplied with L_m/y. Afterwards the squared maximum of these values is taken and divided by the stone properties. See also §8.4.1 and figure 8.2 in Hofland (2005) for a visualization.

Hoan (2008) Hoan created a formula which uses a probabilistic approach for the derivation of an amount of transport. Instead of a contribution of $\sqrt{k}$ as in the formulae by Jongeling et al. and Hofland, the standard deviation of the flow velocity $\sigma(u)$ is used. Hoan defines this value as $\sigma(u) = \sqrt{\overline{u'^2}}$. The k-ε model does not provide this value and therefore this formula is difficult to implement with RANS-models. The final stability parameter reads:

$$\Psi_{u-\sigma(u)} = \frac{\left\langle [u + \alpha\sigma(u)]^2 \times \sqrt{1 - z/h} \right\rangle_h}{\Delta g d} \tag{Hoa08}$$

in which:

$\Psi_{u-\sigma(u)}$	Hoan stability parameter [-]
u	Horizontal flow velocity at each depth level [m/s]
α	Empirical turbulence magnification factor, fitted to a value of 3 [-]
$\sigma(u)$	Standard deviation of the flow velocity, defined as $\sigma(u) = \sqrt{\overline{u'^2}}$ [m/s]
z	Measurement level above the bed; $z = 0$ at the theoretical bed level [m]
h	Water level above the bed [m]
$\langle \ldots \rangle_h$	Spatial average over the water column above the bed
d	Stone diameter; from §3.3 in Hoan (2008) it can be assumed that it is probably the D_{n50}-value [m]

Steenstra (2014) Steenstra did additional research to the effects of accelerating flow and tried to combine this with knowledge gained on turbulence in the work by Jongeling et al. (2003), Hofland (2005) and Hoan (2008). From available experiment data and numerical simulations a stability parameter is derived which is based on the Hofland stability parameter. An extra term is added which accounts for the acceleration and which is comparable to the Dessens (2004) approach. Since the formula by Hofland was not intended for

waves, this might also hold for this formula. The formula reads:

$$\Psi_{RS} = \frac{\left(\max\left[\left\langle \bar{u} + \alpha\sqrt{k}\right\rangle_{L_m}\frac{L_m}{z}\right]^2\right) + C_{m:b}\left(\bar{u}\frac{\partial \bar{u}}{\partial x}\right)_{h_a} d}{K(\beta)\cdot\Delta g d} \tag{Ste14}$$

in which:

Ψ_{RS}	Steenstra stability parameter [-]
$(\max\ldots)$	See the Hofland (2005) formula
z	Measurement level above the bed; $z = 0$ at the theoretical bed level [m]
α	Empirical turbulence magnification factor, fitted to a value of 3.75 [-]
$C_{m:b}$	Empirical coefficient for turbulence and acceleration, fitted to a value of 23.0 [-]
$(\ldots)_{h_a}$	Values and derivative taken at a level of $z = h_a$
h_a	The level above the bed where the advective acceleration should be measured, fitted to a value of $9.0 D_{n50}$ [m]
d	Stone diameter; from §2.4 and 3 in Steenstra (2014) it can be assumed that it is probably the D_{n50}-value [m]
$K(\beta)$	Correction factor for the bed slope [-] $K(\beta) = \begin{cases} \frac{\sin(\phi+\beta)}{\sin\phi} & \text{upward slope} \\ \frac{\sin(\phi-\beta)}{\sin\phi} & \text{downward slope} \end{cases}$
β	Angle of the bed slope in the direction of the flow [-]
ϕ	Angle of repose of the bed material [-]

Peters (2014b) During the course of this research Ruben Peters published his Master's thesis, in which the stability of individual stones in a rubble mound breakwater toe was investigated. He defined a critical moment, caused by the acting forces on a single stone, above which the stone will dislocate. It therefore gives a criterion of motion. The formula incorporates drag, lift, weight and shear forces, see figure 2.2. The shear force turned out to be negligible. Prediction of motion was found to be quite accurate and promising for further research. The formulae read:

$$\begin{aligned} M_A &= F_L \cdot o_{wl} - F_W \cdot o_{wl} + F_D \cdot o_d \\ F_L &= (p_{under} - p_{above}) \cdot D_{n50}^2 \\ F_W &= (\rho_s - \rho_w) \cdot D_{n50}^3 \cdot g \\ F_D &= \frac{1}{2} C_D \rho_w A_f u|u| \end{aligned} \tag{Pet14}$$

in which:

M_A Moment; motion if $M_B > 0$ [Nm]

F_L Lift force [N]

F_W Weight force (submerged) [N]

F_D Drag force [N]

o_{wl} Lever arm for lift and weight force [m]

o_d Lever arm for drag force [m]

p Pressure above/below stones in the top layer of the toe [Pa]

C_D Drag coefficient based on Hofland (2005), with a value of 0.23 [-]

A_f Frontal area of the stone, attacked by flow [m^2]

u Flow velocity at a level of $0.15D_{n50}$ above the toe bed, though estimated here as $0.9u_{\text{free flow}}$ [m/s]

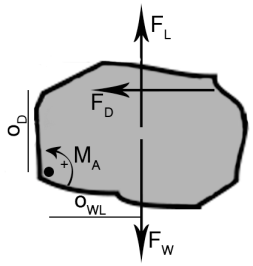

Figure 2.2: Forces acting on a stone. Flow velocity is from right to left.
Image courtesy of R.B.M. Peters

Overview and selection The formulae will now be tested against the requirements. This is done with use of table 2.1. We can see that already five of the ten formulae fulfil the strict requirements and two formulae can be used if a subjective threshold value is imposed. The Izbash formula was originally rejected since definition of flow velocity is unclear. However during evaluation in chapter 5 it was decided to use the formula as others appeared to perform not very well. Formulae by Shields and Sleath were regarded as inappropriate due to the use of a diagram, the correction factor K_v for non-uniform flow and the difficulty to measure shear stresses. The Rance and Warren formula is kept since it is also used in Baart (2008). Regarding turbulence it is dangerous to use a formula that requires a value for turbulence intensity k, since the current version of the IH-2VOF model can only calculate the instantaneous production. Besides turbulence, non-stationary flow by wave attack was not investigated either. Care must be taken to use this formula for the purpose of breakwater stability. Only the most recent formula will be tested for reference, i.e. the formula by Steenstra. A subjective threshold value should be chosen. The formula by Dessens is also retained since it is a simple formula which includes acceleration and which accounts for turbulence with a bulk coefficient.

The formula by Peters was also selected as it is state of the art and appeared to be quite promising. However two problems arose. First problem was the necessity of accurate stone dimensions to find moment lever arms and frontal area. Second and most important problem was necessity of pressures above and below the toe bed level in F_L. Peters' work was published only *after* the Ebbens cases (see chapter 5) were run in IH-2VOF and therefore it was not known that pressures calculated should be stored. Both problems were overcome by making assumptions and simplifications, which will be elaborated in section 5.3.

To conclude this section we will discuss which model output is required. Izbash requires flow velocities above the toe. It is decided to use velocities at $1.0D_{n50}$ above the toe, see section 5.3. The Rance and Warren formula requires a local period and orbital horizontal flow velocity, which can be derived from horizontal

Table 2.1: Overview of motion formulae properties

	Izbash	Shields	**Rance and Warren**	Sleath	Jongeling et al.	**Dessens**	Hofland	Hoan	**Steenstra**	**Peters**
Non-uniform flow (s)	✓	x	✓	✓	✓	✓	✓	✓	✓	✓
RANS-model applicability (s)	✓	x	✓	x	✓	✓	✓	x	✓	✓
Coarse material	✓	x	✓	x	x	✓	✓	✓	✓	✓
Threshold criterion	✓	✓	✓	✓	✓	✓	~	~	~	✓
Requires k	x	x	x	x	✓	x	✓	x	✓	x
Fulfils requirements	✓	x	✓	x	✓	✓	~	x	~	✓
Chosen after review	✓		✓			✓			✓	✓

(s) strict requirement, ✓ possible/available, x not possible/unavailable, ~ available with subjective limit

flow velocity records above the toe. They have to be measured at each grid cell border and at a couple of levels in vertical direction. The same holds for the Dessens formula, since the flow acceleration in space can be derived from multiple velocity measurements in space. The Steenstra formula requires u and k values measured over the full water column. It is therefore chosen to place u- and k-gauges at each vertical cell border over the full toe width. The gauges store the necessary time records at each water level. Output of the water level gauges is also retained. In section 5.2 configuration is explained in more detail.

2.3. HISTORICAL EXPERIMENT DATA

Both phase one and two in this research require appropriate datasets. These datasets can be found in historical experiments, as reported in appendix A. In this section it is described which datasets will be used and how they are composed. In Appendix C a full description of datasets used is given.

In phase one the IH-2VOF model will be validated regarding toe stability. Two researchers at Delft University of Technology have performed flume tests in which flow velocities and pressures are measured, namely Julia Nammuni-Krohn and Ruben Peters. The velocities and pressures measured can be compared with the results of the IH-2VOF model. The particularities of their datasets will now be described.

Julia Nammuni-Krohn (2009) performed flume tests to obtain the required data by which the hypothesis by Baart (2008) could be proven. For this she reconstructed the experiments by Gerding (1993). The main difference with his experiments is that she did not measure the amount of damage, but the flow velocities above the toe. This was done on several locations with mainly regular waves. A total of 80 test cases is investigated, of which 26 have irregular (JONSWAP) waves. Her research data are available at the Dutch 3TU.Datacentrum[1] and consists mainly of horizontal flow velocities. In fact she recorded flow velocities in all directions, but she did not review the other directions in her report. Therefore it is chosen to validate only the horizontal flow velocities with the IH-2VOF model.

Ruben Peters (2014) recently held flume tests dedicated to movement of single stones. For this he created a single breakwater layout in which all stones were glued together, except for a couple of stones at the toe. He recorded flow velocities above the toe and fluid pressure above and under the loose stones. Peters validated

[1] http://data.3tu.nl/

the IH-2VOF model on his test data in an additional thesis project, therefore his dataset will not be used for this Master's thesis. Section 4.5 provides a review of his work.

Phase two of this research requires datasets in which toe damage was recorded. This is done in the work by Gerding, Docters van Leeuwen, Ebbens, Van Gent and Van der Werf, Burcharth and Liu, and Sayao. Datasets of the latter two could not be obtained. The other four datasets will be discussed below.

E. Gerding (1993) presented a systematic way of describing damage and recorded this visually for a set of flume tests. He performed 171 different test cases with irregular waves. The data are presented in the report.

Linda Docters van Leeuwen (1996) validated the formula by Gerding for different stone densities. For this she recreated Gerding's flume layout to some extent. She also recorded damage visually. The data available is presented in her report. She states that 96 cases were performed, though in the dataset 98 different cases can be observed.

Reinder Ebbens (2009) performed tests in the flume of Delta Marine Consultants (BAM Infraconsult) with focus on very shallow water. 296 different test cases with irregular waves were constructed. His method of counting stones differs from previous work in the sense that damage was visually counted with help of a computer. The armour layer in his structure consists of Xbloc units, for which he gives a D_{n50}-value. Experiment data are given in the report appendices.

Marcel van Gent and Ivo van der Werf (2014) held tests in one of the small-scale Deltares flumes. Although they describe test set-up and parameter ranges in their paper, the final experiment data are not published. Experimental results of Van Gent and Van der Werf (2014) have been digitised from plotted data in their paper. The test conditions have been analysed backwards from these digitised data and from additional information in the paper. Only test conditions and test results that could be clearly identified by this procedure have been included. These are 122 of 192 tests conducted.

The experiment data for phase two were already gathered by Markus Muttray in 2014. He was so kind to make this combined dataset available for this thesis project. The test cases by Nammuni-Krohn have been appended to this database. A total of 767 test cases is obtained.

To be able to model these tests with the IH-2VOF model details of the structure are required. Often original reports do not give information on e.g. stone porosity, coefficients of the Forchheimer equation or detailed dimensions. This requires assumptions and approximations which might influence results, though it is expected that the trends will stay the same since fundamental processes are not influenced. The final structure details are given in appendix E.

Phase 1 – Evaluation of IH-2VOF

3

Running IH-2VOF

This chapter gives a description of the computational fluid dynamics model used in this research. Some basic information on the model configuration is provided. To discover best settings for simulation performance some convergence tests have been performed. Results are given in section 3.3. During testing some unexpected behaviour was observed. In section 3.4 the phenomena are analysed. At the same time it was discovered that the turbulence calculation of IH-2VOF does not work properly. Details on this matter are given in section 3.5.

3.1. Description of the model

The IH-2VOF model is a computational fluid dynamics (CFD) model. It has been developed by the Spanish Instituto de Hidráulica Ambiental "IH Cantabria" (Environmental Hydraulics Institute "IH Cantabria"). For a full description and mathematical formulation reference is made to IH Cantabria (2012) and Lara et al. (2011). The most important features are summarized here. The model:

- is two-dimensional, providing a 'side view' model of a flume;
- can simulate on model and prototype scale;
- solves the Reynolds-averaged Navier-Stokes (RANS) equations in the clear fluid region;
- uses the nonlinear k-ε turbulence model when required (Lin and P. L.-F. Liu, 1999) (see also section 3.5);
- accounts for porous media by applying volume averaging in porous regions, resulting in the volume-averaged RANS equations (P. L.-F. Liu et al., 1999). The additional terms due to volume averaging are closed using the extended Forchheimer equation (P. L.-F. Liu et al., 1999; Van Gent, 1995);
- calculates free surface by applying the Volume of Fluid (VOF) technique (Lin and P. L.-F. Liu, 1999);
- provides flow velocities, pressure, turbulence intensity and VOF-values at each grid cell;
- uses grid generator Coral to set up the geometry;
- is written in Fortran and C++ and has been compiled for Windows and Linux computers. It is distributed with a MATLAB-based graphical user interface (GUI) which makes pre- and post-processing very easy.

The department of Coastal Engineering at Delft University of Technology has adopted the IH-2VOF model due to its capability of simulating porous flow, excellent pre- and post-processing facilities, portability and reasonable pricing. It is valuable for modelling coastal structures since it can model wave overtopping, wave transmission and resultant forces on structures.

The model is built to run on a single computer. Often a large number of simulations is needed for research purposes and therefore the use of a computer cluster is useful. For this Master's thesis the computer rooms at the faculty of Civil Engineering of Delft University of Technology were used. Each computer could efficiently run three simulations simultaneously. A description of how the program can operate on a computer cluster is given in appendix I and J.

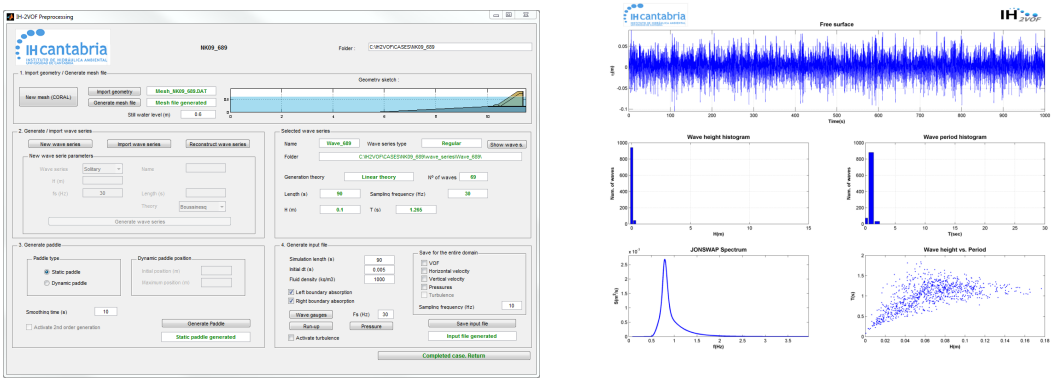

Figure 3.1: Arbitrary screenshots of the IH-2VOF GUI

3.2. CONFIGURATION

3.2.1. WORKFLOW

The workflow for a typical simulation is pictured in figure 3.2. Pre-processing starts by creating the geometry (water, air, solids and porous media) and the calculation grid (also called mesh) by using program Coral. Next the incoming waves are generated using the GUI, which is able to generate solitary, regular and irregular waves. Finally one can choose which output is stored, whether flume boundaries are absorptive and whether turbulence should be included. All input and output values are in SI units. Now the calculation process can start. Duration of calculation is dependent on structure modelled and computational power, but it quickly reaches hours or days with a nowadays desktop computer. See appendix E for some values. When calculation is finished the GUI enables quick data exploration by graphically showing the calculation results. With data-analysing software more detailed post-processing is possible.

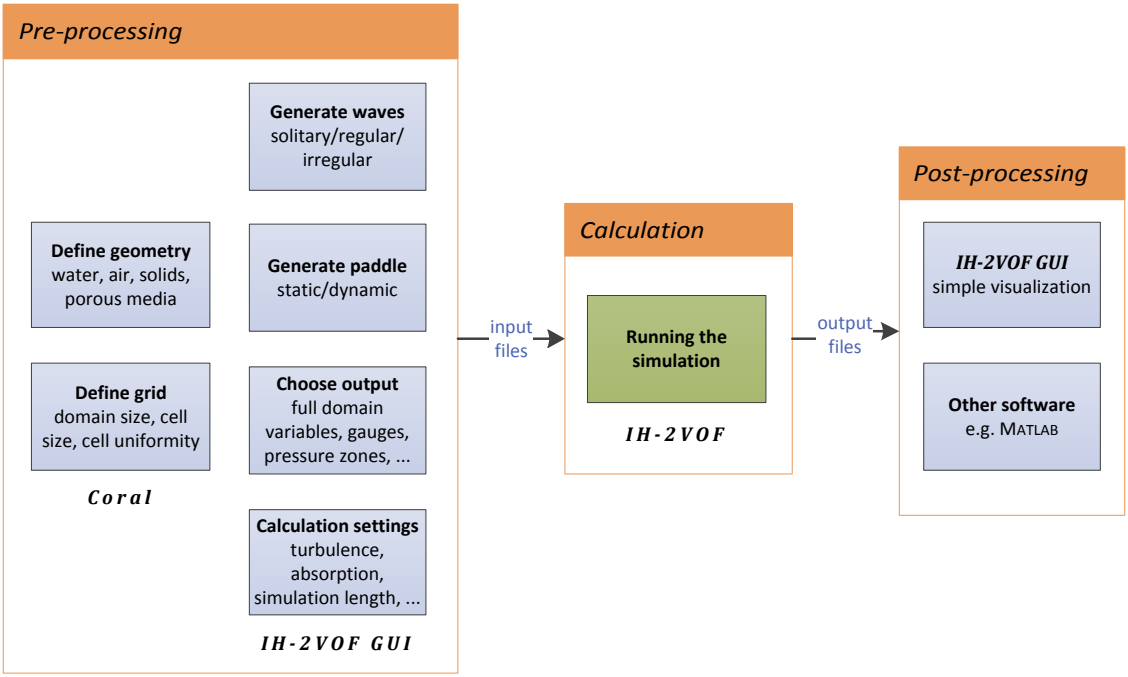

Figure 3.2: Workflow in IH-2VOF simulations

3.2.2. GRID PROPERTIES

Accuracy of a computational fluid dynamics model is dependent on the computational grid. The IH-2VOF model has a grid with rectangular elements. The IH-2VOF manual imposes a limit of $\Delta x/\Delta y < 2.5$ to avoid false breaking effects, see IH Cantabria (2012). Element orientation is along the horizontal x-axis and vertical y-axis. Origin of these axes is at the intersection between flume floor and wave generator, like shown in figure 3.3. Convergence tests are required to check when accuracy of the model is sufficient. Computational efficiency is investigated as well: a very dense grid is more accurate but implies a problematic computation duration. For this report three types of convergence tests have been performed: one on flume length in front of the structure, one on cell size in x-direction (their width, Δx) and one on cell size in y-direction (their height, Δy). Since a lot of issues were encountered during these convergence tests, they will be discussed in a separate section, see section 3.3 hereafter.

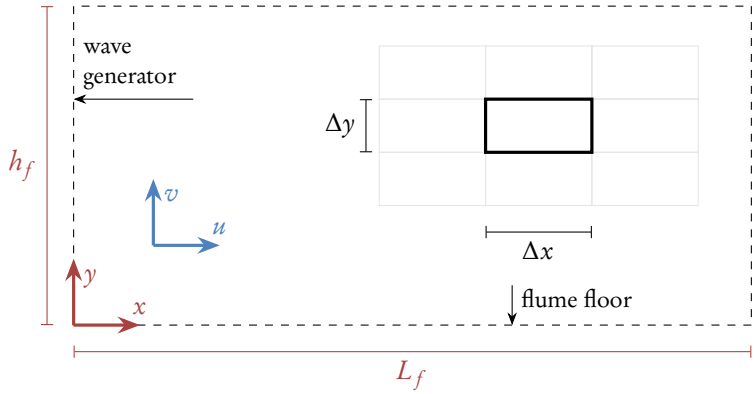

Figure 3.3: Defintions in the computational grid

With grid generator Coral one can create both a uniform and a non-uniform grid, in which cell dimensions are respectively constant or variable along the domain. This could be interesting to get a higher level of detail near the region of interest. In the IH-2VOF manual it is strongly advised to use uniform grids because of numerical errors in finite difference schemes. In the work by Arets (2013) this has been investigated. It appears that constructing a non-uniform grid in x-direction gives severe changes and errors in calculation. A non-uniform grid in y-direction has nearly no effect on accuracy, but it does not improve computation time. Based on these observations and recommendations it is chosen to use a uniform grid in both directions.

3.2.3. PROPERTIES OF POROUS MEDIA

The IH-2VOF model uses the extended Forchheimer equation to solve the volume-averaged RANS equations (P. L.-F. Liu et al., 1999). The Forchheimer equation has its basis in Darcy's law, by giving the relation between pressure gradient $\partial p/\partial x$ and a forcing due to turbulent flow through a porous medium. When non-stationary flow is present, the classical Forchheimer must be extended with an additional term: accelerating flow leads to the 'added mass phenomenon'. This can be explained by the fact that it takes more momentum to accelerate a volume of water in a porous medium than in unhindered flow. In Van Gent (1995, eq. 3.5 and 3.16) the extended Forchheimer equation is given as

$$I = au + bu|u| + c\frac{\partial u}{\partial t}$$

with coefficients

$$a = \alpha \frac{(1-n)^2}{n^3} \frac{\nu}{g D_{n50}^2}$$
$$b = \beta_c \left(1 + \frac{7.5}{\mathrm{KC}}\right) \frac{1-n}{n^3} \frac{1}{g D_{n50}}$$
$$c = \frac{1 + \gamma \frac{1-n}{n}}{ng}$$

Coefficient a belongs to the linear contribution of the shear stress (according to Darcy's law), b accounts for turbulence and convective transport and c is result of accelerating flow. The coefficients a, b and c are dimensional and contain dimensionless parameters α, β_c and γ. It can clearly be seen that the coefficients, and therefore the porous flow gradient, are largely determined by the porosity and the nominal stone diameter. The KC denotes the Keulegan-Carpenter number and is given as $\mathrm{KC} = \hat{u}T/nD_{n50}$. In literature following definitions are also found:

$$\beta = \beta_c \left(1 + \frac{7.5}{\mathrm{KC}}\right)$$
$$c_A = \gamma \frac{1-n}{n}$$

This leads to some confusion, as β is sometimes mixed up with β_c, and γ with c_A. By analysing the computer source code, the following can be found on how Forchheimer is implemented in IH-2VOF:

Parameter α is called the *linear friction coefficient* in grid generator Coral. This is correct and indeed the α value in the Forchheimer equation. Lara et al. (2011) advises to use $\alpha = 4409.22 \cdot D_{n50}^{0.43}$ (with $[D_{n50}] = m$) as an estimation when no calibration tests have been performed.

Parameter β_c is called the *non-linear friction coefficient* in Coral. In the IH-2VOF manual this is mixed up with β in equation 30: according to Van Gent (1995) one can use $\beta_c = 1.1$ as an estimation, though in the IH-2VOF manual and in Hsu et al. (2002) it is stated that $\beta = 1.1$ should be taken. In P. L.-F. Liu et al. (1999), on which the article of Hsu et al. (2002) is based, it is however correctly written that $\beta_c = 1.1$ ($\beta_c = \beta_p$ in the article). The IH-2VOF model calculates the KC number for each time step and grid cell, and converts β_c to β accordingly.

Parameter γ is called the *added mass coefficient* in Coral. This is incorrect since in literature this name is given to c_A. One should therefore simply fill in the advised value of $\gamma = 0.34$ in Coral. The IH-2VOF model subsequently adds the factor $(1-n)/n$.

In source code following calculations are performed in `MCoralFiles.F90`:

$$\texttt{xa(n)} : ga = \alpha \frac{(1-n)^2}{n^3} \frac{\nu}{D_{n50}^2}$$
$$\texttt{xxb(n)} : \frac{gb}{1 + \frac{7.5}{\mathrm{KC}}} = \beta_c \frac{1-n}{n^3} \frac{1}{D_{n50}}$$
$$\texttt{gc(n)} : gc = \frac{1 + \gamma \frac{1-n}{n}}{n}$$

with α, β_c, γ, n and D_{n50} given in the mesh file from Coral. Thereafter in both `IHC_deltadj.F90` and `CVTilde.cpp` the gb-value is obtained by multiplying `xxb(n)` with $1 + 7.5/\mathrm{KC}$.

Usually a and b coefficients for a specific material are determined experimentally. This was not done during the reviewed experiments on toe stability. The values are therefore estimated by using the recommendations described above:

$$\alpha = 4409.22 \cdot D_{n50}^{0.43} \text{ with } [D_{n50}] = m,\ \beta_c = 1.1 \text{ and } \gamma = 0.34 \tag{3.1}$$

3.2.4. Wave generation

The IH-2VOF GUI allows for easy wave generation. Users can choose amongst different wave types and wave generation methods. In this research regular (harmonic, using the linear wave theory) and irregular (using a JONSWAP spectrum) waves are used. The generation scripts make sure that a realistic record is obtained.

In Van den Heuvel (2013, appendix A) it has been investigated how many waves should be simulated to obtain a full irregular wave spectrum; fewer waves imply a shorter simulation time and thus a reduction in computation time. It was found that a minimum of 1000 waves are required. This coincides with most of flume experiments conducted. When investigating processes like overtopping or forces on structures, extrema are important and a more developed spectrum with 1000 waves is necessary. However, the creators of the IH-2VOF model use only 300-500 waves when investigating flow velocities. This is sufficient when extrema are less important. It certainly reduces computation time.

For regular (harmonic) waves one can simply fill in the required wave height and period H and T. For irregular waves the value of H_{m0}, T_p and the JONSWAP γ-value should be given. The script then generates waves according to the spectrum. All parameters are target values at the wave generator. Simulation duration should also be filled in. When one wants to obtain n waves, one can use following approximations for the simulation duration:

$$t_{end} = n \cdot T \qquad \text{(regular waves)}$$
$$t_{end} \approx n \cdot 0.8 T_p \qquad \text{(irregular waves)}$$

In the IH-2VOF model two methods of wave generation are possible: one is by using a Dirichlet boundary condition ('static paddle'), the other by using a moving boundary ('dynamic paddle'). The latter produces waves as how they would be generated in a laboratory flume by simulating a moving paddle. It therefore requires a larger horizontal domain, which increases computation time. According to IH Cantabria (2012) and Van den Heuvel (2013) the static paddle generates the same waves as the dynamic paddle. It is therefore chosen to use the static paddle in this study.

3.3. Convergence tests

Convergence tests were performed to obtain sufficient simulation accuracy at a not too high cost of computation time. In this section these convergence tests are described in detail since outcome is important for modelling. Observations made during testing led to additional tests, which gave essential information on how the model should be used later on. The convergence tests were made together with Ruben Peters, see Peters (2014a). His findings and methodology are almost identical to these hereafter.

As mentioned earlier before three convergence tests have been performed: one on flume length, one on cell width and one on cell height. The outcome of each test has been implemented in the next one. This might lead to some conservative values, since more efficient combinations of grid properties might exist outside these limits. In other words: some cell size ratios within the limit of $\Delta x/\Delta y < 2.5$ have not been considered. Due to time restrictions this was not investigated further; the method used gave sufficient accuracy and workable computation durations.

Test set-up is based on Nammuni-Krohn experiment NK09-R016-L, see appendix E. This case was chosen based on high influence of bottom friction (low water level), high chance of breaking (high steepness with low water level) and low wave height. This results in smallest Δx and Δy. In appendix D the full test set-up is described in more detail. Focus was put on peak values of the horizontal flow velocities, since the u values will be compared with data from the Nammuni-Krohn tests. Verification of convergence is done in a similar fashion for all tests. In short the following steps were taken:

1. Get the horizontal velocity record at each wave gauge, over the full vertical and for each case.

2. Shift the time domain so that velocity records coincide for different flume lengths.

3. Find the maximal difference in peak velocity after a certain spin-up time.

4. Use this maximal difference to calculate a relative error in the following way:

$$\text{rel.error} = \left| \frac{\text{max. difference}}{\max\left\{\text{peakvalue}_{reference}, \text{peakvalue}_{current}\right\}} \right|$$

5. Take the mean relative error over the wave gauge and subsequently the mean over the full flume.

It would be interesting to have errors less than 5%, since this is the typical accuracy of laboratory wave gauges and velocity measurement devices. Appendix D contains a detailed description of step 1 to 3.

Flume length convergence tests In the IH-2VOF manual it was advised to extend the flume (horizontal domain) with at least 0.5 times the governing wave length, at both sides of the structure. This has been tested with values of 0.5, 1.0, 1.5, 2.0, 2.5, 3.0, 3.5 and 4.0 times $L_0 = 2.08$ m of 'free' flume in front of the foreshore. The structure itself has not been changed, nor wave parameters. After running the cases horizontal flow velocities have been compared against the case with the longest flume. This is the reference case as it is expected to have the most accurate solution.

In figure 3.4 a flume has been sketched. At each common gauge position the mean relative error over this gauge has been plotted for the different flume lengths. The figure shows that with $0.5 - 2.0L_0$ the relative error varies quite a lot over the flume. Near the toe errors fluctuate a lot due to wave breaking processes. It seems that convergence is present since the errors diminish with longer flumes. When observing the relative error for each case separately, we can observe a zigzag pattern over the gauges. This zigzag pattern becomes regular starting from the $2.0L_0$-case.

When we average relative errors over the gauges, we obtain figure 3.5b. The relative error diminishes linearly. With convergence the error should approach a horizontal asymptote at zero like in figure 3.5a, but this is clearly not the case. Convergence is thus not perceivable. One could argue that with $4.0L_0$ the relative error would probably be zero, which would be ideal. This is not true, since we are comparing with a reference case for which it is not proven that it contains correct (converged) results; we cannot be sure that with $4.5L_0$ flow velocities would be the same as with $4.0L_0$. To illustrate this, imagine taking $2.5L_0$ as reference case and assessing only shorter flume lengths[1]. The ideal case would then seem to be $2.5L_0$ as it would have a relative error of zero.

In the next section the linear pattern will be analysed and it will be proven that convergence is indeed not present. Still a choice must be made on what flume extension in front of the breakwater should be. A low value is preferable as it reduces the computational domain and thus the computation duration. The criterion chosen is the stability of the fluctuating relative error pattern (the zigzag pattern) in figure 3.4. Starting from $2.0L_0$ the pattern fluctuates regularly around its mean value, in range of x from 0 m to 4.5 m. It is therefore advised to extend the flume with $2.0L_0$ in front of the structure. The relative error is expected to be less than 10%, although this cannot be verified completely.

Cell width convergence tests In Van den Bos et al. (2014) it was advised to use about 150 grid cells per wave length. This has been tested with values for $L_0/\Delta x$ of approximately 50, 100, 150, 200 and 250. The 250-case has the smallest grid cells and is the reference case. The flume length determined in the previous paragraph has been implemented. Due to rounding the flume lengths have been extended at the back of the breakwater for some cases. This has no influence at all on flow pattern in front of the breakwater since the back of the breakwater is an impermeable plate.

The averaged relative errors per gauge are plotted in figure 3.6. Diminishing relative errors for smaller cells can be seen over all gauges. The case with $L_0/\Delta x = 50.7$ show large deviations. This can be result of false breaking since this case has $\Delta x/\Delta y = 4.1 > 2.5$. In figure 3.7 we can clearly observe convergence, in contrary with the convergence tests for flume length. Starting from $L_0/\Delta x = 104$ the calculations appear to stabilize with an error of less than 10% compared with the reference case.

[1] In fact this was the first set-up of the convergence tests. Based on the expectations of non-convergence it was chosen to run additional tests with flume extensions up to $4.0L_0$, to verify whether this was indeed the case.

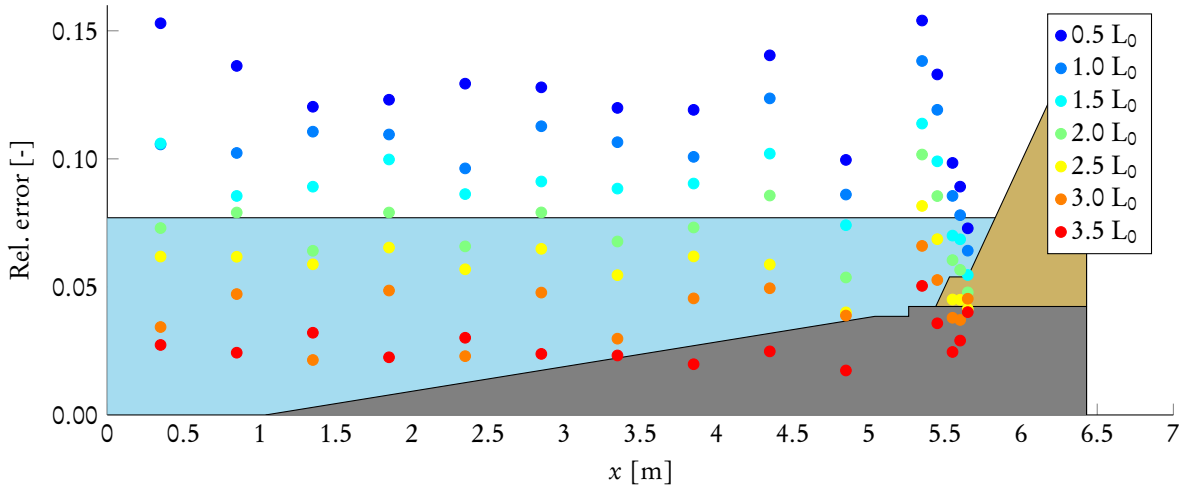

Figure 3.4: Mean relative error per gauge for different flume lengths

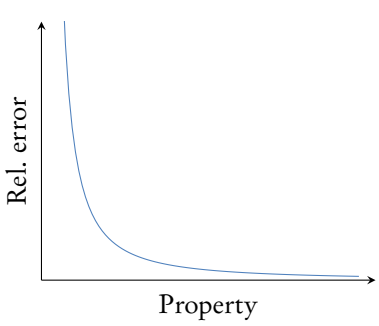

(a) Expected pattern for convergence

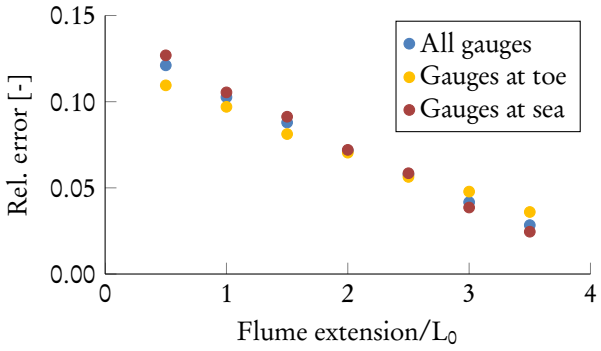

(b) Measured

Figure 3.5: Total relative error over all gauges for different flume lengths

Computation time increases with the number of grid cells. Based on these observations and computation durations it is advised to use a horizontal grid resolution of about $L_0/\Delta x = 150$. The error is about 5% compared with the reference case.

Cell height convergence tests Finally cell height convergence tests have been performed. The IH-2VOF manual gives a recommendation of 10 cells per wave height. In Van den Bos et al. (2014) it was found that cell height was not of big importance. Therefore cell height configurations with values for $H/\Delta y$ of about 5, 10, 15 and 20 have been tested. The 20-case has smallest grid cells and is the reference case. Flume length and cell width recommendations from previous paragraphs have been implemented, without having to change flume (domain) height.

Figure 3.8 shows diminishing relative errors with smaller cell heights. The $H/\Delta y = 5$-case is clearly unreliable as it has errors up to 40%. In figure 3.9 convergence is visible, although there are few data points. With the $H/\Delta y = 16.7$-case the relative error is less than 10% and differences between toe and 'sea' gauges are nearly gone. Unfortunately computation time increases rapidly with smaller Δy: the total number of cells increases with the number of cells in x-direction n_x for every step in n_y. Accuracy on the other hand is very important to get realistic results.

Based on observations and computation duration it is advised to use a vertical grid resolution of about $H/\Delta y = 15$. The error is about 5% compared with the reference case.

Summary Based on analysis of convergence tests the following conclusions are drawn:

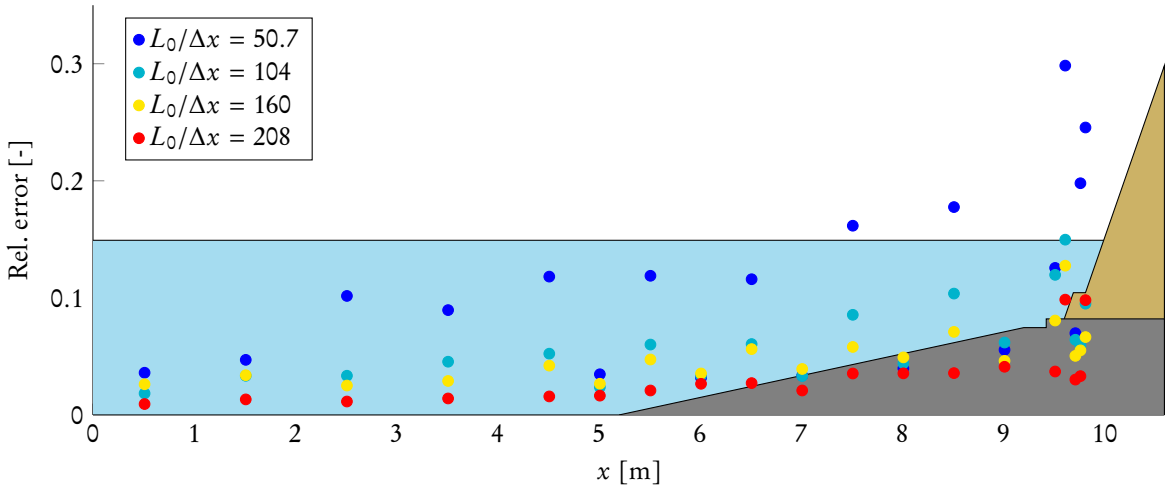

Figure 3.6: Mean relative error per gauge for different cell widths

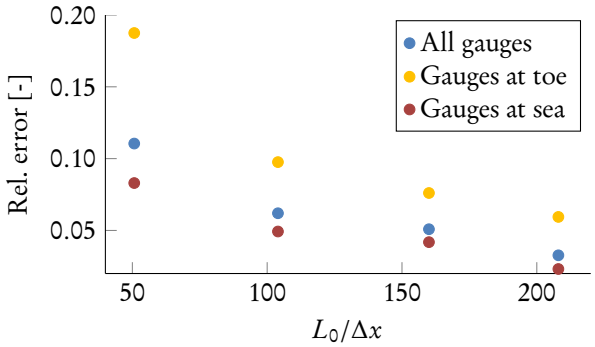

Figure 3.7: Mean relative error over all gauges for different cell widths

- A uniform grid should be used, based on advice in the IH-2VOF manual and the work by Arets (2013).
- The flume requires an extension of $2.0L_0$ in front of the breakwater structure. A longer flume does not increase accuracy, since other effects change the waves.
- A higher flume does not change computation time or accuracy, as long as the largest wave stays within the domain.
- A uniform grid density of $L_0/\Delta x \approx 150$ and $H/\Delta y \approx 15$ gives a good trade-off between accuracy and computation time.
- The cell size ratio is limited by the restriction $\Delta x/\Delta y < 2.5$. For some wave characteristics this will imply that more dense grids must be constructed than these given in the previous point. It is chosen to adapt the Δx-value to fulfil the demand. This results in less additional grid cells than when adapting Δy, which is beneficial for the computation time.

3.4. REFLECTION, FRICTION AND ABSORPTION ISSUES

During convergence tests on flume length it was discovered that total relative error decreases linearly with increasing flume length, see figure 3.5b. We also saw a typical zigzag pattern of the relative error over subsequent gauges, see figure 3.4, 3.6 and 3.8. In this section an effort is made to understand what causes these phenomena and whether they are of influence on succeeding research steps.

A couple of possible explanations – in fact hypotheses – are investigated. In short the following will be tested:

- Is there a substantial effect of wall friction, impacting wave energy?

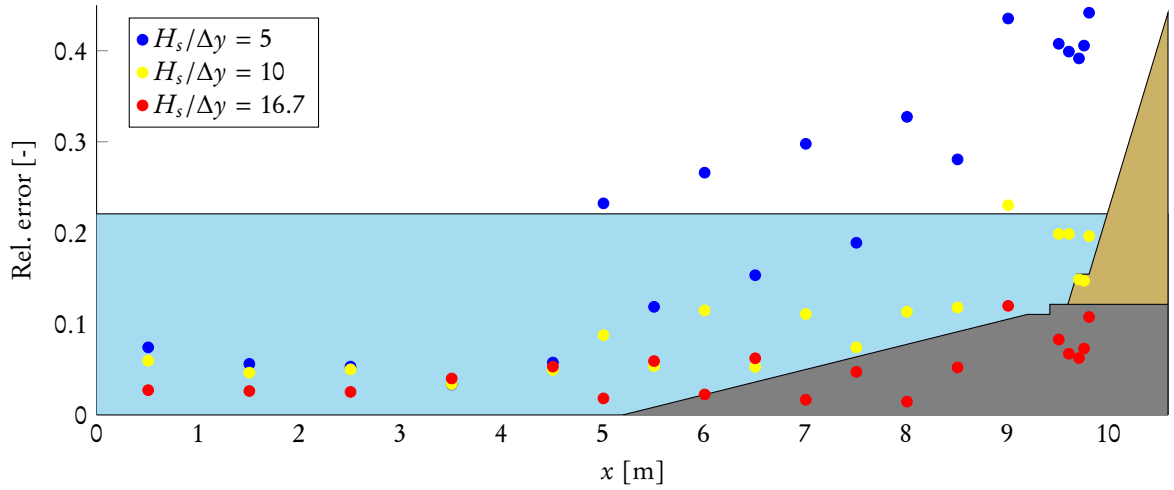

Figure 3.8: Mean relative error per gauge for different cell heights

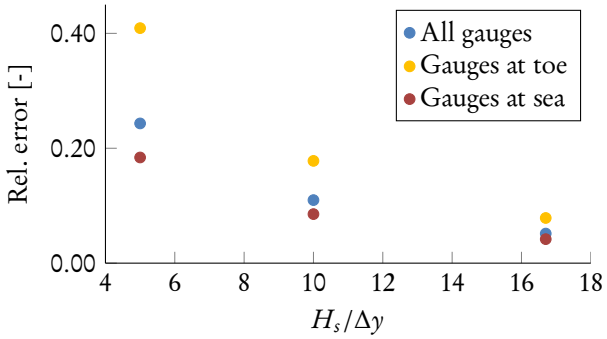

Figure 3.9: Mean relative error over all gauges for different cell heights

- To which extent does reflection create a standing wave pattern and what is the effect of this pattern? What influences the standing wave?
- What is the contribution of numerical diffusion in the IH-2VOF model?

3.4.1. WALL FRICTION

A first explanation for the linear trend was sought in wall friction. In the IH-2VOF model wall friction on a smooth surface is included and modelled with a Von Kármán logarithmic velocity profile (IH Cantabria, 2012, eq. 54). The hypothesis is the following:

> *A progressive wave in a flume is influenced by wall friction and will therefore loose energy over the flume. A longer flume will thus have smaller waves at the same gauge and convergence will not occur since different waves are measured.*

Figure 3.10 shows the principle. The hypothesis will be verified by some basic checks. No in-depth study is made since it is far beyond the scope of this Master's thesis.

First it has been verified whether flow velocities diminish indeed with increasing flume length. In figure 3.11 an example of two subsequent positive peaks in a velocity record is plotted. We see peak velocity values for different flume lengths. Velocity decreases with longer flumes, except for the $3.5L_0$-case. The same trend is observed at other measurement positions in front of the breakwater and at other depth levels. This agrees with the decreasing relative error.

Additional model tests have been performed to investigate whether floor friction is the cause of the lower velocities. For this a flume without structure was modelled with different flume lengths L_f. The hydraulic conditions of NK09-R016-L were implemented with absorptive boundaries at both flume ends. Multiple wave gauges were positioned with equal distance from the right boundary (i.e. the boundary at $x = L_f$). Flume

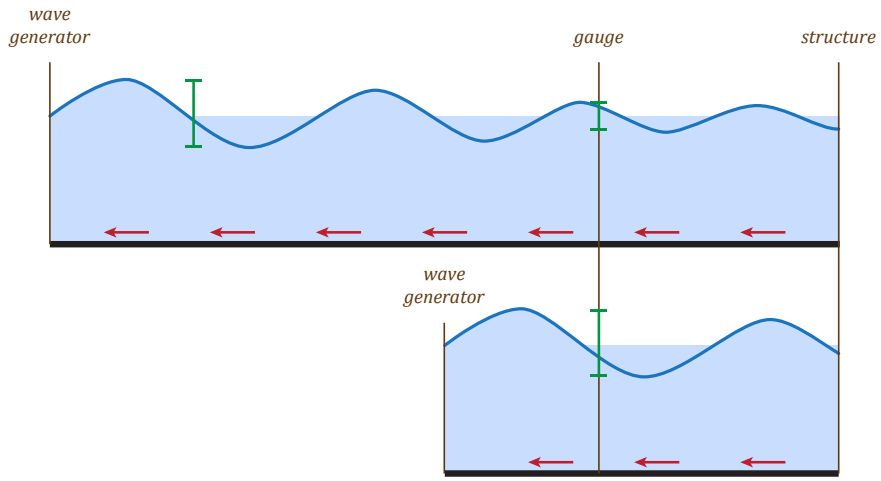

Figure 3.10: Principle of flume floor friction

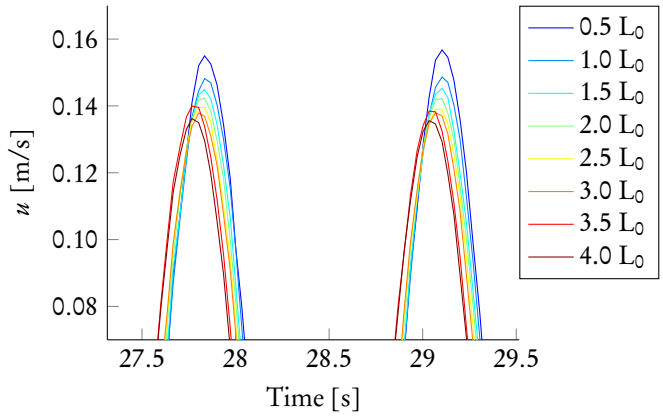

Figure 3.11: Measured velocity peaks at leftmost gauge and $y = 0.2$ m. Velocity data are time-shifted gauge data.

lengths of 1.5 to 4.0 times L_0 were tested. After calculation the *surface elevation* was read at the gauge positions. The mean peak value after spin-up time was taken as envelope value. Note the use of surface elevation η instead of flow velocities. This was done since it was easier to measure and since flow velocity is coupled to surface elevation.

If friction would be present, one would expect that 1) the envelope value decreases with increasing x-position (further away from the wave generator) for the same flume length, and 2) the envelope value at a certain gauge decreases for longer flume lengths. In figure 3.12a these principles are sketched. The simulated values are plotted in figure 3.12b and 3.12c (they have been split up in two figures for readability). It is clear that observations 1) and 2) cannot be made: the envelope values vary seemingly arbitrarily over the different positions. Wall friction does not seem to impact waves to a large extent. An interesting observation however is the zigzag pattern of the dot groups around a certain mean value, in a similar way as in figure 3.4.

A final check is made using velocity data over the full domain. At two depth levels the envelope of velocity data was composed for each flume length. Values are shown in figure 3.13; for readability only the positive envelope is given. Here also some decrease of the velocity can be seen, though withouth a regular pattern. The differences are less than 5%. In the figure an additional observation can be made, namely that the absorptive boundaries seem not to be working efficiently: a standing wave pattern can be seen with a clear node on the right boundary. This coincides with the zigzag pattern observed in 3.12. With perfect absorption a flat

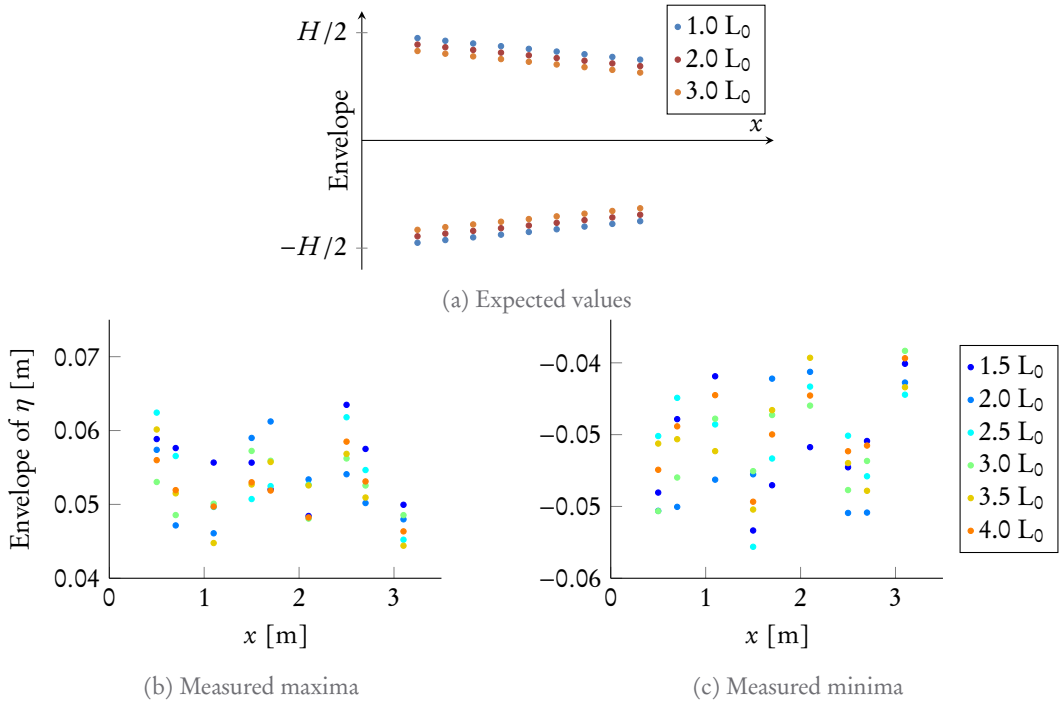

(a) Expected values

(b) Measured maxima

(c) Measured minima

Figure 3.12: Envelope values of η over the flume. Waves propagate to the right.

envelope should be found. This phenomenon will be discussed later.

The basic checks on wall friction give verification nor disproof of the hypothesis. It seems that friction does not influence the waves to a large extent; presumably it is only of interest for much longer flumes.

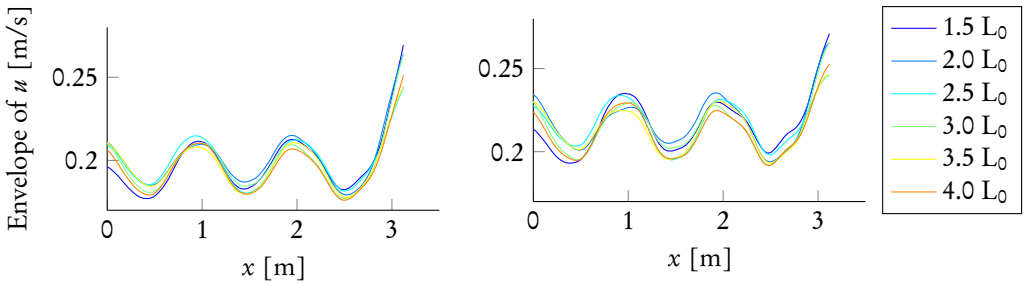

(a) $y = 0.20m$

(b) $y = 0.25m$

Figure 3.13: Full positive velocity envelope of u over the flume

3.4.2. Reflection and standing waves

In the previous paragraphs and figures often a zigzag pattern was observed in the relative error and the wave envelope was sinusoidal. This pattern is certainly result of reflection, as will be proven in the following paragraphs. First we have to check whether reflection indeed exists and what its order of magnitude is. Next some mathematics on standing waves will be given. With this we can give an explanation for the zigzag pattern. Finally we will try to find an explanation for the linear decrease in relative error.

Verification of reflection Progressive waves reflect on a breakwater. A lot of research has been carried out to quantify the amount of reflection, see e.g. Zanuttigh and Van der Meer (2007). Reflection is quantified using reflection coefficient K_r defined as reflected wave height divided by incoming wave height. Typical values

of K_r for rubble mound breakwaters are between 0.1 and 0.7, so it is a process which should certainly be investigated.

To verify the magnitude of reflection in the convergence tests, the surface elevation records at the three gauges in front of the foreshore have been decomposed in an incoming and reflected wave using the method by Zelt and Skjelbreia (1992). Variance density spectra and zeroth order moments of both components have been derived using Brodtkorb et al. (2000). The reflection coefficient is then $K_r = \sqrt{m_{0,r}/m_{0,i}}$ (Goda, 2010). Its value can be compared with the value measured by Nammuni-Krohn and with the value from the prediction formula in Zanuttigh and Van der Meer (2007). Nammuni-Krohn also used decomposition by Zelt and Skjelbreia (1992) and incoming and reflected wave energy based on wave spectra. The formula in Zanuttigh and Van der Meer (2007) is an empirical formula intended for irregular waves and can therefore also deviate slightly; bandwidth of the fit is in the order of 0.1.

In table 3.1 the values are presented. It appears that reflection in model and flume is equal. The prediction formula gives a slightly lower value. Without any further analysis we can conclude that a considerable amount of reflection is present.

Table 3.1: Measured and estimated reflection coefficients for case NK09-R016-L

	IH-2VOF	**Nammuni-Krohn (2009)**	**Zanuttigh and Van der Meer (2007)**
K_r	0.358	0.360	0.329 ± 0.05

Mathematics of a standing wave Reflection creates a standing wave, for an extensive description reference is made to Holthuijsen (2007, §7.3.6). When the incoming wave is not reflected entirely (i.e. when $K_r < 1$) a partially standing wave is created. This is typical for a rubble mound breakwater.

It is useful to give a simple model for the reflection pattern. Since orbital velocity is related to the surface elevation, we will model surface elevation η for simplicity. The story for velocity goes completely analogously. In Holthuijsen (2007, §7.3.6) a mathematical formulation for a partially standing wave is given, composed of an incoming propagating wave with amplitude a_i and a reflected wave – propagating backwards – with amplitude a_r. The amplitudes are related through the reflection coefficient: $a_r = K_r a_i$. The domain is a flume with length L_f with an open boundary at $x = 0$ and a partially reflective boundary at $x = L_f$. The formula for surface elevation now reads:

$$\eta(x,t) = a_i \sin(\omega t - kx) + a_r \sin(\omega t + kx) \tag{3.2}$$

with $\omega = 2\pi/T$ and $k = 2\pi/L$. This equation holds for a situation in which flume length L_f is an exact multiplication of wave length L. In other situations there will be a phase shift for the reflected wave: it takes $\frac{L_f}{c} = \frac{L_f}{L}T$ before the first incoming wave reaches the reflective boundary. The reflected wave will start under the following conditions:

$$\begin{aligned}\eta_r(x,t) &= a_r \sin\left(\omega\left(t - \frac{L_f}{L}T\right) + k(x - L_f)\right)\\ &= a_r \sin(\omega t + kx - 2kL_f)\end{aligned}$$

The phase difference is therefore $\varphi_L = 2kL_f$. Equation (3.2) thus becomes:

$$\eta(x,t) = a_i \sin(\omega t - kx) + a_r \sin(\omega t + kx - \varphi_L) \tag{3.3}$$

In figure 3.14 we can see the effect of phase difference for an arbitrary wave. Surface elevation is plotted over flume length at an arbitrary point in time. Note the position of reflected wave peaks (yellow) in respect to incoming wave peaks (green). It is also interesting to have a look at the envelope, since it takes away time-dependence of the gauge record. The envelope shows the maximum and minimum value that η can have at each x-position. If the envelope of the maxima would be denoted as $m_\eta(x)$ then it can be calculated as $m_\eta(x) = \max_t\{\eta(x,t)\}$. An example of such an envelope can be found in figure 3.15. Note the anti-node at the reflective boundary on the right.

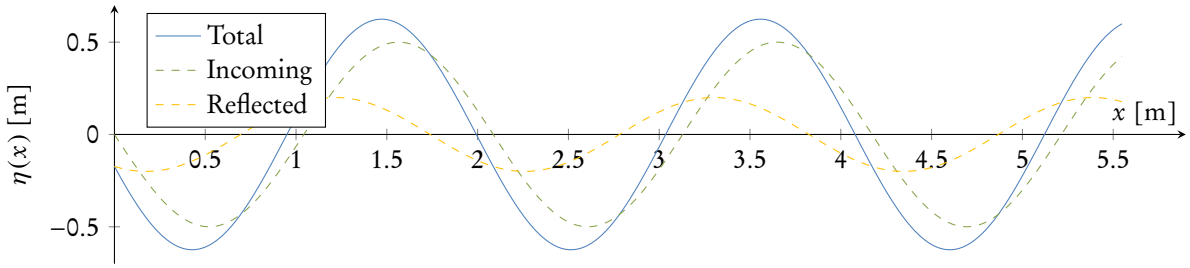

(a) $L_f = 2L \cdot 1$, $\varphi_L = 8\pi$

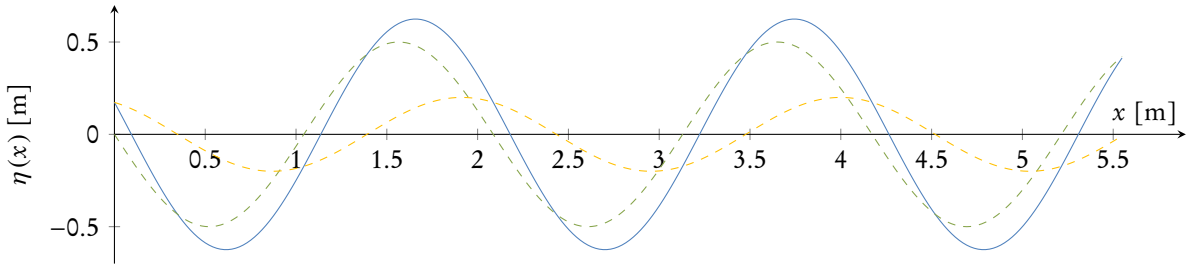

(b) $L_f = 2L \cdot 4/3$, $\varphi_L = 10\frac{2}{3}\pi$

Figure 3.14: Flume view of a partially standing wave, with different phases

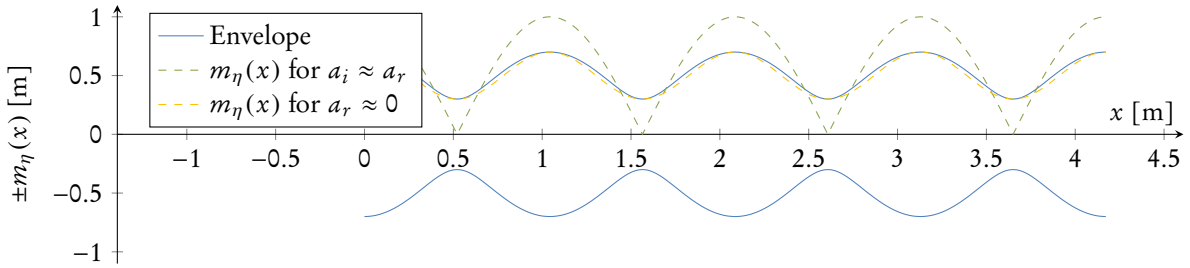

Figure 3.15: Envelope of a partially standing wave ($L_f = 2L_0$)

The phase shift due to a change in flume length does not lead to a phase shift in the envelope. This can be verified by finding an analytical description of the envelope. Curve fitting has been used to find the functions. There seem to be two limit states, one for $a_r \approx 0$ and one for $a_r \approx a_i$ (see the dashed lines in figure 3.15). A transitional function could not be obtained within the time available. The limit functions are:

$$m_\eta(x) = \begin{cases} \left|2a_i \cos\left(kx - \frac{\varphi_L}{2}\right)\right| & \text{if } a_r = a_i \\ a_i + a_r \cos(2kx - \varphi_L) & \text{if } a_r \gtrsim 0 \\ a_i & \text{if } a_r = 0 \end{cases} \tag{3.4}$$

The function for $a_r \gtrsim 0$ seems to represent the envelope quite well for values of K_r up to 0.6. Let us now verify whether the change in flume length always imposes an anti-node at the reflective boundary:

$$m_{\eta,(a_r=a_i)}(L_f) = \left|2a_i \cos\left(kL_f - \frac{2kL_f}{2}\right)\right| = 2a_i$$
$$m_{\eta,(a_r\gtrsim 0)}(L_f) = a_i + a_r \cos(2kL_f - 2kL_f) = a_i + a_r$$

So indeed there will always be an anti-node at the reflective boundary. The same can be proven for a change in wave length L.

The mathematical model can now be used to explain the observations in the convergence tests.

Zigzag pattern in the relative error In the plots of the relative error over the flume in figure 3.4, 3.6 and 3.8, a zigzag pattern was observed. The hypothesis is the following:

> *The zigzag pattern of the relative error is caused by standing wave pattern and specific inter-gauge distance.*

Since the velocity difference is divided by maximum velocity at that point, the value of the envelope is of importance. In figure 3.16 the velocity envelope is plotted with arbitrary values. The gauges have a spacing of 0.5 m $\approx L_0/4$ and are thus positioned (in the worst case scenario) at the nodes and anti-nodes of the envelope. Velocity difference is then divided by a very large and a very small velocity value, resulting in different relative errors although the difference Δu itself stays the same. In formulae:

$$\begin{aligned} u_{\text{max, A}} &< u_{\text{max, B}} \\ \frac{\Delta u}{u_{\text{max, A}}} &> \frac{\Delta u}{u_{\text{max, B}}} \\ \text{relerror}_{\text{A}} &> \text{relerror}_{\text{B}} \end{aligned}$$

The result is indeed a fluctuating pattern of the relative error. Note that the position of wave gauges within the envelope is extremely important. If all gauges would be positioned halfway between the nodes and anti-nodes the zigzag pattern would not be present.

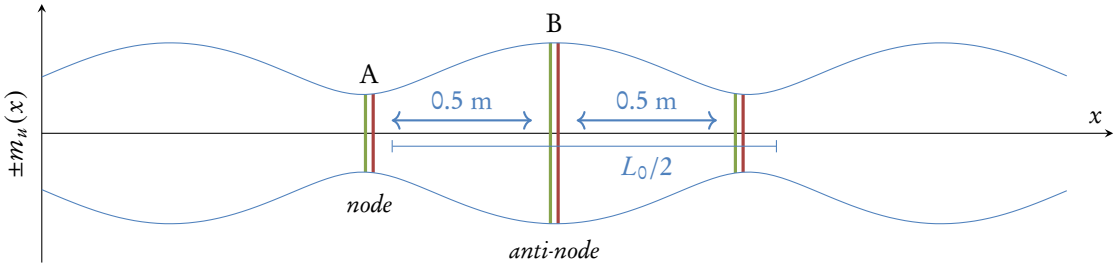

Figure 3.16: Gauge positions within the velocity envelope.
Red and green represent two different cases.

Impact of phase difference on velocities The envelope position is important when assessing measurements of hydraulic parameters. Therefore the following hypothesis is formulated:

> *Reflection creates a partial standing wave. Decrease of flow velocities, as found in figure 3.4 and 3.11, is result of different measurement positions within the envelope of this wave.*

For clarification of the hypothesis, two sets of wave gauges are plotted in figure 3.16 (coloured in green and red) for which it is clear that they will measure different maxima.

First we will discuss what generates a change in measurement position. We can start by excluding the possibility of *different gauge positions*: the structure itself is the same for all flume lengths and wave gauges are positioned relative to the structure. Differences due to rounding are not present, as the flume length is extended with an exact multitude of the cell width.

Perhaps *the structure itself* creates a change in position of the envelope: due to the complex shape of a breakwater, one should see the reflection point as a virtual 'wall' on the breakwater. Position of this reflection point is depending on breakwater layout, wave parameters and breakwater materials. Schoemaker and Thijsse (1949) observed this effect when measuring harmonic waves on an impermeable slope. Scheffer and Kohlhase (1986) investigated this analytically for irregular waves. Work by Büsching (2010) confirms this experimentally for slopes with hollow revetment elements. The latter two papers represent the change of the reflection point as a change in the phase difference of the reflected wave. This phase difference, caused by the structure properties, will now be called φ_S and must not be confused with φ_L, which was result of a change in flume length.

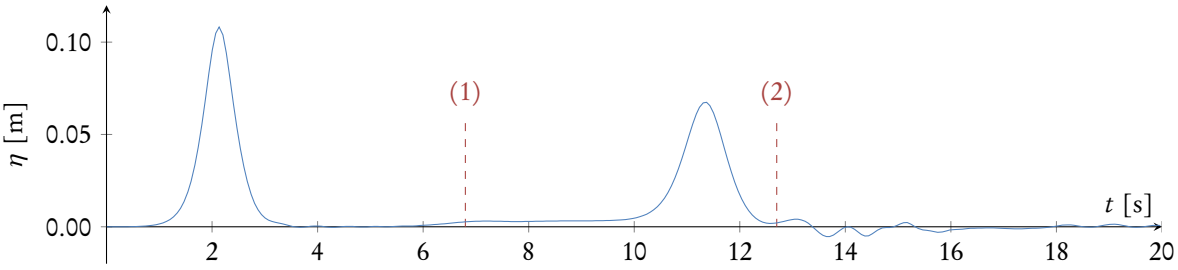

Figure 3.17: Wave record at gauge 1
(1) Reflection at breakwater, (2) reflection at wave generator

Table 3.2: Reflection coefficients K_r for a single wave in case NK09-R016-L

Gauge	x	Breakwater	Wave generator
1	1.00 m	0.62	0.08
2	5.11 m	0.65	0.10

Equation (3.3) and its envelope now becomes:

$$\eta(x,t) = a_i \sin(\omega t - kx) + a_r \sin(\omega t + kx - \varphi_L - \varphi_S) \tag{3.5}$$

$$m_\eta(x) = \begin{cases} \left|2a_i \cos\left(kx - \frac{\varphi_L+\varphi_S}{2}\right)\right| & \text{if } a_r = a_i \\ a_i + a_r \cos(2kx - \varphi_L - \varphi_S) & \text{if } a_r \gtrsim 0 \\ a_i & \text{if } a_r = 0 \end{cases} \tag{3.6}$$

In the mathematical description of the standing wave it was found that change of flume length (change in φ_L) does not change position of the anti-node. This is still the case in equation (3.6). To the contrary, it must be stressed that change in φ_S certainly might change position of the envelope with respect to the breakwater. This will be very important for the next research steps. For now we can conclude that since structure nor hydraulic parameters change in the different cases, phase difference φ_S will not change either. A change of measurement position within the envelope is therefore not obtained.

A final cause of changing measurement positions is sought in *wave reflection on the wave generator*. An incoming wave will first reflect on the breakwater and subsequently re-reflect on the wave generator. The IH-2VOF model applies absorption on this boundary, but it might be insufficient. Unfortunately the method by Zelt and Skjelbreia (1992) does not filter out higher harmonics and can therefore not be used to find the amount of reflection on the wave generator. A simple check is thus performed: the NK09-R016-L model is run again with a single (solitary) wave. The wave is generated by the IH-2VOF GUI and follows Boussinesq theory. The wave has a height of 0.1 meter and a duration of about 3 seconds. Two wave gauges have been placed in the model: one in front of the wave generator and one at the beginning of the foreshore. The wave record at the first gauge is shown in figure 3.17; the reflection coefficients in table 3.2. From the figure we can observe that wave absorption on the generator is not perfect: some spurious oscillations are present after $t = 13$ s. The table shows a rather high reflection coefficient of about 10% at the wave generator[1].

With this it is proven that re-reflected waves do exist. Even very small, they might lead to a change of the envelope. The effect of a re-reflected wave can be described mathematically as follows:

$$\eta(x,t) = a_i \sin(\omega t - kx) + a_r \sin(\omega t + kx - \varphi_L - \varphi_S) + a_{rr} \sin(\omega t - kx - \varphi_L - \varphi_S) \tag{3.7}$$

[1]Note that the reflection coefficient at the breakwater differs from the value for the original tests with regular waves (table 3.1). They should not be compared since hydraulic conditions are totally different. It was originally tried to make a simulation with a wave train of a couple of harmonic waves, but the GUI imposes some smoothing function over the boundary conditions. The result is that it takes some waves before the target wave height is reached. Too many waves are then present within the flume. From a physical point of view this is understandable, but for a reflection check it is undesirable.

Also here a phase shift could occur during the absorption process at the wave generator, but it has been neglected for convenience. From the analysis before, it is obvious that the third component, travelling with the same phase speed as the other wave components, will contribute to a change in envelope height. It is beyond the scope of this research to describe this analytically, therefore some numerical simulations with MATLAB have been performed. It appears that envelope magnitude is influenced by the relation between a_r, a_{rr} and L_f. When $L_f = n \cdot L$ (with $n = 1, 2, ...$) the envelope will always increase, in other situations the envelope can both increase and decrease. Also envelope phase is slightly shifted, though this is very limited.

We can thus conclude that the re-reflected wave on the wave generator causes significant changes in the envelope, in both magnitude and phase. The latter causes a change in measurement position.

Since a plausible cause for a change in measurement position has been found, it is analysed to which extent a change in envelope really exists. The envelope of the convergence test on flume length is plotted in figure 3.18. Positive peaks are marked with circles. The second envelope is taken at a deeper level, intersecting foreshore at $x = 5$ m. First observation is the clear and regular decrease of the envelope with larger flume lengths. The decrease goes with constant steps, agreeing with the linear decrease in relative error. A second observation is that peaks also present a very small phase shift with increasing flume length. The phenomena coincide very well with what was found for reflection on the wave generator.

Based on these observations we can finally review the hypothesis: it seems indeed that reflection on the wave generator causes a change in the envelope. The change is however more present in magnitude than in phase. Linear decrease in relative error is result of this decrease in envelope magnitude.

Observation of non-linear effects For completeness it must be mentioned that during calculations of the envelope non-linear effects have been observed. Gauge records of the surface elevation η show higher maxima than minima. In addition spectra at all wave gauges (see figure 3.19 for some examples) show additional peaks at higher harmonics of the wave period, i.e. at $2T^{-1} = 1.58$ Hz. These phenomena are caused by non-linear wave effects, as described in Holthuijsen (2007, §5.6). With $H/(gT^2) = 6.4 \cdot 10^{-3}$ and $d/(gT^2) = 2.5 \cdot 10^{-2}$ we can expect 2nd order non-linear Stokes waves according to figure 5.12 in the work cited. This kind of waves has a higher harmonic with $2\omega t$, which creates the second peak in the wave spectrum.

3.4.3. NUMERICAL DIFFUSION

The third hypothesis on linear decrease in relative error was on the contribution of numerical diffusion. The hypothesis is the following:

> *The IH-2VOF model uses finite difference schemes (IH Cantabria, 2012). Depending on the scheme some numerical diffusion may exist. This diffusion causes a loss of energy during numerical wave propagation and therefore an additional change in relative error.*

We already considered wall friction as a possible explanation for wave energy loss. With numerical diffusion the same effect would be obtained, i.e. that two different waves are measured and compared. According to dr.ir. Marcel Zijlema from Delft University of Technology numerical diffusion is only of importance for longer flumes. The hypothesis will therefore be left unproven.

Combination of wall friction, bad absorption on the wave generator and numerical diffusion will certainly contribute all together to reduction of wave energy and therefore to a decrease in relative error. No further research will be done on the reduction of relative error since some plausible causes have been found and since the error is probably less than 10%, which is acceptable.

3.4.4. SUMMARY

In this section an explanation for linear decrease in relative error was sought. Also the zigzag pattern of relative error over the gauges was analysed. Model case NK09-016-L was used. During analysis some interesting observations were made, which impose very important limitations on the model evaluation process. Here is a brief summary:

- Reflection on the breakwater creates a partially standing wave pattern.
- The zigzag pattern of relative error is caused by measuring at different positions within the standing wave envelope.

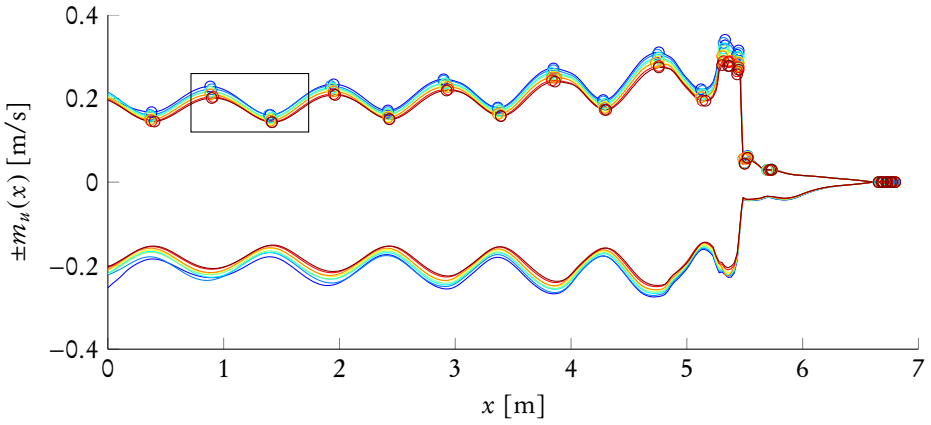

(a) $y = 0.25$ m

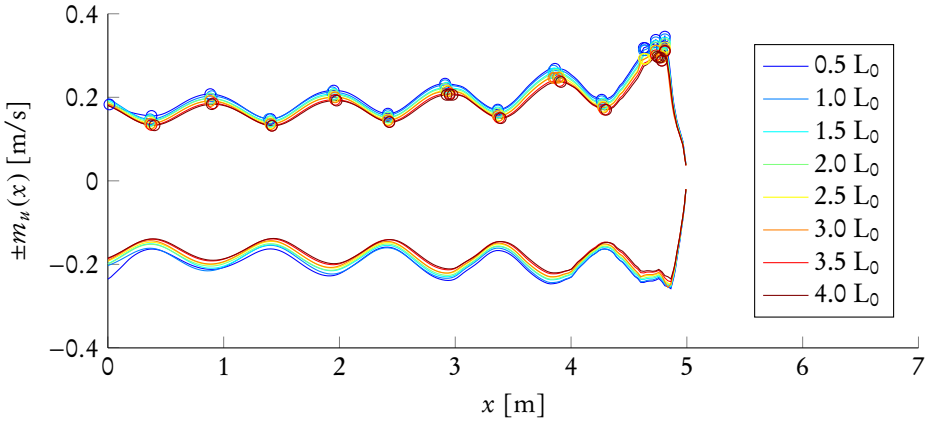

(b) $y = 0.20$ m

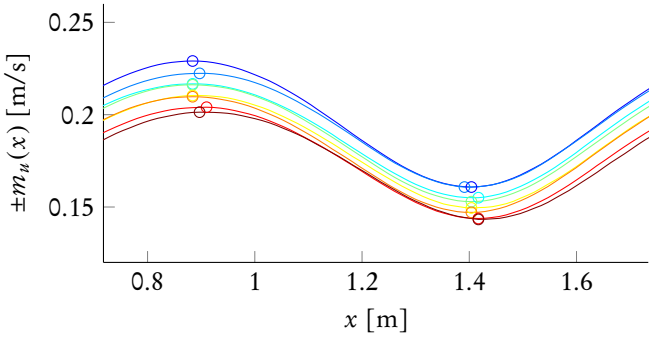

(c) Detailed version of the box in $y = 0.25$ m

Figure 3.18: Full envelope of u over the flume with positive extrema marked

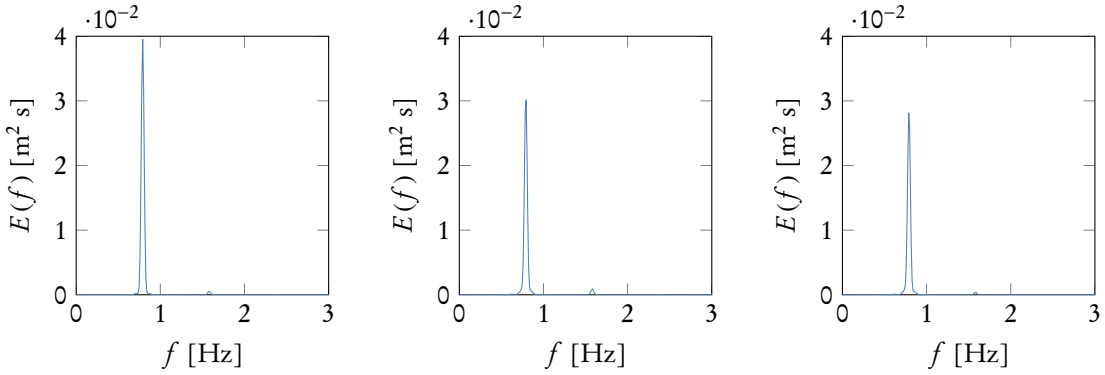

(a) $0.5L_0$ (b) $2.5L_0$ (c) $4.0L_0$

Figure 3.19: Variance density spectra for $\eta(t)$ at the beginning of the foreshore

- Linear decrease of relative error is caused by the effect of bad absorption on the wave generator boundary. It might also be caused, to a limited extent, by wall friction and numerical diffusion. Longer flumes will eventually result in smaller waves since less wave energy will be present and since less reflection on the wave generator is possible.
- Causes in the previous point will not affect the convergence tests on cell width and cell height as the standing wave pattern does not change in these tests.
- The position of the virtual reflection point of the breakwater, and with that the position of the envelope of the partially standing wave, is influenced by structure details. This is true both for regular and for irregular waves.
- The position of a wave gauge within the envelope is of major importance when comparing different tests. This applies to both numerical and physical tests. It imposes a severe limitation on the possibilities of quantitative evaluation.
- According to Holthuijsen (2007, §5.6) 2nd order non-linear Stokes waves should be present, which is confirmed by analysing gauge records and wave spectra.

In the chapter hereafter the model will be evaluated by comparing model results with physical measurements by Nammuni-Krohn. The conclusions above impose limitations on quantitative evaluation, which will be described in section 4.1.

3.5. Turbulence issues

The IH-2VOF model uses the k-ε model for turbulence. Without going too deep into this matter, one can simply state that turbulence is the governing process determining the flow pattern in non-laminar flow. Especially in and near porous media turbulence plays an important role. Turbulence and flow velocities influence each other mutually. During the course of this research it was discovered that turbulence calculation in IH-2VOF did not function properly. This section shortly discusses the flaws discovered and the implications for this research.

Let us start by presenting the RANS equations for the clear fluid domain:

$$\frac{\partial \overline{u_i}}{\partial t} + \bar{u}_j \frac{\partial \overline{u_i}}{\partial x_j} = -\frac{1}{\rho}\frac{\partial \overline{p}}{\partial x_i} + g_i + \frac{1}{\rho}\frac{\partial \overline{\tau_{ij}}}{\partial x_j} - \frac{\partial \left(\overline{u_i' u_j'}\right)}{\partial x_j}$$

Herein contains $\overline{\tau_{ij}}$ the molecular viscosity. The final term is result of Reynolds averaging, leading to the so-called Reynolds stress tensor $\overline{u_i' u_j'}$. It is this term which is defined by the k-ε model as:

$$\overline{u_i' u_j'} = \frac{2}{3}k\delta_{ij} - C_d\frac{k^2}{\varepsilon}(\ldots) - \frac{k^3}{\varepsilon^2}(\ldots)$$

One can find the eddy (turbulent) viscosity as $\nu_t = C_d k^2/\varepsilon$. In porous media the Forchheimer relation is added, for which the k-ε model should be volume-averaged. Complete equations can be found in the IH-2VOF manual (IH Cantabria, 2012).

In IH-2VOF the principal calculation cycle goes as shown in figure 3.20. Each time step the previously calculated viscosity (composed from molecular and eddy viscosity) is used to determine velocities. Together with newly found pressures the Reynolds stress tensor is calculated. Also a small amount of turbulence is produced as a random disturbance. From stress tensor and additional turbulence the values for k, ε and ν_t are derived. Together with the stress tensor by kinematic viscosity everything is then available to obtain velocities in the subsequent time step.

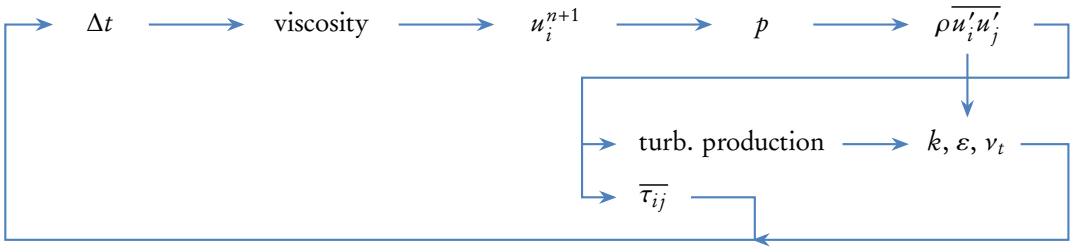

Figure 3.20: Desired turbulence calculation in IH-2VOF

Now when the IH-2VOF model is configured to use the k-ε model, the input files (see figure 3.2) contain a certain setting representing the k-ε model. The IH-2VOF program itself uses an internal flag which should be based on the input file setting, but this very flag is set *before* the input file is read. It results in an interruption of the turbulence calculation loop, see figure 3.21. Velocities are then influenced by the molecular viscosity only.

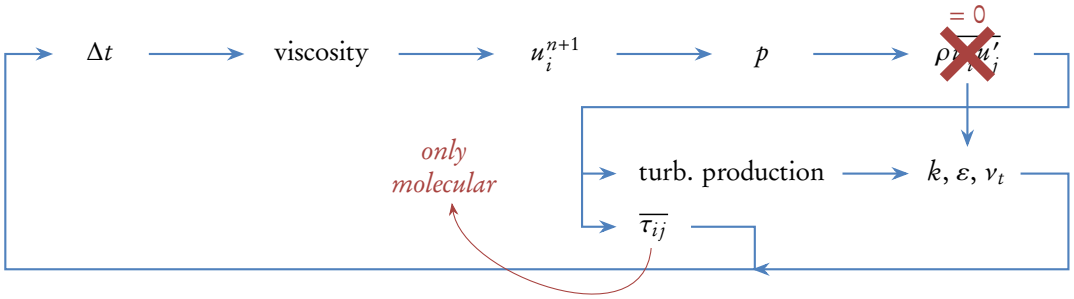

Figure 3.21: True implementation of turbulence calculation in IH-2VOF

Efforts to repair this programmatic flaw resulted in yet even more errors, stating that the "Linear Eddy Visc turbulence model is not yet implemented". Manual nor GUI contain any clue that the k-ε model is not working properly. Only by analysing the code or by comparing measured velocities one can come to this conclusion. No time is available for any other repair trials or to wait for a fix by IH Cantabria.

> *Together with the graduation committee it has been decided to accept this shortcoming and continue research without turbulence modelling. The assumption made is that turbulence has a negligible effect on hydraulic conditions near the toe structure. We cannot verify whether this assumption is valid and therefore great care must be taken when using results of this report in further work or for design purposes.*

4

Evaluating IH-2VOF

This chapter contains the evaluation of the IH-2VOF model. Evaluation is done by simulating the Nammuni-Krohn (2009) tests with the model and comparing flow velocities and surface elevations measured with focus on extrema.

The tests by Nammuni-Krohn (2009) (in short NK09) consists of 54 cases with regular waves and 26 with irregular (JONSWAP) waves. All cases are simulated with the IH-2VOF model. The recommendations on grid properties in section 3.3 are applied. No turbulence calculation was performed. In appendix E the implemented model layout and configuration is shown. Required grid files are automatically generated using scripting language PHP[1]. Generation of cases in the IH-2VOF GUI was automated by using the program SikuliX[2]. Simulations were run on computers of Delft University of Technology, see appendix E for details on the simulations.

This chapter will start by analysing possibilities and restrictions for comparison of physical and numerical measurements. It forms basis of criteria on which the NK09 tests can be evaluated. Before evaluation results are presented some clarification on evaluation calculations is given. In addition to the NK09 evaluation also evaluation results of the Peters (2014a) tests are reviewed. Finally conclusions on usability of the IH-2VOF model will be drawn.

4.1. Possibilities and restrictions

The evaluation of the NK09 tests is limited by some major restrictions. It is essential to mention them so that the remaining evaluation possibilities are found. In section 3.4 impact of wave reflection was discussed. The conclusions form basis of the topics in this section. Thereafter some important remarks on the NK09 dataset will be given.

Change in envelope position The standing wave pattern, formed by wave reflection on the breakwater under regular waves, is characterized by its envelope. Envelope position, i.e. its phase, depends on reflection properties and might differ between physical and numerical tests. It was proven that it also might be the case with irregular waves. Therefore one should be careful when comparing two corresponding gauges: in the worst case scenario one gauge would be measuring at a node and the other at an anti-node. The flow velocities change accordingly.

The true error can be estimated with linear wave theory if the position of the envelope would be known. This requires surface elevation gauges in deep water, which are not present in the NK09 dataset (see further). For that reason only the maximal error range can be given. Depending on the difference between node and anti-node and depending on the phase difference between physical and numerical test, a difference in maximal flow velocity may be present.

Note that for brevity and to avoid confusion this error and its estimation will now be addressed as *the phase shift velocity error*.

[1] `http://php.net/`
[2] `http://www.sikuli.org/` and `http://www.sikulix.com/`

2nd order Stokes waves It was discovered that 2nd order non-linear Stokes waves are present in the NK09 tests. Figure 4.1 shows to which wave theory all NK09 cases belong according to Holthuijsen (2007, §5.6). We can even expect 3th order Stokes waves and cnoidal waves due to the relative shallow water. If the IH-2VOF model performs well, no difference should be present between physical and numerical waves: the wave shape should be the same. On the other hand use of linear wave theory for estimating the phase shift velocity error range can only give an approximation of the real non-linear waves.

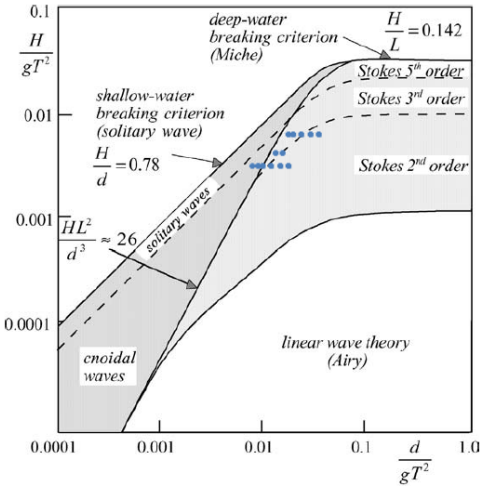

Figure 4.1: Applicable wave theory for the NK09 tests. Background image courtesy of L.H. Holthuijsen

Qualitative versus quantitative evaluation A lot of uncertainties and differences are present between the physical and numerical tests. For one thing the report by Nammuni-Krohn lacks detailed information on the model she made. Approximations and assumptions were made to obtain all dimensions and parameters required for the numerical model. Also wave generation is not exactly the same: the physical wave generator produced different waves than requested, see Nammuni-Krohn (2009, p. 12, 16 and 32). We cannot assess this since deep water wave gauge data lack. Uncertainties are also present for wave absorption on the wave generator. For the numerical tests it is already proven that absorption is not perfect. For the physical tests nothing is reported.

The influence of all these differences on the model results remains unknown, though we can expect that they could be of importance. The utility of a quantitative analysis might thus be very low. Qualitative evaluation is probably the best option. Two methods will be used. The first is the graphical presentation of some representative, 'typical' situations. The second is the graphical presentation of bulk data points.

Dimensionless analysis could also be used to verify whether similar trends exist: does flow velocity increase with e.g. higher waves? It is chosen not to perform this analysis because 1) it requires dimensionless parameters (which again creates uncertainties by choice of the combinations), 2) still a selection of cases must be made when plotting them (which might hide deviating, thus very informative cases) and 3) because of time limitations.

Lack of physical offshore gauge data In the NK09 dataset no processed data are available of the surface elevation measured at the three deep water wave gauges. Calibration information is not present so we cannot safely retrieve the surface elevation from the raw data files. A lot of important properties can therefore not be derived: no reflection coefficient, no real generated wave height and period, no envelope phase, no wave spectrum, etc. On the other hand the reflection coefficient is given in the 'decomp' files in the dataset, though these 'decomp' files are not available for all cases.

Irregular wave simulations Analysis of simulation results with irregular waves differ strongly from these with regular waves. While regular waves give the possibility to hold short simulation durations and derive 'average' waves, irregular waves require a statistical approach. Focus should be on extreme (peak) values: most of the dislocating forces for stones are proportional to flow velocity, so movement will start at peak values.

The phase shift velocity error is still present with irregular waves. No estimation of the error can be made based on the incoming wave height as the envelope will constantly shift. Perhaps the random nature might smooth out effects a bit. The reflection coefficient K_r can still be derived from the spectra.

Nammuni-Krohn did not analyse her experiments with irregular waves; in §5.2 of her report she warns that they are not reliable. We can thus expect large discrepancies with numerical results. The amount of 'decomp' files is also limited.

Simulation settings Besides the assumptions on model dimensions and stone properties, some limitations exist by the grid properties. Cell size and flume length were chosen based on the convergence tests. Together with the recommendation to use a uniform grid, this results occasionally in a rather coarse grid near the

toe. Structure edges are shifted towards the cell edges by number rounding. A sloping border for instance is modelled as a staircase border. This lack of detail might lead to slightly different results.

4.2. EVALUATION CRITERIA

Considerations from the previous section result in a set of evaluation criteria. They will be discussed hereafter. Some criteria are dedicated to (ir)regular waves, some to both wave types.

Numerical performance A first important check is to compare numerical model output versus requested wave properties. If wave production is not sufficiently accurate a comparison against physical tests would be useless. Waves are characterized by their amplitude and period. The wave generator should produce waves in such a way that the wave measured at offshore wave gauges should correspond to the required wave. We know that envelope position can create differences in wave height with regular waves. A split-up in incoming and reflected wave forms the solution. The qualitative evaluation followed will be the one of bulk data points. Each time a scatter plot will be made with data points for all cases available (i.e. cases for which both numerical and physical data are available). The scatter plots contain a 1:1-line with the 10% deviation area. The closer all data points are to this 1:1-line, the better the performance. The following checks will be made:

Regular waves:

- Wave period: requested T versus generated $T_{m01} = m_0/m_1$ representing mean wave period
- Wave height: requested H versus generated H_{m0}
- Wave height: requested $H/2$ (amplitude) versus time-averaged generated incoming amplitude $\overline{a_i}$ at offshore wave gauges. The latter is derived by reflection decomposition.

Irregular waves:

- Wave period: requested T_p versus generated T_p
- Wave height: requested H_s versus generated H_{m0}

Reflection performance Wave reflection influences flow velocities above the toe. It is result of the breakwater structure: its dimensions and stone properties. By comparing the reflection coefficient we can get insight in the modelling capabilities for porous media and fluid-solids interfaces. Three sources of data are present: the numerical simulations with offshore surface elevation data, the K_r values in the 'decomp' analysis provided by Nammuni-Krohn and the empirical formula in Zanuttigh and Van der Meer (2007). Numerical data have to be processed, more on this in the following section. The 'decomp' analysis uses $K_r = \sqrt{m_{0,r}/m_{0,i}} = H_{m0,r}/H_{m0,i}$ from the decomposed wave spectra. The formula by Zanuttigh goes as follows:

$$K_r = \tanh\left(a\xi_0^b\right) \tag{4.1}$$

$$\text{with: } \xi_0 = \frac{\tan\alpha_{arm}}{\sqrt{\left(2\pi H_{m0,t}\right) / \left(g T_{m-1,0}^2\right)}} \tag{4.2}$$

The values for a and b are taken for permeable rock being 0.12 and 0.87 respectively. The armour layer slope is 2:3. Wave characteristics are measured at the toe, which might give a deviation when shoaling processes are not modelled correctly.

The three values will be compared qualitatively with 1:1-scatter plots. High correspondence between physical/analytical and numerical coefficients signifies good fluid-structure interaction.

Local qualitative analyses The third evaluation will be zooming in on the processes near the toe: how accurate is the local flow pattern modelled? Since we posses a full numerical velocity profile at each time step at each wave gauge, it is interesting to plot the envelopes of these (see also the following section for envelope definitions and calculations used). Physical velocity measurements are in fact discrete points on these envelopes. For regular waves the error by possible phase shift due to reflection is estimated with linear wave theory. In Van Gent and Van der Werf (2014) it was stated that an estimate for the flow velocity could be made using linear wave theory. This approach will also be included in the envelope plots. A more complete

estimation using linear wave theory and shoaling processes is also shown. Each case has its plot for each gauge. Only the first, middle and last toe gauge will be shown for representative cases to reduce the amount of plots.

The flow pattern over time might also be of interest. Therefore some typical velocity and surface elevation records (i.e. $u(t)$ and $\eta(t)$) will be plotted. Wave shape and amount of spikes in both signals can be compared between physical and numerical tests.

In case of irregular waves some wave variance density spectra at the toe gauges will be plotted to verify whether the full spectrum is present and similar. This is possible since surface elevation data are available at all these gauges.

Summarizing the following plots will be made:

- Some representative velocity envelope over the vertical (profiles). Three discrete velocity values will also be shown: 1) physical data points, 2) the estimate by Van Gent and Van der Werf (2014) right above the toe bed, and 3) the estimate using linear wave theory and shoaling calculation at the physical data levels.
- Some representative $u(t)$ and $\eta(t)$-records at interesting gauge positions and water levels (for regular waves only).
- Some representative variance density spectra at toe gauges (for irregular waves only).

Bulk peak velocity analysis To get a global view on velocity modelling all data points from the velocity envelopes will be presented in 1:1-scatter plots. Envelope values at all physical gauge positions will be shown. Again we possess four data sources: numerical measurements, physical measurements, the estimation by Van Gent and Van der Werf (2014) and the extended estimation with linear wave theory and shoaling. The Van Gent estimation is only available for the lowest gauge positions (right above the bed). For regular waves the standard deviation of peak values can be shown; the larger this deviation the less reliable the measurement data are. Figure 4.2 is of help when assessing the relative magnitude of a certain value in a 1:1-scatter plot.

Following analyses will be made:

- Numerical versus physical data
- Numerical and physical data versus linear wave theory and shoaling
- Numerical and physical data versus the Van Gent estimation

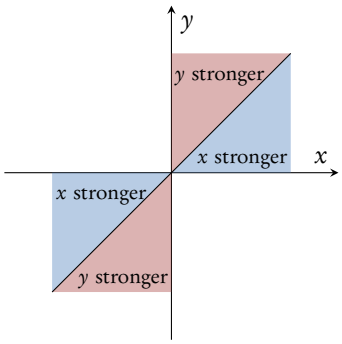

Figure 4.2: Octants in a 1:1-scatter plot

4.3. Preparation of evaluation

A lot of post-processing has to be done on simulation results. This section describes the outline of the most important calculations.

4.3.1. General

Post-processing software used is Matlab version R2014a. Wave records were split up in an incoming and reflected wave using the method by Zelt and Skjelbreia (1992). This method was coded to a Matlab script by Barbara Zanuttigh. For common wave analysis, i.e. determination of wave statistics and energy density spectra, the Matlab toolbox wafo was used (Brodtkorb et al., 2000; WAFO-group, 2000).

Post-processing is split up in cases with regular and irregular waves. In appendix H the outline of corresponding Matlab routines is shown. Cases were given a code and a numeric identifier: e.g. NK09_xxx for regular waves and NK09ir_xxx for irregular waves. In appendix E all cases are listed.

Two data sources are available. First data source is the numerical simulation data, i.e. output from IH-2VOF. Second data source is the Nammuni-Krohn dataset. Her data have been summarized so that only necessary data are retained. In her test set-up two different toe stone sizes were modelled at the same time. For convenience these data are split up into two different cases. Numerical and physical output files are read and processed with Matlab.

4.3.2. Gauge coupling

Numerical wave and velocity gauges were placed at the same x-positions as in the physical tests. The output of velocity gauges in IH-2VOF contains a $u(t)$ record at all y-levels. Levels corresponding with these of the

physical tests must be found. At first the horizontal cell border closest to the physical y-level was taken. This gave unrealistic results, probably because of structure edge shifting (see section 4.1). Best results were found when numerical y was taken near physical y plus one D_{n50}.

4.3.3. WAVE ANALYSIS

Spin-up time The numerical model requires some time before the original wave has run through the full flume length and reflected on the breakwater. From visual observation of regular wave records spin-up time is about 40 seconds, after which wave shape stabilizes. With 90 seconds of model time 50 seconds remain for analysis. The same spin-up time is kept for irregular waves. Physical tests on the other hand do not posses such spin-up time, likely because Nammuni-Krohn only started recording after the flume was filled with waves.

Reflection analysis As already discussed the waves measured at offshore wave gauges (i.e. at the beginning of the foreshore) have to be split up in an incoming and reflected part. The method by Zelt and Skjelbreia (1992) uses a minimum and maximum frequency which are set to 0 Hz and $4T^{-1}$ respectively. This method returns an incoming and reflected surface elevation and wave amplitude record. The reflection coefficient is then obtained as follows:

$$K_r = \begin{cases} \overline{a_r}/\overline{a_i} & \text{for regular waves} \\ \sqrt{m_{0,r}/m_{0,i}} & \text{for irregular waves} \end{cases} \tag{4.3}$$

in which $\overline{a}$ is the time-averaged wave amplitude and m_0 the zeroth order moment of the wave spectrum. Note that the 'decomp' files by Nammuni-Krohn use the same method.

Wave spectra and derived values Wave properties are based on wave spectra. The WAFO toolbox provides function `dat2spec()` which calculates the one-dimensional frequency energy density spectrum $E(f)$. A smoothing function is used, see WAFO-group (2000). A set of wave properties is then obtained with function `spec2char()`. At offshore wave gauges following values are derived:

- $m_{0,i}$ and $m_{0,r}$ for incoming and reflected wave
- $H_{m0} = 4\sqrt{m_0}$ as significant wave height
- $T_{m0,1} = m_0/m_1$ as mean wave period
- T_p as peak wave period.
- $T_{m-1,0} = m_{-1}/m_0$ as energy period for the velocity estimation by Van Gent and Van der Werf (2014)

At the first toe gauge H_{m0} and $T_{m-1,0}$ are also calculated for the reflection estimation by Zanuttigh and Van der Meer (2007).

4.3.4. LINEAR WAVE THEORY IMPLEMENTATION

A set of calculations using linear wave theory is performed. Target is to obtain horizontal flow velocity amplitude at a certain depth level, i.e. $\hat{u}(y)$. Point of start is wave amplitude and period offshore. By solving the dispersion relationship wave number k can be found both offshore and above the toe.

$$\omega^2 = gk\tanh(kd) \tag{4.4}$$

Shoaling coefficient K_{sh} is proportional to the ratio of group velocity c_g.

$$K_{sh} = \sqrt{c_{g,0}/c_{g,t}}$$

$$c_g = \frac{1}{2}\left(1 + \frac{2kd}{\sinh(2kd)}\right)\sqrt{\frac{g}{k}\tanh(kd)}$$

in which d is local water depth. Multiplying shoaling coefficient with deep water wave amplitude gives us the local amplitude above the toe. This local amplitude is then transformed to orbital velocity.

$$a_t = a_0 \cdot K_{sh}$$

$$\hat{u}(y) = \omega a_t \frac{\cosh(ky)}{\sinh(kd)}$$

in which y is zero at bed level.

For estimation of deviation by the partially standing wave, the $\hat{u}$ value is calculated based on time-averaged amplitude of the reflected wave offshore, i.e. $\overline{a}_{r,0}$. It represents possible deviation of peak velocity and will be shown in plots as a hatched area around the envelope value measured. Of course this is only a rough estimation as there exist non-linear and breaking waves.

Finally the velocity estimation proposed by Van Gent and Van der Werf (2014) is given. It estimates the velocity right above the toe bed with a deep water approximation. Values of H_{m0} and $T_{m-1,0}$ are based on the first offshore gauge record.

$$k = \frac{4\pi^2}{g T_{m-1,0}^2}$$
$$\hat{u}(y=0) = \frac{\pi H_{m0}}{T_{m-1,0}} \frac{1}{\sinh(k h_t)}$$

4.3.5. Envelope and peak values

Definition of the peak value is different for both wave types. For regular waves the peak value is defined as average maximum velocity per wave. For irregular waves maxima per wave are ordered in magnitude and the 2% value is taken as peak value. Taking the 5% or 10% value did not change results noticeably. For both waves peak values are obtained for both maxima and minima, i.e. the flow respectively towards and returning from the breakwater.

The method requires the wave record to be split up in multiple waves. For this the surface elevation record $\eta(t)$ is taken first and split up at downcrossings of the still water level, which is a common approach in wave analysis. Velocity record $u(t)$ is then split up at the same time steps and the minimum and maximum is taken. Figure 4.4 shows the method.

The velocity signal had often a lot of spikes (spurious peaks). This would give false extrema. For regular waves the requirement is set that every single wave should have a duration of at least $0.8T$. For irregular waves this method is not applicable since the period is changing constantly. Therefore a smoothing function is applied on the velocity signal. The WAFO function `smooth()` uses a cubic spline interpolation. The smoothing parameter was fitted by the eye and needed to be about 0.999. Figure 4.5 shows an example of the smoothed signal.

For regular waves not only the mean peak value is taken, but also the standard deviation σ of these peaks. The standard deviation is a measure for reliability of the record: the lower the value, the more constant and stable waves are. It will be shown in graphs as a shaded area around the mean value, see figure 4.3. Officially the maxima are Rayleigh distributed, see e.g. Holthuijsen (2007, §4.2.2). Standard deviation is then a different measure than the more common definition for a normal distribution.

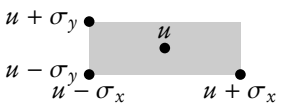

Figure 4.3: Visualization of standard deviation

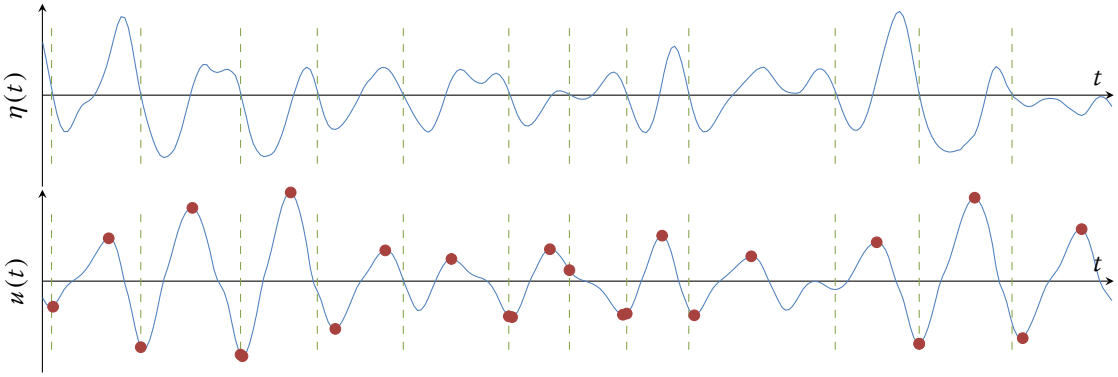

Figure 4.4: Method of wave splitting on an irregular wave record. Red dots are the selected minima and maxima.

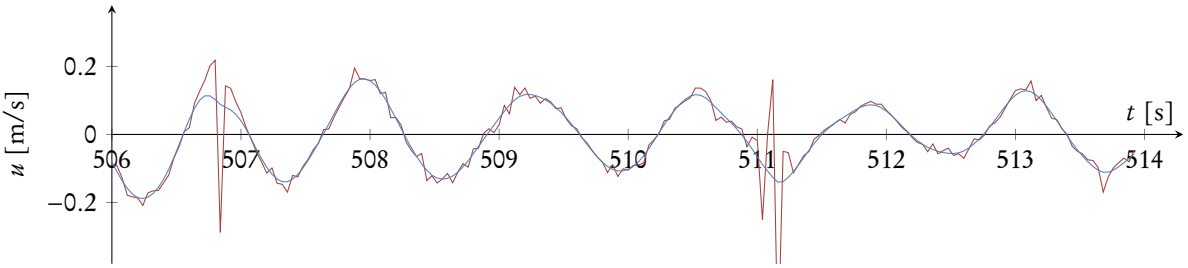

Figure 4.5: Method of wave smoothing on an irregular wave record. The red line is the original signal.

4.4. PERFORMANCE OF THE IH-2VOF MODEL

In the paragraphs hereafter evaluation results are presented. Each section starts on a separate page with a description of results after which corresponding graphs are shown. Note that graphs are grouped and ordered according to wave type.

4.4.1. NUMERICAL PERFORMANCE

With both regular and irregular waves generation of waves in the IH-2VOF model is in general very good, see figure 4.6 to 4.8. All values are within the 10 – 20% range. In generation of regular waves the expected problem with shifting envelope positions is clearly visible in comparison of wave heights (figure 4.7a). After retrieving mean amplitude of the incoming wave a good production is found (figure 4.8a).

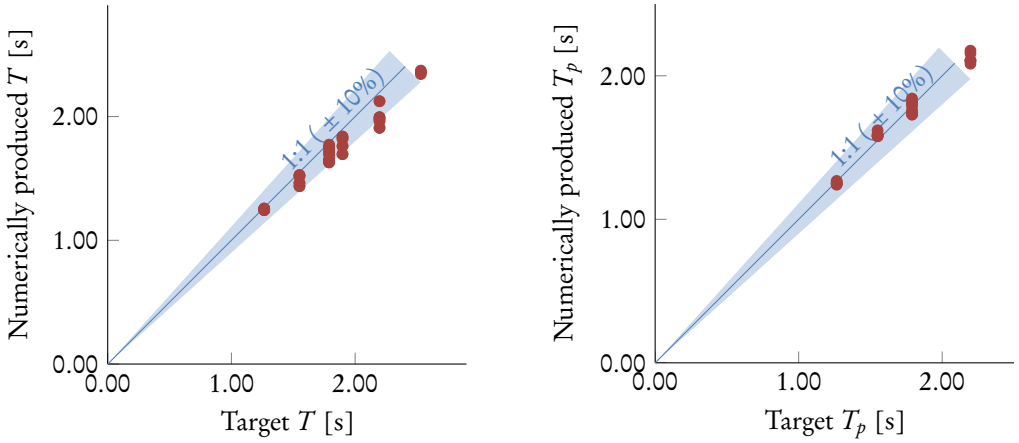

(a) Regular waves (b) Irregular waves

Figure 4.6: Wave period production

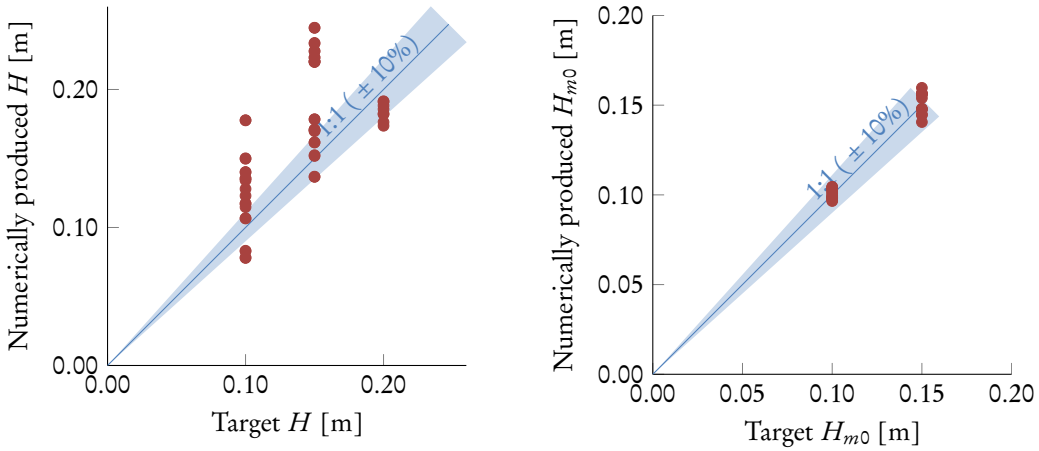

(a) Regular waves (b) Irregular waves

Figure 4.7: Wave height production

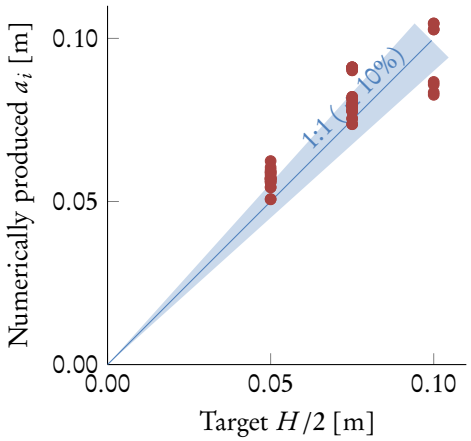

(a) Regular waves

Figure 4.8: Incoming wave amplitude production

4.4.2. REFLECTION PERFORMANCE

Regular waves Before comparing reflected waves, let us validate the incoming wave amplitude in deep water. This is feasible since Nammuni-Krohn provided this value in her 'decomp' files and since calculation methods in her and this report are equal. High correlation is visible in figure 4.9a. Higher waves are within the 10% range, lower waves in the 30% range.

Now since the incoming wave is equal we can safely use the K_r value to assess reflection properties. When comparing numerical and physical values there is low correlation, see figure 4.9b. Reflection seems to be modelled badly. There is no consistent over- or underestimation of reflected wave amplitude. Possible causes are estimated stone properties and dimension dimensions, and incorrect Forchheimer coefficients.

Can we rely on physical K_r values? A verification is made by using the formula by Zanuttigh and Van der Meer (2007). Values seem to correspond better than numerical values, see figure 4.10a. Since the formula uses $H_{m0,t}$ and $T_{m-1,0}$ measured with numerical data, possibility of a phase shift velocity error is still present. Furthermore the formula is not intended for regular waves.

Irregular waves Nammuni-Krohn only provided a very limited amount of 'decomp' files in which the reflection coefficient was present. A comparison between numerical and physical results is thus impossible. Figure 4.10b shows how the Zanuttigh-formula performs. More than 50% difference is encountered; Zanuttigh predicts much stronger reflection. The same reasoning as with regular waves can be kept.

Reflection modelling in IH-2VOF is all together not very reliable. Maybe better values for stone properties and dimensions would yield better results. This would prove on the other hand that sensitivity to these parameters is high.

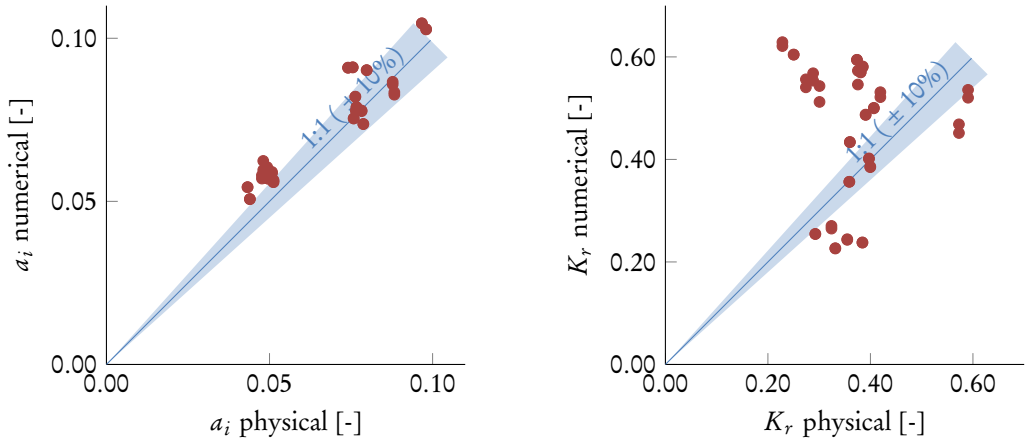

(a) Wave amplitude

(b) Reflection coefficient

Figure 4.9: Numerical reflection performance with regular waves

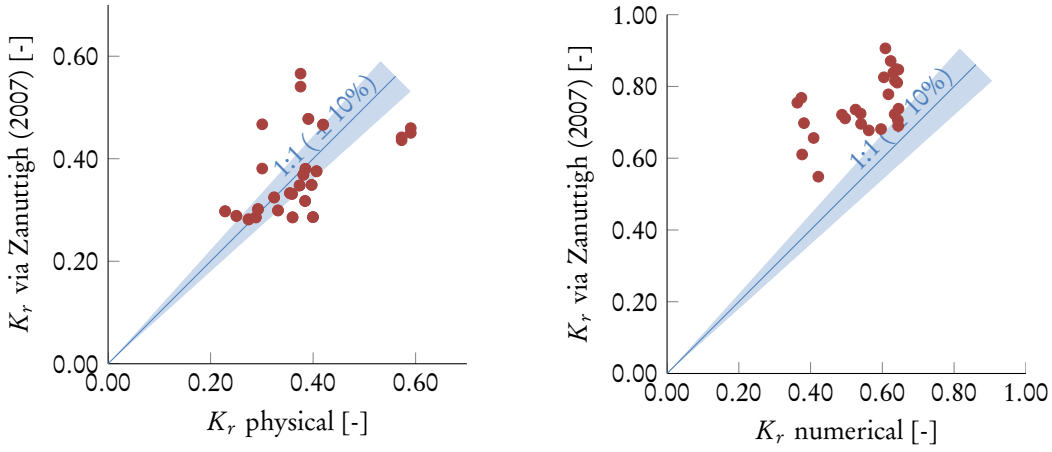

(a) Regular waves

(b) Irregular waves

Figure 4.10: Estimation of K_r by Zanuttigh and Van der Meer (2007)

4.4.3. VELOCITY ENVELOPE PROFILES

Regular waves A couple of typical velocity envelope profiles, showing mean peak velocity in seaward and landward direction, are given in figure 4.11. The different flow regimes near solids, porous media and free surface are visible in the numerical profile. In other words structural definition of the model results in realistic flow patterns. Wall friction is also modelled as we see a velocity gradient near the fluid-porous interface.

Correspondence between numerical and physical results is rather good if one takes the possible deviation by the phase shift velocity error into account. The latter is shown by the grey boxes, which have a range of $\pm\hat{u}$. Flow right above the bed level is numerically lower than in physical measurements. It is unknown whether this is result of shifted structure dimensions, by too strong modelling of wall friction or by inaccurate parameters for porous media. This is an important observation as it shows sensitivity of the flow measurement level.

Analytical approximation by linear wave theory and shoaling performs well. Note that wall friction is not implemented and indeed, pure horizontal non-zero fluid motion above the bed is present, which is stated in linear wave theory. Compared with physical tests linear wave theory always underestimates flow velocity with a minimum of about 60% of the physical value. Possibly higher order effects or turbulence give slightly higher velocities than predicted by linear wave theory.

The Van Gent estimation is mostly overestimating physical values, up to a factor of 2. Note that the estimation uses values for H_{m0} and $T_{m-1,0}$ at a certain gauge; the possibility of a phase shift velocity error is therefore also present.

To conclude regular wave analysis it must be noted that near the corner between toe and armour layer the observations above do not hold consistently. This can be explained by the local flow pattern which has to change its direction from horizontal to sloping motion. Local eddies can easily be formed.

Irregular waves With irregular waves no estimation of the possible phase shift velocity error can be made. It is expected that the effect with irregular waves is lower than with regular waves. Waves in the Nammuni-Krohn measurements were reported to be lower, so lower velocities are to be expected.

In figure 4.12 some typical profiles of the 2% highest velocities are shown. The numerical profiles are not as symmetric compared with regular waves. When comparing physical and numerical values one can observe that they are quite corresponding once again, though the shape over the vertical is not always consistent. The latter is difficult to compare since only a few measurement positions are available. Physical measurements are slightly lower than numerical values, as expected.

The approximations with linear wave theory are very close to the physical values. Again a slight underestimation is present. The Van Gent estimation on the other hand is overestimating physical measurements.

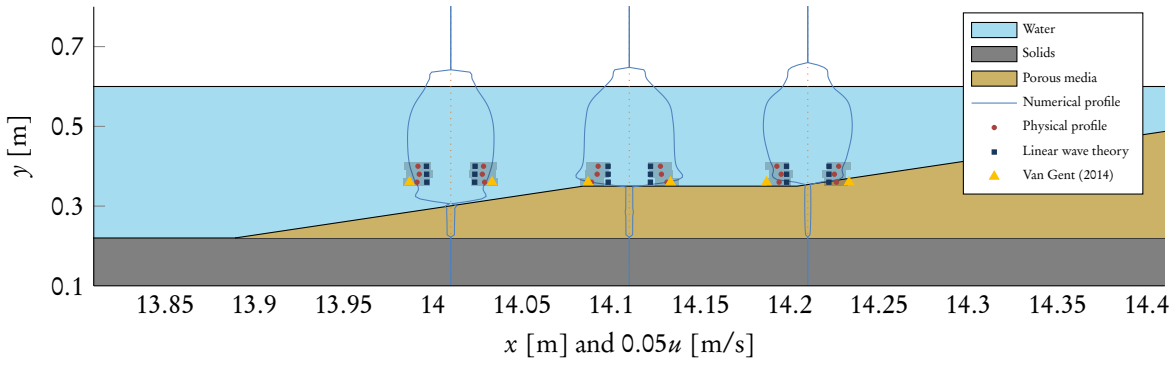

(a) NK09_711

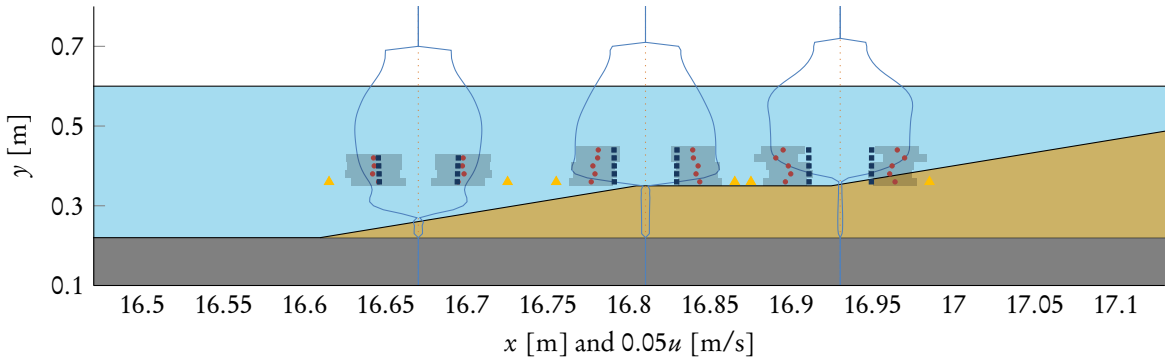

(b) NK09_713

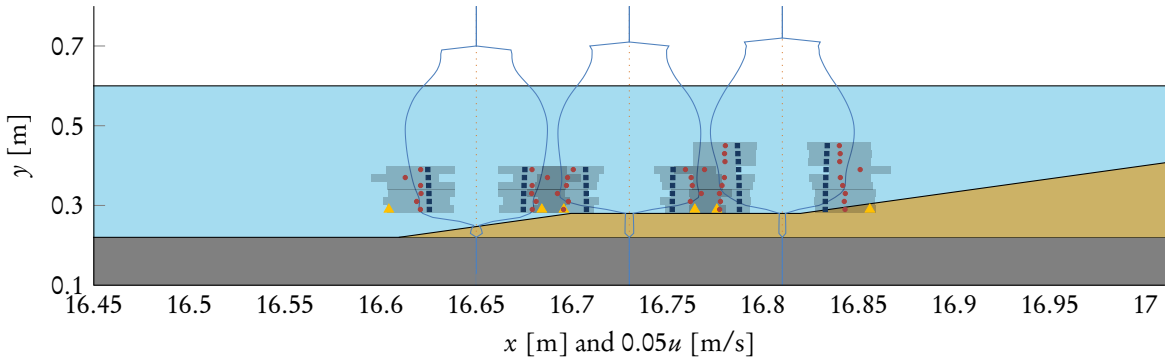

(c) NK09_730

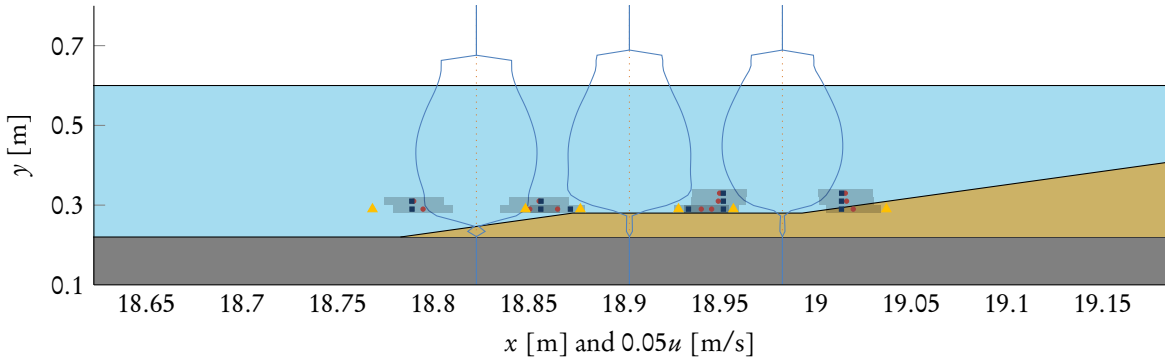

(d) NK09_733

Figure 4.11: Regular wave envelopes

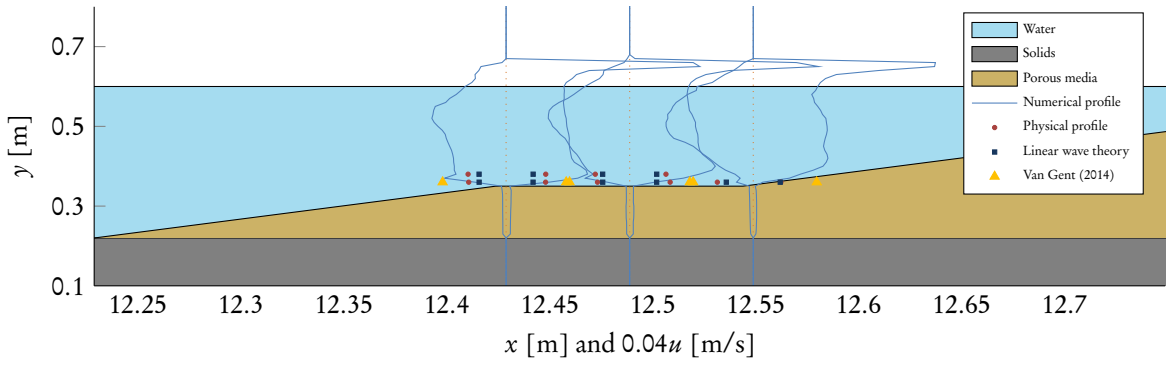

(a) NK09ir_726

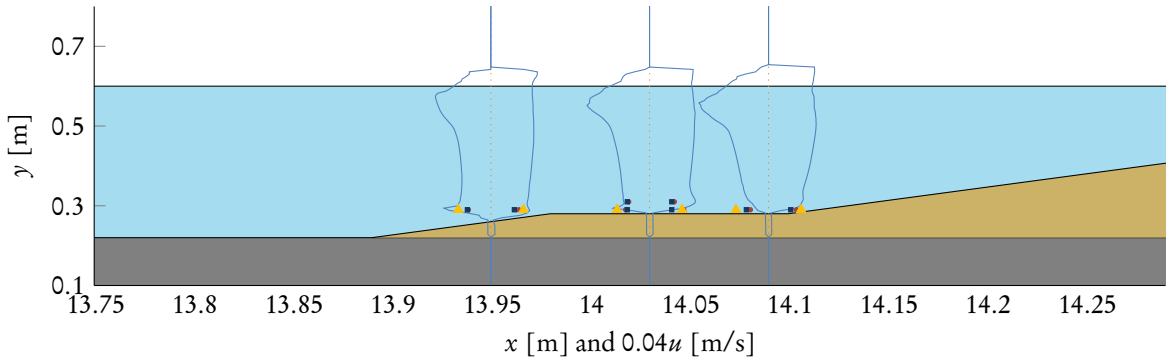

(b) NK09ir_743

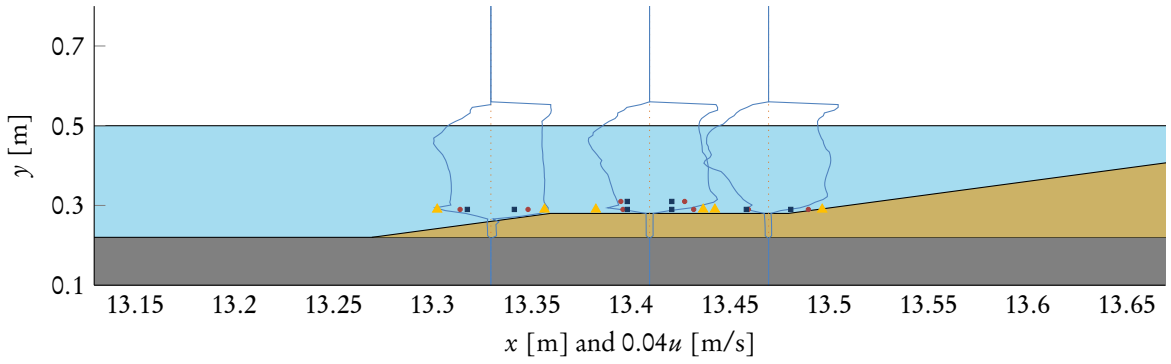

(c) NK09ir_747

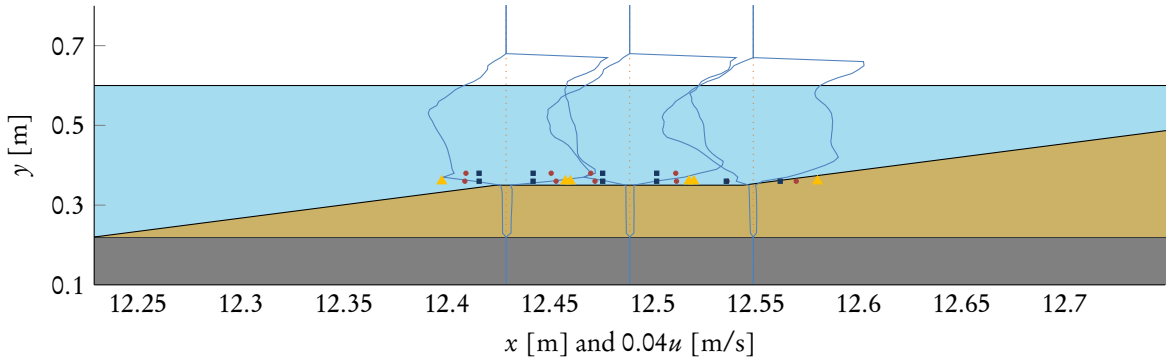

(d) NK09ir_766

Figure 4.12: Irregular wave envelopes, taken as $u_{2\%}$

4.4.4. Representative records

Figure 4.13 shows a couple of typical free surface elevation records at multiple gauge positions. Wave shape in both numerical and physical records is quite consistent. Magnitude is not always the same, probably by the envelope phase shift. Note that the physical signal is shifted slightly upwards. This may result from how the still water level is defined and measured.

Figure 4.14 shows typical horizontal velocity records. Physical records are often disturbed by spikes in the signal. Certainly measurements in the corner between toe and armour layer are affected. For other measurement positions often the positive (landward) velocity peak was not measured properly. When ignoring the spikes one can observe that shape and magnitude are quite comparable between numerical and physical signals.

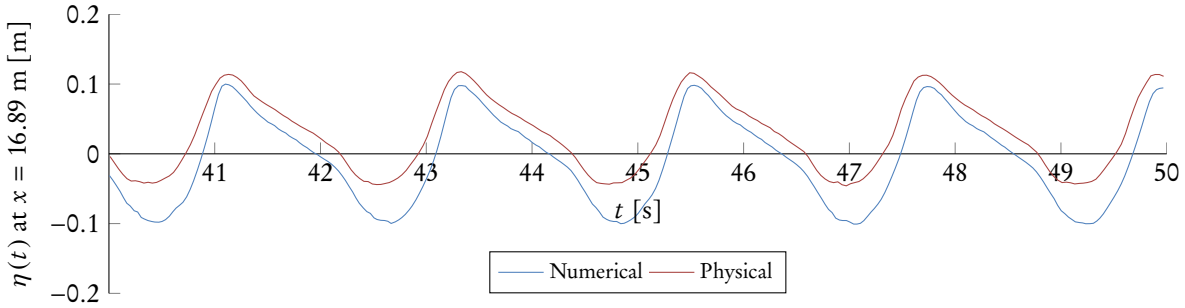

(a) NK09_713

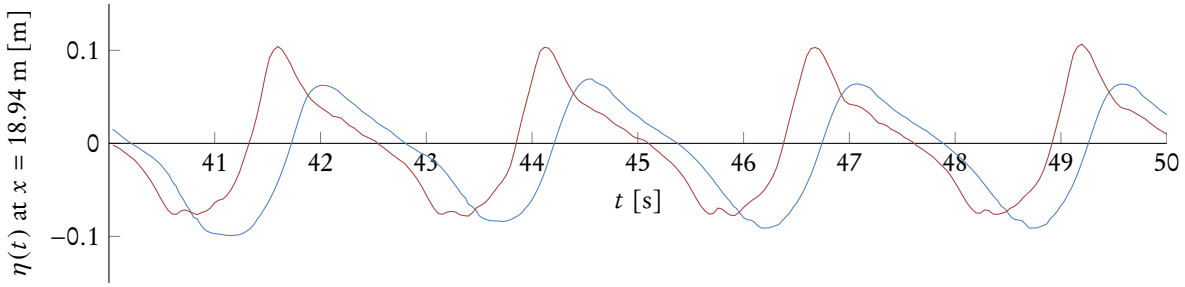

(b) NK09_733

Figure 4.13: Surface elevation records

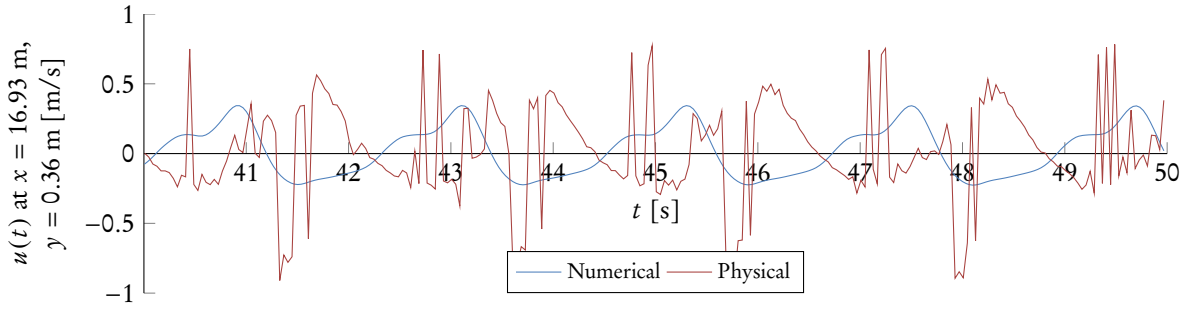

(a) NK09_713

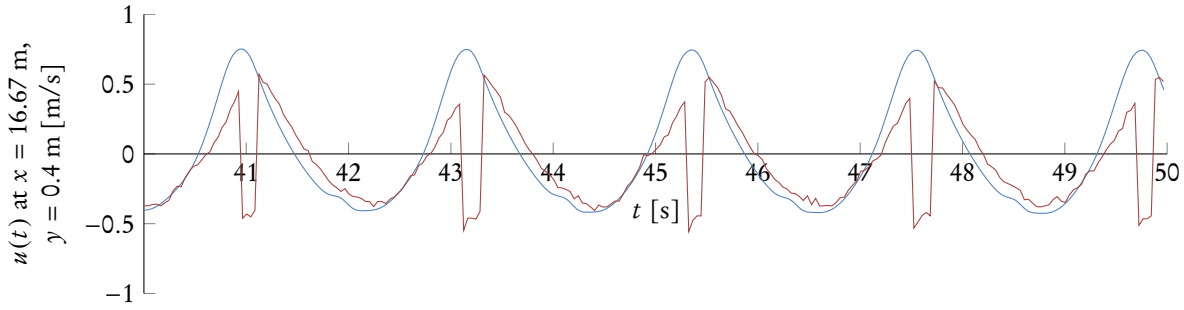

(b) NK09_713

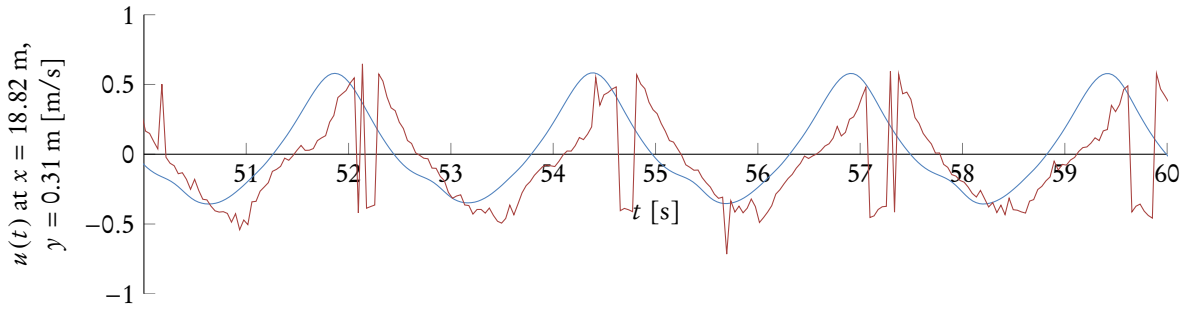

(c) NK09_733

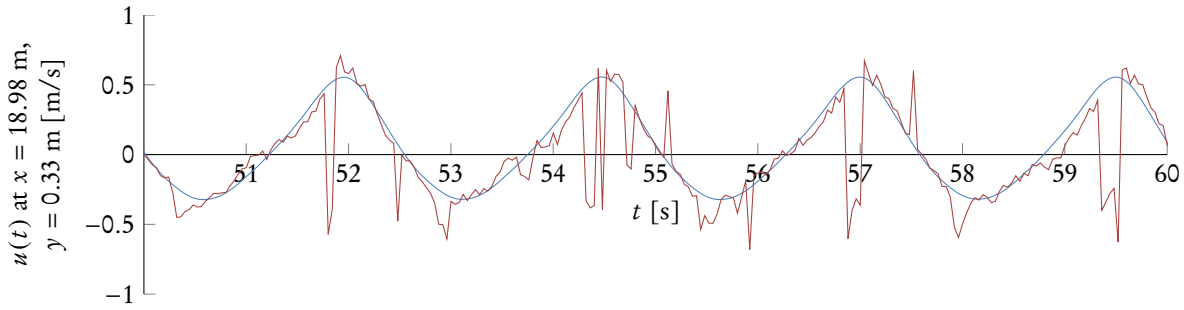

(d) NK09_733

Figure 4.14: Horizontal velocity records

4.4.5. VARIANCE DENSITY SPECTRA

For irregular waves some wave variance density spectra are shown in figure 4.15. For each case the spectrum is made at three gauge positions above the toe for both numerical and physical measurements. At first sight spectra correspond quite well in shape. The physical spectrum is always lower than the numerical, which is expected by the lower generated waves. One can also observe that the peak value is not always highest at the first or last gauge. This might point at the phase shift difference in the standing wave envelope. Finally one can often find a secondary peak at a lower frequency in the numerical signal. It is not known what causes this peak.

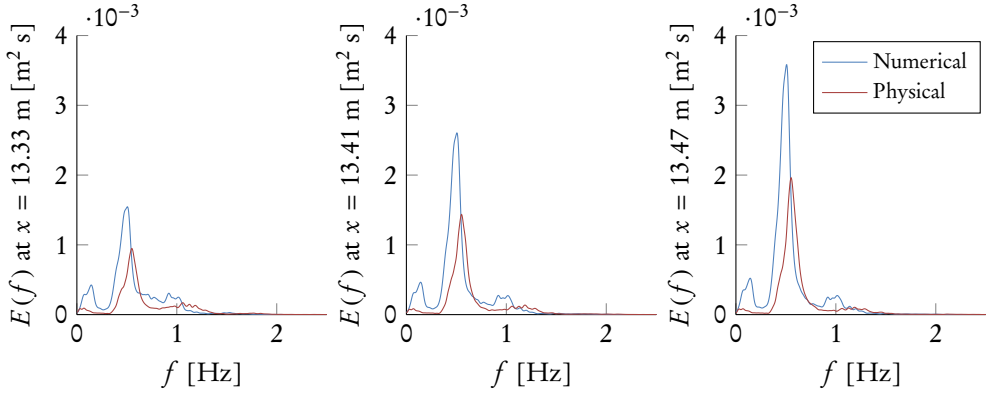

(a) NK09ir_707

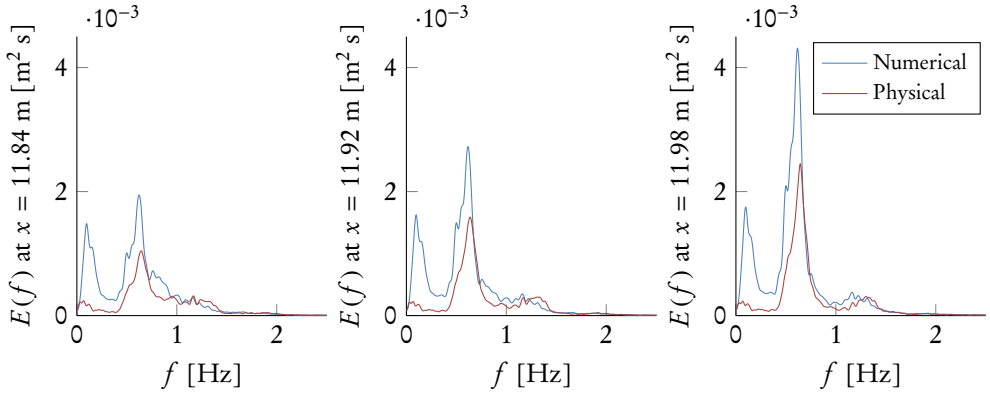

(b) NK09ir_710

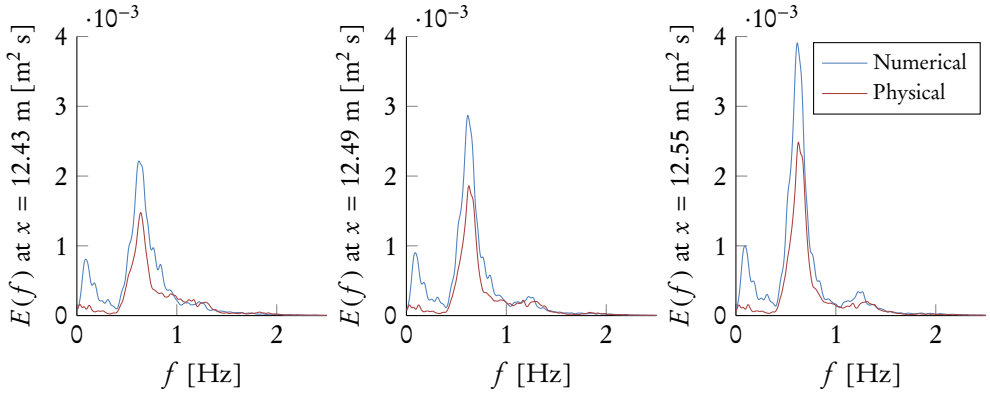

(c) NK09ir_726

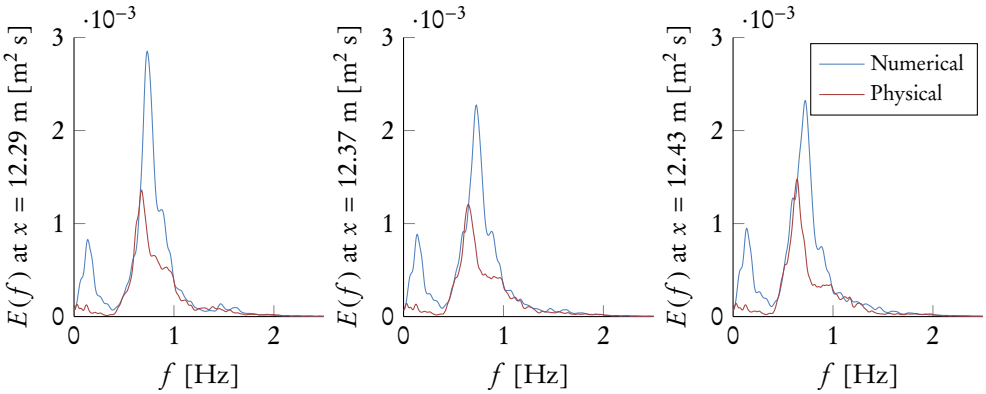

(d) NK09ir_746

Figure 4.15: Variance density spectra

4.4.6. Bulk peak velocity analysis

Regular waves The scatter plots show peak velocity values at each physical gauge. Colouring of the dots corresponds to different cases. It was tried to colour them according to the case parameters, but this did not give any valuable extra information.

We will start again by comparing physical and numerical values in figure 4.16a. For landward (positive) flow most data points are within the 30 – 40% range. Seaward flow has larger deviations, up to more than 50%. With most velocities less than 0.5 m/s it is also less strong than landward flow, which has velocities up to 1.0 m/s. There are some serious outliers, which seem to be from certain cases.

As we now plot the standard deviation of peaks as a grey box in figure 4.16b, we can see that these outliers often have a large standard deviation in physical direction. The darkest area (most overlapping points) is still within the 40% range for landward flow and within the 50% range for seaward flow. Numerical standard deviation is in most cases very low. For a couple of cases with large standard deviation the velocity record is analysed. Two scenarios can be found. The first is visible in figure 4.17: a constant pattern and smooth signal is available, but physical peaks are not constant. This is a natural effect. The second scenario is shown in figure 4.18 where a signal disturbed with a lot of spikes and irregularities is found. These irregularities result in a high standard deviation.

When comparing physical values with the linear wave theory approximation in figure 4.19a, we see quite inconsistent results. When compared with numerical results in figure 4.19b better results are found. Accuracy is still low: for seaward flow the error is up to 50%, for landward flow even higher.

Finally the Van Gent approximation is compared with numerical and physical measurements in figure 4.20a and 4.20b. Values are only shown for lowest gauge levels, for which the formula is intended. As expected from velocity envelope profile analysis, a big overestimation is present, up to a factor 3. It seems that the approximation is not very reliable for regular waves. Note again that the approximation is based on wave statistics from a numerical wave gauge, which will probably differ from the physical record.

Irregular waves With irregular waves the error between physical and numerical values in figure 4.21 seems to be the other way around: now seaward flow has a slightly lower deviation (but still up to 40%). Landward flow has deviations up to 60% and is again stronger than seaward flow. Note that nearly all dots are positioned in the octants where numerical flow is stronger than physical flow, which is expected by the lower waves.

When linear wave theory approximation is compared with numerical values in figure 4.22b low correspondence is found, certainly for landward flow. Linear wave theory is strongly underestimating flow velocities. Compared to physical values in figure 4.22a better results are found, within the 30 – 40% range. Note however that physical velocities are higher, while this should not be the case since waves were lower. In that way linear wave theory might again underestimate flow velocity.

Finally the approximation by Van Gent is analysed. With numerical results in figure 4.23b a remarkable good correspondence is found for landward flow (up to 30%), while for seaward flow it overestimates the velocity with an error up to 60%. Compared to physical results a constant overestimation up to 60% is found, see figure 4.23a.

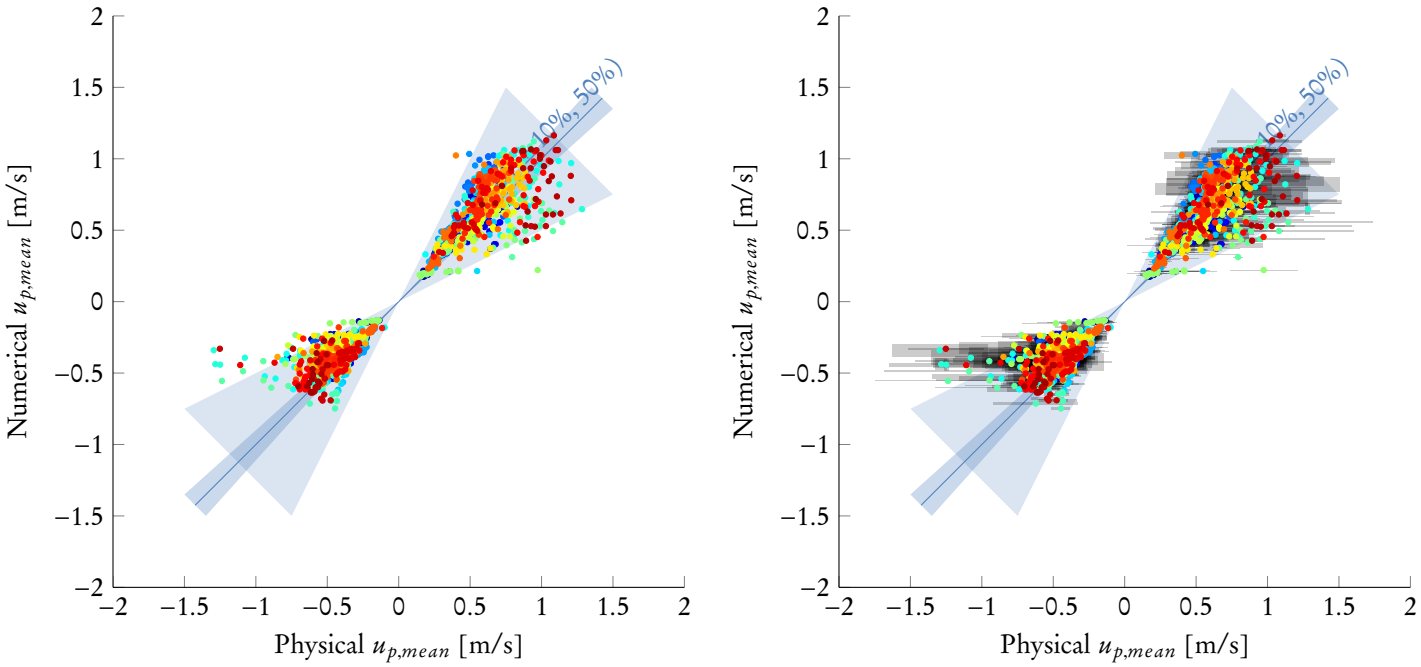

(a) Original

(b) With standard deviation

Figure 4.16: Regular waves, numerical versus physical data

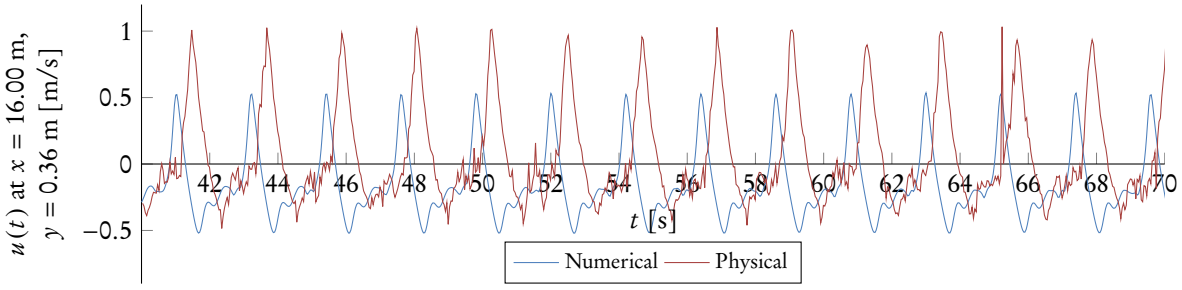

Figure 4.17: Horizontal velocity record for case NK09_720

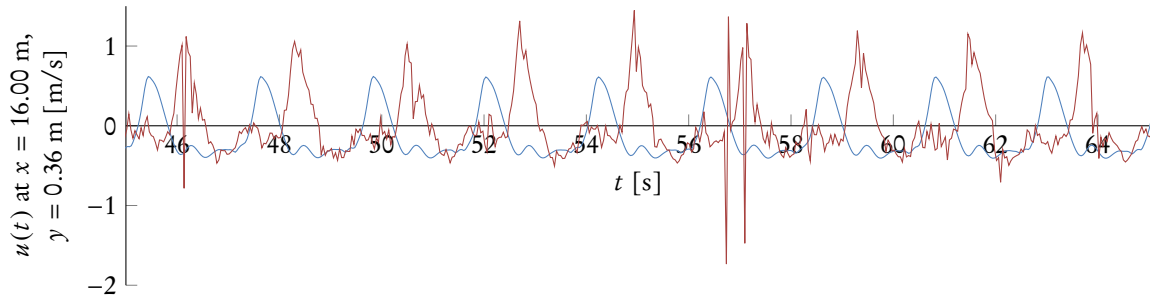

Figure 4.18: Horizontal velocity record for case NK09_760

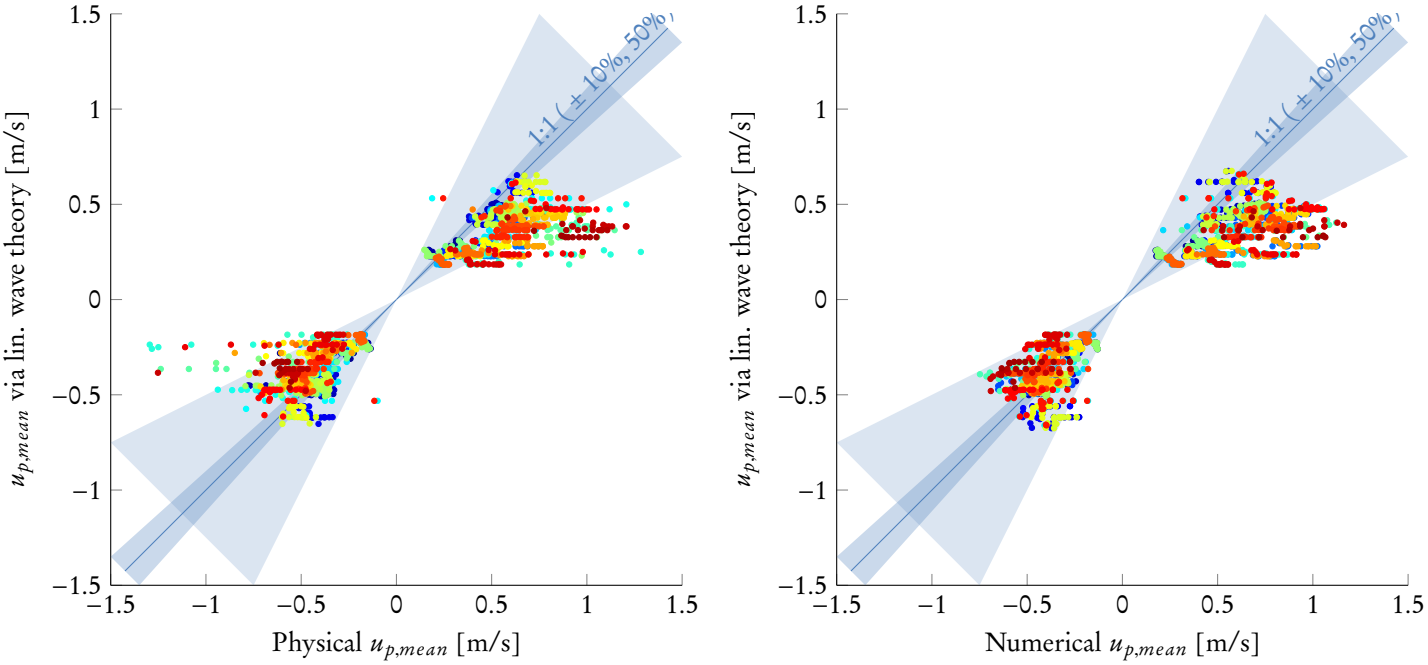

(a) Versus physical data

(b) Versus numerical data

Figure 4.19: Regular waves, comparison with linear wave theory

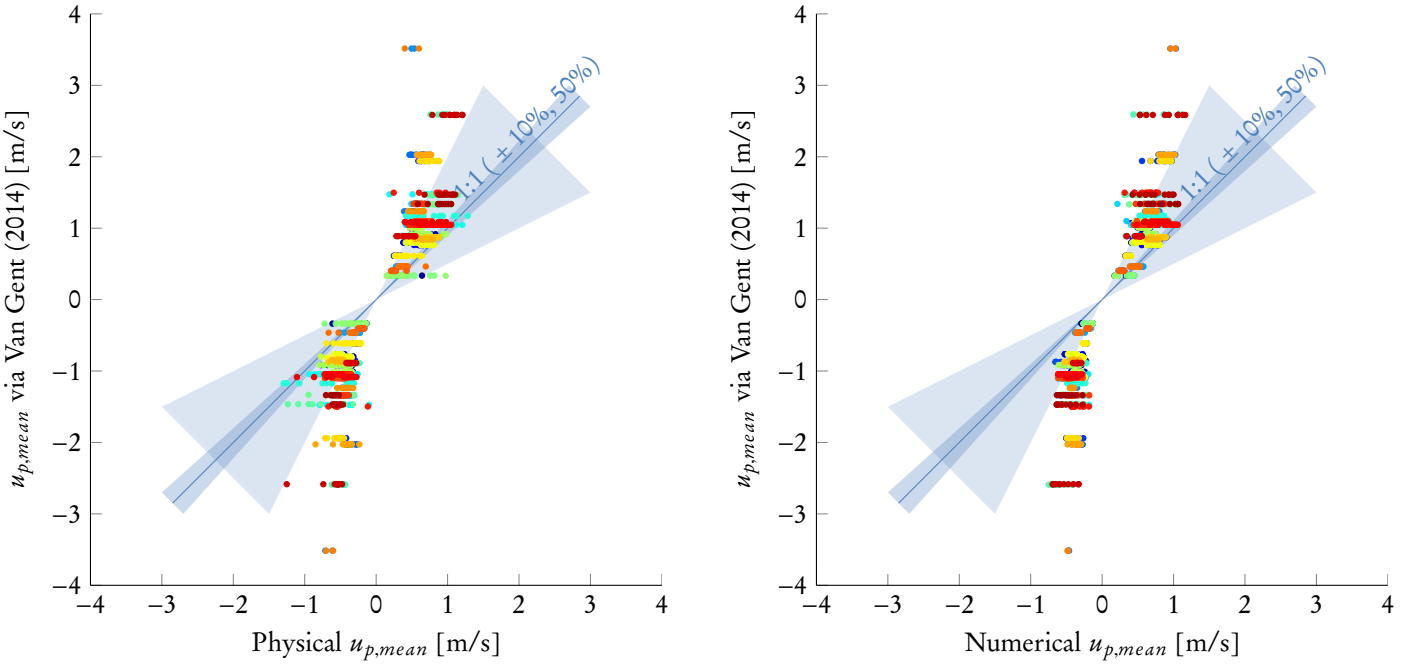

(a) Versus physical data

(b) Versus numerical data

Figure 4.20: Regular waves, comparison with Van Gent and Van der Werf (2014)

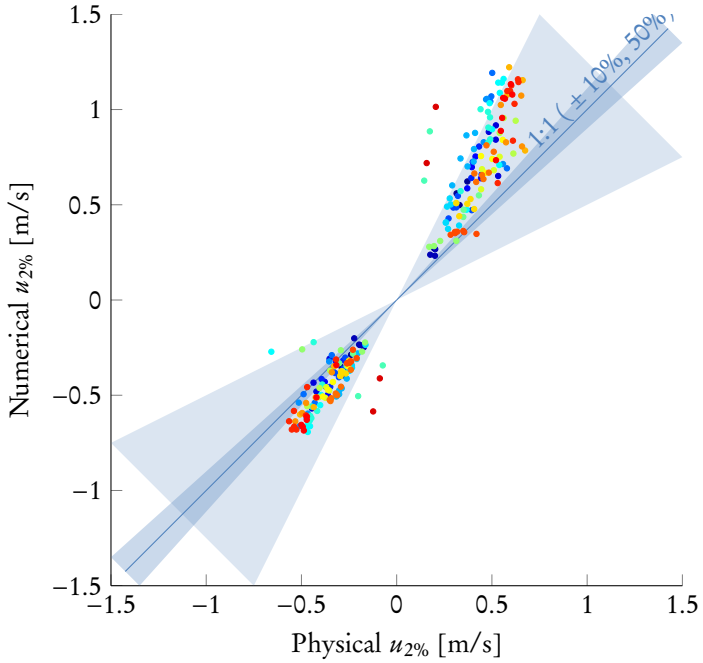

Figure 4.21: Irregular waves, numerical versus physical data

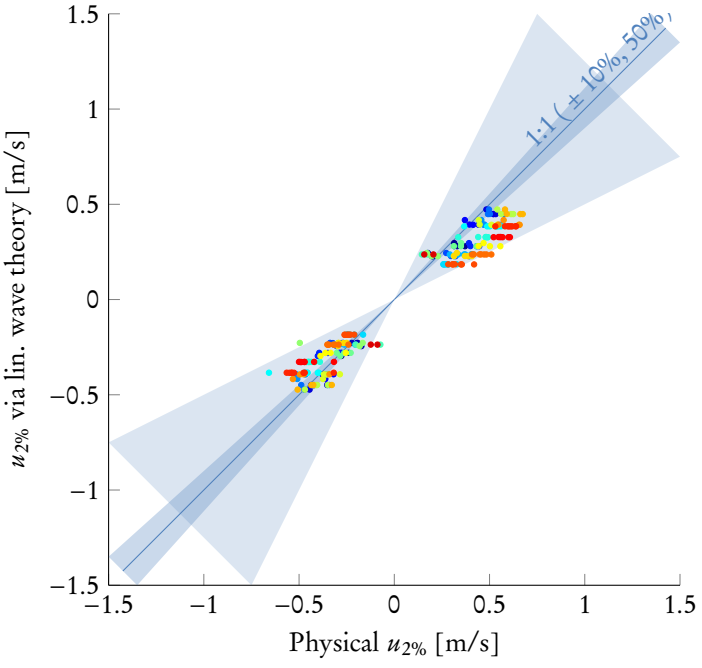

(a) Versus physical data

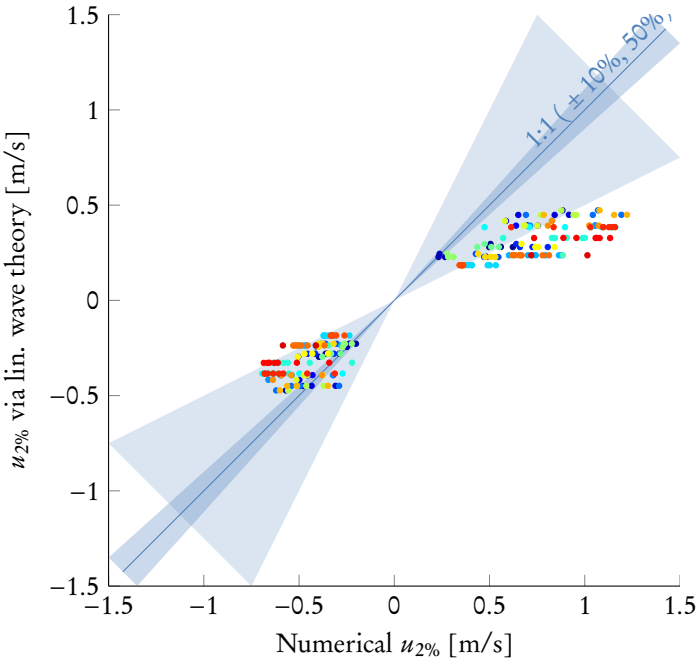

(b) Versus numerical data

Figure 4.22: Irregular waves, comparison with linear wave theory

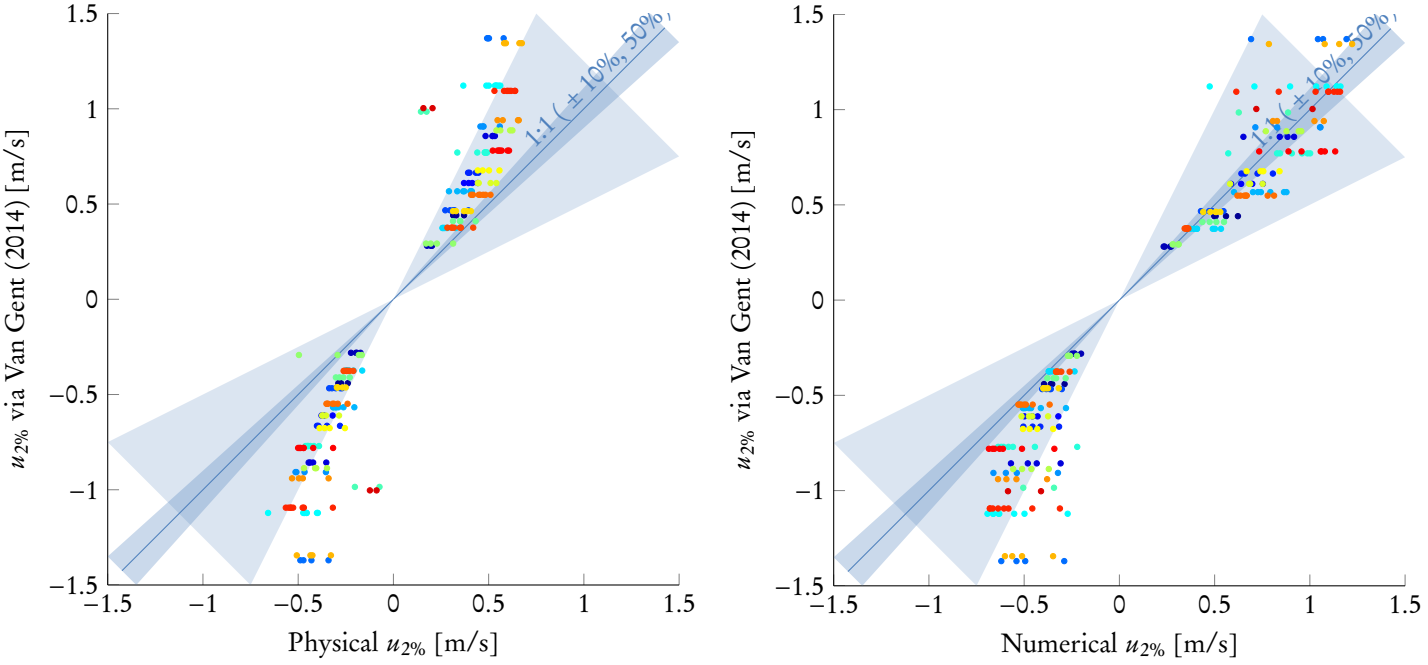

(a) Versus physical data

(b) Versus numerical data

Figure 4.23: Irregular waves, comparison with Van Gent and Van der Werf (2014)

4.4.7. SUMMARY

The analyses performed will now be summarized in next few points:

- Numerical performance is very good: requested waves are well present in the model results.
- Modelling of reflection in IH-2VOF is not consistent with results measured in the flume. The formula by Zanuttigh and Van der Meer (2007) gives good values compared with physical tests. Though since the formula uses input from the numerical model and since it is not intended for regular waves, one should be careful to draw conclusions from this observation.
- Physical tests with irregular waves show too low produced waves as expected. This was found in velocity comparison and in variance density spectra. Velocity records contain a lot of spikes. For regular waves this resulted in high standard deviations for velocity peaks. For irregular waves numerical smoothing of the signal was essential.
- Approximation with linear wave theory and shoaling underestimates velocities with respect to both physical and numerical tests.
- Approximation by Van Gent and Van der Werf (2014) gives only good results for landward flow under irregular waves. With respect to physical values, an overestimation up to 60% is visible. It must be noted that wave properties were derived from numerical results.
- Numerical and physical velocity envelope profiles have often an inconsistent shape near the bed. Probably wall friction is modelled too strong, giving a high velocity gradient. It is therefore difficult to compare values right above the bed. The measurement level seems to be very sensitive to variations.
- From bulk velocity analysis one can see that landward flow is stronger than seaward flow, up to factor 2.

There are too many unknowns (model layout, stone properties, turbulence, reflection modelling, etc.) to give well-founded advice on applicability of the IH-2VOF model to this research. Lack of information makes it difficult to compare Nammuni-Krohn measurements with numerical model output. If the estimations made would be correct, one could state that overall numerical results are *not* very reliable for detailed work on extrema, even given the restrictions discussed in section 4.1 and the fact that turbulence is not modelled correctly.

Analytical approaches do not provide consistent solutions either, with physical nor with numerical values. On the other hand they could be used to give a lower and upper limit for velocities, as it turned out that the Van Gent approximation often overestimates, and linear wave theory with shoaling underestimates flow velocities.

Since velocities by IH-2VOF are within the values by analytical approaches, one could state that the order of magnitude is correct. Therefore one might use IH-2VOF to get information on trends rather than on absolute values. For design purposes, relative behaviour analysis of different breakwater layouts is possible.

4.5. RUBEN PETERS' EVALUATION

Parallel to this research Ruben Peters validated his experimental data with the IH-2VOF model. He prepared flume experiments in such way that good numerical modelling was possible, with as few uncertainties as possible. In Peters (2014a) his findings were reported, which will be summarized here.

Contrary to the Nammuni-Krohn experiments Peters did measure the Forchheimer coefficients for the stones used. Next to surface elevation and horizontal flow velocity he recorded pressure data. Peters modelled 63 cases with regular waves. Parameters changed were water depth, wave height and wave period; breakwater dimensions remained the same. No turbulence calculation was performed. The convergence tests on the computational grid were performed in an equal fashion as for this research. Following recommendations were used:

- Use of a uniform grid.
- Flume extension length ratio of $3.5L_0$ (here $2.0L_0$).
- Cell width ratio of $L_0/\Delta x = 200$ (here ≈ 150).
- Cell height ratio of $H/\Delta y = 15$ (equal here).

During analysis a clear and distinct boundary layer was observed on the interface between fluid and solids/porous media. It has a thickness of about one cell. The hydraulic conditions within these cells were found to be unreliable.

To compare physical and numerical measurements, Peters concentrated on the signal extrema. The root mean squared value of the extrema and a relative error were calculated with following formulae:

$$u_{rms} = \sqrt{\frac{1}{N}\sum_{i=1}^{N} u_i^2}$$

$$\text{error} = \frac{u_{rms,measured} - u_{rms,IH2VOF}}{u_{rms,measured}} \cdot 100\%$$

For horizontal flow velocities a mean error of 18% for landward flow and 6% for seaward flow was found. The standard deviation of the error was respectively 9% and 16%. In nearly all cases the IH-2VOF results were lower than measured.

The free surface record had larger errors, between 13% and 30% with standard deviations of 16 to 30%. The waves in the model were clearly lower than in the flume.

Pressures finally were measured above and within the toe structure. They appeared to be modelled very accurately: with an error in the range of 10-20% and standard deviations of less than 10% a very consistent result was found.

Peters therefore concludes his research as follows:

> "[...] it can be concluded that IH2VOF performs reasonably well at computing the hydraulic properties near breakwater toes. Since a lot of the computed errors are relatively consistent they can be accounted for in further analysis."
>
> *(Cited from Peters (2014a), page 26)*

The experiment by Peters points out that IH-2VOF is rather capable of correctly modelling the flow. What causes then poor results in the Nammuni-Krohn cases? Following the experience of the graduation committee it is found that the IH-2VOF model is very sensitive to the Forchheimer coefficients, which had to be estimated for this research. Even if they are measured in detail for modelling purposes, some amount of calibration work is still necessary. For prototype modelling this poses a problem since measuring the coefficients is in such circumstances rather infeasible.

Peters did measure the Forchheimer coefficients in detail for his research. In table 4.1 his measured Forchheimer coefficients are shown. They were taken as the average value of a couple of experiments per stone class. In the same table the estimated coefficients according to equation 3.1 are given. It seems that linear friction coefficient α is highly variable. The equation both over- and underestimates the value measured up to 50%. Non-linear friction coefficient β_c has a smaller spread, though again the equation deviates up to 30%. Peters assumed that the non-linear coefficient is more important since flow within breakwaters is expected to be highly turbulent.

All together it seems that estimation of the coefficients is not very reliable. Together with high sensitivity to these parameters, it is likely the most important cause of bad resemblance between Nammuni-Krohn data and data from IH-2VOF

Table 4.1: Measured and estimated Forchheimer coefficients in Peters (2014a)

		α [-]			β_c [-]		
	D_{n50} [m]	**Range**	**Average**	**Eq. 3.1**	**Range**	**Average**	**Eq. 3.1**
Armour	0.044	1816 - 1836	1826	1151	1.70 - 1.71	1.70	1.1
Core	0.022	483 - 830	627	854	1.34 - 1.39	1.36	1.1
Toe	0.025	496 - 688	591	903	1.12 - 1.33	1.23	1.1

4.6. Summary

In this chapter the first research question was answered: can the IH-2VOF model be used to simulate physical flume experiments on breakwater toe stability? Evaluation was performed by comparing physical measurements by Nammuni-Krohn with the numerical model outcome. Work by Ruben Peters was also reviewed. Focus was on extrema in horizontal flow velocity above the toe. Qualitative evaluations were found to be most appropriate for the comparisons.

Next to a validation of model results it was tested to which extent linear wave theory could provide an alternative for physical and numerical tests. Two applications with linear wave theory were investigated: one incorporating shoaling effects and one based on deep water situations, as proposed in Van Gent and Van der Werf (2014).

Modelling the Nammuni-Krohn flume required estimation of several breakwater dimensions and stone properties. Wave parameters were set to values which Nammuni-Krohn used to configure the physical wave generator; physical irregular waves turned out to be smaller than requested. The numerical model did not incorporate effects of turbulence, i.e. fluid viscosity was always the molecular viscosity.

The IH-2VOF model produced the waves requested with sufficient accuracy. Comparison between numerical and physical flow velocities gave generally poor results with relative differences up to 50%. Linear wave theory with shoaling mostly underestimated velocities while the Van Gent estimation overestimated them. They were not very consistent with numerical measurements either.

Question is now whether numerical or physical measurements are reliable. We know that IH-2VOF does not model turbulence correctly and that estimated dimensions and properties are used. The Nammuni-Krohn dataset on the other hand is also incomplete, lacking deep water gauge data, corresponding calibration results and reflection properties. The IH-2VOF model was also evaluated by Ruben Peters against a different physical dataset. He found much better results with relative errors of at most 20% for flow velocities. Also pressures were modelled with high accuracy. Moreover errors were much more consistent and standard deviation of the error had low values of less than 15%. A note was made on the existence of a distinct boundary layer between fluid and solids/porous media, in which measurements should be avoided.

The work by Peters points out that the Nammuni-Krohn tests and dataset are not appropriate for this evaluation. Assumptions had to be made on dimensions and stone properties, and certain information lacked in dataset and report. It was found that Forchheimer coefficients impact the reflection process to a large extent, impacting velocities in its turn. We must be aware that IH-2VOF is very sensitive to inaccuracies in model definition.

It is decided to continue using the IH-2VOF model since flow velocities are modelled quite accurately. The model is considered to be appropriate to model flume experiments on breakwater toe stability *given* the availability of accurate dimensions and stone properties. For continuation of this research this imposes no problem: estimated values are used in both IH-2VOF and the toe stability methods. No discrepancies between model and method parameters will then exist.

Phase 2 – Evaluation of stability methods

5

Evaluating stability methods

Phase two of this study focuses on evaluation of the stability methods. This is done by simulating the Ebbens (2009) tests (in short Eb09) with IH-2VOF and using the local hydraulic conditions to predict motion by means of motion formulae from section 2.2.4. This prediction will be compared with prediction by the stability methods.

This chapter starts with a detailed description of the approach. Modelling of the Eb09 cases is then discussed. Section 5.3 presents main steps taken to couple stability methods and motion formulae to the output data from IH-2VOF. Full conversion of the formulae is given in appendix F. After applying the motion formulae on output data, it appeared that some calibration was necessary, this is discussed in section 5.4. Finally comparison results are presented and discussed.

5.1. Evaluation procedure

5.1.1. Evaluation target

Target of evaluation is to see which toe stability method has the most consistent prediction of motion. A set of cases is run, for which motion is determined using motion formulae from section 2.2.4. Of course validity of the formulae should be taken into account. In the end one can find a percentage for each stability method, giving the amount of equal motion respectively immobility predictions.

5.1.2. Evaluation steps

In figure 5.1 a scheme shows the stepwise evaluation procedure. Point of start is the set of Ebbens cases, defined by breakwater layout, wave climate and stone properties. The cases are modelled in IH-2VOF to find velocities, surface elevation and turbulence intensities above the toe. These values are put into the motion formulae. Calibration is then applied to verify when one can consider the case as having motion. This way for each case motion is predicted.

Left side of the scheme shows the route which is taken for the stability methods. They directly accept parameters of the breakwater structure. For some methods wave properties are required, which are derived from deep water surface elevation data. Each formula predicts an amount of damage, which can be transformed to a prediction of motion using a subjective threshold. This threshold is based on the description of damage given in the corresponding reports.

Finally prediction of motion by both routes are compared in light of evaluation target. Details on all steps are found in the sections hereafter.

An additional evaluation will be performed in which validity ranges for parameters in the stability method are ignored. With this we obtain information on prediction capacity of the methods outside their validity limits. No new calibration is necessary since the motion formulae are not affected.

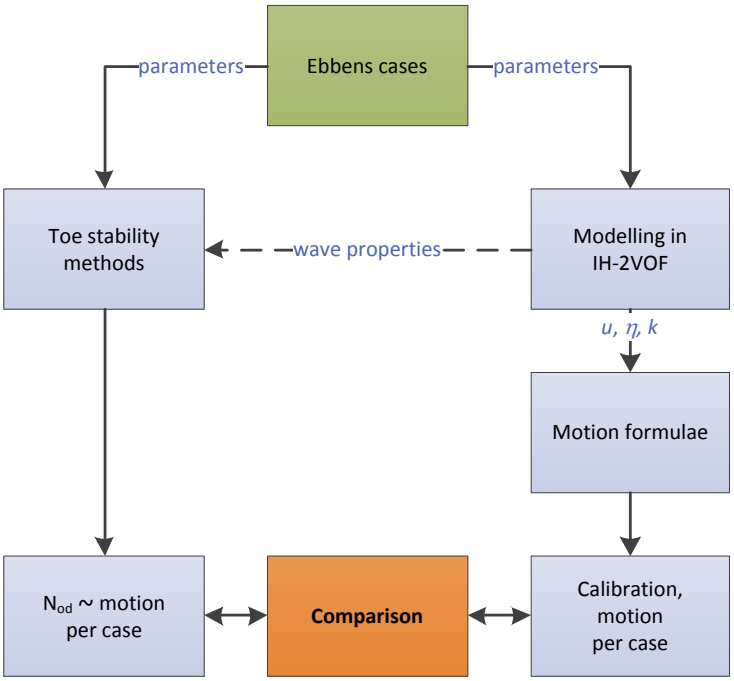

Figure 5.1: Scheme of the evaluation procedure

5.1.3. Sensitivity analysis

Subjectivity of the threshold of motion should be investigated with a sensitivity analysis. As a matter of fact the transition zone from immobility to motion is always given as a range of the damage parameter. Sensitivity analysis is performed as follows: firstly limits of the transition zone are obtained from original reports, secondly an intermediate value is taken as the base situation, finally for each formula individually this threshold value is taken towards the range limits and motion prediction is reassessed. The different situations are shown in table 5.4 below.

5.1.4. Output presentation

For each case and for each stability formula we get an indicator whether there is motion or not. A tabular overview can be made on prediction performance. Validity of these formulae should also be shown: if a certain formula is very accurate but only for a very limited range of case parameters, it might be questionable whether the formula is universally applicable. Note that the tables below contain arbitrary values.

Prediction table 5.1 depicts the main evaluation results. It shows how often predictions match. Bold figures show performance of toe stability methods as the average over all motion formulae (vertically). In "xx% (yy%)" the values are defined as follows:

$$xx = \frac{\#\text{ joint motion} + \#\text{ joint immobility}}{\#\text{joint valid}} \cdot 100\% \quad \text{percentage of joint equal prediction for cases where both formulae are valid}$$

$$yy = \frac{\#\text{joint valid}}{\#\text{cases}} \cdot 100\% \quad \text{percentage of cases where both formulae are valid}$$

For sensitivity analysis the final row of the prediction table will be shown for each situation. This forms *sensitivity* table 5.2. Validity ranges do not change in the situations. Finally *motion* table 5.3 will be constructed for reference. It shows motion prediction per case.

Table 5.1: Layout of the prediction table

	VdM91	...	Mut14	Performance motion formulae
Izb30	60% (100%)	...	80% (60%)	70% (80%)
...	...	...	...	...
Ste14	70% (80%)	...	90% (80%)	80% (80%)
Performance toe stability formulae	**65% (95%)**	**...**	**85% (80%)**	

Table 5.2: Layout of the sensitivity table

	VdM91	...	Mut14
Base	**65%**	**...**	**85%**
Validity	95%	...	80%
Situation 2	80%	...	87%
...	...	...	...
Situation 10	70%	...	85%

Table 5.3: Layout of the motion table

	VdM91	...	Mut14	Izb30	...	Ste14	% valid	% motion if valid
Case 1	x	...	✓	✓	...	x	90	40
...	...	...	...	...	...	...	...	...
Case n	-	...	✓	-	...	x	90	40
% valid	30	...	85	70	...	65		
% motion if valid	75	...	35	85	...	50		

Table 5.4: Situations for sensitivity analysis.
Values equal to the base case are omitted for clarity.

	$N_{od,c}$	$N_{\%,c}$	F_S	$\Psi_{RS,c}$	$\Psi_{MS,c}$
Min.	0.4	5%	0.91	0.54	0.25
Max.	0.8	20%	0.95	0.79	0.35
(Base) 1	0.6	10%	0.95	0.6	0.3
2	0.4				
3	0.8				
4		5%			
5		10%			
6			0.91		
7				0.55	
8				0.65	
9					0.25
10					0.35

$N_{od,c}$ based on Baart (2008), used for Ger93a, Bur95, VdM98, VGe14 and Mut14

$N_{\%,c}$ based on Ebbens (2009), used for Ebb09, Mut13

F_S safety factor for Baa08, not to be confused with Γ in his fitting procedure

$\Psi_{RS,c}$ based on figure 8.11 and 8.12 in Hofland (2005): stone movement started for $\Phi_E \in \left[10^{-10}, 10^{-9}\right] \Leftrightarrow \Psi_{RS_c} \in [0.54, 0.79]$

$\Psi_{MS,c}$ based on figure 5.19 in Dessens (2004)

5.2. THE EBBENS MODEL

Global description of the Eb09 cases was already given in section 2.3. All 296 cases were modelled in IH-2VOF. Configuration was made based on recommendations and principles of chapter 3. All configuration data are given in appendix E. Note that for the longest foreshore (slope 1:50) it was decided to use only 1000 mm as flume extension to reduce grid size. The model layout is shown in appendix E as well. Just like with the NK09 cases pre-processing was automated with PHP and SikuliX.

For stone properties again some estimations had to be made. Forchheimer coefficients had to be estimated once again with formula 3.1. For the porosity of the core and the underlayer an estimated value is used. Porosity of the armour layer was obtained from the Xbloc brochure. Note that the back side of the breakwater is modelled as a vertical slope. This is physically impossible without a wall structure, but it turned out to be necessary for the calculation process. It is expected not to be of any problem since the right boundary is absorptive.

Simulations were also run on university computers. Some cases took too much time to complete in a weekend. In the end 185 cases (63%) were finished. It is not expected that simulating the rest of the cases would add much relevant information to the evaluation hereafter. Details on the simulations can be found in appendix E.

(Very) shallow water is defined as situations in which $\gamma = H_s/h_m \geqslant 0.5$. The Eb09 cases had both deep and shallow water situations. From the cases which were run successfully 78% have shallow water conditions.

Requirements on output data were given in section 2.2.4. To fulfil the requirements three sets of wave gauges are placed in the model, each recording local surface elevation and values for u and k in every grid cell in vertical direction. The three sets are the following:

- Three offshore (deep water) gauges: spaced 200 mm and 650 mm right in front of the foreshore
- Three onshore gauges: spaced 160 mm and 240 mm right in front of the bedding layer
- A number of wave gauges, spaced Δx, spanning at least 150 mm and positioned above the toe. The number of gauges is ranging between 13 and 23.

Spacing for offshore and onshore gauges is kept the same as in the original Eb09 model. In general the minimum spacing for gauges is Δx.

Regarding turbulence the remarks from section 3.5 should be kept in mind. The formula by Steenstra requires turbulence intensity k so the partial turbulence calculation had to be switched on. The k value is then the instantaneous production and might be very inaccurate.

5.3. IMPLEMENTATION OF FORMULAE

A large number of formulae and methods was used to determine motion for each case. MATLAB was used for post-processing. This chapter describes the most important calculations aspects. Converted stability methods and motion formulae are given in detail in appendix F. From now on abbreviated formula names will be used.

Motion in stability methods Nearly all stability methods give a relation between damage, wave and structure parameters. This is converted into a stability criterion, i.e. a relation in the form:

$$\text{motion occurs if } 1 \geqslant f\ (H_s, D_{n50}, N_{od}, \ldots)$$

In this criterion the damage parameter is then set to a defined critical value. The formula provides a single indication of motion per case.

Discrete value probing For Des04 and Ste14 velocity, turbulence intensity and advective acceleration are determined pairwise per gauge couple. This is allowed for small Δx, see e.g. §4.4 in Steenstra (2014). Following conventions are used, in which the index denotes the gauge:

$$u \approx \frac{u_i + u_{i+1}}{2}$$
$$k \approx \frac{k_i + k_{i+1}}{2}$$
$$a \approx u\frac{u_{i+1} - u_i}{\Delta x}$$

Wave properties Several formulae need wave properties as input. They should be established as values for the undisturbed situation (i.e. without breakwater) in all cases. This is achieved through wave decomposition in an incoming and reflected wave with the method by Zelt and Skjelbreia (1992). Methods in the WAFO toolbox are then applied on the incoming wave signal. To obtain wave lengths the dispersion relation from equation 4.4 is used.

One exception is on value L_{0m}, based on mean wave period in deep water T_{0m}. In Holthuijsen (2007, §4.2.2) it was discouraged to use the estimate $\sqrt{m_2/m_0}$. The mean wave period is thus determined by splitting the wave signal on its downcrossings and simply taking the average of the individual periods.

Validity ranges Most formulae have validity ranges for certain parameters, outside which the formula may not be used. If the Eb09 case investigated does not comply to the requirements of a certain formula, it is not evaluated. For motion formulae it is additionally verified whether measurement level lies above the still water level. Three exceptions are made to prevent the formulae being inappropriate for all cases.

- Stability method VGe14 requires the armour layer to have a slope of 1:2. This has been ignored since the Eb09 model slope is 2:3.
- As described in table 5.4 $\Psi_{RS,c}$ for Ste14 should be in the range $[0.54, 0.79]$ which is smaller than the minimum 0.9 (Steenstra, 2014, eq. 6-3).

– Where measurement level h_g lies outside the range for α and $C_{m:b}$ in Ste14, the closest defined value is used (see further).

For the second evaluation validity ranges of the stability methods will be ignored completely.

Measurement levels Except for Pet14 all motion formulae have one major drawback in common: they do not define a (practical) measurement level for hydraulic properties. In the original experiments for Ran68a an oscillating water tunnel was used, for which the (mean) velocity is simply discharge divided by area. Formulae Des04 and Ste14 used stationary situations with rather deep water. In Ste14 advective acceleration should be measured at a level h_a above toe level, which is above the still water level in 90% of the Eb09 cases.

The formulae use input data from the free flow region. Due to relatively low water level the velocity profile is somewhat blockwise shaped when flow is maximal in a direction. This can be seen in figure 5.2. It is then acceptable to let the measurement level be halfway the water column, i.e. at $h_g = (h_t + \eta)/2$. Drawback of this choice is that there might be an overestimation of motion due to higher velocities.

For Izb30 an exception is made since it is intended for individual stones, requiring local flow forces. It is chosen to take the flow velocity at a level of $h_g = 1.0D_{n50}$ as a workaround for modelling effects in the boundary layer, as described in Peters (2014a).

Pet14 finally measures velocities at $h_g = 0.05$ m as described in Peters (2014b, §4.2).

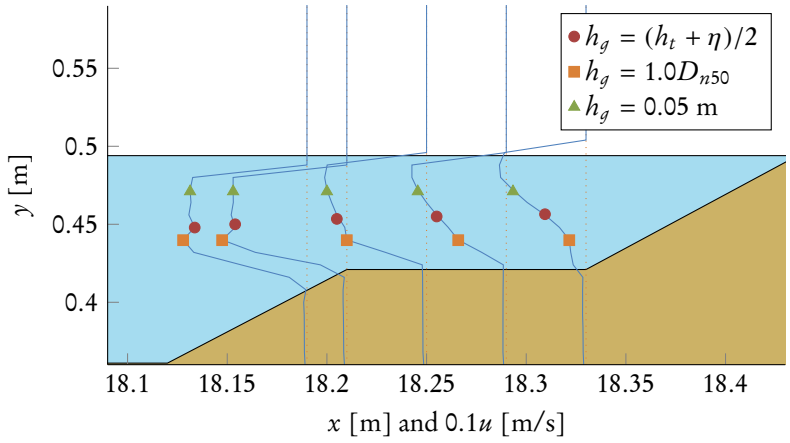

Figure 5.2: Velocity profiles and measurement levels h_g in a typical situation

Baa08 Baart provided an analytical description which is completed with formulae in the Rock Manual (CIRIA et al., 2007) to determine values for wave run-up and run-down. All formulae are presented in appendix F. In the main stability check a safety factor 0.91–0.95 is given (noted as F_S in this report) which is varied in sensitivity analysis.

Ran68a The formula by Rance and Warren is applied per wave. For this the surface elevation record is split at downcrossings and corresponding velocity record parts are obtained. Orbital velocity and period is then obtained as depicted in figure 5.3a. Note that velocity is about in phase with surface elevation, so down- or zerocrossings take place almost simultaneously.

Ste14 The formula by Steenstra contains a complex moving-average calculation together with measurement of the advective acceleration at a certain level. This level was defined to be at $9.0D_{n50}$ since it gave highest correlation for entrainment. Figure 5-3 in his report showed however that correlation for lower levels is not much worse ($R^2 \in [0.69, 0.80]$). It is therefore acceptable to use the measurement level halfway the water column.

Coefficients α and $C_{m:b}$ in the formula are dependent on the measurement level. Since h_g is chosen to be dependent on η, coefficients are updated at every time step. It is chosen to use interpolation with splines

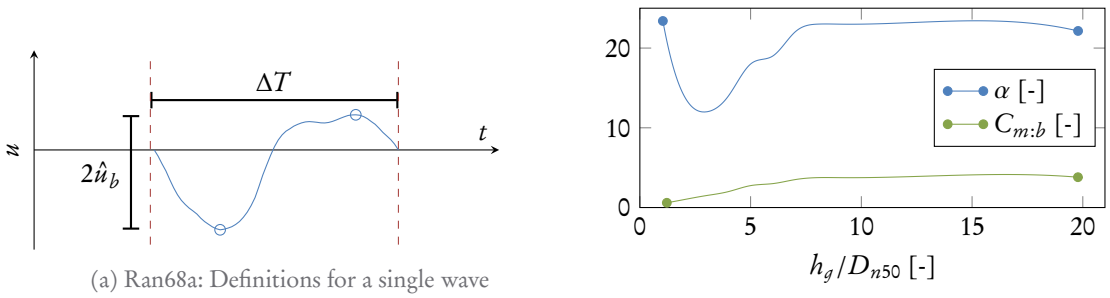

(a) Ran68a: Definitions for a single wave

(b) Ste14: Coefficient values

Figure 5.3: Details on Ran68a and Ste14

between the fitted values from table 5-2 in the report. For measurement levels outside the fitted range, values for the closest measurement level defined are used (shown as dots in figure 5.3b).

Pet14 Peters' formula uses detailed information on stone dimensions. Individual stones are not modelled in IH-2VOF and therefore this information should be estimated. It is chosen to consider stones as randomly placed cubes[1]. It can then be argued that average frontal area is $0.5D_{n50}^2$. It is advised to perform sensitivity analysis on this estimation in further research.

Pressures required for Peters' formula were unfortunately not stored. With output available the Bernoulli approach for pressures above the stones (as presented by Peters) can still be used:

$$p_{above} \approx \left(h_t + \eta + \frac{u|u|}{2g}\right)\rho g$$

Within the toe one could use the Forchheimer formula to obtain pressures. In that case an accurate boundary condition is required, though unavailable. This method was consequently considered inappropriate. It was then tried to approximate pressures with a hydrostatic approach, which is acceptable since velocities within the toe are relatively low:

$$p_{under} \approx (h_t + \eta)\,\rho g$$

This approximation agreed well with measurement data by Peters. Pressure difference then becomes $\Delta p = \frac{1}{2}\rho u|u|$.

Regarding stability lift force is always upwards: velocities above the stones are higher than within the toe, thus resulting in lower pressure above. Drag force also destabilizes stones. Stone weight is consequently the single stabilizing force. Under oscillatory flow the pivot point position depends on flow direction. Therefore it is chosen to take absolute values of flow velocity (i.e. squared values) and account for correct directions in the moment calculation.

5.4. CALIBRATION OF MOTION FORMULAE

5.4.1. NECESSITY

Contrary to stability methods, the motion formulae should be applied over all time steps and all toe wave gauges. Should a case then be considered as having motion when the criterion is passed a single moment in all these steps? This would be nonsense, as it takes some time to dislocate the stone. A minimum period of subsequent motion indications could be interesting to define, but elaboration of this approach is beyond the scope of this research. A practical approach is then to measure the percentage of motion indications in time/position and calibrate them to the original Eb09 damage recordings. Determination of stability is then

[1]This is defendable based on definition of D_{n50}.

performed in these steps:

$$\text{motion-\%} = \frac{\sum_x \sum_t \text{motion at } (x_i, t_i)}{\sum_x \sum_t 1} \cdot 100\%$$

$$\text{motion occurs if motion-\%} \geqslant \text{calibrated motion-\%}$$

For Ran68a motion is counted per wave rather than per time step.

5.4.2. APPROACH

For every Eb09 case a damage recording was reported by Ebbens, i.e. a N_{od} value. By imposing a limit on this value one can state per case whether motion has occurred in the flume. The limit chosen is taken equally to the value in the base situation in table 5.4: $N_{od,c} = 0.6$. Of course some natural randomness is present in the Eb09 tests: depending on stone configuration and waves more displacement will occur, or there might be no displacement at all. This uncertainty was already described in literature study in section 1.2. Therefore two calibration steps will be taken.

In the first calibration step the number of Eb09 cases with recorded (physical) motion is counted. The numerical cases are analysed and for each case the motion percentage is obtained. Ordered on this percentage a cumulative distribution can be made. Let $C(p_m)$ be the value at motion percentage p_m, then the following holds:

$$C(p_m) = (\#\text{ cases with motion-\%} \leqslant p_m) \cap \text{ valid cases}$$

$C(100\%)$ will consequently be the number of cases for which the motion formula gave valid results. The percentage for which $C(p_m)$ is equal to the Eb09 count, is then the calibrated motion percentage. The principle advantage of this step is that information on the distribution of motion percentages is obtained.

In figure 5.4a some ideal graphs of $C(p_m)$ are shown as green curves. The blue line is the amount of cases for which Eb09 recorded motion. It would be good to have a single very steep slope at the intersection: low sensitivity to N_{od} is then present.

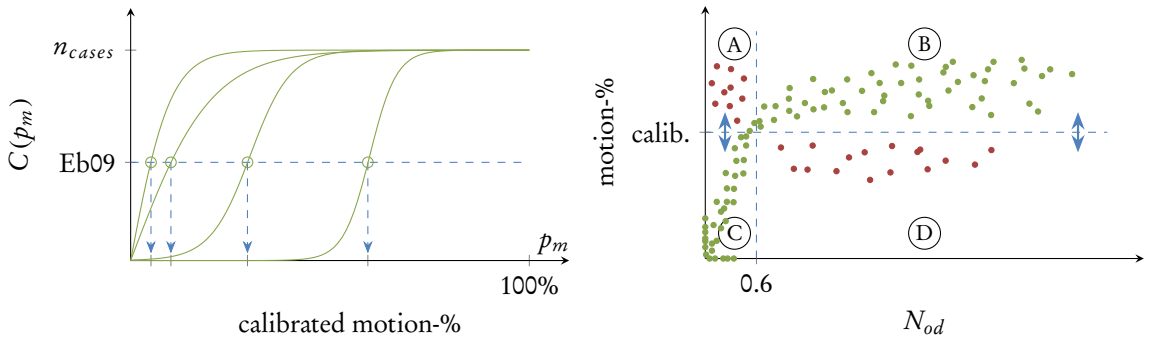

(a) First step

(b) Second step

Figure 5.4: Calibration graphs

A drawback of the first step is that no information is given on whether there is consistency in predicting motion: if many cases with physical motion would be predicted as having immobility, a very dangerous situation is present. In the second step measurements and predictions are compared casewise.

Figure 5.4b shows how the check will be made. All N_{od} and motion percentage combinations are shown as single dots. The green dots together represent an almost ideal situation. Two lines are drawn at the chosen calibration levels. Area B and C contain points in which motion is given equally by formula and measurement. Note that area C mostly contains points created by initial instabilities. For points within area A the motion formula would give an overestimation of motion; area D consequently represents underestimation.

Now with help of the first step a preliminary estimate of the calibrated motion percentage is made. The second step is then used to get best joint equal prediction, i.e. the amount of points in region B and C should be maximized by shifting the horizontal division line.

5.4.3. CALIBRATION RESULTS AND SELECTION

Now it has been discussed what kind of results we would like to get, we will present the values calculated. In figure 5.5 to 5.8 the two calibration graphs are presented for each motion formula.

Izb30 gives reasonably good results. A low sensitivity on N_{od} is present. The first step gives 48%, which is refined to 55% in the second step. The joint equal prediction is then 75%. Unfortunately quite some points exist in region A and C. Moreover the points are grouped closely together, giving quite some sensitivity on joint equal prediction. We can also see that in all cases the Izb30 criterion predicts much instability. This is perhaps due to the measurement level of $1.0D_{n50}$, giving higher velocities than right above the bed.

Ran68a is a reliable formula. It fulfils the requirement in the first step by which 0.03% is found as first estimate. The second step tunes the estimate to 0.1%. A joint equal prediction of 78% is then found. Interesting to see is that there are a lot of points in area C where Ran68a does not predict stone motion. This is a sign that the formula gives a good indication of real stone displacement. Even though a lot of points in area A is found, reliability is considered to be best.

Des04 has high sensitivity to N_{od} according to the first calibration step. 5.5% is taken as a first calibrated value. Unfortunately in the second step one can see a lot of points in area A and D. The formula thus over- and underestimates motion. This might be result of taking the measurement level halfway the water column, since flow velocities are higher there. By tuning the calibration level a joint equal prediction of 72% is found.

Ste14 gives almost random results. Both over- and underestimation of motion is present, with a very curious white area around 60% motion. The first calibration step gives us a calibrated percentage of 38% but sensitivity to N_{od} at this point is very high. Next to the problem with measurement level, as in Des04, the incorrect calculation of turbulence might lead to the nearly random results. A calibrated motion percentage of 37% is maintained, giving a joint equal prediction of 45%.

Pet14 has equal behaviour as Ran68a and is also considered to be reliable. The first estimate gave 0.08%, which was refined to 0.6% in the second step. Joint equal prediction went up to 84%. With this prediction agreement Pet14 performs best of the five motion formulae, even though pressures and stone sizes were estimated.

All together most formulae perform reasonably well in calibration, except for Ste14. Agreement of more than 70% is obtained, which is a sign that the decoupled model approach is capable of predicting stone motion. No perfect prediction is present, though. Overestimation of motion is present in all formulae, but this would not lead to an unsafe design. The undefined or infeasible measurement level for velocities might be a cause. Lower measurement levels might give more reliable results, but as it was shown in section 4.5 flow modelling in the boundary layer right above the toe bed is not reliable either.

Table 5.5 summarizes calibration results. Ran68a and Pet14 are considered as best predictors: they have highest joint equal prediction and a low amount of cases in which motion is underestimated (leading to an insecure design). Furthermore they have very low motion percentages, so almost no calibration is required. This makes them more robust and perhaps more generally applicable. Evaluation of stability methods will be made based on these two formulae.

Izb30 and Des04 perform acceptably good, though more points with over- and underestimation are present. Ste14 is considered as inappropriate due to the incorrect turbulence calculation. Results from these three formulae will be given for reference purposes.

Table 5.5: Calibration results

Motion formula	Motion percentage	Joint equal prediction	Reliability
Izb30	55%	75%	medium
Ran68a	0.1%	78%	high
Des04	8%	72%	medium
Ste14	37%	45%	very low
Pet14	0.6%	84%	high

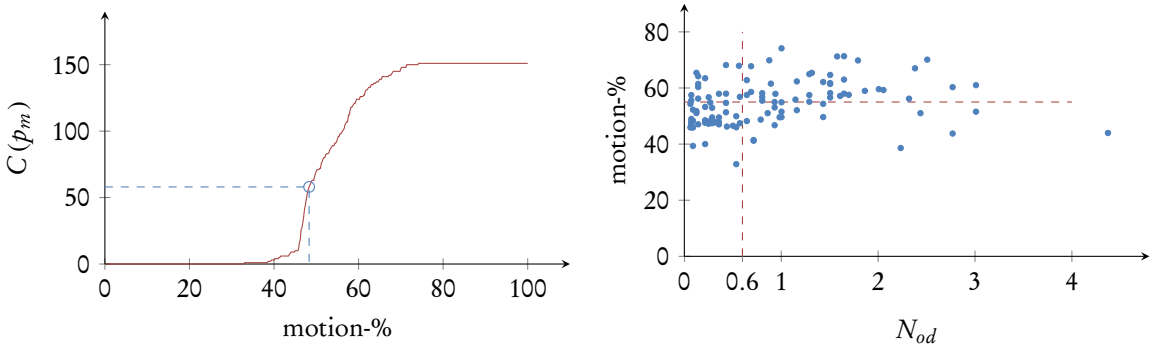

(a) First step (48%)

(b) Second step (55%)

Figure 5.5: Calibration of Izb30

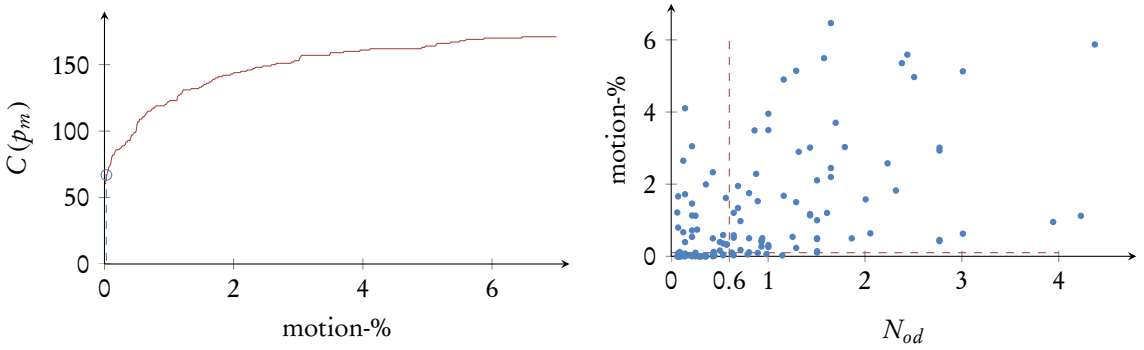

(a) First step (0.03%)

(b) Second step (0.1%)

Figure 5.6: Calibration of Ran68a

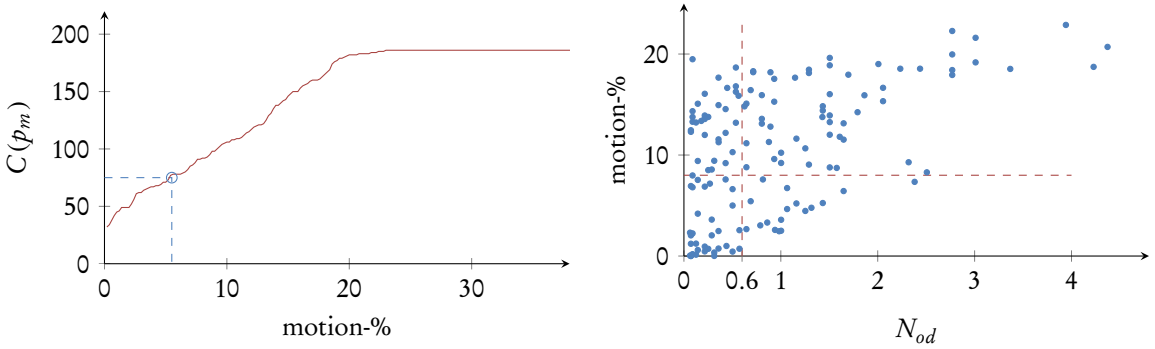

(a) First step (5.5%)

(b) Second step (8%)

Figure 5.7: Calibration of Des04

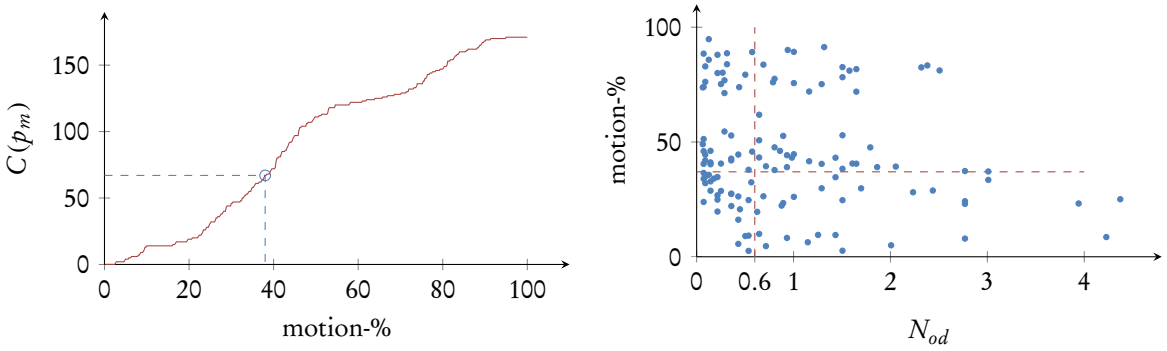

(a) First step (38%)

(b) Second step (37%)

Figure 5.8: Calibration of Ste14

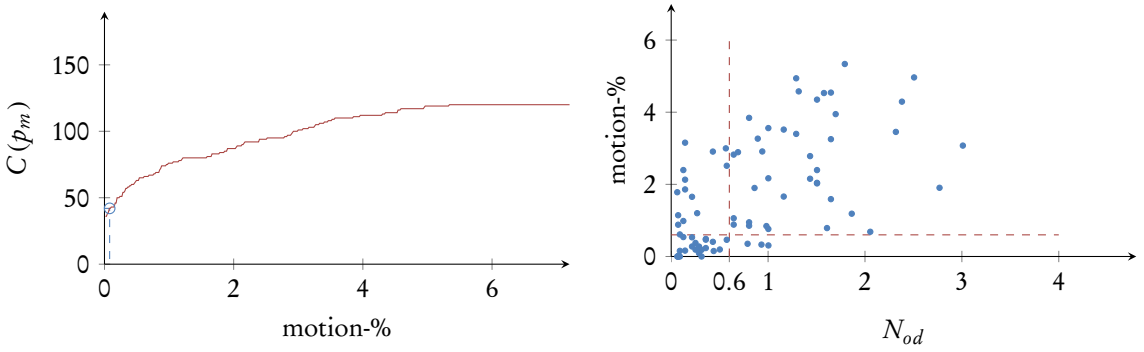

(a) First step (0.08%)

(b) Second step (0.6%)

Figure 5.9: Calibration of Pet14

5.5. Results

5.5.1. Validity

Now calibration has given us the percentages determining motion for the four motion formulae, we can continue evaluation. Motion has been recalculated for all cases and the motion table is constructed. In appendix G the full list is given for reference purposes. Interesting in the motion table is the second last row. It contains for each method and formula the percentage of cases where it is valid. It is repeated here.

Table 5.6: Validity of methods and formulae (excerpt from the motion table)

	VdM91	Ger93a	Bur95	VdM98	Say07	Baa08	Ebb09	Mut13	VGe14	Mut14	Izb30	Ran68a	Des04	Ste14	Pet14
% valid	29%	41%	100%	41%	100%	76%	66%	96%	3%	100%	81%	92%	100%	92%	65%

The validity range is quite low for some cases. Most extreme is VGe14: even after making exception for armour layer slope, the formula is hardly applicable for the Eb09 cases. The validity parameter violating its limits is t_t/h_m, being larger than 0.3 for most cases (i.e. a too low water level above the toe). For Bur95, Say07 and Mut14 no validity limits were imposed, hence the 100%. Pet14 encountered many cases in which measurement level was above the still water level.

5.5.2. Prediction

In table 5.7 main evaluation results are presented. Figure 5.10a and 5.10b give a graphical representation. Average performance is measured over Ran68a and Pet14 only since calibration showed that they are most reliable in determining motion. As somehow expected performance of the motion formulae – given the reliability of the stability methods – is almost equal for Izb30, Ran68a, Des04 and Pet14 (coloured in purple). As expected Ste14 performs much worse.

Bold values show prediction by stability methods compared with Ran68a and Pet14. Best predictors are VdM91, Ger93a and VdM98, but with low joint validity. They have been coloured in blue. Mut13 and Mut14 are reliable as well according to Pet14. Finally Baa08 and Ebb09 are the two worst predictors. For Ebb09 this is surprising since his cases are modelled and high agreement was found during calibration. It is questionable how robust this top three is, since their validity is low and statistical sensitivity accordingly high.

In the second evaluation validity ranges are ignored. The adapted motion table is also given in appendix G. Table 5.8 shows new evaluation results. In general one can conclude that the range of performance values becomes narrower. VdM91, Ger93a and VdM98 are still at the top, but with slightly lower agreement (about 75% instead of 80%). However now VGe14 and Mut14 are joining the top (coloured in orange), something both Ran68a and Pet14 agree upon. VGe14 even has an agreement of 91% with Pet14. Based on these results one could argue that the stability methods have too strict validity limits. Baa08 and Ebb09 are least reliable.

5.5.3. Sensitivity

Before drawing any final conclusions on prediction capacity, results of sensitivity analysis should be reviewed. Table 5.9 shows these results. Note that analysis is performed on the average prediction by Ran68a and Pet14. Combinations where parameters were not changed for that method are left out for readability.

In general sensitivity to the damage parameters chosen is rather low. Mostly a maximum of 5% deviation is found. Exceptions are Ger93a, Mut13 and VGe14. The first two have deviations of up to 8%, which might still be acceptable. Sensitivity of VGe14 is not of interest since only six (3%) valid cases were tested. For the other stability methods we can thus rely on prediction values found in the prediction table.

For situation 7 to 10 critical stability for Ste14 and Des04 is varied. Sensitivity cannot be tested since this analysis is based on Ran68a and Pet14 only. When verified individually it turned out that changing these parameters gave at most 1% difference with the base case.

Sensitivity analysis for the second evaluation (without validity limits) was also performed. Only for VGe14 new interesting information was found: for situation 2 and 3 prediction performance went to 68% and 80% respectively (base performance 77%).

Table 5.7: The prediction table with joint equal prediction percentages. Average is based on Ran68a and Pet14. (Joint validity percentages between parentheses.)

	VdM91	Ger93a	Bur95	VdM98	Say07	Baa08	Ebb09	Mut13	VGe14	Mut14	Performance motion formulae
Izb30	91% (29%)	71% (41%)	60% (81%)	83% (41%)	71% (81%)	45% (69%)	41% (47%)	61% (77%)	67% (3%)	68% (81%)	66% (55%)
Ran68a	**83% (29%)**	**71% (41%)**	**51% (92%)**	**81% (41%)**	**67% (92%)**	**36% (76%)**	**53% (58%)**	**53% (88%)**	**67% (3%)**	**65% (92%)**	**63% (61%)**
Des04	89% (29%)	60% (41%)	70% (100%)	74% (41%)	77% (100%)	49% (76%)	33% (66%)	74% (96%)	67% (3%)	73% (100%)	67% (65%)
Ste14	26% (29%)	58% (41%)	46% (92%)	44% (41%)	28% (92%)	70% (76%)	50% (58%)	47% (88%)	33% (3%)	43% (92%)	45% (61%)
Pet14	**78% (29%)**	**84% (41%)**	**75% (65%)**	**88% (41%)**	**72% (65%)**	**51% (53%)**	**21% (31%)**	**80% (61%)**	**67% (3%)**	**83% (65%)**	**70% (45%)**
Average	**81% (29%)**	**78% (41%)**	**63% (78%)**	**84% (41%)**	**69% (78%)**	**44% (64%)**	**37% (44%)**	**66% (74%)**	**67% (3%)**	**74% (78%)**	

Table 5.8: The prediction table with the equal prediction percentages *with ignored validity ranges*

	VdM91	Ger93a	Bur95	VdM98	Say07	Baa08	Ebb09	Mut13	VGe14	Mut14	Joint validity	Performance motion formulae
Izb30	77%	66%	60%	73%	71%	50%	61%	61%	73%	68%	81%	66%
Ran68a	**64%**	**58%**	**51%**	**68%**	**67%**	**40%**	**66%**	**53%**	**64%**	**65%**	**92%**	**60%**
Des04	86%	76%	70%	80%	77%	59%	52%	73%	79%	73%	100%	72%
Ste14	30%	44%	46%	37%	28%	63%	40%	48%	39%	43%	95%	42%
Pet14	**83%**	**85%**	**75%**	**87%**	**72%**	**56%**	**54%**	**78%**	**91%**	**83%**	**65%**	**76%**
Average	**74%**	**71%**	**63%**	**78%**	**69%**	**48%**	**60%**	**66%**	**77%**	**74%**		

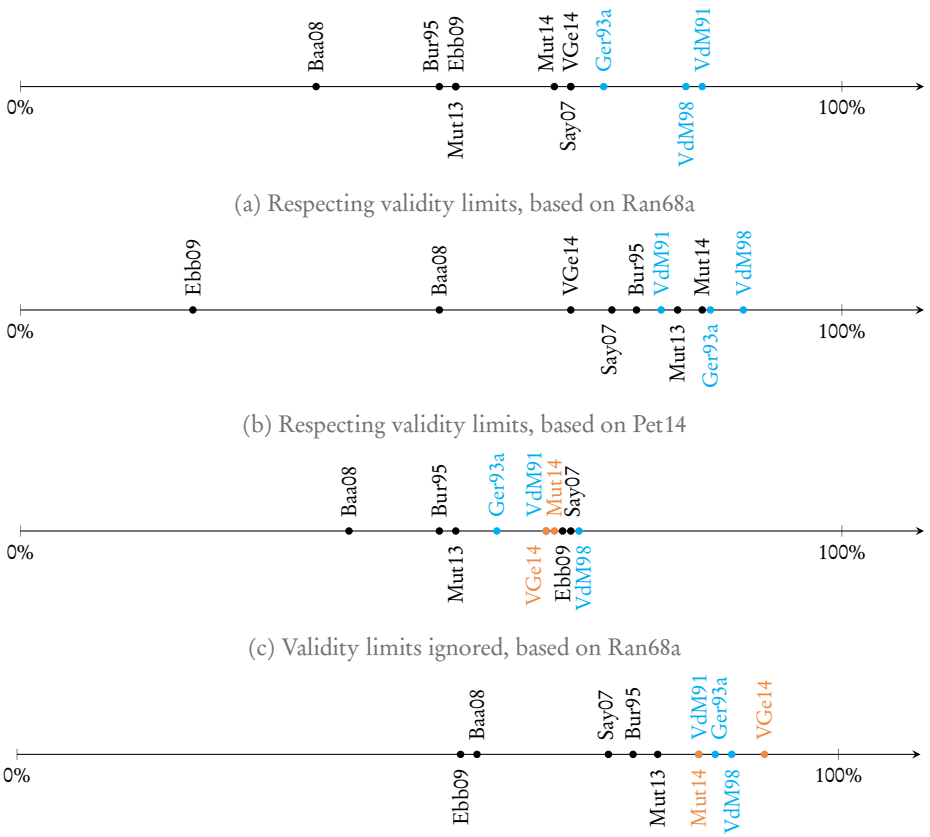

(a) Respecting validity limits, based on Ran68a

(b) Respecting validity limits, based on Pet14

(c) Validity limits ignored, based on Ran68a

(d) Validity limits ignored, based on Pet14

Figure 5.10: Performance of the stability methods

Table 5.9: The sensitivity table with joint equal prediction based on Ran68a and Pet14

		VdM91	**Ger93a**	**Bur95**	**VdM98**	**Say07**	**Baa08**	**Ebb09**	**Mut13**	**VGe14**	**Mut14**
	Base	**81%**	**78%**	**63%**	**84%**	**69%**	**44%**	**37%**	**66%**	**67%**	**74%**
	Validity	29%	41%	78%	41%	78%	64%	44%	74%	3%	78%
Sit. 2	$N_{od,c} \downarrow$		71%	60%	83%					33%	69%
Sit. 3	$N_{od,c} \uparrow$		78%	64%	84%					83%	74%
Sit. 4	$N_{\%,c} \downarrow$							40%	58%		
Sit. 5	$N_{\%,c} \uparrow$							35%	71%		
Sit. 6	$F_S \downarrow$						44%				
Sit. 7	$\Psi_{RS,c} \downarrow$					— Ste14 not reviewed —					
Sit. 8	$\Psi_{RS,c} \uparrow$					— Ste14 not reviewed —					
Sit. 9	$\Psi_{MS,c} \downarrow$					— Des04 not reviewed —					
Sit. 10	$\Psi_{MS,c} \uparrow$					— Des04 not reviewed —					

5.6. SUMMARY

In this chapter toe stability methods are tested on their motion prediction. After modelling the Eb09 cases with IH-2VOF five motion formulae are applied on model output. These formulae were calibrated to give a distinct prediction of motion. Joint equal prediction of the toe stability methods was then calculated and presented.

The calibration *approach* is generally applicable. However without any further verification one cannot be certain that calibration *results* may be applied on other datasets. They are directly linked to the Eb09 cases by hydraulic situation and stone motion definition.

Measurement level for hydraulic conditions is a serious issue. In the calibration process it was clear that all formulae, maybe except for Ran68a and Pet14, suffer from this problem: they overestimate motion due to higher measured velocities. Only Ran68a and Pet14 predicted damage reliably, possibly without necessity of calibration. Izb30 and Des04 do not perform all too bad, though calibration is required and a certain amount of cases is present in which motion is underestimated. Ste14 is considered as inappropriate for this study due to an incorrect turbulence calculation and measurement level issues.

When prediction of motion by Ran68a and Pet14 is compared with the toe stability methods, three formulae give rather good agreement: VdM91, Ger93a and VdM98. Agreement is about 80% for cases for which the formulae are valid. They have a limited validity range though. All three formulae have low sensitivity to their damage number N_{od}. Verified against Pet14 only, Mut13 and Mut14 perform quite good as well. The method VGe14 could not be verified since it was only applicable in 3% of the cases. It is clearly not intended for shallow water conditions. Baa08 and Ebb09 performed worst.

A second evaluation was performed, in which validity limits of the toe stability methods were ignored. VdM91, Ger93a and VdM98 still perform well, but now VGe14 and Mut14 join the top. Agreement is about 75% in average.

Note that the relatively low validity ranges are result of shallow water situations. Recall that 78% of cases used for this evaluation are such. Evaluation results should therefore not be generalized without additional research.

In the Rock Manual (CIRIA et al., 2007) the methods Ger93a and VdM98 are presented in equation 5.187 and 5.188. This manual is widely used by coastal engineers. Fortunately these methods performed relatively good in evaluation, making the constructed breakwaters in the world a bit more trustworthy given the reliability of the decoupled model approach.

Now one can speculate on the value of the evaluation results for design purposes. There are so many summarizing calculations, statistical variations, uncertainties and adaptations required to get the decoupled model approach implemented, that it is highly questionable whether we can rely on the outcome of this evaluation at this stage. In further research aspects of this approach can be investigated further. Interesting routes are:

- Find a better measurement level of hydraulic conditions under wave action
- Develop a new motion formula
- Define a minimum period of subsequent motion indications so that real stone dislocation can be determined
- Verify whether calibration results are generally applicable, so for other damage recordings and other hydraulic conditions
- Evaluate more situations with deep water conditions
- Verify the boundary layer at the toe-fluid interface and, if modelled correctly, check performance of Izb30 on water levels closer to the toe
- Implement a correct turbulence calculation

6

Conclusions and recommendations

Target of this research was to give advice on stability methods for breakwater toe stability. For this the decoupled model approach was applied using numerical model IH-2VOF and general formulae for stone motion. This chapter contains answers to the research questions, general conclusions, recommendations for further studies and a discussion on value of the research outcome.

6.1. Answers to the research questions

This section gives a brief answer to research questions posed in section 1.3. Report sections which answer the questions in detail are appended.

Main research question 1 *Can the IH-2VOF model be used to simulate physical flume experiments on breakwater toe stability?*
The IH-2VOF model is able to determine local hydraulic conditions near the toe. Accuracy is sufficient to determine toe stability. Still some fundamental defects are present, i.e. the broken turbulence calculation and incorrect Forchheimer coefficient definitions in grid generator Coral. Aspects which should be studied in more detail are the high sensitivity to properties of porous media (D_{n50}, porosity, Forchheimer coefficients) and the boundary layer effects. (§4.6)

Main research question 2 *Which existing method on breakwater toe stability gives, using the decoupled model approach and based on calculations with a VOF model, best results for prediction of the threshold of motion?*
The formulae by Van der Meer (1991), Gerding (1993) and Van der Meer (1998) give good agreement with motion prediction by Rance and Warren (1968) and Peters (2014b). Their validity range is small however. When validity limits of all methods are ignored, formulae by Van Gent and Van der Werf (2014) and Muttray et al. (2014) also performed well.
Note that additional verification on turbulence and calibration is recommended before using this answer for design purposes. (§5.6)

Sub-question a *Which are criteria on which VOF models should be evaluated in light of the target of research?*
Four criteria have been defined (§4.2):

- Numerical performance: does the model produce the waves requested?
- Reflection performance: is reflection behaviour of the breakwater similar?
- Local qualitative analysis: how accurate is the local flow pattern modelled?
- Bulk peak velocity analysis: are the maximal flow velocities similar?

Sub-question b *Which formula or method is best to determine whether toe stones will start to displace under influence of the hydraulic load?*
No motion formula is fully suitable for purpose of determining toe stone motion. From ten formulae reviewed

five have been retained: Izbash (1930), Rance and Warren (1968), Dessens (2004), Steenstra (2014) and Peters (2014b). By calibration it was found that Rance and Warren (1968) and Peters (2014b) are most reliable. Possibly they do not require calibration at all. Izbash (1930) and Dessens (2004) also give good agreement but lack a practical definition of flow velocity. Steenstra (2014) was not suitable for this study since turbulence calculation in IH-2VOF is incorrect. (§2.2.4, 5.4)

Sub-question c *How can stability prediction by toe stability methods be transformed into a threshold of motion?*
A critical value is given to the damage parameter in the stability method. Motion occurs when this value is exceeded. Sensitivity of the critical value has been tested. (§5.1, 5.3, 5.5).

Sub-question d *Which are criteria on which toe stability methods should be evaluated in light of the target of research?*
Prediction of motion should be equal to prediction by the motion formulae. Agreement should be as high as possible, preferably with a large number of cases for which the method is valid. (§5.1)

6.2. Conclusions

Many aspects of toe stability modelling have been studied. Per aspect some conclusions are given, together with a reference to relevant report sections.

Numerical modelling with IH-2VOF (general)

- IH-2VOF is a user friendly computational fluid dynamics model. Setting up a case is straightforward and simple visualization of results for a first impression is available. (§3.1, 3.2)
- Grid generator Coral uses incorrect and ambiguous descriptions for the Forchheimer coefficients. By following the recommendations in §3.2.3 this issue can be overcome. (§3.2.3)
- Wall friction and numerical diffusion were not of substantial importance for the models considered in this research. (§3.4)
- Reflection absorption at model boundaries is not perfect. For the model considered 10% of the reflected wave was re-reflected at the wave generator. (§3.4)
- Turbulence modelling in IH-2VOF is not performed, even when the model is requested to do so. (§3.5)
- IH-2VOF produces requested waves in a reliable way. (§4.4)
- IH-2VOF models are sensitive to stone properties (D_{n50}, porosity and Forchheimer coefficients). (§4.6)
- Simulating a large set of cases requires modifications to the model output and is best performed on a set of computers. Parallel computing is not supported. When run on Windows computers each process is best assigned to a single CPU core with high priority. (§I, J)

Numerical modelling of breakwaters with IH-2VOF

- Convergence tests gave the following recommendations for calculation grid layout (§3.3):
  - Use a uniform grid
  - Extend the flume with a minimum length of $2.0L_0$ on seaward side of the structure
  - Use a grid density of $L_0/\Delta x \approx 150$ and $H_s/\Delta y \approx 15$ for a good trade-off between accuracy and computation time
- Under regular waves a partially standing wave pattern is generated in front of a breakwater. According to Scheffer and Kohlhase (1986) and Büsching (2010) this phenomenon also exists under irregular waves. The position of the standing wave envelope, and with that the position of wave gauges, is of major importance when hydraulic conditions are compared quantitatively. (§3.4)
- Linear wave theory with an estimation of shoaling underestimates flow velocities above the toe. This is partly result of non-linear wave effects. (§3.4, 4.1, 4.4)
- Velocity estimation by Van Gent and Van der Werf (2014) overestimates flow velocities above the toe, because it is a deep water approximation. (§4.4)
- The model by Nammuni-Krohn (2009) was simulated with IH-2VOF. The dataset with physical measurements was found to be inappropriate for this research because certain model information required for numerical modelling lacked. Agreement between numerical and physical measurements was low. (§4.4)

- In Peters (2014a) much better agreement was found between IH-2VOF and physical measurements, than for the Nammuni-Krohn (2009) measurements. This is because Peters measured parameters required for numerical modelling in detail. (§4.5)
- A distinct boundary layer is present on the interface between fluid and solids/porous media. Within this boundary layer it is questionable whether hydraulic conditions are reliable. (§4.4, 4.5)

Decoupled model approach

- The decoupled model approach, which determines toe stability in two steps by calculating local hydraulic conditions at the toe, is appropriate for toe stability. It is capable to predict stone motion for the Ebbens (2009) cases with an accuracy up to 84%. (§1.2.2, 2.1, 5.4, 5.6)
- Major advantage of the decoupled model approach is the ability of modelling other breakwater geometries and sea states than those which are accounted for in classical toe stability methods. (§1.2.2)
- Determining a threshold of motion is presumably the only way how historical toe stability tests can be compared, since damage definitions and counting methods are unlike. (§1.2, 2.2.4)
- No general formula for stone motion was found which is perfectly applicable for toe stability, except for Peters (2014b). Wave action is often not accounted for or flow velocity measurement is not feasible. Peters' formula on the other hand requires detailed information on stone dimensions. (§2.2.4, 5.3, 5.4)
- Calibration of motion formulae is possible by comparing numerical prediction with original damage measurements in the lab. The approach is generally applicable, though current knowledge implies that recalibration of formulae to each new dataset is mandatory. The motion formulae by Rance and Warren (1968) and Peters (2014b) probably do not need calibration and are therefore interesting for design purposes. (§5.4)
- Large scatter in motion prediction by the motion formulae is present. Toe stability is a stochastic process. (§5.4)

Toe stability methods

- No reliable conclusions on the toe stability methods can be drawn without any further verification of the impact of the incorrect turbulence calculation in IH-2VOF.

The conclusions hereafter are applicable under the assumption that turbulence is not of large importance in toe stability. The motion formula by Steenstra (2014) was not suited for this research since it requires information on turbulence. (§3.5)

- The toe stability methods have been tested against the Ebbens (2009) cases. In 78% of cases modelled shallow water was present, i.e. $H_s/h_m \geqslant 0.5$. (§5.2)
- The motion formulae by Rance and Warren (1968) and Peters (2014b) give on average similar results for the performance of toe stability methods. (§5.5)
- When respecting validity limits of the toe stability methods, the formulae by Van der Meer (1991), Gerding (1993) and Van der Meer (1998) give good agreement with motion prediction by Rance and Warren (1968) and Peters (2014b). The validity range is however small. (§5.5)
- When ignoring validity limits of the toe stability methods, methods from previous point still perform well. Also Van Gent and Van der Werf (2014) and Muttray et al. (2014) give good agreement with prediction by the decoupled model approach. Validity ranges of current toe stability methods might therefore be too strict. (§5.5)
- Sensitivity to the damage parameters is generally low, giving less than 5% deviation in performance prediction. Gerding (1993), Muttray (2013) and Van Gent and Van der Werf (2014) are more sensitive, up to 10% deviation. (§5.5)

6.3. Discussion

In this research an effort is made to determine toe stability using the decoupled model approach. Many problems had to be solved, mostly arising from non-complementary research or incomplete model descriptions. One should certainly be cautious when conclusions above are used for design purposes. On the other hand motion was predicted successfully with agreement of more than 70%. What then is the value of the DMA for design purposes?

Stone stability and damage Stability prediction was done in terms of motion rather than an amount of damage. For design purposes often the first is more suitable since clients tend to choose a conservative design, i.e. no motion may be present. A toe structure consists of a small amount of stones, so when one stone is removed out of the toe the situation may already become dangerous. Motion is also a more comprehensible and practical measure for non-experts.

One may question the utility of a damage parameter. Motion is initiated when certain hydraulic conditions are present. The longer the conditions are present, the more stones can displace. This process however is highly dependent on exact stone dimensions, wave variation and duration of the conditions. This is an issue which is not studied in detail in historical research – one often tests for a 'design' storm of 1000 waves. In numerical research this time dependency is not modelled either. A threshold of motion is then a more practical and less time dependent measure than a cumulative damage parameter. The subjectivity on the exact threshold is probably a minor problem for toe structures.

Decoupled model approach Regarding results of the DMA it seems that the approach yields reasonable results, despite all estimations and limitations. Performance is in the range of 70 – 90% — it could have been much worse. This is an indicator that the DMA is suitable for further use. Moreover it provides a method to verify toe stability in complex breakwater geometries. For design purposes a stability method consisting of one or more formulae would be preferable though. This is useful for conceptual design to get a first insight into stability, without the need for a time-consuming numerical model.

An additional problem encountered was sensitivity of IH-2VOF to stone properties. For real-life breakwaters it is difficult to determine accurately all properties required for a numerical model. On the other hand it shows that stone properties have influence on local hydraulic conditions, and with that on toe stability. This influence is not accounted for in current stability methods, making them possibly incomplete in representation of physical processes involved. Further research should verify relative importance of stone properties for toe stability.

Decoupled model approach in practice Does a lack of detailed information on stone properties imply that the DMA cannot be used for design purposes? Probably not. In practice a certain breakwater layout is often tested with a physical model. On beforehand the DMA can assist in conceptual design and benchmarking. For instance an engineer could design a couple of breakwater layouts and test them using IH-2VOF. Complex geometries can be accounted for. Keeping wave climate and grid definition constant between layouts is recommended. Model output is then transformed into a prediction of stone motion with the formulae by Rance and Warren (1968) and Peters (2014b), which possibly do not require calibration. Also deep water conditions might change calibration results. Note that it is advised to verify this behaviour in further research.

Calibration also provides a tool to get higher safety. By shifting the calibrated motion percentage in such way that the amount of underestimations of motion is reduced to an acceptable amount, say e.g. 5%, one can benchmark toe stability methods for a more safe design. In other words one should take the calibrated motion percentage low enough so that area D in figure 5.4b is almost empty. A drawback of this approach is that the outcome is still linked to the Ebbens cases.

In an ideal situation one should be able to use the DMA with a numerical model to create a new stability method without requirement of physical flume test (perhaps except for calibration purposes). Much larger validity ranges can then be explored, something which is highly desirable for designs purposes. With more detailed numerical models and more appropriate motion formulae this ideal situation may perhaps be reached in the future.

6.4. Recommendations

For further research a couple of recommendations are given hereafter. They intend to give more insight in toe stability with use of the decoupled model approach. At this time not all suggestions are feasible by practical limitations, though it is expected that it will be achievable in the near future.

- Repair the turbulence calculation in IH-2VOF or find an other suitable computational fluid dynamics model.
- Obtain better estimations for the Forchheimer coefficients.

- Find or derive a more suitable formula for motion, or improve current formulae.
- Calibrate motion formulae on other datasets, preferably with deep water situations. Compare them with current calibration results to discover whether calibrated motion percentages are universally applicable in toe stability and whether Rance and Warren (1968) and Peters (2014b) do not require calibration.
- Model other toe stability tests (e.g. Gerding (1993), Docters van Leeuwen (1996) and Van Gent and Van der Werf (2014)) to study performance of the toe stability methods in these cases.
- Investigate reliability of hydraulic conditions in the boundary layer as modelled by IH-2VOF.
- Use a 3D-model in which single stones are modelled. This is interesting since the toe structure often consists of a small amount of stones. Statistical research on stability of these stones is then possible.
- Verify where and how long the stability criterion of the motion formulae is exceeded.
- Obtain insight in the influence of certain model and structure parameters on stability.

An integrated study towards toe stability is maybe the most interesting step forward in toe stability research. It would comprise physical flume tests to calibrate motion, numerical modelling of these tests and the derivation of a (new) formula for motion of single stones under wave action. By this one can calibrate the numerical model and use it to explore a large number of breakwater layouts and sea states. A new toe stability method might then be obtained.

References

Arets, K. (2013). 'Modellering van de stroomsnelheid bij de teen van een golfbreker'. Bachelor's thesis. Delft University of Technology. URL: http://resolver.tudelft.nl/uuid:5483d5a9-f03b-401d-a913-2838c2711407.

Baart, S. A. (2008). 'Toe structures for rubble mound breakwaters'. Master's thesis. Delft University of Technology. URL: http://dx.doi.org/10.4233/uuid:1eceacb8-23c8-48ff-9cec-772434559b00.

Baart, S. A., Ebbens, R. E. et al. (2010). 'Toe rock stability for rubble mound breakwaters'. In: *Proceedings of the 32nd International Conference on Coastal Engineering, ICCE 2010*. ASCE - Texas Digital Library. URL: http://resolver.tudelft.nl/uuid:2532b50a-4fe4-442e-aa96-412c85477119.

Brodtkorb, P. A., Johannesson, P. et al. (2000). 'WAFO - A Matlab toolbox for analysis of random waves and loads'. In: *Proceedings of the 10th International Offshore and Polar Engineering Conference*. Seattle, USA, pages 343–350. URL: http://www.kennisbank-waterbouw.nl/. Related work: WAFO-group. *WAFO - A matlab toolbox for analysis of random waves and loads*. Math. Stat., Center for Math. Sci., Lund University. Lund, Sweden, 2000. URL: http://www.maths.lth.se/matstat/wafo/index.html.

Bruun, P., editor (1985). *Design and construction of mounds for breakwaters and coastal protection*. Amsterdam, The Netherlands: Elsevier. ISBN: 978-0-444-60045-5.

Burcharth, H. F. and Liu, Z. (1995). 'Rubble mound breakwater failure modes'. In: *Proceedings of the Final (MAS-CT92-0042) Workshop: Rubble mound failure modes*. Sorrento, Italy. URL: http://vbn.aau.dk/en/publications/rubble-mound-breakwater-failure-modes(0199c909-85d1-49f7-b226-9040574e3b15).html.

Büsching, F. (2010). 'Phase jump due to partial reflection of irregular water waves at steep slopes'. In: *Proceedings of the 3rd International Conference on the Application of Physical Modelling to Port and Coastal Protection (Coastlab'10)*. Barcelona, Spain: IAHR. URL: http://www.digibib.tu-bs.de/?docid=00047044.

CERC (1984). *Shore Protection Manual*. 4th edition. USACE, Washington DC. URL: http://resolver.tudelft.nl/uuid:98791127-e7ae-40a1-b850-67d575fa1289.

CIRIA, CUR and CETMEF (2007). *The Rock Manual. The use of rock in hydraulic engineering*. 2nd edition. CIRIA, London.

Dessens, M. (2004). 'The influence of flow acceleration on stone stability'. Master's thesis. Delft University of Technology. URL: http://resolver.tudelft.nl/uuid:17f63722-b650-4207-b71d-1ef657f75a0b.

Docters van Leeuwen, L. (1996). 'Toe stability of rubble-mound breakwaters'. Master's thesis. Delft University of Technology. URL: http://resolver.tudelft.nl/uuid:d8b9924f-2109-44e6-b6fd-24f93eadfa63.

Ebbens, R. E. (2009). 'Toe structures of rubble mound breakwaters'. Master's thesis. Delft University of Technology. URL: http://resolver.tudelft.nl/uuid:04a06a0a-c790-4fac-9b8e-d3508b3e7762.

Eckert, J. W. (1983). 'Design of toe protection for coastal structures'. In: *Coastal Structures '83*. Edited by J. R. Weggel. Arlington, Virginia, USA: ASCE, New York, pages 331–341.

Gerding, E. (1993). 'Toe structure stability of rubble mound breakwaters'. Master's thesis. Delft University of Technology. URL: http://resolver.tudelft.nl/uuid:51af1788-de9f-4ef3-8115-ffefb2e26f76.

Goda, Y. (2010). *Random seas and design of maritime structures*. 3rd edition. Volume 33. Advanced Series on Ocean Engineering. Singapore: World Scientific. ISBN: 978-981-4282-39-0.

Gravesen, H. and Sørensen, T. (1977). 'Stability of rubble mound breakwaters'. In: *Proceedings of the 24th International Navigation Congress, PIANC*. Leningrad, Russia.

Hoan, N. T. (2008). 'Stone stability under non-uniform flow'. PhD thesis. Delft University of Technology. URL: http://resolver.tudelft.nl/uuid:fbf294c2-0cae-4a04-8dac-d07e051a6081.

Hofland, B. (2005). 'Rock & roll: Turbulence-induced damage to granular bed protections'. PhD thesis. Delft University of Technology. URL: http://resolver.tudelft.nl/uuid:90796c07-7666-4550-b73b-2b8f70057768.

Holthuijsen, L. H. (2007). *Waves in Oceanic and Coastal Waters*. New York: Cambridge University Press. ISBN: 978-0-521-12995-4.

Hovestad, M. (2005). 'Breakwaters on steep foreshores'. Master's thesis. Delft University of Technology. DOI: 10.4233/uuid:d528450c-5941-4cf3-addc-29e33be28818.

Hsu, T.-J., Sakakiyama, T. and Liu, P. L.-F. (2002). 'A numerical model for wave motions and turbulence flows in front of a composite breakwater'. In: *Coastal Engineering* 46, pages 25–50. DOI: 10.1016/S0378-3839(02)00045-5.

IH Cantabria (2012). *IH-2VOF Course and Manual*. Santander, Spain.

Jongeling, T. H. G., Blom, A. et al. (2003). *Ontwerpmethodiek granulaire verdedigingen*. Technical report. Delft, The Netherlands: WL|Delft Hydraulics. URL: http://resolver.tudelft.nl/uuid:e1f172c7-eeeb-42cf-bb66-26eb6494c5de.

Lara, J. L., Losada, I. J. et al. (2011). 'Breaking solitary wave evolution over a porous underwater step'. In: *Coastal Engineering* 58, pages 837–850. DOI: 10.1016/j.coastaleng.2011.05.008.

Lin, P. and Liu, P. L.-F. (1999). 'A numerical study of breaking waves in the surf zone'. In: *Journal of Fluid Mechanics* 359, pages 239–264. DOI: 10.1017/S002211209700846X.

Liu, P. L.-F., Lin, P. et al. (1999). 'Numerical modelling of wave interaction with porous structures'. In: *Journal of Waterway, Port, Coastal, and Ocean Engineering* 125 (6), pages 322–330. DOI: 10.1061/(ASCE)0733-950X(1999)125:6(322).

Markle, D. G. (1989). *Stability at toe berm armor stone and toe buttressing stone on rubble-mound breakwaters and jetties*. Technical report. Washington, DC: US Army Corps of Engineers. DOI: 10.5962/bhl.title.48211.

Muttray, M. (2013). 'A pragmatic approach to rock toe stability'. In: *Coastal Engineering* 82, pages 56–63. DOI: 10.1016/j.coastaleng.2013.08.002.

Muttray, M., Reedijk, B. et al. (2014). 'Investigations on quarry stone toe berm stability'. In: *Coastal Engineering, Proceedings of 34th Conference on Coastal Engineering*. Seoul, Korea. DOI: 10.9753/icce.v34.structures.77.

Nammuni-Krohn, J. (2009). *Flow velocity at rubble mound breakwater toes*. Additional Master's thesis. Delft University of Technology. DOI: 10.4233/uuid:fe20c5e2-051e-45fe-aaa5-aac0bb113e18.

Peters, R. B. M. (2014a). *Evaluation of the IH2VOF model for modelling of hydraulic properties near breakwater toes*. Additional Master's thesis. Delft University of Technology. DOI: http://resolver.tudelft.nl/uuid:db75aaec-074f-4fd0-97f0-ede53bad9a4d.

Peters, R. B. M. (2014b). 'Stone stability in breakwater toes based on local hydraulic conditions'. Master's thesis. Delft University of Technology. DOI: 10.4121/uuid:4eb8d0ae-53e6-4914-b241-7b53a04169ea.

Rance, P. J. and Warren, N. F. (1968). 'The threshold of movement of coarse material in oscillatory flow'. In: *Proceedings of the 11th Conference on Coastal Engineering*. London, United Kingdom, pages 487–491. URL: https://journals.tdl.org/icce/index.php/icce/article/view/2533.

Sayao, O. J. (2007). 'Toe protection design for rubble mound breakwaters'. In: *Proceedings of the Coastal Structures Conference*. Venice, Italy. URL: http://www.kennisbank-waterbouw.nl/.

Scheffer, H.-J. and Kohlhase, S. (1986). 'Reflection of irregular waves at partially reflective structures including oblique wave approach'. In: *Coastal Engineering, Proceedings of the 20th Conference on Coastal Engineering*. Taipei, Taiwan: ASCE, New York. Chapter 162, pages 2203–2211. URL: https://journals.tdl.org/icce/index.php/icce/article/view/4163.

Schiereck, G. J. and Fontijn, H. L. (1996). 'Pipeline protection in the surf zone'. In: *Coastal Engineering, Proceedings of the 25th Conference on Coastal Engineering*. Orlando, Florida, USA: ASCE, New York. Chapter 327, pages 4228–4241. URL: https://journals.tdl.org/icce/index.php/icce/article/view/5543.

Schiereck, G. J. and Verhagen, H. J. (2012). *Introduction to bed, bank and shore protection*. 2nd edition. Delft, The Netherlands: VSSD.

Schoemaker, H. J. and Thijsse, J. T. (1949). 'Investigation of the reflection of waves'. In: *Proceedings of the 3rd IAHR World Congress*. Grenoble, France. URL: http://resolver.tudelft.nl/uuid:2faff62a-c38c-4ed7-83a7-ca08ad93a461.

Shields, A. (1936). 'Anwendung der Aehnlichkeitsmechanik und der Turbulenzforschung auf die Geschiebebewegung'. PhD thesis. Berlin, Germany. URL: http://resolver.tudelft.nl/uuid:a66ea380-ffa3-449b-b59f-38a35b2c6658.

Sleath, J. F. A. (1978). 'Measurements of bed load in oscillatory flow'. In: *Journal of the Waterway Port Coastal and Ocean Division* 104, pages 291–307.

Steenstra, R. S. (2014). 'Incorporation of the effects of accelerating flow in the design of granular bed protections'. Master's thesis. Delft University of Technology. DOI: http://resolver.tudelft.nl/uuid:60aa407c-0e87-46b6-97bc-34c0fe3a6183.

Technical Committee CSB/17 (1991). *British Standard 6349. Maritime structures. Part 7: Guide to the design and construction of breakwaters*. United Kingdom: BSI. ISBN: 978-0-580-69608-4.

Van den Bos, J., Verhagen, H. J. et al. (2014). 'Towards a practical application of numerical models to predict wave-structure interaction: an initial validation'. In: *Proceedings of the 34th Conference on Coastal Engineering*. DOI: 10.9753/icce.v34.structures.50.

Van den Heuvel, H. P. A. (2013). 'The effect of multiple storms on the stability of near-bed structures'. Master's thesis. Delft University of Technology. URL: http://resolver.tudelft.nl/uuid:e8e20512-eb3a-40e5-a1a6-ab0af4833aa3.

Van der Meer, J. W. (1998). 'Geometrical design of coastal structures'. In: *Dikes and Revetments*. Edited by K. W. Pilarczyk. Balkema, Rotterdam. Chapter 9, pages 161–175. URL: http://books.google.com/books?id=VJhTkRoCbGsC.

Van der Meer, J. W., d'Angremond, K. and Gerding, E. (1995). 'Toe structure stability of rubble mound breakwaters'. In: *Proceedings of the Advances in Coastal Structures and Breakwaters Conference*. Thomas Telford, London, pages 308–321. URL: http://books.google.com/books?id=2vaHgOuUEtIC.

Van Gent, M. R. A. (1995). 'Wave interaction with permeable coastal structures'. PhD thesis. Delft University of Technology. URL: http://resolver.tudelft.nl/uuid:7bbff8e4-215d-4bfc-a3af-51cdecb754bd.

Van Gent, M. R. A. and Van der Werf, I. M. (2014). 'Rock toe stability of rubble mound breakwaters'. In: *Coastal Engineering* 83, pages 166–176. DOI: 10.1016/j.coastaleng.2013.10.012.

WAFO-group (2000). *WAFO - A matlab toolbox for analysis of random waves and loads*. Math. Stat., Center for Math. Sci., Lund University. Lund, Sweden. URL: http://www.maths.lth.se/matstat/wafo/index.html.

Zanuttigh, B. and Van der Meer, J. W. (2007). 'Wave reflection from composite slopes'. In: *Proceedings of the Coastal Structures Conference*. Venice, Italy. URL: http://www.kennisbank-waterbouw.nl/.

Zelt, J. A. and Skjelbreia, J. E. (1992). 'Estimating incident and reflected wave fields using an arbitrary number of wave gauges'. In: *Coastal Engineering, Proceedings of the 23rd International Conference on Coastal Engineering*. Venice, Italy: ASCE, New York, pages 777–789. URL: https://journals.tdl.org/icce/index.php/icce/article/view/4736.

List of symbols

Common indices and mathematical symbols

Symbol	Description
x_b	Value measured at or near the bed level
x_{cr}, x_c	Critical value for x
x_{dr}	Value for wave run-down (downrush)
x_g	Measurement level (gauge level)
x_i	Value for the incoming wave
x_i, x_j	Value in a certain dimension (Einstein notation)
x_m	Mean value
x_{m0}	Based on the zeroth order moment of the wave spectrum
x_{m01}	Based on the zeroth and first order moment of the wave spectrum
$x_{m-1,0}$	Based on the first negative and zeroth order moment of the wave spectrum
x^n	Value at time step n
x_p	Peak value of x
x_r	Value for the reflected wave
x_{rr}	Value for the re-reflected wave
x_s	Significant, or based on H_s
x_t	Value measured at the toe
x_0	Value measured in deep water/offshore
x_{0m}	Mean value measured in deep water
$x_{\#\%}$	Value that is exceeded by #% of the values in a dataset
$\bar{x}$	Mean value of x, often time-averaged
$\hat{x}$	Amplitude of x
$\tan^{-1}\alpha$	Denotes a slope of 1:$\tan^{-1}\alpha$ (V:H); $\tan^{-1}\alpha \equiv \cot\alpha$
$\propto$	Proportional to

Roman symbols

Symbol	Unit	Description
a	m	1. Wave amplitude
	m/s^2	2. Flow acceleration in space, $a \equiv u\frac{\partial u}{\partial x}$
	s/m	3. Forchheimer coefficient (linear contribution)
A_e	m^2	Eroded area, in Van Gent and Van der Werf (2014)
A_f	m^2	Frontal stone area, in Peters (2014b)

Symbol	Unit	Description
b	s^2/m^2	Forchheimer coefficient (turbulent contribution)
B_t	m	Toe width (measured along wave ray)
c	m/s	1. Wave celerity or phase speed, $c \equiv L/T$
	s^2/m	2. Forchheimer coefficient (added mass contribution)
c_g	m/s	Group velocity of a wave
C_B	-	Bulk coefficient for drag and turbulence, in Dessens (2004)
C_d	-	Empirical coefficient for the eddy viscosity
C_D	-	Drag coefficient, in Peters (2014b)
$C_{m:b}$	-	Coefficient for turbulence and acceleration, in Steenstra (2014)
C_M	-	Inertia coefficient, in Dessens (2004)
C_{PF}	-	Factor to account for porous flow, in Baart (2008)
$C(p_m)$	-	Amount of valid cases with motion percentage lower than p_m
d	m	1. Water depth
	m	2. Stone diameter
D_{n50}	m	Median nominal (rock) diameter
$E(f)$	$m^2 s$	Variance density spectrum
f	Hz	Frequency
f_B	-	Correction factor for toe damage, in Van Gent and Van der Werf (2014)
F_S	-	Safety factor, in Baart (2008)
F	N	Force on stone, in Peters (2014b)
g	m/s^2	Gravitational acceleration
h	m	Water depth
h_a	m	Level where the advective acceleration should be measured, in Steenstra (2014)
h_f	m	Flume height
h_m	m	Mean water depth in front of the toe
h_t	m	Water depth above the toe
H	m	Wave height
i	-	Head gradient over the toe, in Baart (2008)
I	-	Forchheimer pressure gradient
k	m^{-1}	1. Wave number, $k \equiv 2\pi/L$
	m^2/s^2	2. Turbulence intensity
$K(\beta)$	-	Correction factor for the bed slope, in Steenstra (2014)
KC	-	Keulegan-Carpenter number
K_r	-	Reflection coefficient, $K_r \equiv H_i/H_r$
K_{sh}	-	Shoaling coefficient, $K_{sh} = a_t/a_0$
L	m	1. Wave length
	m	2. Toe length (measured along wave crest)
L_f	m	Flume length
L_m	m	Bahkmetev mixing length, $L_m = \kappa \cdot y\sqrt{1 - y/h}$, in Steenstra (2014)

Symbol	Unit	Description
L_{TA}	m	Distance determining φ_{TA}, in Baart (2008)
m	-	Foreshore slope, in Sayao (2007) and Muttray et al. (2014)
$m_{\#}$		#'th order moment of the wave spectrum. Unit depends on the order.
$m_y(x)$		Envelope of a wave record $y(x,t)$, taken over the extrema in time, $m_y(x) \equiv \max_t \{y(x,t)\}$
$M_{\#}$	kg	Mass of the element that is exceeded by #% of the elements
n	-	Porosity, volume of voids divided by total volume
n_t	-	Toe front slope, in Muttray et al. (2014)
n_x	-	Number of grid cells in x-direction (horizontally)
n_y	-	Number of grid cells in y-direction (vertically)
N	-	1. Number of displaced toe elements
	-	2. Number of waves
N_{od}	-	Damage parameter, standardized number of displacements
N_{odB}	-	Damage parameter including toe width, in Baart (2008)
N_s	-	Stability number, $N_s \equiv H_s/\Delta D_{n50}$
$N_{\%}$	-	Percentual damage parameter (definition varies)
o	m	Moment lever arm, in Peters (2014b)
p	Pa	Pressure
p_m	-	Motion percentage
P	-	Notional permeability factor
R^2	-	Coefficient of determination
R_d	m	Wave run-down, in Baart (2008)
R_u	m	Wave run-up, in Baart (2008)
s	-	Wave steepness, $s \equiv H/L$
S	-	Damage parameter based on erosion profile, in Van Gent and Van der Werf (2014)
t	s	Time
t_b	m	Bedding layer thickness
t_{end}	s	End time of the simulation (model time)
t_t	m	Toe thickness, measured above mean bed level
T	s	Wave period
$\hat{u}_\delta$	m/s	Characteristic velocity amplitude at the toe, in Van Gent and Van der Werf (2014)
u	m/s	1. Velocity (no direction defined)
	m/s	2. Horizontal flow velocity
v	m/s	1. Velocity (no direction defined)
	m/s	2. Vertical flow velocity
V	m^3	Volume
x	m	Horizontal coordinate, various definitions
y	m	Vertical coordinate, various definitions
z	m	Vertical coordinate, various definitions

GREEK SYMBOLS

Symbol	Unit	Description
α	rad	1. Steepness of a slope (armour/foreshore/toe), $1 : \tan^{-1}\alpha$
	-	2. Turbulence magnification factor, in Steenstra (2014)
	-	3. Parameter in the Forchheimer a-coefficient; called *linear friction coefficient* in Coral
β_c	-	Parameter in the Forchheimer b-coefficient; called *non-linear friction coefficient* in Coral
γ	-	1. Breaker index, $\gamma \equiv H/h$
	-	2. JONSWAP peak-enhancement factor
	-	3. Parameter in the Forchheimer c-coefficient; incorrectly called *added mass coefficient* in Coral
γ_{dr}	-	Coefficient for wave run-down, in Baart (2008)
γ_{fore}	-	Correction factor for foreshore steepness, in Baart et al. (2010)
Γ	-	Fit coefficient, in Baart (2008)
δ_{ij}	-	Kronecker delta
Δ	-	1. Relative density, $\Delta \equiv \rho_s/\rho_w - 1$
	-	2. Difference
Δx	m	Grid cell width (horizontal dimension)
Δy	m	Grid cell height (vertical dimension)
ε	m^2/s^3	Turbulent dissipation rate
η	m	Surface elevation
κ	-	Von Kármán constant, $\kappa = 0.41$
ν	m^2/s	Kinematic viscosity of water
ν_t	m^2/s	Eddy (turbulent) viscosity
ξ	-	Surf similarity number or Iribarren number, $\xi \equiv \tan\alpha/\sqrt{s}$
ρ_s	kg/m^3	Density of stones or sediment
ρ_w	kg/m^3	Density of water
σ		Standard deviation of a dataset
τ	N/m^2	Shear stress
φ_L	rad	Phase difference between incoming and reflected wave, due to flume length
φ_S	rad	Phase difference between incoming and reflected wave, due to the structure
φ_{TA}	rad	Phase difference due to wave run-down, in Baart (2008)
Φ	-	Dimensionless transport parameter
Ψ	-	Dimensionless stability parameter. Ψ_{MS} in Dessens (2004), Ψ_{RS} in Steenstra (2014).
ω	Hz	Wave period, $\omega \equiv 2\pi/T$

Descriptions are partly based on Schiereck and Verhagen (2012) and CIRIA et al. (2007).
For motion formulae in section 2.2.4 which have not been retained, their particular symbols are not shown above. They were already described in that section.

List of terms

Acoustic Doppler Velocimeter (ADV) A measurement device that makes use of the Doppler shift effect to measure flow velocities at a certain point. Nammuni-Krohn used ADVs in her research.

Computation time/duration Real-world time it takes a computer to perform its modelling tasks.

Computer cluster A 'computer cluster' or 'cluster computing system' consists of several linked computers which together form a powerful system. Computation speed is heavily increased by executing tasks in parallel.

Damage parameter Parameters in stability methods expressing the amount of damage, i.e. the amount of moved rock. Typical examples are N_{od} and $N_{\%}$.

Decoupled model approach (DMA) Approach for toe stability applied in this research. It uses local hydraulic conditions above the toe bed to decouple wave and structure properties from stone stability. Also see §1.2.2.

Empirical curve fitting approach (ECFA) Approach for toe stability which uses experimental models and curve fitting methods. Also see §1.2.2.

Envelope An envelope is a curve that connects all extrema of a signal. The extrema can be measured in any dimension, but often time is taken. The dataset is then reduced with this dimension.

Graphical user interface (GUI) Part of a computer program that interacts with the user by means of visual elements rather than with pure text or code. Common elements are e.g. buttons and text fields.

Grid A 'grid' or 'mesh' divides a certain space into smaller cells. It is required for numerical modelling, since governing equations are applied per grid cell.

Mesh See 'grid'.

Model time/duration Time scale of the computed model.

Motion formula A formula which gives information on stone stability in general situations. Examples are the formulae by Rance and Warren (1968) or Dessens (2004).

Moving average (filter) A signal filtering technique that uses averaging over a certain subset of data. For each new point the subset is taken around that point.

Numerical diffusion A process in numerical calculations where energy is diffused faster than what would happen in reality.

Reynolds-averaged Navier-Stokes (RANS) equations A particular set of equations describing fluid motion.

Shoaling The process in which a wave becomes higher when it moves from deep to shallow water.

Spectrum A 'wave spectrum' or 'variance density spectrum' represents distribution of wave energy over different frequencies in an irregular wave record. The JONSWAP spectrum is a standardized spectrum of the wave climate in the North Sea.

Stability method A single or multiple formulae together which determine whether a breakwater toe structure is stable under the prevailing wave climate. Examples are the formulae by Gerding (1993) or Muttray (2013).

Stability number The dimensionless $N_s = H_s/\Delta D_{n50}$ value for breakwater stone stability. The stability number implies that higher values of N_s allow for smaller or lighter stones under equal wave attack.

Stability parameter The typical dimensionless parameter Ψ in motion formulae. It is often related to transport parameter Φ.

Uniform flow Flow in which acceleration in *space* is zero. Not to be confused with stationary flow, in which acceleration in *time* is zero.

Validity range/limits Limits set to parameters of a certain formula. They define the range of parameters for which the formula may be used.

Velocity profile A graphical representation of flow velocity along a certain cross-section. One axis follows the cross-section, the other gives the velocity.

Volume of fluid (VOF) A method in numerical fluid modelling by which the free surface can be determined.

Appendices

A

Diagram of historical research

On the following page a diagram of historical research can be found. This diagram displays in a chronological order how research and experiments are related. Blue boxes are papers, theses and other reports; green boxes are physical experiments conducted.

The left branch of the graph contains the empirical curve fitting approach, as described in section 1.2.2. The right branch contains research based on the decoupled model approach. Central on the graph commonly used experimental data are placed.

Diagram of historical research

Empirical curve fitting approach

Gravesen and Sørensen (1977)
Eckert (1983)
Shore Protection Manual, CERC (1984)
Bruun (1985)
Markle (1989)
Rock Manual, CIRIA/CUR (1991)
BSI 6349 (1991)

N_{od}, $H_{2\%}$
Damage levels

Gerding
1993

Aalborg University

Burcharth and Liu
1995

Concrete
cubes

Submitted as paper
$H_{2\%}$ is not of use anymore

Van der Meer et al.
1995

Check on Δ
New def. N_{od}

Docters van Leeuwen
1996

New formula based
on Gerding (1993)

Hovestad (2005),
CSIR Stellenbosch
(2005, unpublished)

Van der Meer
1998

Sayao
2007

ξ, foreshore

Rock Manual, CIRIA/CUR
2007

Shallow water,
ξ, foreshore

Ebbens
2009

Overview of stab. methods,
theoretical via Izbash,
N_{fo}, $N_{s,cr}$

Muttray
2013

Determination of N_{od} instead of N_s,
damage $N_{od} \cdot f_b$

Avoid interdependency
of parameters

Muttray et al.
2014

USACE
1987

Markle
1989

Van der Meer
1991

MAST I
1992

Gerding
1993

Docters van Leeuwen
1996

Ebbens
2009

Nammuni-Krohn
2009

Van Gent et al.
2014

Van Gent and Van der Werf
2014

Decoupled model approach

2-step model, $\hat{u}_c$,
threshold of motion

Baart
2008

Determination $\hat{u}_c$
by experiments

Nammuni-Krohn
2009

Combined in a paper

Baart et al.
2010

Analysis irregular waves,
characteristic velocity $\hat{u}_b$

Motion of single stones

VOF-model for
Nammuni-Krohn (2009)

Arets
2013

Peters
2014

Experiments — data are used in → Research

adaptation

Research

Underlined: data available
Italic: not in reference list

Legend

B

Stability methods

This appendix contains all stability methods reviewed in this study. An important remark: to make comparison between stability methods possible, parameters used are uniformized. In the sketch below the most important parameters are given. The 'undisturbed' situation is the situation without a breakwater, i.e. without reflection.

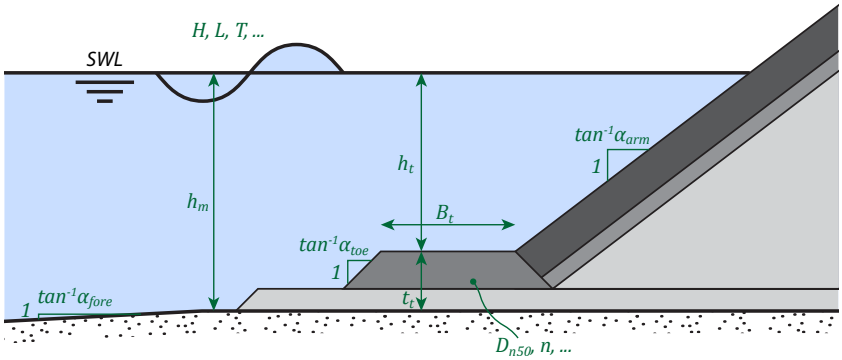

Figure B.1: Uniformized parameters

B.1. Stability and damage methods

B.1.1. Van der Meer (1991)

As found in the CUR/CIRIA Rock Manual (1991).

$$\frac{h_t}{h_m} = 0.22\left(\frac{H_s}{\Delta \cdot D_{n50}}\right)^{0.7} \qquad \text{(VdM91)}$$

$$\frac{H_s}{\Delta \cdot D_{n50}} = 8.7\left(\frac{h_t}{h_m}\right)^{1.4}$$

No information on where to take the wave characteristics.
Validity: $0.5 < h_t/h_m < 0.8$

B.1.2. Gerding (1993), Van der Meer et al. (1995)

Formula with H_s:

$$\frac{H_s}{\Delta \cdot D_{n50}} = \left(0.24\frac{h_t}{D_{n50}} + 1.6\right) N_{od}^{0.15} \qquad \text{(Ger93a)}$$

Formula with $H_{2\%}$ (disposed of in Van der Meer et al. (1995)):

$$\frac{H_{2\%}}{\Delta \cdot D_{n50}} = \left(0.34 \frac{h_t}{D_{n50}} + 2.2\right) N_{od}^{0.15} \tag{Ger93b}$$

Wave characteristics measured at the toe in the undisturbed situation.
Validity:

$$\begin{aligned} 0.4 < h_t/h_m &< 0.9 \\ 3 < h_t/D_{n50} &< 25 \end{aligned}$$

B.1.3. Burcharth and Liu (1995)

Modified Gerding (1993) for concrete cubes:

$$\frac{H_s}{\Delta \cdot D_{n50}} = \frac{1.6}{N_{od}^{-0.15} - 0.4 \frac{h_t}{H_s}} \tag{Bur95}$$

No information on where to take wave characteristics.

B.1.4. Van der Meer (1998)

Based on work by Gerding (1993):

$$\frac{H_s}{\Delta \cdot D_{n50}} = \left(6.2 \left(\frac{h_t}{h_m}\right)^{2.7} + 2\right) N_{od}^{0.15} \tag{VdM98}$$

Wave characteristics measured at the toe in the undisturbed situation.
Validity:

$$\begin{aligned} 0.4 < h_t/h_m &< 0.9 \\ 3 < h_t/D_{n50} &< 25 \end{aligned}$$

B.1.5. Sayao (2007)

Re-written to conventional indices, with m being the foreshore slope and ξ_{0p} the Iribarren number based on H_s and L_{0p}.

$$\frac{\rho_s \cdot H_s^3}{\Delta^3 \cdot M_{50}} = 4.5 m^{-2/3} \cdot \mathrm{e}^{5.67 h_t/h_m - 0.63 \xi_{0p}} \tag{Say07}$$

Herein: $m = \tan \alpha_{fore}$ and $\xi_{0p} = \tan \alpha_{arm} / \sqrt{H_s/L_{0p}}$. The significant wave height is measured at the toe. The wave length is measured in deep water. From the case study in the report it can be assumed that peak wave length should be used. No information is given on whether they should be measured in an undisturbed situation.

B.1.6. Baart (2008)

The method proposed by Baart is a two-step model, which gives a critical velocity:

$$\hat{u}_{bc} = \left(0.46 \sqrt{T} \cdot \left(\left(\Delta - C_{PF} \cdot i\right) g\right)^{1.5} \cdot D_{n50}\right)^{2.5^{-1}}$$

$$\text{with } i = \frac{H/2 + R_u}{L_{TA} + R_u / \tan \alpha_{arm}}$$

etc.

and a load:

$$\hat{u}_b = \sqrt{(\hat{u}_{bi} \cdot \sin\varphi_{TA})^2 + (\hat{u}_{bi} \cdot \cos\varphi_{TA} + \hat{u}_{bdr})^2}$$
$$\text{with } \hat{u}_{bdr} = \gamma_{dr}\sqrt{2g\,(R_u/3 + R_d/2)}$$
$$\hat{u}_{bi} = \omega\frac{H}{2}\frac{\cosh\left(k\left(h_m - h_t\right)\right)}{\sinh\left(kh_m\right)}$$
$$\varphi_{TA} = kx = \frac{2\pi}{L}\cdot L_{TA}$$

Finally a design criterion is given, using the relative load with an overall fit factor Γ:

$$\Gamma \cdot \frac{\hat{u}_b}{\hat{u}_{bc}} = 0.91 - 0.95 \tag{Baa08}$$

which can be plotted against N_{od} for test results.
For the derivation of $\hat{u}_{bc}$ Baart uses T_p and H_s (in i).
For the derivation of $\hat{u}_{bi}$ and φ_{TA} one should take the H_s, $T_{m-1,0}$ and $L_{m-1,0}$ values measured at the toe.
Baart used formulae from the Rock Manual (CIRIA et al., 2007) to determine R_u and R_d.

Validity:

$$H_s/h_t > 0.5$$
$$H_s/h_m > 0.35$$
$$\tan\alpha_{arm} \approx 0.67$$

permeable rubble mound breakwater with a rough front slope

B.1.7. EBBENS (2009)

Stability for very shallow water:

$$\frac{H_s}{\Delta \cdot D_{n50}} = 3.0 \cdot \frac{N_{\%}^{1/3}}{\sqrt{\xi_{0p}}} \tag{Ebb09}$$

Herein: $\xi_{0p} = \tan\alpha_{fore}/\sqrt{H_s/L_{0p}}$.
The significant wave height is measured at the toe. Peak wave length is measured in deep water. It is not reported specifically that wave characteristics should be taken in the undisturbed situation, but since Ebbens performed reflection analysis with multiple wave gauges it can be assumed that the formula is based on the incoming wave characteristics.
Validity: $h_m/H_s < 2.0$

B.1.8. BAART ET AL. (2010)

Adding foreshore slope to Baart (2008) to match values of Docters van Leeuwen (1996):

$$\hat{u}_b \rightarrow \hat{u}_b \cdot \gamma_{fore}$$
$$\gamma_{fore} = \left(\frac{\tan\alpha_{fore}}{0.05}\right)^{0.5}$$

B.1.9. MUTTRAY (2013)

Theoretical derivation.

$$\sqrt[3]{N_{od}} = \frac{N_s}{N_{s,cr}}$$
$$\frac{H_s}{\Delta \cdot D_{n50}} = \frac{2.4N_{od}^{1/3}}{1.4 - 0.4\frac{h_t}{H_s}} \tag{Mut13}$$

The method by Muttray is based on old experiments which *probably* use wave characteristics for the undisturbed situation. Muttray states that H_s in his formula should be the local, incoming significant wave height. Validity: $h_t/H_s < 3$

B.1.10. VAN GENT AND VAN DER WERF (2014)

No stability number, but a prediction of damage:

$$N_{od} = 0.032 \left(\frac{t_t}{H_s}\right)\left(\frac{B_t}{H_s}\right)^{0.3}\left(\frac{H_s}{\Delta \cdot D_{n50}}\right)^3\left(\frac{\hat{u}_\delta}{\sqrt{gH_s}}\right) \tag{vGe14}$$

$$\text{with } \hat{u}_\delta = \frac{\pi H_s}{T_{m-1,0}} \frac{1}{\sinh kh_t}$$

$$k = \frac{2\pi}{L_{m-1,0}} = \frac{2\pi^2}{\frac{g}{2\pi}T_{m-1,0}^2}$$

The wave characteristics are taken for the undisturbed situation. For the estimation of $\hat{u}_\delta$ Van Gent and Van der Werf use linear deep water theory, "irrespective of the actual situation being in deep water or in shallow water". The wave characteristics should therefore be measured at the toe. Validity:

$$0.1 < t_t/h_m < 0.3$$
$$\tan\alpha_{arm} = 1:2$$
$$1.2 < h_m/H_s < 4.5$$

B.1.11. MUTTRAY ET AL. (2014)

Muttray provided two formulae. The formula with the toe berm slope is presented here. Muttray warns that the formula is not intended for design purposes.

$$\frac{H_s}{\Delta \cdot D_{n50}} = \left((4n_t)^{1/3} + \frac{h_t}{L_p}m\right) N_{od}^{\frac{1}{3}} \tag{Mut14}$$

with parameter limits:

$$N_{od} = \max\{N_{od}, 0.25\}$$
$$h_t = \max\{h_t, 0\}$$
$$m = \min\{m, 50\}$$
$$n_t \approx 1.5$$

Herein: $m = \tan^{-1}\alpha_{fore}$ and $n_t = \tan^{-1}\alpha_{toe}$. The wave characteristics should probably be measured in the undisturbed situation. L_p is measured at the toe. No validity limits are given; this is somewhat included in the parameter limits.

B.2. DEFINITION OF DAMAGE

B.2.1. GERDING (1993)

N_{od} is defined as number of stones removed from the toe structure in a strip with a width of 1 D_{n50}, i.e.:

$$N_{od} = \frac{\text{total number of removed stones}}{\text{number of strips}} = \frac{\text{total number of removed stones}}{\text{toe bund length}/D_{n50}}$$

This definition is also used in Van der Meer et al. (1995). Baart (2008) makes the definition more concrete for 'removed': *"The damage number N_{od} is the amount of elements that have actually displaced from the toe bund edge, with respect to the amount of elements that were lying on the toe bund edge before the test."* (Baart, 2008, p. 62)

B.2.2. Docters van Leeuwen (1996)

N_{od} is defined as the number of stones removed from the toe structure *in seaward direction* **divided by the number of stones** in a strip with a width of 1 D_{n50}, i.e.:

$$N_{od} = \frac{\text{total number of removed stones}}{\text{mean number of stones in a strip}}$$

B.2.3. Baart (2008)

As a second option, Baart proposes a percentual damage: *"The damage number N_{odB} is the amount of elements that have actually displaced from **top surface** layer of the toe bund, with respect to the amount of elements that were lying in this layer before the test."* (Baart, 2008, p. 64)

$$N_{odB} = \frac{\text{total number of removed stones}}{\frac{\text{toe bund length}}{D_{n50}} \cdot \frac{\text{toe bund width}}{D_{n50}}} = \frac{N}{\frac{L}{D_{n50}} \cdot \frac{B_t}{D_{n50}}}$$

Baart concludes that N_{odB} is not significantly better than N_{od}, although the definition of damage has proven not to be very important.

B.2.4. Ebbens (2009)

A "displaced" stone is defined as a stone which is not in place anymore after the test, i.e. moved (in a detectable way by using digital image processing) in any direction.

New percentual damage, using porosity, as percentage of the total volume:

$$N_{\%} = N \cdot \frac{D_{n50}^3}{(1-n)V_{tot}}\%$$

B.2.5. Muttray (2013)

New percentual damage, based on volumes:

$$N_{\%} = \frac{\text{displaced stone volume}}{\text{total stone volume}} = \frac{N_{od} D_{n50}^2}{(t_t - t_b)\bar{B}(1-n)}$$

B.2.6. Van Gent and Van der Werf (2014)

The value for N_{od} is based on the amount of stones which have been replaced over more than one stone diameter. It seems that this value can also be approximated using the erosion profile ($S = A_e/D_{n50}^2$) and a conversion formula from S to N_{od}.

B.3. Damage levels

B.3.1. Gerding (1993)

$N_{od} = 0.5$ hardly any damage
$N_{od} = 2$ acceptable damage, design criteria
$N_{od} = 4$ unacceptable damage
Confirmed in Van der Meer et al. (1995) and Van der Meer (1998).

B.3.2. Baart (2008)

$N_{od} < 0.4$ insignificant damage
$0.4 < N_{od} < 0.8$ transition
$0.8 < N_{od}$ significant damage

B.3.3. Ebbens (2009)

For interlocking armour units:
$N_{\%} = 5\%$ for swell waves ($s_{0p} = 0.01$)
$N_{\%} = 10\%$ for wind waves ($s_{0p} = 0.035$)

B.3.4. MUTTRAY (2013)

$N_{\%} < 5\%$ insignificant damage
$5\% < N_{\%} < 10\%$ start of damage
$20\% < N_{\%} < 40\%$ flattening, still functional
$N_{\%} > 50\%$ loss of functionality

B.3.5. VAN GENT AND VAN DER WERF (2014)

Multiply the damage level values of Gerding (1993) with a factor f_B:

$$f_B = \left(\frac{B_t}{3D_{n50}} \right)^{0.5}$$

B.4. Tabular overview of datasets and formulae

Research	Approach	Target	New dataset	Wave type	Material	Dependency	Damage parameter
Rock Manual (1991)	ECFA	Design formula	Yes	?	Rock	h_t/h_m	-
Gerding (1993) **Van der Meer et al. (1995)** **CIRIA et al. (2007)**	ECFA	Systematic approach, reliable parameters	Yes	Irregular	Rock	h_t/D_{n50}	N_{od}
Burcharth and Z. Liu (1995)	ECFA	Formula for concrete cubes	Yes	?	Concrete cubes	h_t/H_s	N_{od}
Docters van Leeuwen (1996)	ECFA	Proof of Gerding (1993) for Δ	Yes	Irregular	Rock	-	N_{od} (new)
Van der Meer (1998) **Rock Manual (2007)**	ECFA	New formula based on work by Gerding (1993)	No	-	Rock	h_t/h_m	N_{od}
Sayao (2007)	ECFA	Encorporate foreshore slope, steepness, breaker index	Yes	?	Rock	α_{fore}, h_t/h_m, ξ_{0p}	-
Baart (2008)	DMA, analytical	Define critical load via threshold of motion	No	Regular and irregular	Rock	L, H, R_u, R_d, L_{TA}, h_t, h_m	N_{od}, N_{odB} (rejected)
Ebbens (2009)	ECFA	Very shallow water	Yes	Irregular	Rock	ξ	$N_{\%}$
Nammuni-Krohn (2009)	-	Measure u_{max}	Yes	Regular and irregular	(Rock)	-	-
Baart et al. (2010)	-	Combine Baart (2008), Ebbens (2009) and Nammuni-Krohn (2009)	No	-	Rock	$\hat{u}_b \cdot \gamma_{fore}$	N_{od}, $N_{\%}$
Muttray (2013)	ECFA	Analytical derivation of 'classical' stability formula	No	-	Rock	h_t/H_s	N_{od}, $N_{\%}$ (new)
Arets (2013)	DMA, numerical	Numerical simulation of Nammuni-Krohn (2009)	No	Regular	(Rock)	-	-
Van Gent and Van der Werf (2014)	DMA and decoupled model	Gain higher accuracy by combining both methods, validate more toe dimensions	Yes	Irregular	Rock, concrete V-units	t_t/H_s, B_t/H_s, $\hat{u}_\delta/\sqrt{gH_s}$	N_{od}
Muttray et al. (2014)	ECFA	Step-by-step derivation of simple benchmark formula, avoiding interdependency of parameters	No	Irregular	Rock	h_t/L_p, α_{fore}, α_{toe}	N_{od}

ECFA = empirical curve fitting approach
DMA = decoupled model approach

C

Datasets

On the following pages historical datasets used for this research are described in detail. For Nammuni-Krohn (2009) and Ebbens (2009) a structure drawing of the model implemented in IH-2VOF can be found in appendix E. Per dataset the following topics are given as complete as possible:

- Where to obtain data
- Number of tests
- Test set-up, flume and wave characteristics, method of measurement
- Particularities
- Parameters changed with their ranges
- Constant parameters
- Measured/derived values available

C.1. Gerding (1993)

- Data in report, page 91-100
- 171 test composed as 57 cases x 3 stone sizes
- Irregular waves, JONSWAP-spectrum, γ unknown, 1000 waves per run
- Wave height and wave period are measured using wave gauges, at the wave generator and at the toe. Damage is recorded as stones removed completely from the toe.
- Parameters changed:

  B_t = 0.12, 0.20, 0.30 m

  D_{n50} = 0.017, 0.025, 0.035, 0.040 m

  h_m = 0.3, 0.4, 0.5 m

  H_s = 0.15, 0.20, 0.25 m (target at toe)

  s_{0p} = 0.02, 0.03, 0.04 (target at wave generator)

  t_t = 0.08, 0.15, 0.22 m
- Constant parameters:

  ρ_s = 2680 kg/m^3

  ρ_w = 1000 kg/m^3

  Δ = 1.68

  D_{85}/D_{15} = 1.15 – 1.30
- Measured/derived values:

  At wave generator: $H_{2\%,0}$
  At toe: T_p, $H_{2\%}$, damage

C.2. Docters van Leeuwen (1996)

- Data in report, page 102-106 (appendix C1)
- 98 tests composed as 16 cases x 6 stone types and 2 additional runs
- Irregular waves, JONSWAP-spectrum, $\gamma = 3.3$, 2000 waves per run
- Wave height and wave period are measured using wave gauges, at the wave generator and at the toe. Damage is recorded as stones removed completely from the toe in seaward direction.
- Parameters changed:
  $D_{n50} = 0.0098, 0.0102, 0.0144, 0.0151, 0.021, 0.0231$ m
  $h_m = 0.30, 0.45$ m
  $H_s = 0.10, 0.14, 0.17, 0.20$ m (target at toe)
  $t_t = 0.08, 0.15$ m
  $\rho_s = 1900, 2550, 2850$ kg/m^3 $\rightarrow \Delta = 0.90, 1.55, 1.85$
- Constant parameters:
  $s_{0p} = 0.04$ (target at wave generator)
  $\rho_w = 1000$ kg/m^3
- Measured/derived values:
  T_p (probably at toe)
  Damage

C.3. Ebbens (2009)

- Data in report, page 102-114
- 296 tests
- Irregular waves, JONSWAP-spectrum, $\gamma = 3.3$, 1000 waves per run. The armour layer consists of Xbloc-elements.
- Wave height and period are measured using wave gauges, at the wave generator and in front of toe. The 'toe' measurement was at a position where the bed level was 4.2 cm lower than the bed level at the toe (i.e. water level 4.2 cm larger than h_m). This means that H_s at the toe is different due to shoaling. Muttray corrected this by assuming no change in H_s if no breaking was present ($\frac{H_{s,0}}{h_m + 42 \text{ mm}} < 0.6$). When wave breaking was present, an adaption was made, see Muttray (2013).
  Damage is presumably recorded as stones removed completely from the toe (separately up/down), though his choice is not clear since he wrote: *"A division can be made in stones moving downwards (away from the breakwater), stones moving upwards (to primary armour layer) and movind [moving] within the toe profile (more than its own diameter)."* (Ebbens, 2009, p. 20). He did not give the values for the last measurement though.
- Parameters changed:
  $\tan(\alpha_{fore}) =$ 1:10,1:20,1:50
  $D_{n50} = 18.8, 21.5, 26.8$ mm with $\rho_s = 2650, 2700, 2750$ kg/m^3 and $n = 0.36, 0.33, 0.32$
  $h_t = 0.00, 0.02, 0.04, 0.06, 0.08, 0.13, 0.18, 0.266$ m
  h_t should be corrected with -0.07 m (Ebbens, 2009, p. 44).
  $H_s = 0.06, 0.08, 0.10, 0.12$ m (target at wave generator)
  $s_{0p} = 0.02, 0.03, 0.04$ (target at wave generator)
- Constant parameters:
  $\rho_w = 1000$ kg/m^3
  Armour layer: Xbloc, $D_{n50} = 0.040$ m , $M_{50} = 49 \cdot 10^{-3}$ kg
  First underlayer: $D_{n50} = 0.0124$ m, $M_{50} = 5.0 \cdot 10^{-3}$ kg
  Core: $D_{n50} = 0.0111$ m, $M_{50} = 3.6 \cdot 10^{-3}$ kg
  Structure dimensions are constant, except foreshore steepness
- Measured/derived values:

At wave generator: T_p
At toe: H_{m0}, T_p, $T_{m-1,0}$, $H_{1/3}$, $H_{2\%}$, damage

- See appendix E for the structure layout as implemented in IH-2VOF.

C.4. NAMMUNI-KROHN (2009)

- Data at 3TU.Datacentrum. An additional (though incomplete) table with calculations can be found in the report on page 84-95.
  `http://dx.doi.org/10.4121/uuid:91312903-7701-406e-a1b0-2d7bc456155c`.
- 80 tests composed as 40 cases x 2 stone sizes
- The toe structure has two toe rock sizes, horizontally divided. 27 cases have regular waves, 50 waves per run. 13 cases have irregular waves, JONSWAP-spectrum, γ unknown, 1000 waves per run.
- Wave height and wave period are measured using wave gauges, at the wave generator and at the toe. Flow velocities are measured with an ADV (Acoustic Doppler Velocimeter). ADV1 is located in the centre line of the larger rock section, ADV2 at the smaller rock section. The orientation of both ADVs is not the same, see Table 2 in the report.
- Parameters changed:

$D_{n50} = 0.035, 0.025$ m
$h_m = 0.2, 0.3, 0.4$ m
$H_s = 0.10, 0.15, 0.20$ m (target in front of foreshore)
$h_t = 0.08, 0.15$ m
$s_p = 0.02, 0.04$ (target in front of foreshore)

- Constant parameters:

$\rho_w = 1000$ kg/m^3
$D_{85}/D_{15} = 1.15 - 1.30$

- Measured/derived values: H_{m0} and T_p at the wave generator, from spectral analysis
- See appendix E for the structure layout as implemented in IH-2VOF.

C.5. VAN GENT AND VAN DER WERF (2014)

- Test set-up in article.
- 192 tests. For 122 of them a dataset could be obtained from the digitised data and additional information in the paper.
- Wave height and wave period are measured using wave gauges, at the wave generator and at the toe. Damage is recorded as stones which have moved over a distance more than D_{n50}.
- Parameters changed:

$D_{n50} = 14.6, 23.3$ mm
$B_t = 0.044, 0.070, 0.131, 0.210$ m
$t_t = 29, 47, 58$ mm
$h_m = 0.2, 0.3, 0.4$ m
$s_{p0} = 0.018, 0.048$ mm

- Constant parameters:

$\Delta = 1.7$
$D_{n85}/D_{n15} = 1.17$
$\rho_w = 1000$ kg/m^3

- Measured/derived values: H_s and T_p at the toe

D

Convergence tests

Convergence tests were performed to obtain sufficient simulation accuracy at a not too high cost of computation time, see section 3.3. In this appendix some additional details and figures on the convergence tests are presented. Details on the exact grid properties are given in appendix E.

D.1. Set-up of the base case

Three convergence tests have been performed. The recommendation of each set of tests has been implemented in the next. The base case NK09-R016-L by Nammuni-Krohn was implemented in grid generator Coral after estimating missing structure dimensions. Porosity has been set on 0.4 and standard[1] Forchheimer coefficients were used, i.e. $\alpha = 200$, $\beta = 1.1$ and $\gamma = 0.34$. Wave length is calculated from wave period for transitional water depths, see Schiereck and Verhagen (2012, p. 175). The calculation resulted in $L_0 = 2.086$ m, which has been rounded to $L_0 = 2.08$ m for easy model set-up. The base domain, grid size and simulation settings have been chosen as follows:

Flume length In the IH-2VOF manual it was advised to let the grid extend at both sides of the structure with at least half a wave length. This formed the case with the minimum flume length. The 'structure' includes the foreshore. Behind the structure the grid was extended only 0.195 m, since the structure contained a vertical impermeable wall and since overtopping was not expected.

Flume height The original flume height of 0.9 m was taken. Higher flume heights do not influence calculations since this only adds air. It is only important that the domain is sufficiently high so that wave crest do not reach the edge.

Grid uniformity As described in section 3.2 a uniform grid has been used.

Cell width Cell width is the cell size in horizontal (x) direction. In Van den Bos et al. (2014) use of at least 150 cells per wave length was advised ($L/\Delta x \geqslant 150$). The IH-2VOF manual additionally puts the criterion $\Delta x < 2.5\Delta y$ to prevent false breaking effects. In the base case it is therefore chosen to take $\Delta x = 0.013$ m which gives $L_0/\Delta x = 160$.

Cell height Cell height is the cell size in vertical (y) direction. The IH-2VOF manual advises to use a minimum of 10 cells per wave height. A criterion of $H/\Delta y \geqslant 10$ is thus advised. For the base case this resulted in $\Delta y = 0.01$ m with $H/\Delta y = 10$. The $\Delta x/\Delta y$-criterion is fulfilled.

[1] Extensive study to the Forchheimer coefficients was not yet performed when working on the convergence tests.

Simulation settings All simulations have been performed with regular waves with initial duration of 180 s. Wave height is 0.10 m and wave period is 1.265 s, both measured in 'deep' water i.e. near the wave generator. A typical plot of the flow velocity over time is shown in figure D.1. It can be seen that it takes about 30 seconds of spin-up time to let waves reach their regular pattern. Therefore it is chosen to reduce simulation duration to 90 seconds, so that for the longest flume a sufficient 50 seconds of stable waves is obtained. Other simulation settings are as follows:

- Linear wave generation theory
- Static paddle
- Left and right boundary absorption. No turbulence calculation.
- Wave gauges are positioned relative to the structure to make comparison possible. At the toe they are positioned with spacing of 0.05 m and 0.10 m; in front of the toe spacing is 0.50 m.
- Only output of wave gauge data, with a sampling frequency of 30 Hz. The convergence tests on flume length have been re-run in a later stage to obtain u-data over the full domain.

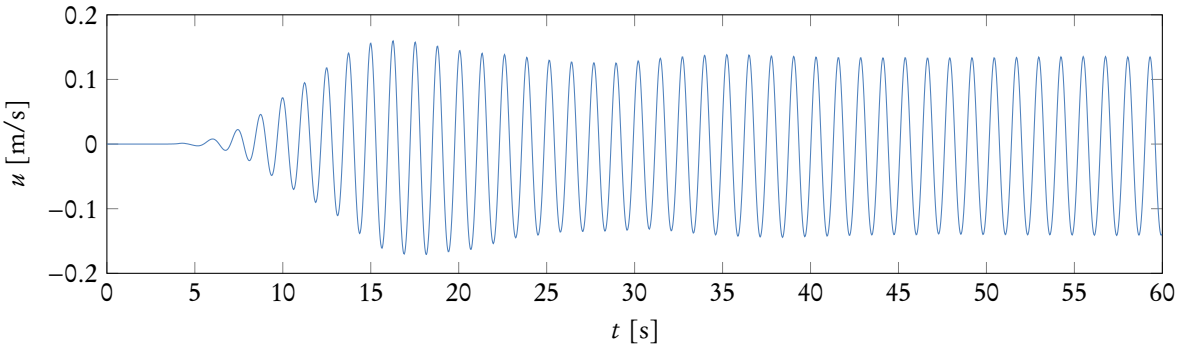

Figure D.1: Typical record of horizontal flow velocity over time.
Note the time required for the wave to reach the structure (~5 s) and the spin-up time (~35 s).

The dataset consists of a time record of horizontal flow velocities u at all y-grid points at each wave gauge (see figure D.1 for an example). They have to be compared in some way. Figure D.2 represents the method. A first trial was to simply subtract one velocity record from the reference case, at each x-y-point. For this wave records have been resampled at the time points of the reference case. This has been done with linear interpolation, which is sufficiently accurate due to the high sampling frequency. Differences in flume length imply a time shift between cases, for when the first wave reaches the gauge. Therefore all velocity records have been shifted to the 'left' in the time domain, so that they start at the 5^{th} positive peak. Choice for the 5^{th} peak is result of trial and error. Now the velocity records can be subtracted.

Unfortunately this resulted in a unworkable solution due to small phase shifts over the record, giving false differences (see figure D.2c). Since toe stone stability is presumably result of velocity peaks, it is chosen to compare the values of the velocity peaks (for now only the positive peaks). At x-y-points where air is sometimes present (near the still water level) false peaks can occur: the velocity suddenly drops to zero when no fluid is present. Peaks are therefore filtered so that time difference between two peaks should be more than $0.9T_0$. Finally peaks can be subtracted, resulting in a stable description of the velocity variation (see figure D.2d).

The relative error is calculated as the difference in peak velocity divided by the highest peak velocity at that peak. The maximum over the time record (after spin-up time) is taken and subsequently the average per gauge is calculated. It must be remarked that relative error is not calculated above the still water line, since wave breaking is not of interest. The error within non-permeable cells is also ignored as it is always zero.

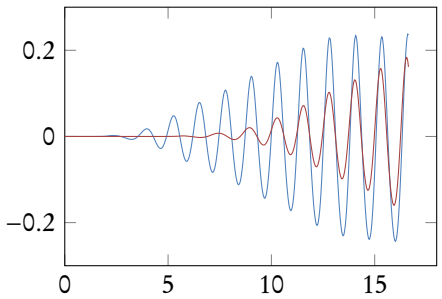

(a) Original gauge data for two gauges

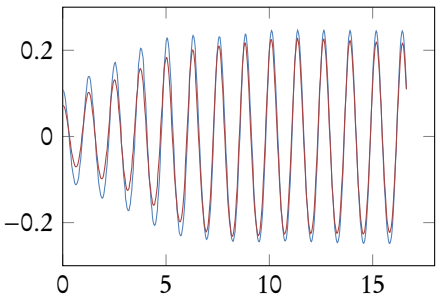

(b) Resampled and shifted gauge data

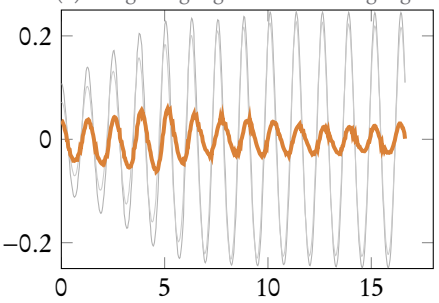

(c) Subtraction of the gauge data (inappropriate due to phase shifts)

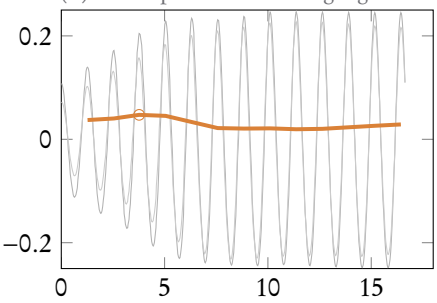

(d) Difference in positive peaks with its maximum marked

Figure D.2: Comparison method of time-velocity records.
The horizontal axis is t in seconds, the vertical u in metres per second.

D.2. Additional figures on flume length convergence

In figure D.3 a flume has been represented. At all wave gauges maximal peak difference per x-y position has been plotted. We can observe that around the still water level and near the toe there is greater difference with the reference case due to wave breaking. When we zoom in on the toe, we see that velocity records seem to converge with increasing flume length. A clear answer to which flume length is best is not obvious.

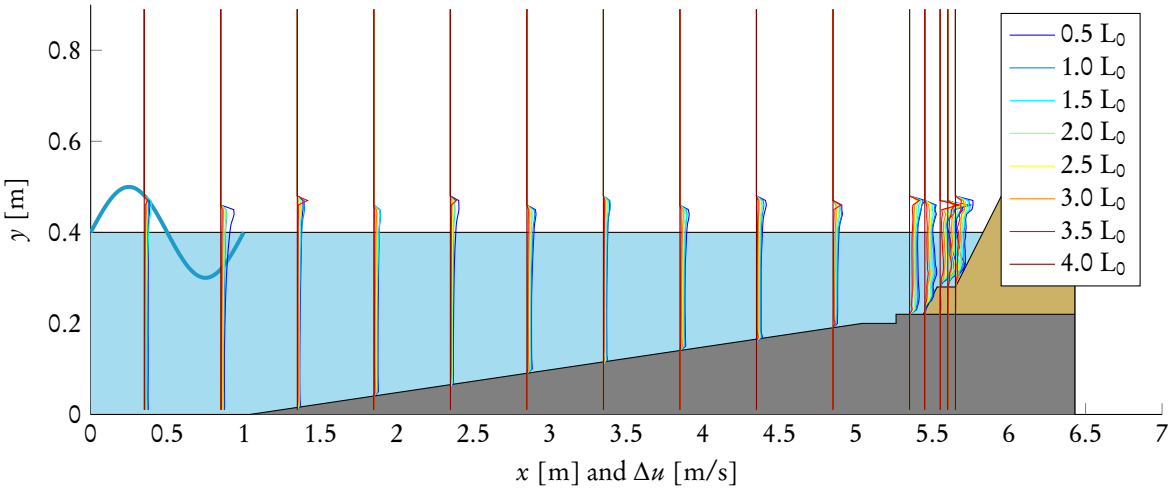

(a) Full width

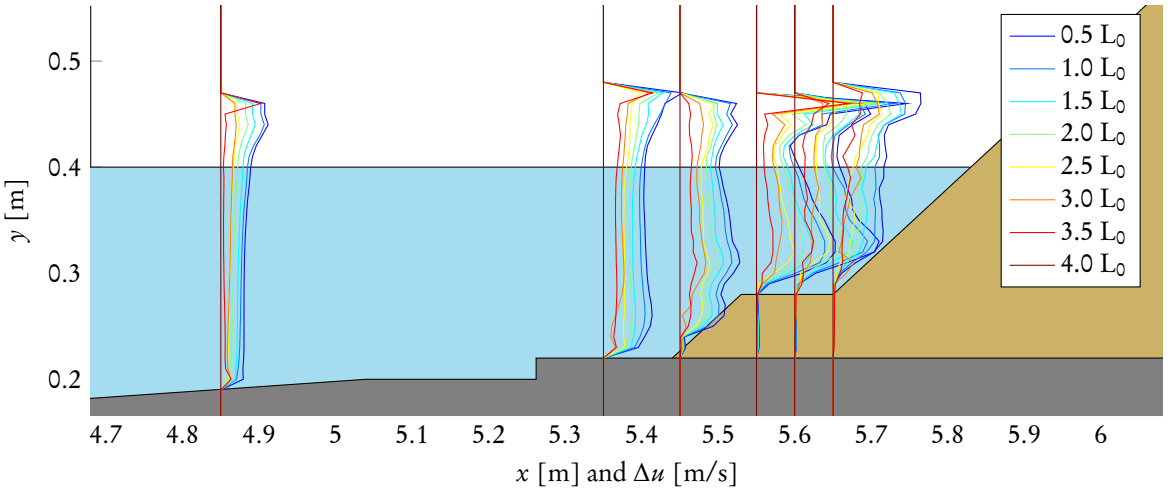

(b) Zoomed in

Figure D.3: Maximal peak difference at each gauge x-y-position for different flume lengths

D.3. ADDITIONAL FIGURES ON CELL WIDTH CONVERGENCE

Maximal peak difference at each gauge position is plotted in figure D.4 with a zoomed in version in figure D.4b. It shows convergence for smaller cells. The case with a $L_0/\Delta x$-value of 50.7 shows large deviations and may certainly not be used.

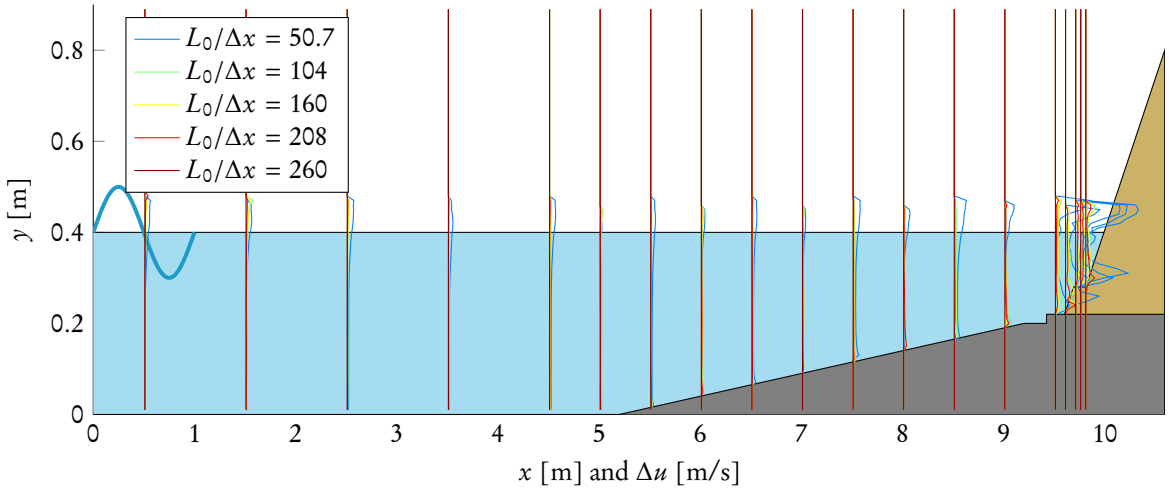

(a) Full width

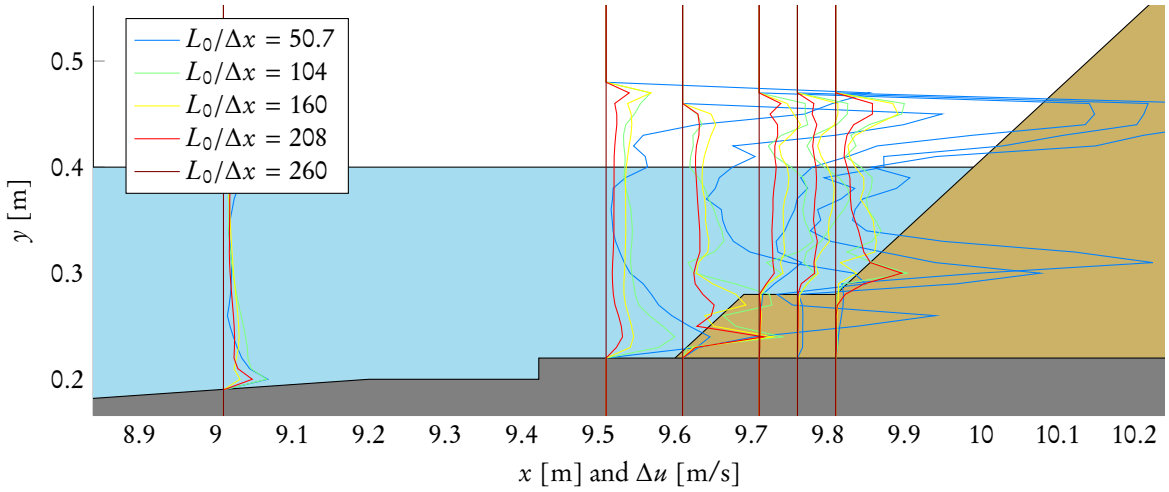

(b) Zoomed in

Figure D.4: Maximal peak difference at each gauge x-y-position for different cell widths

D.4. Additional figures on cell height convergence

In figure D.5 we can observe convergence in cell height. Certainly the case with $H/\Delta y = 5$ still has large errors. The same can be seen in figure 3.8 as well. Although calculation with $H/\Delta y = 10$ seems to be much more accurate, it still shows extensive fluctuations over the wave gauges. This is largely gone with $H/\Delta y = 16.7$.

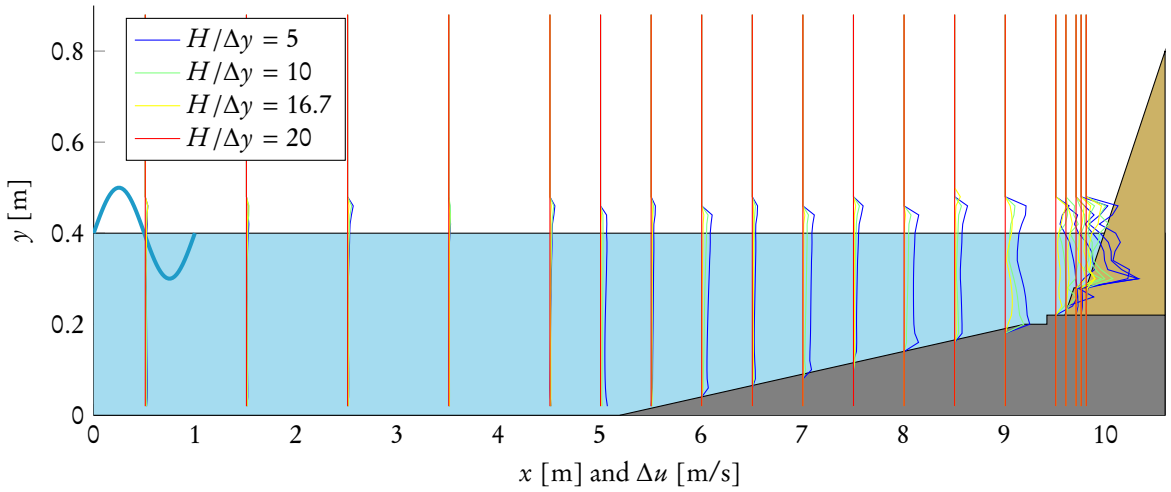

(a) Full width

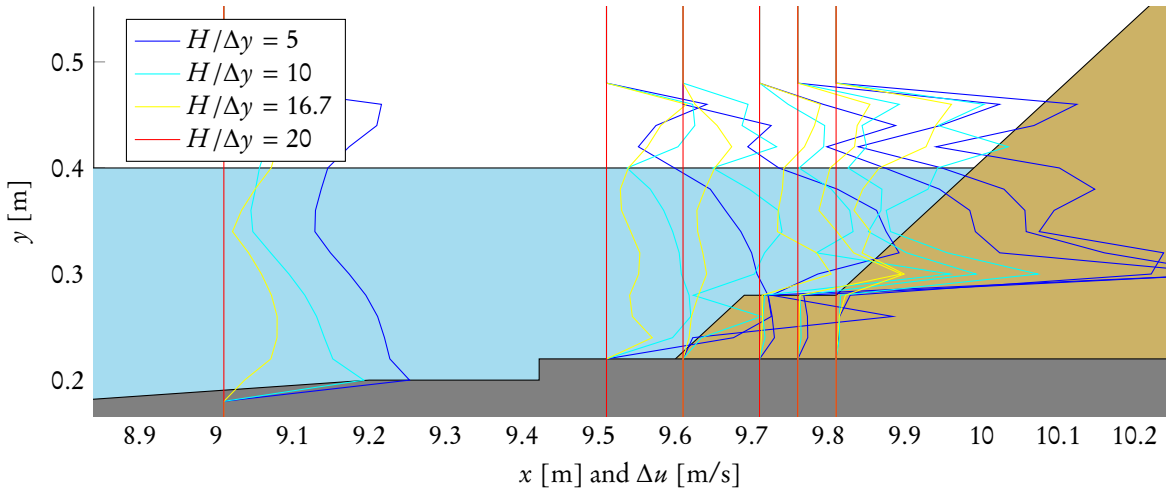

(b) Zoomed in

Figure D.5: Maximal peak difference at each gauge x-y-position for different cell heights

E

Model configurations

The following pages show configurations for the IH-2VOF models. Three models have been made:

- The convergence test model, based on NK09-R016-L (simulation ID NK09_741)
- The NK09 (Nammuni-Krohn, 2009) models (simulation ID NK09_688 to NK09_767)
- The Eb09 (Ebbens, 2009) models (simulation ID Eb09_172 to Eb09_467)

Simulation IDs are identifiers used in this research. In fact all Gerding (1993), Docters van Leeuwen (1996) and Van Gent and Van der Werf (2014) cases have also been assigned an ID, though they are not modelled with IH-2VOF due to time limitations.

For NK09 and Eb09 the model implemented is drawn. The model is dependent on case parameters. Then a table follows in which the configuration per case is shown. Only relevant parameters which cannot be deduced from the model drawing are given. Estimated values are shown between parentheses.

At the end of the chapter a table is presented containing information on the performance of the calculations.

E.1. Convergence tests

The convergence tests are based on test NK09_741. See also section 3.3 and appendix D for details on the choices made. The model layout is given in the NK09 model description.

Table E.1: Flume length convergence

Flume extension	L_f [m]	h_f [m]	Δx [m]	Δy [m]	n_x [-]	n_y [-]
$0.5L_0$	6.825	0.900	0.013	0.01	525	90
$1.0L_0$	7.865	0.900	0.013	0.01	605	90
$1.5L_0$	8.905	0.900	0.013	0.01	685	90
$2.0L_0$	9.945	0.900	0.013	0.01	765	90
$2.5L_0$	10.985	0.900	0.013	0.01	845	90
$3.0L_0$	12.025	0.900	0.013	0.01	925	90
$3.5L_0$	13.065	0.900	0.013	0.01	1005	90
$4.0L_0$	14.105	0.900	0.013	0.01	1085	90

Table E.2: Cell width convergence

$L_0/\Delta x$ [-]	L_f [m]	h_f [m]	Δx [m]	Δy [m]	n_x [-]	n_y [-]
50.7	10.988	0.900	0.041	0.01	268	90
104	11.000	0.900	0.020	0.01	550	90
160	10.985	0.900	0.013	0.01	845	90
208	10.990	0.900	0.010	0.01	1099	90
260	10.992	0.900	0.008	0.01	1374	90

Table E.3: Cell height convergence

$H/\Delta y$ [-]	L_f [m]	h_f [m]	Δx [m]	Δy [m]	n_x [-]	n_y [-]
5	10.985	0.900	0.013	0.020	845	45
10	10.985	0.900	0.013	0.010	845	90
16.7	10.985	0.900	0.013	0.006	845	150
20	10.985	0.900	0.013	0.005	845	180

Table E.4: Friction check, see §3.4.1

Flume extension	L_f [m]	h_f [m]	Δx [m]	Δy [m]	n_x [-]	n_y [-]
$1.5L_0$	3.133	0.9	0.013	0.006	241	150
$2.0L_0$	4.173	0.9	0.013	0.006	321	150
$2.5L_0$	5.226	0.9	0.013	0.006	402	150
$3.0L_0$	6.266	0.9	0.013	0.006	482	150
$3.5L_0$	7.306	0.9	0.013	0.006	562	150
$4.0L_0$	8.346	0.9	0.013	0.006	642	150

E.2. Nammuni-Krohn (2009)

Some details on the NK09 model:

- The model was reported in low level of detail. Consequently a lot of assumptions on stone properties and dimensions had to be made.
- Three offshore gauges were placed
- Multiple gauges above the toe were placed, according to the x_{ADV} positions in the NK09 report
- The origin of the ADV coordinate system moves with a higher toe

Table E.5: NK09 stone properties

Material	D_{n50} [m]	n [-]	α [-]	β_c [-]	γ [-]
Toe stone 1	0.0250	(0.40)	903	1.1	0.34
Toe stone 2	0.0350	(0.40)	1043	1.1	0.34
Armour	0.0400	(0.40)	1105	1.1	0.34
Core	(0.0111)	(0.38)	637	1.1	0.34

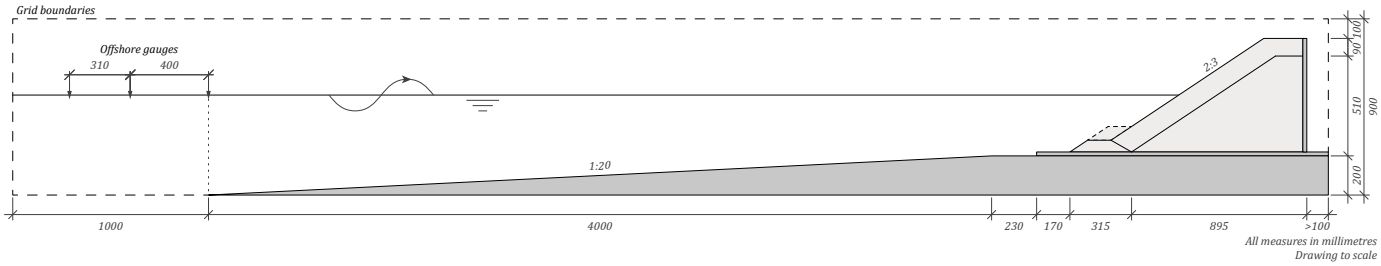

Figure E.1: Geometry of NK09

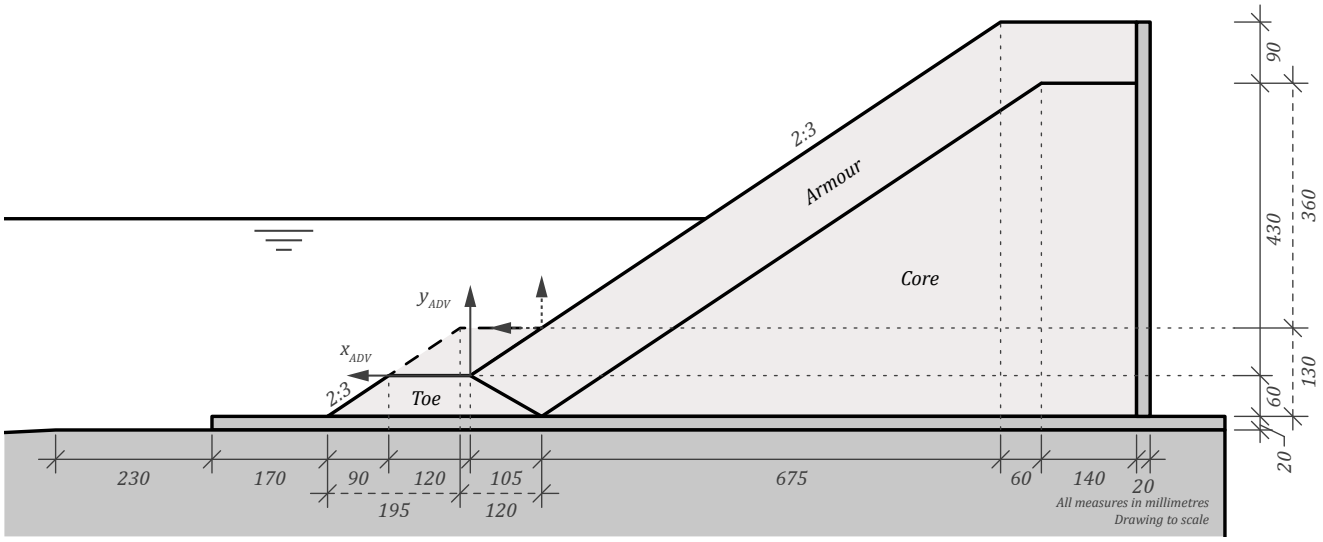

Figure E.2: Detailed geometry of NK09

Table E.6: NK09 configuration with regular waves

Sim. ID	NK09-ID	h_0 [m]	H [m]	T [s]	D_{n50} [m]	t_t [m]	L_0 [m]	L_f [m]	h_f [m]	Δx [m]	Δy [m]	n_x [-]	n_y [-]	t_{end} [s]
688	R001-S	0.6	0.10	1.790	0.025	0.08	3.80	15.210	0.90	0.015	0.006	1014	150	90
689	R002-S	0.6	0.10	1.265	0.025	0.08	2.31	11.505	0.90	0.015	0.006	767	150	90
690	R003-S	0.6	0.15	2.197	0.025	0.08	4.88	17.925	0.90	0.025	0.010	717	90	90
691	R004-S	0.6	0.15	1.898	0.025	0.08	4.09	15.950	0.90	0.025	0.010	638	90	90
692	R005-S	0.6	0.15	1.550	0.025	0.08	3.13	13.540	0.90	0.020	0.010	677	90	90
693	R006-S	0.6	0.20	2.531	0.025	0.08	5.75	20.097	0.91	0.033	0.013	609	70	90
694	R007-S	0.6	0.20	1.789	0.025	0.08	3.79	15.200	0.91	0.025	0.013	608	70	90
695	R008-S	0.5	0.10	1.790	0.025	0.08	3.55	14.580	0.90	0.015	0.006	972	150	90
696	R009-S	0.5	0.10	1.265	0.025	0.08	2.22	11.270	0.90	0.014	0.006	805	150	90
697	R010-S	0.5	0.15	2.197	0.025	0.08	4.53	17.050	0.90	0.025	0.010	682	90	90
698	R011-S	0.5	0.15	1.898	0.025	0.08	3.81	15.250	0.90	0.025	0.010	610	90	90
699	R012-S	0.5	0.15	1.550	0.025	0.08	2.95	13.110	0.90	0.019	0.010	690	90	90
700	R015-S	0.4	0.10	1.789	0.025	0.08	3.25	13.830	0.90	0.015	0.006	922	150	90
701	R016-S	0.4	0.10	1.265	0.025	0.08	2.09	10.933	0.90	0.013	0.006	841	150	90
702	R017-S	0.4	0.15	2.197	0.025	0.08	4.11	16.000	0.90	0.025	0.010	640	90	90
711	R030-S	0.6	0.10	1.790	0.025	0.15	3.80	15.210	0.90	0.015	0.006	1014	150	90
712	R031-S	0.6	0.10	1.265	0.025	0.15	2.31	11.505	0.90	0.015	0.006	767	150	90
713	R032-S	0.6	0.15	2.197	0.025	0.15	4.88	17.925	0.90	0.025	0.010	717	90	90
714	R033-S	0.6	0.15	1.898	0.025	0.15	4.09	15.950	0.90	0.025	0.010	638	90	90
715	R034-S	0.6	0.15	1.550	0.025	0.15	3.13	13.540	0.90	0.020	0.010	677	90	90
716	R035-S	0.6	0.20	2.531	0.025	0.15	5.75	20.097	0.91	0.033	0.013	609	70	90
717	R036-S	0.6	0.20	1.789	0.025	0.15	3.79	15.200	0.91	0.025	0.013	608	70	90
718	R037-S	0.5	0.10	1.790	0.025	0.15	3.55	14.580	0.90	0.015	0.006	972	150	90
719	R038-S	0.5	0.10	1.265	0.025	0.15	2.22	11.270	0.90	0.014	0.006	805	150	90
720	R039-S	0.5	0.15	2.197	0.025	0.15	4.53	17.050	0.90	0.025	0.010	682	90	90
721	R040-S	0.5	0.15	1.898	0.025	0.15	3.81	15.250	0.90	0.025	0.010	610	90	90
722	R041-S	0.5	0.15	1.550	0.025	0.15	2.95	13.110	0.90	0.019	0.010	690	90	90
728	R001-L	0.6	0.10	1.790	0.035	0.08	3.80	15.210	0.90	0.015	0.006	1014	150	90
729	R002-L	0.6	0.10	1.265	0.035	0.08	2.31	11.505	0.90	0.015	0.006	767	150	90
730	R003-L	0.6	0.15	2.197	0.035	0.08	4.88	17.925	0.90	0.025	0.010	717	90	90
731	R004-L	0.6	0.15	1.898	0.035	0.08	4.09	15.950	0.90	0.025	0.010	638	90	90
732	R005-L	0.6	0.15	1.550	0.035	0.08	3.13	13.540	0.90	0.020	0.010	677	90	90
733	R006-L	0.6	0.20	2.531	0.035	0.08	5.75	20.097	0.91	0.033	0.013	609	70	90
734	R007-L	0.6	0.20	1.789	0.035	0.08	3.79	15.200	0.91	0.025	0.013	608	70	90
735	R008-L	0.5	0.10	1.790	0.035	0.08	3.55	14.580	0.90	0.015	0.006	972	150	90
736	R009-L	0.5	0.10	1.265	0.035	0.08	2.22	11.270	0.90	0.014	0.006	805	150	90
737	R010-L	0.5	0.15	2.197	0.035	0.08	4.53	17.050	0.90	0.025	0.010	682	90	90
738	R011-L	0.5	0.15	1.898	0.035	0.08	3.81	15.250	0.90	0.025	0.010	610	90	90
739	R012-L	0.5	0.15	1.550	0.035	0.08	2.95	13.110	0.90	0.019	0.010	690	90	90
740	R015-L	0.4	0.10	1.789	0.035	0.08	3.25	13.830	0.90	0.015	0.006	922	150	90
741	R016-L	0.4	0.10	1.265	0.035	0.08	2.09	10.933	0.90	0.013	0.006	841	150	90
742	R017-L	0.4	0.15	2.197	0.035	0.08	4.11	16.000	0.90	0.025	0.010	640	90	90
751	R030-L	0.6	0.10	1.790	0.035	0.15	3.80	15.210	0.90	0.015	0.006	1014	150	90
752	R031-L	0.6	0.10	1.265	0.035	0.15	2.31	11.505	0.90	0.015	0.006	767	150	90
753	R032-L	0.6	0.15	2.197	0.035	0.15	4.88	17.925	0.90	0.025	0.010	717	90	90
754	R033-L	0.6	0.15	1.898	0.035	0.15	4.09	15.950	0.90	0.025	0.010	638	90	90
755	R034-L	0.6	0.15	1.550	0.035	0.15	3.13	13.540	0.90	0.020	0.010	677	90	90
756	R035-L	0.6	0.20	2.531	0.035	0.15	5.75	20.097	0.91	0.033	0.013	609	70	90
757	R036-L	0.6	0.20	1.789	0.035	0.15	3.79	15.200	0.91	0.025	0.013	608	70	90
758	R037-L	0.5	0.10	1.790	0.035	0.15	3.55	14.580	0.90	0.015	0.006	972	150	90
759	R038-L	0.5	0.10	1.265	0.035	0.15	2.22	11.270	0.90	0.014	0.006	805	150	90
760	R039-L	0.5	0.15	2.197	0.035	0.15	4.53	17.050	0.90	0.025	0.010	682	90	90
761	R040-L	0.5	0.15	1.898	0.035	0.15	3.81	15.250	0.90	0.025	0.010	610	90	90
762	R041-L	0.5	0.15	1.550	0.035	0.15	2.95	13.110	0.90	0.019	0.010	690	90	90
54 cases in total														

Table E.7: NK09 configuration with irregular waves

Sim. ID	NK09-ID	h_0 [m]	H_s [m]	T_p [s]	D_{n50} [m]	t_t [m]	L_{0p} [m]	L_f [m]	h_f [m]	Δx [m]	Δy [m]	n_x [-]	n_y [-]	t_{end} [s]
703	I020-S	0.6	0.10	1.790	0.025	0.08	3.80	15.210	0.90	0.015	0.006	1014	150	716
704	I021-S	0.6	0.10	1.265	0.025	0.08	2.31	11.505	0.90	0.015	0.006	767	150	506
705	I022-S	0.6	0.15	2.197	0.025	0.08	4.88	17.925	0.90	0.025	0.010	717	90	879
706	I023-S	0.6	0.15	1.550	0.025	0.08	3.13	13.540	0.90	0.020	0.010	677	90	620
707	I026-S	0.5	0.10	1.790	0.025	0.08	3.55	14.586	0.90	0.017	0.007	858	129	716
708	I027-S	0.5	0.10	1.265	0.025	0.08	2.22	11.270	0.90	0.014	0.006	805	150	506
709	I028-S	0.5	0.15	2.197	0.025	0.08	4.53	17.050	0.90	0.025	0.010	682	90	879
710	I029-S	0.5	0.15	1.550	0.025	0.08	2.95	13.110	0.90	0.019	0.010	690	90	620
723	I049-S	0.6	0.10	1.790	0.025	0.15	3.80	15.210	0.90	0.015	0.006	1014	150	716
724	I050-S	0.6	0.10	1.265	0.025	0.15	2.31	11.505	0.90	0.015	0.006	767	150	506
725	I051-S	0.6	0.15	2.197	0.025	0.15	4.88	17.925	0.90	0.025	0.010	717	90	879
726	I052-S	0.6	0.15	1.550	0.025	0.15	3.13	13.540	0.90	0.020	0.010	677	90	620
727	I055-S	0.5	0.10	1.790	0.025	0.15	3.55	14.586	0.90	0.017	0.007	858	129	716
743	I020-L	0.6	0.10	1.790	0.035	0.08	3.80	15.210	0.90	0.015	0.006	1014	150	716
744	I021-L	0.6	0.10	1.265	0.035	0.08	2.31	11.505	0.90	0.015	0.006	767	150	506
745	I022-L	0.6	0.15	2.197	0.035	0.08	4.88	17.925	0.90	0.025	0.010	717	90	879
746	I023-L	0.6	0.15	1.550	0.035	0.08	3.13	13.540	0.90	0.020	0.010	677	90	620

Table E.7: NK09 configuration with irregular waves (continued)

Sim. ID	NK09-ID	h_0 [m]	H_s [m]	T_p [s]	D_{n50} [m]	t_t [m]	L_{0p} [m]	L_f [m]	h_f [m]	Δx [m]	Δy [m]	n_x [-]	n_y [-]	t_{end} [s]
747	I026-L	0.5	0.10	1.790	0.035	0.08	3.55	14.586	0.90	0.017	0.007	858	129	716
748	I027-L	0.5	0.10	1.265	0.035	0.08	2.22	11.270	0.90	0.014	0.006	805	150	506
749	I028-L	0.5	0.15	2.197	0.035	0.08	4.53	17.050	0.90	0.025	0.010	682	90	879
750	I029-L	0.5	0.15	1.550	0.035	0.08	2.95	13.110	0.90	0.019	0.010	690	90	620
763	I049-L	0.6	0.10	1.790	0.035	0.15	3.80	15.210	0.90	0.015	0.006	1014	150	716
764	I050-L	0.6	0.10	1.265	0.035	0.15	2.31	11.505	0.90	0.015	0.006	767	150	506
765	I051-L	0.6	0.15	2.197	0.035	0.15	4.88	17.925	0.90	0.025	0.010	717	90	879
766	I052-L	0.6	0.15	1.550	0.035	0.15	3.13	13.540	0.90	0.020	0.010	677	90	620
767	I055-L	0.5	0.10	1.790	0.035	0.15	3.55	14.586	0.90	0.017	0.007	858	129	716
26 cases in total														

E.3. Ebbens (2009)

Some details on the Eb09 model:

- The foreshore slope was varied. For the longest slope a flume extension of only 1000 mm instead of $2.5L_{0p}$ was applied.
- The breakwater dimensions are fixed, i.e. only one geometry was tested
- A number of gauges with spacing Δx was placed above the toe, so that a range of at least 150 mm was covered
- Three offshore and three onshore gauges were placed in addition
- The crown wall dimensions were undefined and estimated
- The back side of the breakwater was cut off and modelled as a vertical edge. This is physically impossible, but the effect on the simulation is negligible.

Table E.8: Eb09 stone properties

Material	D_{n50} [m]	n [-]	α [-]	β_c [-]	γ [-]
Toe stone 1	0.0188	0.360	798	1.1	0.34
Toe stone 2	0.0215	0.330	846	1.1	0.34
Toe stone 3	0.0268	0.320	930	1.1	0.34
Armour	0.0400	0.587	1105	1.1	0.34
Underlayer	0.0124	(0.400)	668	1.1	0.34
Core	0.0111	(0.380)	637	1.1	0.34

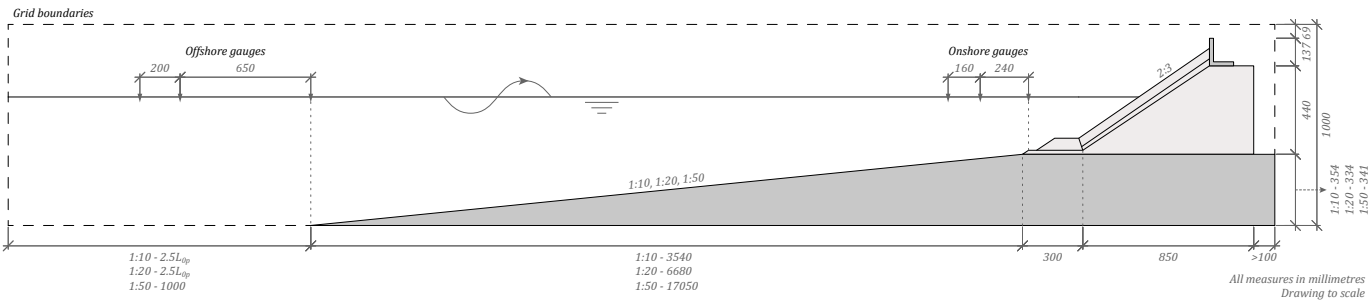

Figure E.3: Geometry of Eb09

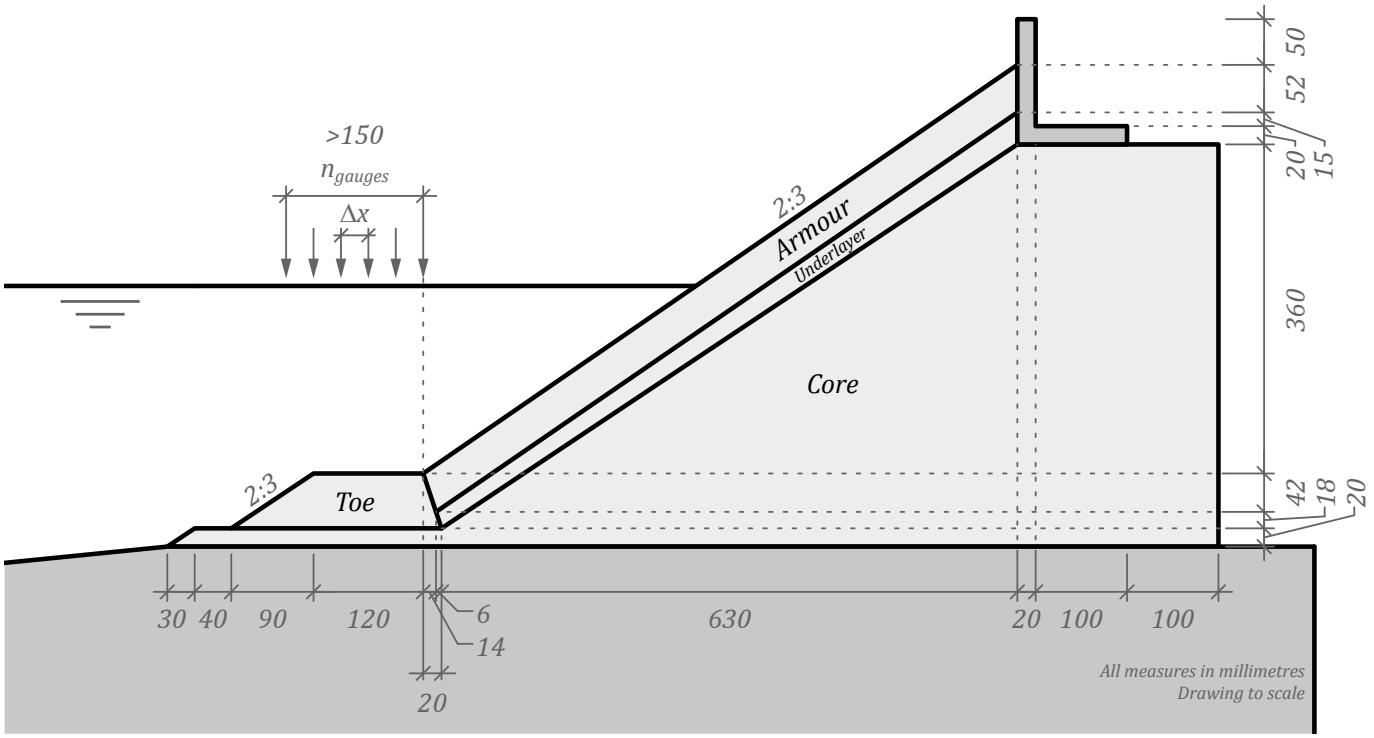

Figure E.4: Detailed geometry of Eb09

Table E.9: Eb09 configuration

Sim. ID	Eb09-ID	$\tan^{-1}\alpha_{fore}$	h_0	H_s	T_p	D_{n50}	t_t	L_{0p}	L_f	h_f	Δx	Δy	n_x	n_y	t_{end}	n_{gauges}
		[-]	[m]	[m]	[s]	[m]	[m]	[m]	[m]	[m]	[m]	[m]	[-]	[-]	[s]	[-]
172	1	50	0.594	0.061	1.16	0.0188	1.65	2.00	19.300	1.000	0.010	0.004	1930	250	464	21
173	2	50	0.594	0.085	1.31	0.0188	1.65	2.44	19.305	1.002	0.015	0.006	1287	167	524	16
174	3	50	0.594	0.115	1.56	0.0188	1.65	3.15	19.300	1.000	0.020	0.008	965	125	624	14
175	4	50	0.594	0.125	1.73	0.0188	1.65	3.62	19.300	1.000	0.020	0.008	965	125	692	14
176	5	50	0.544	0.063	1.16	0.0188	1.65	1.97	19.300	1.000	0.010	0.004	1930	250	464	21
177	6	50	0.544	0.085	1.31	0.0188	1.65	2.39	19.305	1.002	0.015	0.006	1287	167	524	16
178	7	50	0.544	0.106	1.56	0.0188	1.65	3.06	19.312	1.001	0.017	0.007	1136	143	624	15
179	8	50	0.544	0.129	1.73	0.0188	1.65	3.51	19.316	1.008	0.022	0.009	878	112	692	13
180	9	50	0.494	0.058	1.16	0.0188	1.65	1.94	19.300	1.000	0.010	0.004	1930	250	464	21
181	10	50	0.494	0.076	1.33	0.0188	1.65	2.38	19.308	1.000	0.012	0.005	1609	200	532	19
182	11	50	0.494	0.094	1.56	0.0188	1.65	2.97	19.305	1.002	0.015	0.006	1287	167	624	16
183	12	50	0.494	0.113	1.73	0.0188	1.65	3.39	19.300	1.000	0.020	0.008	965	125	692	14
184	13	50	0.474	0.060	1.07	0.0188	1.65	1.69	19.300	1.000	0.010	0.004	1930	250	428	21
185	14	50	0.474	0.063	1.56	0.0188	1.65	2.92	19.308	1.000	0.012	0.005	1609	200	624	19
186	15	50	0.474	0.082	1.21	0.0188	1.65	2.05	19.308	1.000	0.012	0.005	1609	200	484	19
187	16	50	0.474	0.086	2.13	0.0188	1.65	4.27	19.305	1.002	0.015	0.006	1287	167	852	16
188	17	50	0.474	0.103	1.46	0.0188	1.65	2.68	19.312	1.001	0.017	0.007	1136	143	584	15
189	18	50	0.474	0.106	2.56	0.0188	1.65	5.25	19.312	1.001	0.017	0.007	1136	143	1024	15
190	19	50	0.474	0.126	1.73	0.0188	1.65	3.33	19.300	1.000	0.020	0.008	965	125	692	14
191	20	50	0.474	0.126	3.05	0.0188	1.65	6.35	19.300	1.000	0.020	0.008	965	125	1220	14
192	21	50	0.454	0.058	1.07	0.0188	1.65	1.67	19.300	1.000	0.010	0.004	1930	250	428	21
193	22	50	0.454	0.058	1.49	0.0188	1.65	2.71	19.300	1.000	0.010	0.004	1930	250	596	21
194	23	50	0.454	0.078	1.21	0.0188	1.65	2.03	19.308	1.000	0.012	0.005	1609	200	484	19
195	24	50	0.454	0.077	2.07	0.0188	1.65	4.06	19.305	1.002	0.015	0.006	1287	167	828	16
196	25	50	0.454	0.097	1.36	0.0188	1.65	2.40	19.305	1.002	0.015	0.006	1287	167	544	16
197	26	50	0.454	0.099	2.56	0.0188	1.65	5.15	19.312	1.001	0.017	0.007	1136	143	1024	15
198	27	50	0.454	0.117	1.73	0.0188	1.65	3.28	19.300	1.000	0.020	0.008	965	125	692	14
199	28	50	0.454	0.117	3.05	0.0188	1.65	6.23	19.300	1.000	0.020	0.008	965	125	1220	14
200	29	50	0.434	0.061	1.07	0.0188	1.65	1.66	19.300	1.000	0.010	0.004	1930	250	428	21
201	30	50	0.434	0.064	1.73	0.0188	1.65	3.22	19.308	1.000	0.012	0.005	1609	200	692	19
202	31	50	0.434	0.085	1.21	0.0188	1.65	2.00	19.305	1.002	0.013	0.006	1485	167	484	18
203	32	50	0.434	0.084	2.07	0.0188	1.65	3.98	19.305	1.002	0.015	0.006	1287	167	828	16
204	33	50	0.434	0.105	1.36	0.0188	1.65	2.37	19.305	1.001	0.015	0.007	1287	143	544	16
205	34	50	0.434	0.105	2.56	0.0188	1.65	5.05	19.312	1.001	0.017	0.007	1136	143	1024	15
206	35	50	0.434	0.126	1.88	0.0188	1.65	3.56	19.300	1.000	0.020	0.008	965	125	752	14
207	36	50	0.434	0.127	3.05	0.0188	1.65	6.10	19.300	1.000	0.020	0.008	965	125	1220	14

Table E.9: Eb09 configuration (continued)

Sim. ID	Eb09-ID	$\tan^{-1}\alpha_{fore}$ [-]	h_0 [m]	H_s [m]	T_p [s]	D_{n50} [m]	t_t [m]	L_{0p} [m]	L_f [m]	h_f [m]	Δx [m]	Δy [m]	n_x [-]	n_y [-]	t_{end} [s]	n_{gauges} [-]
208	37	50	0.414	0.059	1.07	0.0188	1.65	1.64	19.300	1.000	0.010	0.004	1930	250	428	21
209	38	50	0.414	0.058	1.73	0.0188	1.65	3.16	19.300	1.000	0.010	0.004	1930	250	692	21
210	39	50	0.414	0.078	1.26	0.0188	1.65	2.10	19.308	1.000	0.012	0.005	1609	200	504	19
211	40	50	0.414	0.078	2.29	0.0188	1.65	4.37	19.305	1.002	0.015	0.006	1287	167	916	16
212	41	50	0.414	0.098	1.46	0.0188	1.65	2.56	19.312	1.001	0.017	0.007	1136	143	584	15
213	42	50	0.414	0.097	2.56	0.0188	1.65	4.94	19.312	1.001	0.017	0.007	1136	143	1024	15
214	43	50	0.414	0.118	1.73	0.0188	1.65	3.16	19.300	1.000	0.020	0.008	965	125	692	14
215	44	50	0.414	0.118	3.05	0.0188	1.65	5.96	19.300	1.000	0.020	0.008	965	125	1220	14
216	45	50	0.594	0.061	1.16	0.0215	1.70	2.00	19.300	1.000	0.010	0.004	1930	250	464	21
217	46	50	0.594	0.085	1.31	0.0215	1.70	2.44	19.305	1.002	0.015	0.006	1287	167	524	16
218	47	50	0.594	0.115	1.56	0.0215	1.70	3.15	19.300	1.000	0.020	0.008	965	125	624	14
219	48	50	0.594	0.125	1.73	0.0215	1.70	3.62	19.300	1.000	0.020	0.008	965	125	692	14
220	49	50	0.544	0.063	1.16	0.0215	1.70	1.97	19.300	1.000	0.010	0.004	1930	250	464	21
221	50	50	0.544	0.085	1.31	0.0215	1.70	2.39	19.305	1.002	0.015	0.006	1287	167	524	16
222	51	50	0.544	0.106	1.56	0.0215	1.70	3.06	19.312	1.001	0.017	0.007	1136	143	624	15
223	52	50	0.544	0.129	1.73	0.0215	1.70	3.51	19.316	1.008	0.022	0.009	878	112	692	13
224	53	50	0.494	0.058	1.16	0.0215	1.70	1.94	19.300	1.000	0.010	0.004	1930	250	464	21
225	54	50	0.494	0.076	1.33	0.0215	1.70	2.38	19.308	1.000	0.012	0.005	1609	200	532	19
226	55	50	0.494	0.094	1.56	0.0215	1.70	2.97	19.305	1.002	0.015	0.006	1287	167	624	16
227	56	50	0.494	0.113	1.73	0.0215	1.70	3.39	19.300	1.000	0.020	0.008	965	125	692	14
228	57	50	0.474	0.060	1.07	0.0215	1.70	1.69	19.300	1.000	0.010	0.004	1930	250	428	21
229	58	50	0.474	0.063	1.56	0.0215	1.70	2.92	19.308	1.000	0.012	0.005	1609	200	624	19
230	59	50	0.474	0.082	1.21	0.0215	1.70	2.05	19.308	1.000	0.012	0.005	1609	200	484	19
231	60	50	0.474	0.086	2.13	0.0215	1.70	4.27	19.305	1.002	0.015	0.006	1287	167	852	16
232	61	50	0.474	0.103	1.46	0.0215	1.70	2.68	19.312	1.001	0.017	0.007	1136	143	584	15
233	62	50	0.474	0.106	2.56	0.0215	1.70	5.25	19.312	1.001	0.017	0.007	1136	143	1024	15
234	63	50	0.474	0.126	1.73	0.0215	1.70	3.33	19.300	1.000	0.020	0.008	965	125	692	14
235	64	50	0.474	0.126	3.05	0.0215	1.70	6.35	19.300	1.000	0.020	0.008	965	125	1220	14
236	65	50	0.454	0.058	1.07	0.0215	1.70	1.67	19.300	1.000	0.010	0.004	1930	250	428	21
237	66	50	0.454	0.058	1.49	0.0215	1.70	2.71	19.300	1.000	0.010	0.004	1930	250	596	21
238	67	50	0.454	0.078	1.21	0.0215	1.70	2.03	19.308	1.000	0.012	0.005	1609	200	484	19
239	68	50	0.454	0.077	2.07	0.0215	1.70	4.06	19.305	1.002	0.015	0.006	1287	167	828	16
240	69	50	0.454	0.097	1.36	0.0215	1.70	2.40	19.305	1.002	0.015	0.006	1287	167	544	16
241	70	50	0.454	0.099	2.56	0.0215	1.70	5.15	19.312	1.001	0.017	0.007	1136	143	1024	15
242	71	50	0.454	0.117	1.73	0.0215	1.70	3.28	19.300	1.000	0.020	0.008	965	125	692	14
243	72	50	0.454	0.117	3.05	0.0215	1.70	6.23	19.300	1.000	0.020	0.008	965	125	1220	14
244	73	50	0.434	0.061	1.07	0.0215	1.70	1.66	19.300	1.000	0.010	0.004	1930	250	428	21
245	74	50	0.434	0.064	1.73	0.0215	1.70	3.22	19.308	1.000	0.012	0.005	1609	200	692	19
246	75	50	0.434	0.085	1.21	0.0215	1.70	2.00	19.305	1.002	0.013	0.006	1485	167	484	18
247	76	50	0.434	0.084	2.07	0.0215	1.70	3.98	19.305	1.002	0.015	0.006	1287	167	828	16
248	77	50	0.434	0.105	1.36	0.0215	1.70	2.37	19.305	1.001	0.015	0.007	1287	143	544	16
249	78	50	0.434	0.105	2.56	0.0215	1.70	5.05	19.312	1.001	0.017	0.007	1136	143	1024	15
250	79	50	0.434	0.126	1.88	0.0215	1.70	3.56	19.300	1.000	0.020	0.008	965	125	752	14
251	80	50	0.434	0.127	3.05	0.0215	1.70	6.10	19.300	1.000	0.020	0.008	965	125	1220	14
252	81	50	0.414	0.059	1.07	0.0215	1.70	1.64	19.300	1.000	0.010	0.004	1930	250	428	21
253	82	50	0.414	0.058	1.73	0.0215	1.70	3.16	19.300	1.000	0.010	0.004	1930	250	692	21
254	83	50	0.414	0.078	1.26	0.0215	1.70	2.10	19.308	1.000	0.012	0.005	1609	200	504	19
255	84	50	0.414	0.078	2.29	0.0215	1.70	4.37	19.305	1.002	0.015	0.006	1287	167	916	16
256	85	50	0.414	0.098	1.46	0.0215	1.70	2.56	19.312	1.001	0.017	0.007	1136	143	584	15
257	86	50	0.414	0.097	2.56	0.0215	1.70	4.94	19.312	1.001	0.017	0.007	1136	143	1024	15
258	87	50	0.414	0.118	1.73	0.0215	1.70	3.16	19.300	1.000	0.020	0.008	965	125	692	14
259	88	50	0.414	0.118	3.05	0.0215	1.70	5.96	19.300	1.000	0.020	0.008	965	125	1220	14
260	89	20	0.698	0.062	0.98	0.0188	1.65	1.49	11.664	1.000	0.009	0.004	1296	250	392	23
261	90	20	0.698	0.060	1.56	0.0188	1.65	3.30	16.190	1.000	0.010	0.004	1619	250	624	21
262	91	20	0.698	0.080	1.21	0.0188	1.65	2.20	13.440	1.000	0.012	0.005	1120	200	484	19
263	92	20	0.698	0.088	2.07	0.0188	1.65	4.82	19.995	1.002	0.015	0.006	1333	167	828	16
264	93	20	0.698	0.101	1.28	0.0188	1.65	2.42	14.000	1.001	0.016	0.007	875	143	512	16
265	94	20	0.698	0.114	2.37	0.0188	1.65	5.68	22.140	1.000	0.020	0.008	1107	125	948	14
266	95	20	0.698	0.122	1.46	0.0188	1.65	2.99	15.409	1.000	0.019	0.008	811	125	584	14
267	96	20	0.698	0.129	2.91	0.0188	1.65	7.19	25.916	1.008	0.022	0.009	1178	112	1164	13
268	97	20	0.562	0.061	0.98	0.0188	1.65	1.48	11.619	1.000	0.009	0.004	1291	250	392	23
269	98	20	0.562	0.059	1.56	0.0188	1.65	3.10	15.670	1.000	0.010	0.004	1567	250	624	21
270	99	20	0.562	0.079	1.14	0.0188	1.65	1.93	12.756	1.000	0.012	0.005	1063	200	456	19
271	100	20	0.562	0.084	2.07	0.0188	1.65	4.43	19.020	1.002	0.015	0.006	1268	167	828	16
272	101	20	0.562	0.098	1.31	0.0188	1.65	2.41	13.952	1.001	0.016	0.007	872	143	524	16
273	102	20	0.562	0.109	2.46	0.0188	1.65	5.42	21.471	1.001	0.017	0.007	1263	143	984	15
274	103	20	0.562	0.117	1.56	0.0188	1.65	3.10	15.680	1.000	0.020	0.008	784	125	624	14
275	104	20	0.562	0.129	2.91	0.0188	1.65	6.53	24.266	1.008	0.022	0.009	1103	112	1164	13
276	105	20	0.512	0.060	0.98	0.0188	1.65	1.46	11.592	1.000	0.009	0.004	1288	250	392	23
277	106	20	0.512	0.059	1.46	0.0188	1.65	2.75	14.800	1.000	0.010	0.004	1480	250	584	21
278	107	20	0.512	0.079	1.14	0.0188	1.65	1.90	12.684	1.000	0.012	0.005	1057	200	456	19
279	108	20	0.512	0.089	2.07	0.0188	1.65	4.27	18.600	1.002	0.015	0.006	1240	167	828	16
280	109	20	0.512	0.100	1.28	0.0188	1.65	2.27	13.620	1.001	0.015	0.007	908	143	512	16
281	110	20	0.512	0.112	2.37	0.0188	1.65	4.99	20.400	1.001	0.017	0.007	1200	143	948	15
282	111	20	0.512	0.117	1.56	0.0188	1.65	3.00	15.440	1.000	0.020	0.008	772	125	624	14
283	112	20	0.512	0.121	2.91	0.0188	1.65	6.26	23.580	1.000	0.020	0.008	1179	125	1164	14
284	113	20	0.698	0.062	0.98	0.0215	1.70	1.49	11.664	1.000	0.009	0.004	1296	250	392	23
285	114	20	0.698	0.060	1.56	0.0215	1.70	3.30	16.190	1.000	0.010	0.004	1619	250	624	21
286	115	20	0.698	0.080	1.21	0.0215	1.70	2.20	13.440	1.000	0.012	0.005	1120	200	484	19

Table E.9: Eb09 configuration (continued)

Sim. ID	Eb09-ID	$\tan^{-1}\alpha_{fore}$	h_0	H_s	T_p	D_{n50}	t_t	L_{0p}	L_f	h_f	Δx	Δy	n_x	n_y	t_{end}	n_{gauges}
		[-]	[m]	[m]	[s]	[m]	[m]	[m]	[m]	[m]	[m]	[m]	[-]	[-]	[s]	[-]
287	116	20	0.698	0.088	2.07	0.0215	1.70	4.82	19.995	1.002	0.015	0.006	1333	167	828	16
288	117	20	0.698	0.101	1.28	0.0215	1.70	2.42	14.000	1.001	0.016	0.007	875	143	512	16
289	118	20	0.698	0.114	2.37	0.0215	1.70	5.68	22.140	1.000	0.020	0.008	1107	125	948	14
290	119	20	0.698	0.122	1.46	0.0215	1.70	2.99	15.409	1.000	0.019	0.008	811	125	584	14
291	120	20	0.698	0.129	2.91	0.0215	1.70	7.19	25.916	1.008	0.022	0.009	1178	112	1164	13
292	121	20	0.562	0.061	0.98	0.0215	1.70	1.48	11.619	1.000	0.009	0.004	1291	250	392	23
293	122	20	0.562	0.059	1.56	0.0215	1.70	3.10	15.670	1.000	0.010	0.004	1567	250	624	21
294	123	20	0.562	0.079	1.14	0.0215	1.70	1.93	12.756	1.000	0.012	0.005	1063	200	456	19
295	124	20	0.562	0.084	2.07	0.0215	1.70	4.43	19.020	1.002	0.015	0.006	1268	167	828	16
296	125	20	0.562	0.098	1.31	0.0215	1.70	2.41	13.952	1.001	0.016	0.007	872	143	524	16
297	126	20	0.562	0.109	2.46	0.0215	1.70	5.42	21.471	1.001	0.017	0.007	1263	143	984	15
298	127	20	0.562	0.117	1.56	0.0215	1.70	3.10	15.680	1.000	0.020	0.008	784	125	624	14
299	128	20	0.562	0.129	2.91	0.0215	1.70	6.53	24.266	1.008	0.022	0.009	1103	112	1164	13
300	129	20	0.512	0.060	0.98	0.0215	1.70	1.46	11.592	1.000	0.009	0.004	1288	250	392	23
301	130	20	0.512	0.059	1.46	0.0215	1.70	2.75	14.800	1.000	0.010	0.004	1480	250	584	21
302	131	20	0.512	0.079	1.14	0.0215	1.70	1.90	12.684	1.000	0.012	0.005	1057	200	456	19
303	132	20	0.512	0.089	2.07	0.0215	1.70	4.27	18.600	1.002	0.015	0.006	1240	167	828	16
304	133	20	0.512	0.100	1.28	0.0215	1.70	2.27	13.620	1.001	0.015	0.007	908	143	512	16
305	134	20	0.512	0.112	2.37	0.0215	1.70	4.99	20.400	1.001	0.017	0.007	1200	143	948	15
306	135	20	0.512	0.117	1.56	0.0215	1.70	3.00	15.440	1.000	0.020	0.008	772	125	624	14
307	136	20	0.512	0.121	2.91	0.0215	1.70	6.26	23.580	1.000	0.020	0.008	1179	125	1164	14
308	137	20	0.612	0.059	1.16	0.0215	1.70	2.01	12.960	1.000	0.010	0.004	1296	250	464	21
309	138	20	0.612	0.083	1.33	0.0215	1.70	2.51	14.220	1.002	0.015	0.006	948	167	532	16
310	139	20	0.612	0.107	1.49	0.0215	1.70	2.98	15.385	1.001	0.017	0.007	905	143	596	15
311	140	20	0.612	0.122	1.64	0.0215	1.70	3.41	16.460	1.000	0.020	0.008	823	125	656	14
312	141	20	0.562	0.059	1.16	0.0215	1.70	1.99	12.900	1.000	0.010	0.004	1290	250	464	21
313	142	20	0.562	0.078	1.33	0.0215	1.70	2.46	14.100	1.000	0.012	0.005	1175	200	532	19
314	143	20	0.562	0.098	1.49	0.0215	1.70	2.91	15.198	1.001	0.017	0.007	894	143	596	15
315	144	20	0.562	0.120	1.73	0.0215	1.70	3.55	16.820	1.000	0.020	0.008	841	125	692	14
316	145	20	0.512	0.058	1.16	0.0215	1.70	1.95	12.810	1.000	0.010	0.004	1281	250	464	21
317	146	20	0.512	0.076	1.26	0.0215	1.70	2.22	13.488	1.000	0.012	0.005	1124	200	504	19
318	147	20	0.512	0.095	1.46	0.0215	1.70	2.75	14.805	1.002	0.015	0.006	987	167	584	16
319	148	20	0.512	0.114	1.73	0.0215	1.70	3.43	16.520	1.000	0.020	0.008	826	125	692	14
320	149	20	0.492	0.058	1.02	0.0215	1.70	1.56	11.840	1.000	0.010	0.004	1184	250	408	21
321	150	20	0.492	0.060	1.49	0.0215	1.70	2.79	14.900	1.000	0.010	0.004	1490	250	596	21
322	151	20	0.492	0.078	1.16	0.0215	1.70	1.94	12.768	1.000	0.012	0.005	1064	200	464	19
323	152	20	0.492	0.080	2.07	0.0215	1.70	4.20	18.420	1.002	0.015	0.006	1228	167	828	16
324	153	20	0.492	0.099	1.28	0.0215	1.70	2.25	13.560	1.001	0.015	0.007	904	143	512	16
325	154	20	0.492	0.100	2.37	0.0215	1.70	4.90	20.196	1.001	0.017	0.007	1188	143	948	15
326	155	20	0.492	0.119	1.46	0.0215	1.70	2.71	14.724	1.000	0.018	0.008	818	125	584	15
327	156	20	0.492	0.118	2.91	0.0215	1.70	6.14	23.300	1.000	0.020	0.008	1165	125	1164	14
328	157	20	0.472	0.058	1.02	0.0215	1.70	1.55	11.820	1.000	0.010	0.004	1182	250	408	21
329	158	20	0.472	0.062	1.49	0.0215	1.70	2.75	14.800	1.000	0.010	0.004	1480	250	596	21
330	159	20	0.472	0.080	1.16	0.0215	1.70	1.92	12.732	1.000	0.012	0.005	1061	200	464	19
331	160	20	0.472	0.085	2.07	0.0215	1.70	4.12	18.240	1.002	0.015	0.006	1216	167	828	16
332	161	20	0.472	0.102	1.33	0.0215	1.70	2.35	13.815	1.001	0.015	0.007	921	143	532	16
333	162	20	0.472	0.105	2.37	0.0215	1.70	4.81	19.958	1.001	0.017	0.007	1174	143	948	15
334	163	20	0.472	0.124	1.46	0.0215	1.70	2.68	14.620	1.000	0.017	0.008	860	125	584	15
335	164	20	0.472	0.123	2.91	0.0215	1.70	6.03	23.000	1.000	0.020	0.008	1150	125	1164	14
336	165	20	0.452	0.058	1.02	0.0215	1.70	1.54	11.790	1.000	0.010	0.004	1179	250	408	21
337	166	20	0.452	0.058	1.49	0.0215	1.70	2.71	14.700	1.000	0.010	0.004	1470	250	596	21
338	167	20	0.452	0.079	1.16	0.0215	1.70	1.90	12.684	1.000	0.012	0.005	1057	200	464	19
339	168	20	0.452	0.077	2	0.0215	1.70	3.89	17.670	1.002	0.015	0.006	1178	167	800	16
340	169	20	0.452	0.098	1.33	0.0215	1.70	2.32	13.740	1.001	0.015	0.007	916	143	532	16
341	170	20	0.452	0.098	2.37	0.0215	1.70	4.72	19.737	1.001	0.017	0.007	1161	143	948	15
342	171	20	0.452	0.118	1.52	0.0215	1.70	2.78	14.886	1.000	0.018	0.008	827	125	608	15
343	172	20	0.452	0.116	2.91	0.0215	1.70	5.91	22.700	1.000	0.020	0.008	1135	125	1164	14
344	173	20	0.432	0.062	1.07	0.0215	1.70	1.66	12.080	1.000	0.010	0.004	1208	250	428	21
345	174	20	0.432	0.065	1.49	0.0215	1.70	2.67	14.604	1.000	0.012	0.005	1217	200	596	19
346	175	20	0.432	0.086	1.19	0.0215	1.70	1.95	12.818	1.002	0.013	0.006	986	167	476	18
347	176	20	0.432	0.086	2	0.0215	1.70	3.82	17.475	1.002	0.015	0.006	1165	167	800	16
348	177	20	0.432	0.106	1.33	0.0215	1.70	2.29	13.665	1.001	0.015	0.007	911	143	532	16
349	178	20	0.432	0.105	2.56	0.0215	1.70	5.04	20.536	1.001	0.017	0.007	1208	143	1024	15
350	179	20	0.432	0.126	1.73	0.0215	1.70	3.22	15.980	1.000	0.020	0.008	799	125	692	14
351	180	20	0.432	0.127	2.91	0.0215	1.70	5.79	22.400	1.000	0.020	0.008	1120	125	1164	14
352	181	20	0.612	0.059	1.16	0.0268	1.75	2.01	12.960	1.000	0.010	0.004	1296	250	464	21
353	182	20	0.612	0.083	1.33	0.0268	1.75	2.51	14.220	1.002	0.015	0.006	948	167	532	16
354	183	20	0.612	0.107	1.49	0.0268	1.75	2.98	15.385	1.001	0.017	0.007	905	143	596	15
355	184	20	0.612	0.122	1.64	0.0268	1.75	3.41	16.460	1.000	0.020	0.008	823	125	656	14
356	185	20	0.562	0.059	1.16	0.0268	1.75	1.99	12.900	1.000	0.010	0.004	1290	250	464	21
357	186	20	0.562	0.078	1.33	0.0268	1.75	2.46	14.100	1.000	0.012	0.005	1175	200	532	19
358	187	20	0.562	0.098	1.49	0.0268	1.75	2.91	15.198	1.001	0.017	0.007	894	143	596	15
359	188	20	0.562	0.120	1.73	0.0268	1.75	3.55	16.820	1.000	0.020	0.008	841	125	692	14
360	189	20	0.512	0.058	1.16	0.0268	1.75	1.95	12.810	1.000	0.010	0.004	1281	250	464	21
361	190	20	0.512	0.076	1.26	0.0268	1.75	2.22	13.488	1.000	0.012	0.005	1124	200	504	19
362	191	20	0.512	0.095	1.46	0.0268	1.75	2.75	14.805	1.002	0.015	0.006	987	167	584	16
363	192	20	0.512	0.114	1.73	0.0268	1.75	3.43	16.520	1.000	0.020	0.008	826	125	692	14
364	193	20	0.492	0.058	1.02	0.0268	1.75	1.56	11.840	1.000	0.010	0.004	1184	250	408	21
365	194	20	0.492	0.060	1.49	0.0268	1.75	2.79	14.900	1.000	0.010	0.004	1490	250	596	21

Table E.9: Eb09 configuration (continued)

Sim. ID	Eb09-ID	$\tan^{-1}\alpha_{fore}$ [-]	h_0 [m]	H_s [m]	T_p [s]	D_{n50} [m]	t_t [m]	L_{0p} [m]	L_f [m]	h_f [m]	Δx [m]	Δy [m]	n_x [-]	n_y [-]	t_{end} [s]	n_{gauges} [-]
366	195	20	0.492	0.078	1.16	0.0268	1.75	1.94	12.768	1.000	0.012	0.005	1064	200	464	19
367	196	20	0.492	0.080	2.07	0.0268	1.75	4.20	18.420	1.002	0.015	0.006	1228	167	828	16
368	197	20	0.492	0.099	1.28	0.0268	1.75	2.25	13.560	1.001	0.015	0.007	904	143	512	16
369	198	20	0.492	0.100	2.37	0.0268	1.75	4.90	20.196	1.001	0.017	0.007	1188	143	948	15
370	199	20	0.492	0.119	1.46	0.0268	1.75	2.71	14.724	1.000	0.018	0.008	818	125	584	15
371	200	20	0.492	0.118	2.91	0.0268	1.75	6.14	23.300	1.000	0.020	0.008	1165	125	1164	14
372	201	20	0.472	0.058	1.02	0.0268	1.75	1.55	11.820	1.000	0.010	0.004	1182	250	408	21
373	202	20	0.472	0.062	1.49	0.0268	1.75	2.75	14.800	1.000	0.010	0.004	1480	250	596	21
374	203	20	0.472	0.080	1.16	0.0268	1.75	1.92	12.732	1.000	0.012	0.005	1061	200	464	19
375	204	20	0.472	0.085	2.07	0.0268	1.75	4.12	18.240	1.002	0.015	0.006	1216	167	828	16
376	205	20	0.472	0.102	1.33	0.0268	1.75	2.35	13.815	1.001	0.015	0.007	921	143	532	16
377	206	20	0.472	0.105	2.37	0.0268	1.75	4.81	19.958	1.001	0.017	0.007	1174	143	948	15
378	207	20	0.472	0.124	1.46	0.0268	1.75	2.68	14.620	1.000	0.017	0.008	860	125	584	15
379	208	20	0.472	0.123	2.91	0.0268	1.75	6.03	23.000	1.000	0.020	0.008	1150	125	1164	14
380	209	20	0.452	0.058	1.02	0.0268	1.75	1.54	11.790	1.000	0.010	0.004	1179	250	408	21
381	210	20	0.452	0.058	1.49	0.0268	1.75	2.71	14.700	1.000	0.010	0.004	1470	250	596	21
382	211	20	0.452	0.079	1.16	0.0268	1.75	1.90	12.684	1.000	0.012	0.005	1057	200	464	19
383	212	20	0.452	0.077	2	0.0268	1.75	3.89	17.670	1.002	0.015	0.006	1178	167	800	16
384	213	20	0.452	0.098	1.33	0.0268	1.75	2.32	13.740	1.001	0.015	0.007	916	143	532	16
385	214	20	0.452	0.098	2.37	0.0268	1.75	4.72	19.737	1.001	0.017	0.007	1161	143	948	15
386	215	20	0.452	0.118	1.52	0.0268	1.75	2.78	14.886	1.000	0.018	0.008	827	125	608	15
387	216	20	0.452	0.116	2.91	0.0268	1.75	5.91	22.700	1.000	0.020	0.008	1135	125	1164	14
388	217	20	0.432	0.062	1.07	0.0268	1.75	1.66	12.080	1.000	0.010	0.004	1208	250	428	21
389	218	20	0.432	0.065	1.49	0.0268	1.75	2.67	14.604	1.000	0.012	0.005	1217	200	596	19
390	219	20	0.432	0.086	1.19	0.0268	1.75	1.95	12.818	1.002	0.013	0.006	986	167	476	18
391	220	20	0.432	0.086	2	0.0268	1.75	3.82	17.475	1.002	0.015	0.006	1165	167	800	16
392	221	20	0.432	0.106	1.33	0.0268	1.75	2.29	13.665	1.001	0.015	0.007	911	143	532	16
393	222	20	0.432	0.105	2.56	0.0268	1.75	5.04	20.536	1.001	0.017	0.007	1208	143	1024	15
394	223	20	0.432	0.126	1.73	0.0268	1.75	3.22	15.980	1.000	0.020	0.008	799	125	692	14
395	224	20	0.432	0.127	2.91	0.0268	1.75	5.79	22.400	1.000	0.020	0.008	1120	125	1164	14
396	225	10	0.607	0.061	1.14	0.0215	1.70	1.95	9.670	1.000	0.010	0.004	967	250	456	21
397	226	10	0.607	0.085	1.28	0.0215	1.70	2.36	10.710	1.002	0.015	0.006	714	167	512	16
398	227	10	0.607	0.110	1.46	0.0215	1.70	2.89	12.019	1.001	0.017	0.007	707	143	584	15
399	228	10	0.607	0.126	1.64	0.0215	1.70	3.40	13.280	1.000	0.020	0.008	664	125	656	14
400	229	10	0.557	0.060	1.14	0.0215	1.70	1.93	9.610	1.000	0.010	0.004	961	250	456	21
401	230	10	0.557	0.079	1.31	0.0215	1.70	2.40	10.800	1.000	0.012	0.005	900	200	524	19
402	231	10	0.557	0.099	1.46	0.0215	1.70	2.82	11.832	1.001	0.017	0.007	696	143	584	15
403	232	10	0.557	0.121	1.64	0.0215	1.70	3.30	13.040	1.000	0.020	0.008	652	125	656	14
404	233	10	0.507	0.058	1.14	0.0215	1.70	1.89	9.530	1.000	0.010	0.004	953	250	456	21
405	234	10	0.507	0.076	1.28	0.0215	1.70	2.27	10.464	1.000	0.012	0.005	872	200	512	19
406	235	10	0.507	0.095	1.49	0.0215	1.70	2.81	11.835	1.002	0.015	0.006	789	167	596	16
407	236	10	0.507	0.112	1.73	0.0215	1.70	3.42	13.345	1.001	0.017	0.007	785	143	692	15
408	237	10	0.487	0.059	0.98	0.0215	1.70	1.46	8.433	1.000	0.009	0.004	937	250	392	23
409	238	10	0.487	0.061	1.49	0.0215	1.70	2.78	11.740	1.000	0.010	0.004	1174	250	596	21
410	239	10	0.487	0.080	1.14	0.0215	1.70	1.88	9.492	1.000	0.012	0.005	791	200	456	19
411	240	10	0.487	0.081	2.07	0.0215	1.70	4.18	15.240	1.002	0.015	0.006	1016	167	828	16
412	241	10	0.487	0.099	1.28	0.0215	1.70	2.24	10.402	1.001	0.014	0.007	743	143	512	17
413	242	10	0.487	0.107	2.29	0.0215	1.70	4.69	16.524	1.001	0.017	0.007	972	143	916	15
414	243	10	0.467	0.059	0.98	0.0215	1.70	1.45	8.415	1.000	0.009	0.004	935	250	392	23
415	244	10	0.467	0.061	1.49	0.0215	1.70	2.74	11.640	1.000	0.010	0.004	1164	250	596	21
416	245	10	0.467	0.080	1.14	0.0215	1.70	1.86	9.456	1.000	0.012	0.005	788	200	456	19
417	246	10	0.467	0.085	2.07	0.0215	1.70	4.11	15.060	1.002	0.015	0.006	1004	167	828	16
418	247	10	0.467	0.101	1.28	0.0215	1.70	2.22	10.346	1.001	0.014	0.007	739	143	512	17
419	248	10	0.467	0.103	2.37	0.0215	1.70	4.79	16.779	1.001	0.017	0.007	987	143	948	15
420	249	10	0.447	0.058	0.98	0.0215	1.70	1.44	8.397	1.000	0.009	0.004	933	250	392	23
421	250	10	0.447	0.058	1.56	0.0215	1.70	2.86	11.950	1.000	0.010	0.004	1195	250	624	21
422	251	10	0.447	0.077	1.14	0.0215	1.70	1.85	9.408	1.000	0.012	0.005	784	200	456	19
423	252	10	0.447	0.077	2.07	0.0215	1.70	4.03	14.868	1.000	0.012	0.005	1239	200	828	19
424	253	10	0.447	0.096	1.28	0.0215	1.70	2.19	10.276	1.002	0.014	0.006	734	167	512	17
425	254	10	0.447	0.099	2.56	0.0215	1.70	5.12	17.578	1.001	0.017	0.007	1034	143	1024	15
426	255	10	0.427	0.062	0.98	0.0215	1.70	1.43	8.370	1.000	0.009	0.004	930	250	392	23
427	256	10	0.427	0.064	1.56	0.0215	1.70	2.82	11.830	1.000	0.010	0.004	1183	250	624	21
428	257	10	0.427	0.084	1.14	0.0215	1.70	1.83	9.360	1.002	0.012	0.006	780	167	456	19
429	258	10	0.427	0.085	2.07	0.0215	1.70	3.95	14.670	1.002	0.015	0.006	978	167	828	16
430	259	10	0.427	0.107	1.28	0.0215	1.70	2.16	10.206	1.001	0.014	0.007	729	143	512	17
431	260	10	0.427	0.107	2.37	0.0215	1.70	4.60	16.303	1.001	0.017	0.007	959	143	948	15
432	261	10	0.607	0.061	1.14	0.0268	1.75	1.95	9.670	1.000	0.010	0.004	967	250	456	21
433	262	10	0.607	0.085	1.28	0.0268	1.75	2.36	10.710	1.002	0.015	0.006	714	167	512	16
434	263	10	0.607	0.110	1.46	0.0268	1.75	2.89	12.019	1.001	0.017	0.007	707	143	584	15
435	264	10	0.607	0.126	1.64	0.0268	1.75	3.40	13.280	1.000	0.020	0.008	664	125	656	14
436	265	10	0.557	0.060	1.14	0.0268	1.75	1.93	9.610	1.000	0.010	0.004	961	250	456	21
437	266	10	0.557	0.079	1.31	0.0268	1.75	2.40	10.800	1.000	0.012	0.005	900	200	524	19
438	267	10	0.557	0.099	1.46	0.0268	1.75	2.82	11.832	1.001	0.017	0.007	696	143	584	15
439	268	10	0.557	0.121	1.64	0.0268	1.75	3.30	13.040	1.000	0.020	0.008	652	125	656	14
440	269	10	0.507	0.058	1.14	0.0268	1.75	1.89	9.530	1.000	0.010	0.004	953	250	456	21
441	270	10	0.507	0.076	1.28	0.0268	1.75	2.27	10.464	1.000	0.012	0.005	872	200	512	19
442	271	10	0.507	0.095	1.49	0.0268	1.75	2.81	11.835	1.002	0.015	0.006	789	167	596	16
443	272	10	0.507	0.112	1.73	0.0268	1.75	3.42	13.345	1.001	0.017	0.007	785	143	692	15
444	273	10	0.487	0.059	0.98	0.0268	1.75	1.46	8.433	1.000	0.009	0.004	937	250	392	23

Table E.9: Eb09 configuration (continued)

Sim. ID	Eb09-ID	$\tan^{-1}\alpha_{fore}$ [-]	h_0 [m]	H_s [m]	T_p [s]	D_{n50} [m]	t_t [m]	L_{0p} [m]	L_f [m]	h_f [m]	Δx [m]	Δy [m]	n_x [-]	n_y [-]	t_{end} [s]	n_{gauges} [-]
445	274	10	0.487	0.061	1.49	0.0268	1.75	2.78	11.740	1.000	0.010	0.004	1174	250	596	21
446	275	10	0.487	0.080	1.14	0.0268	1.75	1.88	9.492	1.000	0.012	0.005	791	200	456	19
447	276	10	0.487	0.081	2.07	0.0268	1.75	4.18	15.240	1.002	0.015	0.006	1016	167	828	16
448	277	10	0.487	0.099	1.28	0.0268	1.75	2.24	10.402	1.001	0.014	0.007	743	143	512	17
449	278	10	0.487	0.107	2.29	0.0268	1.75	4.69	16.524	1.001	0.017	0.007	972	143	916	15
450	279	10	0.467	0.059	0.98	0.0268	1.75	1.45	8.415	1.000	0.009	0.004	935	250	392	23
451	280	10	0.467	0.061	1.49	0.0268	1.75	2.74	11.640	1.000	0.010	0.004	1164	250	596	21
452	281	10	0.467	0.080	1.14	0.0268	1.75	1.86	9.456	1.000	0.012	0.005	788	200	456	19
453	282	10	0.467	0.085	2.07	0.0268	1.75	4.11	15.060	1.002	0.015	0.006	1004	167	828	16
454	283	10	0.467	0.101	1.28	0.0268	1.75	2.22	10.346	1.001	0.014	0.007	739	143	512	17
455	284	10	0.467	0.103	2.37	0.0268	1.75	4.79	16.779	1.001	0.017	0.007	987	143	948	15
456	285	10	0.447	0.058	0.98	0.0268	1.75	1.44	8.397	1.000	0.009	0.004	933	250	392	23
457	286	10	0.447	0.058	1.56	0.0268	1.75	2.86	11.950	1.000	0.010	0.004	1195	250	624	21
458	287	10	0.447	0.077	1.14	0.0268	1.75	1.85	9.408	1.000	0.012	0.005	784	200	456	19
459	288	10	0.447	0.077	2.07	0.0268	1.75	4.03	14.868	1.000	0.012	0.005	1239	200	828	19
460	289	10	0.447	0.096	1.28	0.0268	1.75	2.19	10.276	1.002	0.014	0.006	734	167	512	17
461	290	10	0.447	0.099	2.56	0.0268	1.75	5.12	17.578	1.001	0.017	0.007	1034	143	1024	15
462	291	10	0.427	0.062	0.98	0.0268	1.75	1.43	8.370	1.000	0.009	0.004	930	250	392	23
463	292	10	0.427	0.064	1.56	0.0268	1.75	2.82	11.830	1.000	0.010	0.004	1183	250	624	21
464	293	10	0.427	0.084	1.14	0.0268	1.75	1.83	9.360	1.002	0.012	0.006	780	167	456	19
465	294	10	0.427	0.085	2.07	0.0268	1.75	3.95	14.670	1.002	0.015	0.006	978	167	828	16
466	295	10	0.427	0.107	1.28	0.0268	1.75	2.16	10.206	1.001	0.014	0.007	729	143	512	17
467	296	10	0.427	0.107	2.37	0.0268	1.75	4.60	16.303	1.001	0.017	0.007	959	143	948	15
296 cases in total																

E.4. SIMULATION PERFORMANCE

The table below gives some useful information on the simulations run during research. Note that some simulations did not succeed at first, after which they have been re-run. The final (best) result is then shown.

Some details on the column definitions:

- Steps: the number of calculation steps it took IH-2VOF to get to the end. It depends on the numerical time step Δt which is updated every step.
- Field variables: the amount of exported field variables. A field variable is the output of a certain parameter over all cells. It is known that this output is time consuming as writing to the hard disk is rather slow.
- Duration: the computation time it took IH-2VOF to get to the end.
- Performance: a measure for the performance of the model. It is calculated as duration in milliseconds divided by the number of cells and the requested endtime.
- Endtime: the model time t_{end} reached.

Most of the computers used had a Windows 7 operating system and an Intel Core i5 (quad core) CPU.

Table E.10: Simulations

Case	Finished	Steps [-]	Field variables	Duration [s]	Duration [h]	Performance $\left[\frac{\text{ms}}{\text{cell·time}}\right]$	Endtime [s]	Endtime [%]
Convergence tests – flume length								
convtest_length_L0-0.5	✓	32701	1	4395	1.22	0.517		
convtest_length_L0-1.0	✓	32287	1	5113	1.42	0.522		
convtest_length_L0-1.5	✓	31601	1	5708	1.59	0.514		
convtest_length_L0-2.0	✓	31294	1	6715	1.87	0.542		
convtest_length_L0-2.5	✓	14575	1	3928	1.09	0.574		
convtest_length_L0-3.0	✓	30236	1	7776	2.16	0.519		
convtest_length_L0-3.5	✓	14103	1	5486	1.52	0.674		
convtest_length_L0-4.0	✓	14084	1	5741	1.59	0.653		
Convergence tests – cell width								
convtest_dx_50	✓	10313		448	0.12	0.206		
convtest_dx_100	✓	11930		1830	0.51	0.411		
convtest_dx_200	✓	17917		8841	2.46	0.993		
convtest_dx_250	✓	21332		12300	3.42	1.105		
Convergence tests – cell height								
convtest_dy_5	✓	10960		1300	0.36	0.38		
convtest_dy_15	✓	20965		12408	3.45	1.088		
convtest_dy_20	✓	24378		15103	4.2	1.103		
Convergence tests – friction check								
frictioncheck_L0-1.5	✓	14479	2	1692	0.47	0.52		
frictioncheck_L0-2.0	✓	14155	2	2305	0.64	0.532		
frictioncheck_L0-2.5	✓	14339	2	2862	0.79	0.527		

Table E.10: Simulations (continued)

Case	Finished	Steps	Field variables	Duration		Performance	Endtime	
		[-]		[s]	[h]	$\left[\frac{\text{ms}}{\text{cell·time}}\right]$	[s]	[%]
frictioncheck_L0-3.0	✓	14170	2	3415	0.95	0.525		
frictioncheck_L0-3.5	✓	14207	2	4241	1.18	0.559		
frictioncheck_L0-4.0	✓	14196	2	4661	1.29	0.538		
NK09 simulations with regular waves								
NK09_688	✓	18541		10087	2.8	0.737		
NK09_689	✓	19667		8417	2.34	0.813		
NK09_690	✓	14175		2756	0.77	0.474		
NK09_691	✓	13898		2026	0.56	0.392		
NK09_692	✓	16377		2701	0.75	0.492		
NK09_693	✓	90261		6611	1.84	1.723		
NK09_694	✓	14480		1805	0.5	0.471		
NK09_695	✓	82174		30624	8.51	2.334		
NK09_696	✓	19739		8032	2.23	0.739		
NK09_697	✓	14116		2064	0.57	0.374		
NK09_698	✓	30639		3294	0.91	0.667		
NK09_699	✓	16007		2478	0.69	0.443		
NK09_700	✓	22155		6508	1.81	0.523		
NK09_701	✓	21475		10374	2.88	0.914		
NK09_702	✓	18535		2452	0.68	0.473		
NK09_711	✓	17994		21259	5.91	1.553		
NK09_712	✓	19031		5803	1.61	0.56		
NK09_713	✓	14140		2974	0.83	0.512		
NK09_714	✓	14009		3118	0.87	0.603		
NK09_715	✓	15874		3491	0.97	0.637		
NK09_716	✓	89483	2	1775	0.49	0.463		
NK09_717	✓	14501		1776	0.49	0.464		
NK09_718	✓	64862		25041	6.96	1.908		
NK09_719	✓	19493		8089	2.25	0.744		
NK09_720	✓	14164		1943	0.54	0.352		
NK09_721	✓	30319		3186	0.89	0.645		
NK09_722	✓	16152		2427	0.67	0.434		
NK09_728	✓	19462		21964	6.1	1.604		
NK09_729	✓	19601		3280	0.91	0.317		
NK09_730	✓	14176		3281	0.91	0.565		
NK09_731	✓	13950		2031	0.56	0.393		
NK09_732	✓	16429		2686	0.75	0.49		
NK09_733	✓	80171		5905	1.64	1.539		
NK09_734	✓	14538		1784	0.5	0.466		
NK09_735	✓	85315		30305	8.42	2.309		
NK09_736	✓	19760		12214	3.39	1.124		
NK09_737	✓	14124		2101	0.58	0.38		
NK09_738	✓	30707		3412	0.95	0.69		
NK09_739	✓	15986		2574	0.72	0.461		
NK09_740	✓	22201		8783	2.44	0.706		
NK09_741	✓	21492	2	9660	2.68	0.851		
NK09_742	✓	18533		2455	0.68	0.474		
NK09_751	✓	17917		9633	2.68	0.704		
NK09_752	✓	19157		7732	2.15	0.747		
NK09_753	✓	14188		2767	0.77	0.476		
NK09_754	✓	14008		2028	0.56	0.392		
NK09_755	✓	16008		2648	0.74	0.483		
NK09_756	✓	80946		5953	1.65	1.552		
NK09_757	✓	14533		1761	0.49	0.46		
NK09_758	✓	31365		14466	0	0		
NK09_759	✓	19419		13416	3.73	1.234		
NK09_760	✓	14121		2069	0.57	0.374		
NK09_761	✓	30333		3430	0.95	0.694		
NK09_762	✓	16076		2685	0.75	0.48		
NK09 simulations with irregular waves								
NK09ir_703	✓	143068		59618	16.56	0.547		
NK09ir_704	✓	107097		37060	10.29	0.637		
NK09ir_705	✓	128981		33728	9.37	0.595		
NK09ir_706	✓	102913		22537	6.26	0.597		
NK09ir_707	✓	87013		45088	12.52	0.569		
NK09ir_708		69214		31710	8.81	0.519		
NK09ir_709	✓	133923		22419	6.23	0.416		
NK09ir_710	✓	109640		21449	5.96	0.557		
NK09ir_723	✓	140823		62238	17.29	0.571		
NK09ir_724	✓	106852		33320	9.26	0.572		
NK09ir_725	✓	129247		24703	6.86	0.436		
NK09ir_726	✓	103753		21980	6.11	0.582		
NK09ir_727	✓	118766		28525	7.92	0.36		
NK09ir_743		40322		32344	8.98	0.297		
NK09ir_744		55224		32314	8.98	0.555		
NK09ir_745	✓	131326		15853	4.4	0.279		
NK09ir_746	✓	104319		22176	6.16	0.587		
NK09ir_747	✓	118990		29239	8.12	0.369		

Table E.10: Simulations (continued)

Case	Finished	Steps	Field variables	Duration		Performance	Endtime	
		[-]		[s]	[h]	$\left[\frac{ms}{cell\text{-}time}\right]$	[s]	[%]
NK09ir_748	✓	110508		33800	9.39	0.553		
NK09ir_749	✓	133352		31439	8.73	0.583		
NK09ir_750	✓	109462		12922	3.59	0.336		
NK09ir_763	✓	134882		56523	15.7	0.519		
NK09ir_764	✓	106970		47490	13.19	0.816		
NK09ir_765	✓	126775		26329	7.31	0.464		
NK09ir_766	✓	104323		16079	4.47	0.426		
NK09ir_767	✓	117296		29964	8.32	0.378		
Turbulence verification runs								
NK09ke_716	✓	89483	4	13500	3.75	3.519		
NK09ke_741	✓	21640	4	15583	4.33	1.372		
NK09ke_741-ticf1	✓	21500	4	9037	2.51	0.796		
NK09ke_741-edd100	✓	21503	4	15654	4.35	1.379		
Eb09 simulations								
Eb09_172	✓	95948		271228	75.34	1.211	464	100
Eb09_173	✓	96091		100310	27.86	0.891	524	100
Eb09_174	✓	101425		55382	15.38	0.736	624	100
Eb09_175	✓	119884		62317	17.31	0.747	692	100
Eb09_176	✓	97148		261332	72.59	1.167	464	100
Eb09_177		31372		37214	10.34	0.33	173	33
Eb09_178		19832		14742	4.1	0.145	120	19
Eb09_179	✓	117531		37000	10.28	0.544	692	100
Eb09_180		24245		82633	22.95	0.369	114	25
Eb09_181		41979		82820	23.01	0.484	205	39
Eb09_182		74888		82602	22.95	0.616	383	61
Eb09_183	✓	142890		63509	17.64	0.761	692	100
Eb09_184		93048		207654	57.68	1.006	401	94
Eb09_185	✓	113451		162253	45.07	0.808	624	100
Eb09_186		4449		8499	2.36	0.055	25	5
Eb09_187								
Eb09_188								
Eb09_189								
Eb09_190	✓	173390		58549	16.26	0.701	692	100
Eb09_191	✓	356828		98682	27.41	0.671	1220	100
Eb09_192		27158		83094	23.08	0.402	120	28
Eb09_193		59619		169789	47.16	0.59	235	39
Eb09_194		98760		170185	47.27	1.093	406	84
Eb09_195	✓	197302		148806	41.34	0.836	828	100
Eb09_196		27050		26773	7.44	0.229	119	22
Eb09_197		40172		26891	7.47	0.162	146	14
Eb09_198	✓	165277		68658	19.07	0.823	692	100
Eb09_199	✓	337722		119263	33.13	0.81	1220	100
Eb09_200		107341		207384	57.61	1.004	425	99
Eb09_201		36053		57723	16.03	0.259	155	22
Eb09_202		47805		57722	16.03	0.481	215	44
Eb09_203		65675		57980	16.11	0.326	260	31
Eb09_204		17160		12716	3.53	0.127	75	14
Eb09_205		24485		14602	4.06	0.088	90	9
Eb09_206	✓	198392		79686	22.14	0.878	752	100
Eb09_207		36931		14639	4.07	0.099	140	12
Eb09_208		2515		7014	1.95	0.034	15	3
Eb09_209		2630		7040	1.96	0.021	20	3
Eb09_210	✓	143047		185981	51.66	1.147	504	100
Eb09_211	✓	266308		174706	48.53	0.887	916	100
Eb09_212		70314		44294	12.3	0.467	310	53
Eb09_213	✓	301264		125095	34.75	0.752	1024	100
Eb09_214	✓	166723		58182	16.16	0.697	692	100
Eb09_215	✓	344495		103353	28.71	0.702	1220	100
Eb09_216	✓	95569		250667	69.63	1.12	464	100
Eb09_217		20660		25455	7.07	0.226	115	22
Eb09_218		45899		25432	7.06	0.338	277	44
Eb09_219		28058		15904	4.42	0.191	165	24
Eb09_220		4532		15961	4.43	0.071	26	6
Eb09_221		13663		15960	4.43	0.142	83	16
Eb09_222		7703		5622	1.56	0.055	52	8
Eb09_223	✓	116221		40477	11.24	0.595	692	100
Eb09_224	✓	101360		222415	61.78	0.993	464	100
Eb09_225	✓	116973		167310	46.48	0.977	532	100
Eb09_226	✓	124439		108699	30.19	0.81	624	100
Eb09_227	✓	143315		63910	17.75	0.766	692	100
Eb09_228	✓	98672		204362	56.77	0.99	428	100
Eb09_229		12548		23732	6.59	0.118	74	12
Eb09_230		12104		23738	6.59	0.152	61	13
Eb09_231		22957		23358	6.49	0.128	106	12
Eb09_232	✓	126632		71527	19.87	0.754	584	100
Eb09_233	✓	297156		128439	35.68	0.772	1024	100
Eb09_234	✓	174063		66030	18.34	0.791	692	100

Table E.10: Simulations (continued)

Case	Finished	Steps	Field variables	Duration		Performance	Endtime	
		[-]		[s]	[h]	$\left[\frac{ms}{cell \cdot time}\right]$	[s]	[%]
Eb09_235	✓	354845		149301	41.47	1.015	1220	100
Eb09_236		79337		207529	57.65	1.005	331	77
Eb09_237		20239		53682	14.91	0.187	85	14
Eb09_238	✓	121361		151401	42.06	0.972	484	100
Eb09_239	✓	199331		140057	38.9	0.787	828	100
Eb09_240		19078		19318	5.37	0.165	83	15
Eb09_241	✓	282183		124165	34.49	0.746	1024	100
Eb09_242	✓	169166		60850	16.9	0.729	692	100
Eb09_243	✓	344590		106677	29.63	0.725	1220	100
Eb09_244		16118		43012	11.95	0.208	66	15
Eb09_245		149363		207580	57.66	0.932	622	90
Eb09_246	✓	116766		124035	34.45	1.033	484	100
Eb09_247	✓	217961		152532	42.37	0.857	828	100
Eb09_248		10234		8145	2.26	0.081	50	9
Eb09_249		13133		8209	2.28	0.049	48	5
Eb09_250	✓	195662		69390	19.28	0.765	752	100
Eb09_251	✓	364262		113500	31.53	0.771	1220	100
Eb09_252	✓	113951		193127	53.65	0.935	428	100
Eb09_253		3155		8194	2.28	0.025	24	3
Eb09_254		3536		5695	1.58	0.035	21	4
Eb09_255		6659		5704	1.58	0.029	34	4
Eb09_256	✓	137094		65214	18.12	0.687	584	100
Eb09_257	✓	298646		111633	31.01	0.671	1024	100
Eb09_258	✓	163803		54334	15.09	0.651	692	100
Eb09_259		14112		5674	1.58	0.039	56	5
Eb09_260								
Eb09_261	✓	117027		282379	78.44	1.118	624	100
Eb09_262	✓	103775		163087	45.3	1.504	484	100
Eb09_263	✓	130307		167022	46.4	0.906	828	100
Eb09_264	✓	87271		72762	20.21	1.136	512	100
Eb09_265	✓	135073		60223	16.73	0.459	948	100
Eb09_266	✓	97634		37805	10.5	0.639	584	100
Eb09_267								
Eb09_268	✓	92794		186712	51.86	1.476	392	100
Eb09_269	✓	117618		195580	54.33	0.8	624	100
Eb09_270	✓	99916		157129	43.65	1.621	456	100
Eb09_271	✓	122761		112673	31.3	0.643	828	100
Eb09_272	✓	92605		55767	15.49	0.853	524	100
Eb09_273	✓	185036		124456	34.57	0.7	984	100
Eb09_274	✓	107031		38550	10.71	0.63	624	100
Eb09_275	✓	180288		69000	19.17	0.48	1164	100
Eb09_276	✓	92506		199543	55.43	1.581	392	100
Eb09_277	✓	117955		236525	65.7	1.095	584	100
Eb09_278	✓	102166		133140	36.98	1.381	456	100
Eb09_279	✓	158915		147321	40.92	0.859	828	100
Eb09_280	✓	96776		57057	15.85	0.858	512	100
Eb09_281	✓	202111		106078	29.47	0.652	948	100
Eb09_282	✓	123280		43839	12.18	0.728	624	100
Eb09_283	✓	262349		102101	28.36	0.595	1164	100
Eb09_284	✓	90443		229523	63.76	1.807	392	100
Eb09_285	✓	115964		290678	80.74	1.151	624	100
Eb09_286	✓	101489		150521	41.81	1.388	484	100
Eb09_287	✓	131744		157564	43.77	0.855	828	100
Eb09_288	✓	89281		69588	19.33	1.086	512	100
Eb09_289		18346		12530	3.48	0.096	132	14
Eb09_290		24640		12568	3.49	0.212	150	26
Eb09_291		20075		12531	3.48	0.082	147	13
Eb09_292								
Eb09_293								
Eb09_294								
Eb09_295		6965		7923	2.2	0.045	59	7
Eb09_296	✓	92603		48042	13.34	0.735	524	100
Eb09_297	✓	186663		103685	28.8	0.583	984	100
Eb09_298		56072		23705	6.58	0.388	331	53
Eb09_299		48420		24004	6.67	0.167	339	29
Eb09_300		10041		23978	6.66	0.19	47	12
Eb09_301		4304		12008	3.34	0.056	27	5
Eb09_302		8465		12141	3.37	0.126	39	8
Eb09_303		10608		12107	3.36	0.071	74	9
Eb09_304	✓	97797		61386	17.05	0.923	512	100
Eb09_305	✓	206015		125144	34.76	0.769	948	100
Eb09_306	✓	126284		42649	11.85	0.708	624	100
Eb09_307	✓	268449		124431	34.56	0.725	1164	100
Eb09_308	✓	98415		185891	51.64	1.237	464	100
Eb09_309	✓	89093		86790	24.11	1.03	532	100
Eb09_310	✓	109943		79257	22.02	1.028	596	100
Eb09_311								

Table E.10: Simulations (continued)

Case	Finished	Steps	Field variables	Duration		Performance	Endtime	
		[-]		[s]	[h]	$\left[\frac{\text{ms}}{\text{cell-time}}\right]$	[s]	[%]
Eb09_312								
Eb09_313		15243		22564	6.27	0.18	73	14
Eb09_314	✓	105761		53991	15	0.709	596	100
Eb09_315		51784		22784	6.33	0.313	301	43
Eb09_316	✓	102943		175486	48.75	1.181	464	100
Eb09_317	✓	108663		131471	36.52	1.16	504	100
Eb09_318		73001		131471	36.52	1.366	347	59
Eb09_319		31350		13802	3.83	0.193	177	26
Eb09_320	✓	95060		141667	39.35	1.173	408	100
Eb09_321		5273		13784	3.83	0.062	28	5
Eb09_322	✓	105235		108450	30.13	1.098	464	100
Eb09_323		12498		12464	3.46	0.073	60	7
Eb09_324		20031		12463	3.46	0.188	98	19
Eb09_325	✓	217892		124929	34.7	0.776	948	100
Eb09_326	✓	140950		53289	14.8	0.892	584	100
Eb09_327	✓	291043		128370	35.66	0.757	1164	100
Eb09_328	✓	95643		177779	49.38	1.475	408	100
Eb09_329		104679		207452	57.63	0.941	450	76
Eb09_330	✓	113888		138380	38.44	1.405	464	100
Eb09_331	✓	232696		178183	49.5	1.06	828	100
Eb09_332	✓	115637		72587	20.16	1.036	532	100
Eb09_333	✓	280292		167595	46.55	1.053	948	100
Eb09_334	✓	145567		60402	16.78	0.962	584	100
Eb09_335	✓	297128		131782	36.61	0.788	1164	100
Eb09_336	✓	103135		141181	39.22	1.174	408	100
Eb09_337	✓	181715		316570	87.94	1.445	596	100
Eb09_338	✓	121462		136471	37.91	1.391	464	100
Eb09_339	✓	207028		192216	53.39	1.221	800	100
Eb09_340	✓	132784		60621	16.84	0.87	532	100
Eb09_341	✓	251549		108893	30.25	0.692	948	100
Eb09_342	✓	144075		47971	13.33	0.763	608	100
Eb09_343	✓	372728		197550	54.88	1.196	1164	100
Eb09_344		83915		138607	38.5	1.072	309	72
Eb09_345		122632		138643	38.51	0.956	463	78
Eb09_346		9849		7155	1.99	0.091	45	9
Eb09_347		9055		7183	2	0.046	43	5
Eb09_348		14152		7183	2	0.104	67	13
Eb09_349		12336		8151	2.26	0.046	56	5
Eb09_350		25013		8147	2.26	0.118	101	15
Eb09_351		16650		8187	2.27	0.05	74	6
Eb09_352	✓	99778		189190	52.55	1.258	464	100
Eb09_353	✓	89169		87209	24.22	1.035	532	100
Eb09_354	✓	105871		78512	21.81	1.018	596	100
Eb09_355	✓	106725		53970	14.99	0.8	656	100
Eb09_356	✓	101202		204395	56.78	1.366	464	100
Eb09_357	✓	113036		159925	44.42	1.279	532	100
Eb09_358		33940		19186	5.33	0.252	199	33
Eb09_359		47319		19243	5.35	0.265	277	40
Eb09_360		9535		19247	5.35	0.13	49	11
Eb09_361	✓	110205		108906	30.25	0.961	504	100
Eb09_362	✓	127325		86179	23.94	0.895	584	100
Eb09_363	✓	124157		48215	13.39	0.675	692	100
Eb09_364								
Eb09_365								
Eb09_366								
Eb09_367								
Eb09_368								
Eb09_369								
Eb09_370	✓	139627		51794	14.39	0.867	584	100
Eb09_371	✓	303161		131110	36.42	0.773	1164	100
Eb09_372	✓	97720		136078	37.8	1.129	408	100
Eb09_373		24189		59011	16.39	0.268	111	19
Eb09_374		73681		92984	25.83	0.944	305	66
Eb09_375		94526		92928	25.81	0.553	351	42
Eb09_376	✓	115399		59389	16.5	0.848	532	100
Eb09_377	✓	288714		129729	36.04	0.815	948	100
Eb09_378	✓	140365		54571	15.16	0.869	584	100
Eb09_379	✓	291300		157249	43.68	0.94	1164	100
Eb09_380	✓	106396		180701	50.19	1.503	408	100
Eb09_381		111767		207511	57.64	0.947	428	72
Eb09_382								
Eb09_383								
Eb09_384								
Eb09_385	✓	246624		125975	34.99	0.8	948	100
Eb09_386	✓	144462		50149	13.93	0.798	608	100
Eb09_387	✓	369816		140689	39.08	0.852	1164	100
Eb09_388	✓	160786		207539	57.65	1.606	428	100

Table E.10: Simulations (continued)

Case	Finished	Steps	Field variables	Duration		Performance	Endtime	
		[-]		[s]	[h]	$\left[\frac{\text{ms}}{\text{cell·time}}\right]$	[s]	[%]
Eb09_389	✓	155509		163010	45.28	1.124	596	100
Eb09_390	✓	127142		96859	26.91	1.236	476	100
Eb09_391	✓	256807		158787	44.11	1.02	800	100
Eb09_392	✓	144769		67069	18.63	0.968	532	100
Eb09_393	✓	311002		152192	42.28	0.86	1024	100
Eb09_394	✓	194177		61176	16.99	0.885	692	100
Eb09_395	✓	304156		124808	34.67	0.766	1164	100
Eb09_396	✓	97107		137093	38.08	1.244	456	100
Eb09_397	✓	94588		49199	13.67	0.806	512	100
Eb09_398	✓	106603		43284	12.02	0.733	584	100
Eb09_399	✓	120022		37065	10.3	0.681	656	100
Eb09_400	✓	98461		128327	35.65	1.171	456	100
Eb09_401	✓	111423		103585	28.77	1.098	524	100
Eb09_402	✓	111382		49625	13.78	0.854	584	100
Eb09_403	✓	115835		33657	9.35	0.63	656	100
Eb09_404	✓	104459		113530	31.54	1.045	456	100
Eb09_405	✓	127482		92823	25.78	1.04	512	100
Eb09_406	✓	136544		73143	20.32	0.931	596	100
Eb09_407	✓	151296		64861	18.02	0.835	692	100
Eb09_408	✓	97872		109873	30.52	1.197	392	100
Eb09_409	✓	146478		183510	50.98	1.049	596	100
Eb09_410	✓	120435		93488	25.97	1.296	456	100
Eb09_411	✓	162237		112714	31.31	0.802	828	100
Eb09_412	✓	126420		57980	16.11	1.066	512	100
Eb09_413	✓	226235		108989	30.27	0.856	916	100
Eb09_414	✓	105849		122937	34.15	1.342	392	100
Eb09_415	✓	166710		207539	57.65	1.197	596	100
Eb09_416	✓	133506		105238	29.23	1.464	456	100
Eb09_417	✓	201540		134155	37.27	0.966	828	100
Eb09_418	✓	135823		59019	16.39	1.091	512	100
Eb09_419	✓	209447		101962	28.32	0.762	948	100
Eb09_420								
Eb09_421		143108		209770	58.27	1.125	462	74
Eb09_422	✓	155316		123146	34.21	1.722	456	100
Eb09_423		198086		210365	58.43	1.025	498	60
Eb09_424	✓	104369		84205	23.39	1.342	512	100
Eb09_425	✓	254871		141292	39.25	0.933	1024	100
Eb09_426	✓	119628		154763	42.99	1.698	392	100
Eb09_427		183297		209854	58.29	1.137	576	92
Eb09_428	✓	115587		71223	19.78	1.199	456	100
Eb09_429	✓	227903		131861	36.63	0.975	828	100
Eb09_430		36143		15479	4.3	0.29	132	26
Eb09_431		31758		15517	4.31	0.119	121	13
Eb09_432		9002		15532	4.31	0.141	46	10
Eb09_433	✓	95105		47806	13.28	0.783	512	100
Eb09_434	✓	109939		43139	11.98	0.731	584	100
Eb09_435	✓	115764		35510	9.86	0.652	656	100
Eb09_436	✓	99189		129638	36.01	1.183	456	100
Eb09_437	✓	111880		105631	29.34	1.12	524	100
Eb09_438	✓	106731		47551	13.21	0.818	584	100
Eb09_439	✓	116046		33759	9.38	0.631	656	100
Eb09_440	✓	104325		112774	31.33	1.038	456	100
Eb09_441	✓	126728		93355	25.93	1.045	512	100
Eb09_442	✓	134852		79083	21.97	1.007	596	100
Eb09_443	✓	155307		71820	19.95	0.925	692	100
Eb09_444	✓	99972		119253	33.13	1.299	392	100
Eb09_445		12755		23419	6.51	0.134	62	10
Eb09_446		28297		23505	6.53	0.326	108	24
Eb09_447		30280		23485	6.52	0.167	171	21
Eb09_448	✓	116512		54577	15.16	1.003	512	100
Eb09_449	✓	216881		102675	28.52	0.806	916	100
Eb09_450	✓	107411		121276	33.69	1.324	392	100
Eb09_451	✓	164547		206957	57.49	1.193	596	100
Eb09_452	✓	130369		106547	29.6	1.483	456	100
Eb09_453	✓	202868		137202	38.11	0.988	828	100
Eb09_454		65634		29074	8.08	0.537	252	49
Eb09_455	✓	209948		102544	28.48	0.766	948	100
Eb09_456	✓	116315		130091	36.14	1.423	392	100
Eb09_457		146726		207228	57.56	1.112	469	75
Eb09_458	✓	149339		115463	32.07	1.615	456	100
Eb09_459		203615		207607	57.67	1.012	522	63
Eb09_460		145750		74121	20.59	1.181	0	0
Eb09_461	✓	258223		122185	33.94	0.807	1024	100
Eb09_462	✓	119227		130795	36.33	1.435	392	100
Eb09_463								
Eb09_464								
Eb09_465								

Table E.10: Simulations (continued)

Case	Finished	Steps	Field variables	Duration		Performance	Endtime	
		[-]		[s]	[h]	$\left[\frac{\text{ms}}{\text{cell-time}}\right]$	[s]	[%]
Eb09_466	✓	151876		46958	13.04	0.88	512	100
Eb09_467	✓	268886		87588	24.33	0.674	948	100
401 cases in total								

F

Converted formulae

Stability methods (appendix B) and motion formulae (section 2.2.4) are converted into a form by which motion can be determined. The reasoning behind conversion can be found in section 5.3. The formulae hereafter can easily be implemented in computer code, which returns a true/false value for motion by evaluating the final inequality. Inequalities are written so that motion occurs when the inequality holds. Figure F.1 shows definitions of certain toe dimensions and measurement levels.

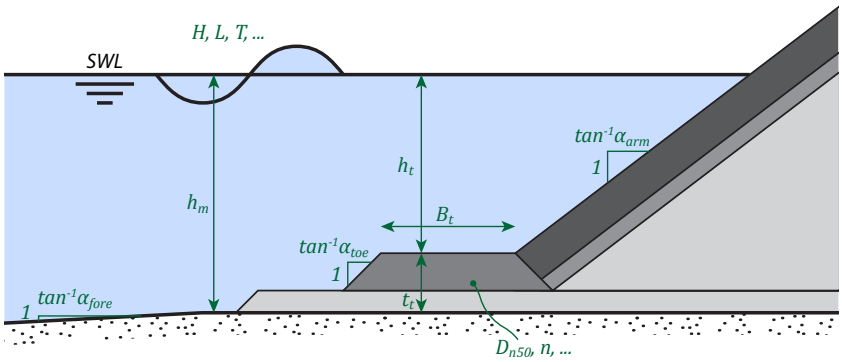

(a)

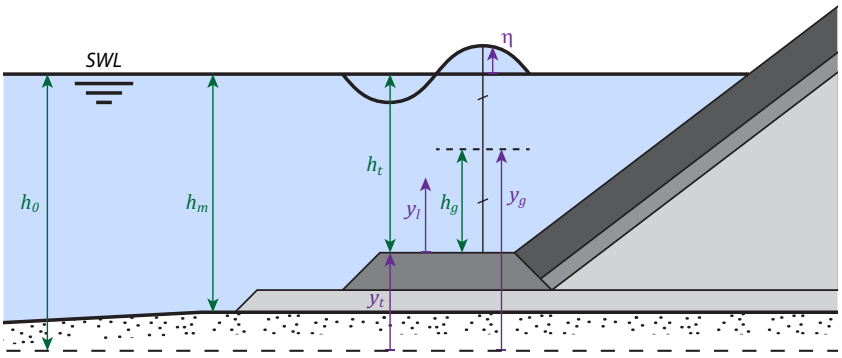

(b)

Figure F.1: Toe dimensions and measurement levels

F.1. STABILITY METHODS

F.1.1. VAN DER MEER (1991)

$$1 \geqslant \frac{\Delta \cdot D_{n50}}{H_s} \cdot 8.7 \left(\frac{h_t}{h_m} \right)^{1.4} \tag{VdM91}$$

F.1.2. GERDING (1993), VAN DER MEER ET AL. (1995)

$$1 \geqslant \frac{\Delta \cdot D_{n50}}{H_s} \left(0.24 \frac{h_t}{D_{n50}} + 1.6 \right) N_{od,c}^{0.15} \tag{Ger93a}$$

F.1.3. BURCHARTH AND LIU (1995)

$$1 \geqslant \frac{\Delta \cdot D_{n50}}{H_s} \left(\frac{1.6}{N_{od,c}^{-0.15} - 0.4 \frac{h_t}{H_s}} \right) \tag{Bur95}$$

F.1.4. VAN DER MEER (1998)

$$1 \geqslant \frac{\Delta \cdot D_{n50}}{H_s} \left(6.2 \left(\frac{h_t}{h_m} \right)^{2.7} + 2 \right) N_{od,c}^{0.15} \tag{VdM98}$$

F.1.5. SAYAO (2007)

Initial calculations:

$$\begin{aligned} \rho_s &= \rho_w \left(\Delta + 1 \right) \\ M_{50} &= \rho_s \cdot D_{n50}^3 \\ m &= \tan \alpha_{fore} \\ \xi_{0p} &= \frac{\tan \alpha_{arm}}{\sqrt{H_s / L_{0p}}} \end{aligned}$$

Stability check:

$$1 \geqslant \frac{M_{50} \cdot \Delta^3}{\rho_s \cdot H_s^3} \cdot 4.5 m^{-2/3} \cdot \mathrm{e}^{5.67 h_t / h_m - 0.63 \xi_{0p}} \tag{Say07}$$

F.1.6. BAART (2008)

Phase difference toe–armour:

$$\begin{aligned} L_{TA} &= \frac{B_t}{2} + \frac{h_t}{\tan \alpha_{arm}} \\ \varphi_{TA} &= \frac{2\pi}{L_{m-1,0}} L_{TA} \end{aligned}$$

Velocity amplitude of the incoming wave:

$$\begin{aligned} \omega &= \frac{2\pi}{T_{m-1,0}} \\ k &= \frac{2\pi}{L_{m-1,0}} \\ \hat{u}_{bi} &= \omega \frac{H_s}{2} \frac{\cosh \left(k \left(h_m - h_t \right) \right)}{\sinh \left(k h_m \right)} \end{aligned}$$

Wave run-up according to the Rock Manual (CIRIA et al., 2007, §5.1.1.2), with rough slope:

$$L_m = \frac{g T_m^2}{2\pi}$$
$$\xi_m = \max\left\{\frac{\tan\alpha_{arm}}{\sqrt{H_s/L_m}}; 1.5\right\}$$
$$R_u = R_{u10\%} = H_s \cdot \max\left(1.45; \begin{cases} 0.77 \cdot \xi_m & \xi_m \leqslant 1.5 \\ 0.94 \cdot \xi_m^{0.42} & \xi_m > 1.5 \end{cases}\right)$$

Wave run-down according to the Rock Manual (CIRIA et al., 2007, box 5.1, p. 499), with porous rubble slopes and $P = 0.4$ (armour layer, filter layer, core):

$$P = 0.4$$
$$s_{0m} = \frac{H_s}{L_{0m}}$$
$$R_d = R_{d2\%} = H_s \cdot \left(2.1\sqrt{\tan\alpha_{arm}} - 1.2P^{0.15} + 1.5\mathrm{e}^{-60\cdot s_{0m}}\right)$$

Velocity amplitude of the down rush:

$$\gamma_{dr} = 0.45 \text{ (from §F.2 in Baart (2008))}$$
$$\hat{u}_{bdr} = \gamma_{dr}\sqrt{2g\left(\frac{R_u}{3} + \frac{R_d}{2}\right)}$$

Combined velocity amplitude from $\hat{u}_{bi}$ and $\hat{u}_{bdr}$:

$$\gamma_{fore} = \left(\frac{\tan\alpha_{fore}}{0.05}\right)^{0.5} \text{ (from Baart et al. (2010))}$$
$$\hat{u}_b = \sqrt{\left(\hat{u}_{bi}\cdot\sin\varphi_{TA}\right)^2 + \left(\hat{u}_{bi}\cdot\cos\varphi_{TA} + \hat{u}_{bdr}\right)^2}\cdot\gamma_{fore}$$

Critical velocity amplitude based on Rance and Warren (1968) adapted for porous flow:

$$T = T_p \text{ (from §A.1 in Baart (2008))}$$
$$C_{PF} = 0.4$$
$$i = \frac{H_s/2 + R_u}{L_{TA} + R_u/\tan\alpha_{arm}}$$
$$\hat{u}_{bc} = \left(0.46\sqrt{T}\left(\left(\Delta - C_{PF}\, i\right) g\right)^{1.5}\cdot D_{n50}\right)^{2.5^{-1}}$$

Fit coefficient: $\Gamma = 1.05$. Safety coefficient for sensitivity analysis: $F_S \in [0.91, 0.95]$. Stability check:

$$1 \geqslant \frac{F_s}{\Gamma}\frac{\hat{u}_{bc}}{\hat{u}_b} \tag{Baa08}$$

F.1.7. EBBENS (2009)

Initial calculations:

$$L_{0p} = \frac{2\pi}{g T_{0p}^2} \text{ (this was the relation used by Ebbens)}$$
$$\xi_{0p} = \frac{\tan\alpha_{fore}}{\sqrt{H_s/L_{0p}}}$$

Stability check:

$$1 \geqslant \frac{\Delta\cdot D_{n50}}{H_s}\cdot 3.0\frac{N_{\%,c}^{1/3}}{\sqrt{\xi_{0p}}} \tag{Ebb09}$$

F.1.8. MUTTRAY (2013)

Conversion of damage number using a bedding layer of 20 mm:

$$N_{od,c} = \frac{N_{\%,c}\,(t_t - 20\text{ mm})\,B_t(1-n)}{D_{n50}^2}$$

Stability check:

$$1 \geqslant \frac{\Delta \cdot D_{n50}}{H_s} \cdot \frac{2.4 N_{od,c}^{1/3}}{1.4 - 0.4\frac{h_t}{H_s}} \tag{Mut13}$$

F.1.9. VAN GENT AND VAN DER WERF (2014)

Initial calculations:

$$f_B = \left(\frac{B_t}{3D_{n50}}\right)^{0.5}$$
$$k = \frac{4\pi^2}{g T_{m-1,0}^2}$$
$$\hat{u}_\delta = \frac{\pi H_s}{T_{m-1,0}} \frac{1}{\sinh k h_t}$$

Stability check:

$$1 \geqslant \frac{N_{od,c} \cdot f_B}{0.032} \left(\frac{H_s}{t_t}\right) \left(\frac{H_s}{B_t}\right)^{0.3} \left(\frac{\Delta \cdot D_{n50}}{H_s}\right)^3 \left(\frac{\sqrt{g H_s}}{\hat{u}_\delta}\right) \tag{VGe14}$$

F.1.10. MUTTRAY (2014)

Initial calculations:

$$n_t = \tan^{-1} \alpha_{toe}$$
$$m = \tan^{-1} \alpha_{fore}$$

Parameter limits:

$$N_{od,c} = \max\left\{N_{od,c}; 0.25\right\}$$
$$h_t = \max\left\{h_t; 0\right\}$$
$$m = \min\left\{m; 50\right\}$$

Stability check:

$$1 \geqslant \frac{\Delta \cdot D_{n50}}{H_s} \left((4n_t)^{1/3} + \frac{h_t}{L_p} m\right) N_{od,c}^{1/3} \tag{Mut14}$$

F.2. MOTION FORMULAE

Most motion formulae are applied per toe gauge (denoted with x) and per time step (denoted with t).

F.2.1. IZBASH (1930)

Velocity is measured at $h_g = 1.0 D_{n50}$.

$$1 \geqslant \frac{1.2\sqrt{2\Delta g D_{n50}}}{u(x,t)} \tag{Izb30}$$

F.2.2. RANCE AND WARREN (1968)

Velocity is measured at $h_g(x,t) = (h_t + \eta(x,t))/2$. This formula is applied per wave. For information on how this is done and for a definition of $\hat{u}_b$ and T, see 5.3.

$$1 \geqslant \frac{1}{\hat{u}_b} \left(2.15^{-1} \sqrt{T}\,(\Delta g)^{1.5} D_{n50}\right)^{1/2.5} \tag{Ran68a}$$

F.2.3. DESSENS (2004)

Velocity and acceleration are measured per toe gauge couple at a level of $h_g(x,t) = (h_t + \eta(x,t))/2$. See 5.3 for more information.
Initial calculations:

$$C_B = 0.10$$
$$C_M = 3.92$$

Stability check:

$$\left| \frac{\frac{1}{2} C_B \bar{u}^2(x,t) + C_M D_{n50} \bar{a}(x,t)}{\Delta g D_{n50}} \right| \geqslant \Psi_{MS,c} \tag{Des04}$$

F.2.4. STEENSTRA (2014)

Initial calculations and definitions:

$$\kappa = 0.41$$
$$L_m = \kappa y_l \sqrt{1 - y_l/ht}$$
$$K(\beta) = 1$$

Velocity and turbulence intensity are measured per gauge couple using a moving average over height L_m. Acceleration is measured per toe gauge couple at a level of $h_g(x,t) = (h_t + \eta(x,t))/2$. See section 5.3 for more information.
Stability check:

$$\left| \frac{\left(\max \left[\left\langle \bar{u} + \alpha \sqrt{\bar{k}} \right\rangle_{L_m} \frac{L_m}{y_l} \right]^2 \right) + C_{m:b} \left(\bar{u} \frac{\partial u}{\partial x} \right)_{h_g} D_{n50}}{K(\beta) \cdot \Delta g D_{n50}} \right| \geqslant \Psi_{RS,c} \tag{Ste14}$$

Herein are u, α, k, L_m, $C_{m:b}$ and $\partial u/\partial x$ functions of (x,t).

The following calculation procedure is used:
1. Initial calculations: κ, $K(\beta)$, ...
2. Per gauge couple (x):
   2.1. Per time step (t):
      2.1.1. Determine h_g
      2.1.2. Find α and $C_{m:b}$ based on $h_g(x,t)$
      2.1.3. Per y_l-level in $[0, h_t]$:
         2.1.3.1. Determine L_m
         2.1.3.2. Go over $y_l \in \left[y_l - \frac{L_m}{2}, y_l + \frac{L_m}{2} \right]$
         2.1.3.3. Take the average of $u + \alpha k$
         2.1.3.4. Multiply with L_m/y_l
      2.1.4. Take the maximum over these levels and square it
      2.1.5. Determine u and $\partial u/\partial x$ at y_g
      2.1.6. Complete the formula
   2.2. Check for motion for all t
3. Check for motion for all x

F.2.5. PETERS (2014)

Initial calculations and definitions:

$$\begin{aligned} C_D &= 0.23 \\ A_f &= 0.5 D_{n50}^2 \\ o_{wl} &\approx 0.5 D_{n50} \\ o_d &\approx 0.75 D_{n50} \end{aligned}$$

Velocity is measured at 0.05 m above the toe. For the drag force it is reduced with a factor 0.9 according to Peters (2014b, §4.2). Absolute (squared) values of velocities are used. See section 5.3 for more information. The forces then become:

$$\begin{aligned} F_L &= \frac{1}{2} \rho u^2(x,t) D_{n50}^2 \\ F_D &= \frac{1}{2} C_D \rho_w A_f \left(0.9 u(x,t)\right)^2 \\ F_W &= (\rho_s - \rho_w) D_{n50}^3 \cdot g \end{aligned}$$

Stability check:

$$F_L \cdot o_{wl} + F_D \cdot o_d - F_W \cdot o_{wl} > 0$$

G

Motion tables

The next two tables are the motion tables belonging to chapter 5. They show motion prediction per case. The first table takes validity ranges defined for the stability methods into account; the second ignores them. The following marks are used:

- ✓ Motion is predicted
- x Immobility is predicted
- – The method or formula is not valid for this case

G.1. Motion table with validity ranges respected

Eb09 ID	Sim. ID	VdM91	Ger93a	Bur95	VdM98	Say07	Baa08	Ebb09	Mut13	VGe14	Mut14	Izb30	Ran68a	Des04	Ste14	Pet14	Izb30 [%]	Ran68a [%]	Des04 [%]	Ste14 [%]	Pet14 [%]	% valid	% motion if valid
1	172	×	×	✓	×	×	–	–	–	–	×	×	×	×	×	×	46.32	0	0	35.35	0	67	10
2	173	×	×	×	×	×	–	–	×	–	×	×	×	×	✓	×	47.03	0	0.03	43.65	0.01	73	9
3	174	×	✓	✓	✓	×	×	–	✓	–	×	×	×	×	✓	✓	53.03	0.64	1.31	48.01	0.86	80	42
4	175	×	✓	✓	✓	×	×	–	✓	–	✓	×	✓	×	✓	✓	54.33	1.21	2.31	49.02	1.78	80	58
5	176	×	×	×	×	×	–	–	×	–	×	×	×	×	✓	×	46.27	0	0.01	65.74	0	73	9
6	179	✓	✓	✓	✓	×	×	×	✓	–	✓	✓	×	×	✓	✓	59.34	0.76	5.13	40.75	3.33	87	62
7	183	–	✓	✓	✓	×	×	×	✓	–	✓	✓	✓	✓	×	✓	65.42	2.65	13.22	35.69	2.4	80	67
8	185	–	–	✓	–	×	×	–	✓	–	×	✓	×	✓	✓	×	56.69	0	8.51	40.6	0.38	60	56
9	190	–	–	✓	–	×	×	×	✓	–	✓	✓	✓	✓	×	✓	67.9	1.62	15.87	32.42	3	67	60
10	191	–	–	✓	–	✓	×	×	✓	–	✓	✓	✓	✓	×	✓	74.14	3.95	9.22	26.1	3.56	67	70
11	195	–	–	✓	–	✓	×	×	✓	–	✓	×	✓	✓	×	–	47.24	1.13	13.77	28.68	–	67	60
12	198	–	–	✓	–	×	×	×	✓	–	✓	✓	✓	✓	×	–	67.76	1.34	16.43	26.35	–	67	60
13	199	–	–	✓	–	✓	×	×	✓	–	✓	✓	✓	✓	×	–	69.87	2.29	11.29	22.28	–	67	70
14	206	–	–	✓	–	✓	×	×	✓	–	✓	–	×	✓	×	–	–	0.54	10.66	9.52	–	60	56
15	210	–	–	✓	–	✓	–	×	✓	–	✓	–	–	✓	–	–	–	–	9.43	–	–	40	83
16	211	–	–	✓	–	✓	–	×	✓	–	✓	–	–	×	–	–	–	–	7.58	–	–	40	67
17	213	–	–	✓	–	✓	–	×	✓	–	✓	–	–	×	–	–	–	–	6.73	–	–	40	67
18	214	–	–	✓	–	✓	–	×	✓	–	✓	–	–	×	–	–	–	–	4.65	–	–	40	67
19	215	–	–	✓	–	✓	–	×	✓	–	✓	–	–	×	–	–	–	–	4.47	–	–	40	67
20	216	×	×	✓	×	×	–	–	–	–	×	×	×	×	×	×	46.39	0	0	27.83	0	67	10
21	223	×	✓	✓	✓	×	×	×	✓	–	✓	✓	×	×	✓	✓	56.22	0.39	4.2	40.29	1.86	87	54
22	224	–	×	×	×	×	×	–	×	–	×	×	×	×	✓	×	46.93	0	0.8	43.56	0	73	9
23	225	–	×	×	×	×	×	–	×	–	×	×	×	×	✓	×	52.1	0	6.24	43.4	0.19	73	9
24	226	–	✓	✓	×	×	×	×	✓	–	×	✓	×	×	✓	✓	55.54	0.8	6.93	40.49	0.88	80	42
25	227	–	✓	✓	✓	×	×	×	✓	–	✓	✓	✓	✓	×	✓	63.48	1.46	13.57	34.74	1.65	80	67
26	228	–	–	✓	–	✓	✓	–	✓	–	✓	×	×	×	✓	×	51.04	0	3.12	46.41	0	60	67
27	232	–	–	✓	–	×	×	×	✓	–	×	✓	✓	✓	×	✓	57.46	1.66	12.3	36.52	1.14	67	50
28	233	–	–	✓	–	×	×	×	✓	–	✓	✓	✓	✓	×	✓	60.34	4.1	9.41	28.79	3.16	67	60
29	234	–	–	✓	–	×	×	×	✓	–	✓	✓	✓	✓	×	✓	64.19	1.72	15.08	32.83	2.13	67	60
30	235	–	–	✓	–	×	×	×	✓	–	✓	✓	✓	✓	×	✓	68.18	2.33	9.2	26.28	2.91	67	60
31	238	–	–	✓	–	×	×	×	✓	–	×	×	×	✓	✓	–	50.12	0.5	14.68	37.79	–	67	40
32	239	–	–	✓	–	×	×	×	✓	–	✓	×	×	✓	×	–	47.06	0.93	13.92	28.73	–	67	40
33	241	–	–	✓	–	×	×	×	✓	–	✓	×	✓	✓	×	–	40.01	3.05	11.99	24.91	–	67	50
34	242	–	–	✓	–	×	×	×	✓	–	✓	×	✓	✓	×	–	53.25	1.13	16.07	26.79	–	67	50
35	243	–	–	✓	–	✓	×	×	✓	–	✓	×	✓	✓	×	–	49.52	1.99	11.27	22.09	–	67	60
36	246	–	–	✓	–	✓	✓	✓	✓	–	✓	–	×	✓	×	–	–	0.09	12.46	23.88	–	60	78
37	247	–	–	✓	–	✓	×	×	✓	–	×	–	×	✓	×	–	–	0.72	13.91	19.7	–	60	44
38	250	–	–	✓	–	✓	×	×	✓	–	✓	–	×	✓	×	–	–	0.39	10.29	9.02	–	60	56
39	251	–	–	✓	–	✓	×	×	✓	–	✓	–	×	✓	×	–	–	0.52	8.79	9.97	–	60	56
40	252	–	–	✓	–	✓	–	×	✓	–	✓	–	–	✓	–	–	–	–	9.89	–	–	40	83
41	256	–	–	✓	–	✓	–	×	×	–	×	–	–	×	–	–	–	–	6.87	–	–	40	33
42	257	–	–	✓	–	✓	–	×	×	–	×	–	–	×	–	–	–	–	6.62	–	–	40	33
43	258	–	–	✓	–	✓	–	×	×	–	✓	–	–	×	–	–	–	–	5	–	–	40	50
44	261	×	×	✓	×	×	–	–	–	–	×	×	×	×	✓	×	47.44	0	0	75.68	0	67	20
45	262	✓	✓	✓	✓	✓	✓	–	✓	–	×	×	×	×	✓	×	45.96	0	0	66.93	0	80	67
46	263	×	×	×	×	×	–	–	×	✓	✓	×	×	×	✓	×	48.69	0	0.06	89.69	0.03	80	25
47	264	×	×	✓	×	×	–	–	×	×	×	×	×	×	✓	×	48.12	0	0	81.11	0	80	17
48	265	×	✓	✓	✓	×	✓	–	✓	✓	✓	×	×	×	✓	×	51.04	0	0.13	94.8	0.54	87	62
49	266	×	×	×	×	×	–	–	×	×	✓	×	×	×	✓	×	47.88	0	0.01	88.65	0	80	17
50	268	×	×	×	×	×	–	–	×	–	×	×	×	×	✓	×	44.81	0	0	49.24	0	73	9
51	269	×	×	×	×	×	✓	–	×	–	×	×	×	×	✓	×	47.78	0	0.01	76.32	0	80	17
52	270	×	×	×	×	×	×	–	×	–	×	×	×	×	✓	×	45.95	0	0.04	73.77	0	80	8
53	271	×	✓	✓	✓	×	✓	–	✓	–	✓	×	×	×	✓	✓	51.74	0.67	1.23	85.84	0.98	80	58
54	272	×	✓	✓	×	×	✓	–	✓	–	✓	×	×	×	✓	×	47.75	0	0.35	83.88	0.18	80	50
55	273	✓	✓	✓	✓	✓	✓	×	✓	–	✓	✓	×	×	✓	✓	57.92	0.5	2.59	90.08	2.91	87	77

Eb09 ID	Sim. ID	VdM91	Ger93a	Bur95	VdM98	Say07	Baa08	Ebb09	Mut13	VGe14	Mut14	Izb30	Ran68a	Des04	Ste14	Pet14	Izb30 [%]	Ran68a [%]	Des04 [%]	Ste14 [%]	Pet14 [%]	% valid	% motion if valid
56	274	✓	✓	✓	✓	×	✓	×	✓	–	✓	×	✓	×	✓	✓	51.55	3.5	2.5	89.27	2.17	87	69
57	275	✓	✓	✓	✓	✓	✓	×	✓	–	✓	✓	✓	×	✓	✓	65.4	2.9	4.78	91.35	4.58	87	85
58	276	–	×	×	×	×	–	–	×	–	×	×	×	×	✓	×	45.74	0	0.03	54.54	0	67	10
59	277	–	×	×	×	×	✓	–	×	–	×	×	×	×	✓	×	48.01	0.1	0.71	75.23	0.19	73	18
60	278	–	✓	✓	×	×	✓	×	✓	–	×	×	×	×	✓	×	46.26	0.12	1	73.88	0.15	80	42
61	279	–	✓	✓	✓	✓	✓	×	✓	–	✓	✓	✓	×	✓	✓	58.59	1.95	5.43	83.71	2.89	80	83
62	280	–	✓	✓	✓	×	✓	×	✓	–	×	×	×	×	✓	✓	49.62	0.31	3.59	75.66	0.76	80	50
63	281	–	✓	✓	✓	✓	✓	×	✓	–	✓	✓	✓	×	✓	✓	67.02	5.35	7.35	83.35	4.29	80	83
64	282	–	✓	✓	✓	✓	✓	×	✓	–	✓	✓	✓	✓	✓	✓	56.19	1.82	9.29	82.5	3.45	80	92
65	283	–	✓	✓	✓	✓	✓	×	✓	–	✓	✓	✓	✓	✓	✓	70.1	4.97	8.29	81.16	4.96	80	92
66	284	×	×	✓	×	×	–	–	–	–	×	×	×	×	×	×	43.49	0	0	22.99	0	67	10
67	285	×	×	✓	×	×	–	–	–	–	×	×	×	×	✓	×	47.39	0	0	68.46	0	67	20
68	286	✓	✓	✓	✓	✓	✓	–	✓	–	×	×	×	×	✓	×	46.26	0	0	60.91	0	80	67
69	287	×	×	×	×	×	–	–	×	×	✓	×	×	×	✓	×	48.96	0	0.06	88.49	0	80	17
70	288	×	×	×	×	×	–	–	×	×	×	×	×	×	✓	×	46.83	0	0	73.97	0	80	8
71	296	×	×	×	×	×	✓	–	✓	–	×	×	×	×	✓	×	46.55	0.16	0.44	79.33	0.19	80	25
72	297	×	✓	✓	✓	×	✓	×	✓	–	✓	✓	×	×	✓	✓	56.84	0.32	2.56	89.18	2.52	87	62
73	304	–	✓	✓	✓	×	✓	×	✓	–	×	×	×	×	✓	×	48.73	0.05	3.03	76.02	0.35	80	50
74	305	–	✓	✓	✓	✓	✓	×	✓	–	✓	✓	✓	×	✓	✓	63	2.45	6.43	81.73	3.25	80	83
75	306	–	✓	✓	✓	×	✓	×	✓	–	✓	✓	×	✓	✓	✓	56.61	0.48	8.77	82.62	2.4	80	75
76	307	–	✓	✓	✓	✓	✓	×	✓	–	✓	✓	✓	✓	✓	✓	71.25	5.49	8.72	81.09	4.53	80	92
77	308	×	×	✓	×	×	–	–	–	–	×	×	×	×	✓	×	46.62	0	0	53.1	0	67	20
78	309	×	×	×	×	×	–	–	×	–	×	×	×	×	✓	×	46.26	0	0	73.01	0	73	9
79	310	×	✓	✓	×	×	✓	–	✓	–	✓	×	×	×	✓	×	48.5	0.54	0.46	88	0.28	80	50
80	314	×	✓	✓	×	×	✓	–	✓	–	✓	×	×	×	✓	×	47.6	0	0.94	80.04	0.53	80	50
81	316	–	×	×	×	×	×	–	×	–	×	×	×	×	✓	×	46.22	0	0.12	63.88	0	73	9
82	317	–	✓	✓	×	×	✓	–	✓	–	×	×	×	×	✓	×	47.45	0	2.05	76.86	0.27	73	45
83	320	–	–	×	–	×	×	–	×	–	×	×	×	×	✓	×	47.11	0	0.18	57.93	0	60	11
84	322	–	–	✓	–	×	✓	×	×	–	×	×	×	×	✓	×	49.52	0	3.61	71.31	0.09	67	30
85	325	–	–	✓	–	✓	✓	×	✓	–	✓	✓	✓	✓	✓	✓	64.96	1.5	9.05	75.2	3.4	67	90
86	326	–	–	✓	–	×	✓	×	✓	–	✓	✓	×	✓	✓	✓	58.19	1	13.92	78.22	2.04	67	70
87	327	–	–	✓	–	✓	✓	×	✓	–	✓	✓	✓	✓	✓	✓	71.33	6.47	11.53	71.92	4.54	67	90
88	328	–	–	×	–	×	✓	×	×	–	×	×	×	×	✓	×	47.66	0	2.04	51.3	0	67	20
89	330	–	–	✓	–	×	✓	×	✓	–	×	×	×	✓	✓	×	52.94	0	8.57	54.57	0.27	67	50
90	331	–	–	✓	–	✓	✓	×	✓	–	✓	✓	×	✓	✓	✓	62.81	0.58	15.09	61.88	2.82	67	80
91	332	–	–	✓	–	×	✓	×	✓	–	✓	✓	×	✓	✓	✓	57.52	0.03	11.17	50.74	0.88	67	70
92	333	–	–	✓	–	✓	✓	×	✓	–	✓	✓	✓	✓	✓	✓	61.44	2.11	13.26	52.92	4.35	67	90
93	334	–	–	✓	–	✓	✓	×	✓	–	✓	✓	×	✓	✓	✓	61.73	0.14	16.02	38.35	2.03	67	80
94	335	–	–	✓	–	✓	✓	×	✓	–	✓	✓	✓	✓	✓	✓	69.82	3.03	14.24	47.65	5.34	67	90
95	336	–	–	✓	–	×	✓	×	✓	–	×	✓	×	×	×	–	57.5	0	5.28	16.69	–	67	40
96	337	–	–	✓	–	✓	✓	×	✓	–	✓	×	×	✓	×	–	54.7	0.03	12.2	16.14	–	67	60
97	338	–	–	✓	–	✓	✓	×	✓	–	✓	✓	×	✓	×	–	57.98	0	14.55	5.62	–	67	70
98	339	–	–	✓	–	✓	✓	×	✓	–	✓	×	×	✓	×	–	53.06	0.41	15.28	8.22	–	67	60
99	340	–	–	✓	–	✓	✓	×	✓	–	✓	✓	×	✓	×	–	55.87	0.02	17.66	6.32	–	67	70
100	341	–	–	✓	–	✓	✓	×	✓	–	✓	×	✓	✓	×	–	49.64	1.17	14.4	9.47	–	67	70
101	342	–	–	✓	–	✓	✓	×	✓	–	✓	✓	×	✓	×	–	64.66	0.1	19.62	2.64	–	67	70
102	343	–	–	✓	–	✓	✓	×	✓	–	✓	✓	✓	✓	×	–	59.59	1.58	19.01	5	–	67	80
103	352	×	×	✓	×	×	–	–	–	–	×	×	×	×	×	×	46.64	0	0	32.51	0	67	10
104	353	×	×	×	×	×	–	–	×	–	×	×	×	×	✓	×	46.35	0	0.01	58.19	0	73	9
105	354	×	×	×	×	×	✓	–	✓	–	×	×	×	×	✓	×	47.72	0	0.38	80.92	0.07	80	25
106	355	×	✓	✓	×	×	✓	–	✓	–	✓	×	×	×	✓	×	47.01	0.16	0.68	85.55	0.32	80	50
107	356	×	×	×	×	×	–	–	×	–	×	×	×	×	✓	×	46.06	0	0.03	45.87	0	73	9
108	357	×	×	×	×	×	×	–	×	–	×	×	×	×	✓	×	47.29	0	0.13	70.06	0.01	80	8
109	361	–	–	×	–	×	✓	–	✓	–	×	×	×	×	✓	×	48.29	0.12	2.24	76.21	0.16	60	33
110	362	–	–	✓	–	×	✓	×	✓	–	✓	×	×	×	✓	✓	52.26	0	6.81	82.94	0.61	67	50
111	363	–	–	✓	–	×	✓	×	✓	–	✓	×	×	×	✓	✓	54.82	0.74	7.17	80.2	1.2	67	50
112	370	–	–	✓	–	×	✓	×	✓	–	✓	✓	×	✓	✓	✓	56.76	0.5	13.11	77.54	0.85	67	70
113	371	–	–	✓	–	✓	✓	×	✓	–	✓	✓	✓	✓	✓	✓	62.35	4.9	11.62	71.99	3.52	67	90

Eb09 ID	Sim. ID	VdM91	Ger93a	Bur95	VdM98	Say07	Baa08	Ebb09	Mut13	VGe14	Mut14	Izb30	Ran68a	Des04	Ste14	Pet14	Izb30 [%]	Ran68a [%]	Des04 [%]	Ste14 [%]	Pet14 [%]	% valid	% motion if valid
114	372	–	–	×	–	×	×	×	×	–	×	×	×	×	✓	×	53.64	0	2.28	52.92	0	67	10
115	376	–	–	✓	–	×	✓	×	✓	–	✓	✓	×	✓	✓	×	57.94	0.03	11.55	52.83	0.49	67	70
116	377	–	–	✓	–	✓	✓	×	✓	–	✓	✓	✓	✓	✓	✓	61.54	1.53	12.81	52.66	3.27	67	90
117	378	–	–	✓	–	×	✓	×	✓	–	✓	✓	×	✓	✓	✓	58.15	0.11	15.93	37.79	0.95	67	70
118	379	–	–	✓	–	✓	✓	×	✓	–	✓	✓	✓	✓	✓	✓	55.47	1.75	13.58	47.66	3.84	67	90
119	380	–	–	×	–	×	✓	×	×	–	×	✓	×	×	×	–	56.53	0	5.29	16.88	–	67	20
120	385	–	–	✓	–	✓	✓	×	✓	–	✓	×	×	✓	×	–	49.94	0.36	13.2	9.22	–	67	60
121	386	–	–	✓	–	✓	✓	×	✓	–	✓	×	×	✓	×	–	45.99	0.05	18.67	2.57	–	67	60
122	387	–	–	✓	–	✓	✓	×	✓	–	✓	×	×	✓	×	–	41.2	0.98	18.2	4.63	–	67	60
123	388	–	–	✓	–	✓	–	×	✓	–	✓	–	×	✓	✓	–	–	0	13.77	41.99	–	53	75
124	389	–	–	✓	–	✓	–	×	✓	–	×	–	×	✓	×	–	–	0.05	19.49	32.06	–	53	50
125	390	–	–	✓	–	✓	–	✓	✓	–	✓	–	×	✓	×	–	–	0	14.34	35.41	–	53	75
126	391	–	–	✓	–	✓	–	×	✓	–	✓	–	×	✓	×	–	–	0	17.66	27.37	–	53	63
127	392	–	–	✓	–	✓	–	×	✓	–	✓	–	×	✓	×	–	–	0	14.94	27.49	–	53	63
128	393	–	–	✓	–	✓	–	×	✓	–	✓	–	×	✓	×	–	–	0.02	16.65	20.67	–	53	63
129	394	–	–	✓	–	✓	–	×	✓	–	✓	–	×	✓	×	–	–	0.03	16.26	24.7	–	53	63
130	395	–	–	✓	–	✓	–	×	✓	–	✓	–	×	✓	×	–	–	0.1	14.82	19.58	–	53	63
131	396	×	×	✓	×	×	–	–	×	–	×	×	×	×	×	×	45.95	0	0	30.37	0	73	9
132	397	×	×	×	×	×	✓	–	×	–	✓	×	×	×	✓	×	46.89	0	0.18	41.67	0	80	25
133	398	×	✓	✓	×	×	✓	–	✓	–	✓	×	×	×	✓	×	47.43	0.33	0.72	45.8	0.46	80	50
134	399	×	✓	✓	✓	×	✓	–	✓	–	✓	×	✓	×	✓	✓	51.03	3.49	3.32	46.13	1.9	80	67
135	400	×	×	×	×	×	–	–	×	–	×	×	×	×	×	×	46.01	0	0.01	33.99	0	73	0
136	401	×	×	×	×	×	✓	–	×	–	✓	×	×	×	✓	×	47.06	0	0.6	41.1	0.16	80	25
137	402	×	✓	✓	×	×	✓	–	✓	–	✓	×	✓	×	✓	✓	48.22	1.21	2.66	43.26	1.06	80	58
138	403	×	✓	✓	✓	×	✓	✓	✓	–	✓	×	✓	×	✓	✓	54.35	3.01	5.25	43.15	2.78	87	69
139	404	–	×	×	×	×	✓	–	×	–	×	×	×	×	✓	×	48	0	1.22	45.99	0.01	73	18
140	405	–	✓	✓	✓	×	✓	–	✓	–	×	×	×	×	✓	×	51.33	0.5	7.58	44.53	0.41	73	55
141	406	–	✓	✓	✓	×	✓	×	✓	–	✓	✓	✓	✓	✓	✓	57.99	2.2	13.14	40.55	1.59	80	83
142	407	–	✓	✓	✓	✓	✓	✓	✓	–	✓	✓	✓	✓	✓	✓	61.01	5.13	19.17	37.16	3.07	80	100
143	408	–	–	×	–	×	✓	–	×	–	×	×	×	×	✓	×	50.66	0.06	2.01	49.52	0.07	60	22
144	409	–	–	✓	–	×	✓	–	×	–	✓	✓	×	✓	✓	×	55	0.44	9.61	44.25	0.33	60	67
145	410	–	–	✓	–	×	✓	×	✓	–	×	×	×	✓	✓	×	54.91	0.26	10.23	44.68	0.31	67	50
146	411	–	–	✓	–	✓	✓	×	✓	–	✓	✓	✓	✓	×	✓	62.13	1.13	14.83	34.65	2.16	67	80
147	412	–	–	✓	–	✓	✓	✓	✓	–	✓	✓	×	✓	✓	✓	58.98	0.5	15.92	39.07	1.19	67	90
148	413	–	–	✓	–	✓	✓	×	✓	–	✓	✓	✓	✓	×	✓	57.48	5.14	18.45	29.83	4.94	67	80
149	414	–	–	×	–	×	✓	×	×	–	×	✓	×	×	✓	–	61.44	0.08	7.54	46.15	–	67	30
150	415	–	–	✓	–	✓	✓	×	✓	–	✓	×	×	✓	✓	–	46.73	0.27	17.54	39.05	–	67	70
151	416	–	–	✓	–	✓	✓	✓	✓	–	✓	✓	×	✓	✓	–	55.11	0.23	18.12	40.48	–	67	90
152	417	–	–	✓	–	✓	✓	×	✓	–	✓	×	✓	✓	×	–	51.02	5.59	18.55	28.86	–	67	70
153	418	–	–	✓	–	✓	✓	✓	✓	–	✓	×	×	✓	×	–	51.56	0.63	21.61	33.5	–	67	70
154	419	–	–	✓	–	✓	✓	×	✓	–	✓	×	✓	✓	×	–	43.97	5.87	20.71	25.07	–	67	70
155	422	–	–	✓	–	✓	✓	×	✓	–	✓	–	×	✓	×	–	–	0.5	18.88	24.64	–	60	67
156	424	–	–	✓	–	✓	✓	✓	✓	–	✓	–	×	✓	×	–	–	0.95	22.88	23.2	–	60	78
157	425	–	–	✓	–	✓	✓	×	✓	–	✓	–	✓	✓	×	–	–	1.12	18.73	8.59	–	60	78
158	426	–	–	✓	–	✓	–	×	✓	–	✓	–	–	✓	–	–	–	–	13.66	–	–	40	83
159	428	–	–	✓	–	✓	–	✓	✓	–	✓	–	–	✓	–	–	–	–	12.01	–	–	40	100
160	429	–	–	✓	–	✓	–	×	✓	–	✓	–	–	✓	–	–	–	–	18.53	–	–	40	83
161	433	×	×	×	×	×	✓	–	×	–	×	×	×	×	×	×	45.91	0	0.19	34.99	0	80	8
162	434	×	×	×	×	×	✓	–	✓	–	✓	×	×	×	✓	×	47.03	0	0.74	41.98	0.23	80	33
163	435	×	✓	✓	×	×	✓	–	✓	–	✓	×	×	×	✓	✓	49.56	0.06	2.45	43.19	0.84	80	50
164	436	×	×	×	×	×	–	–	×	–	×	×	×	×	×	×	46.91	0	0.02	33.09	0	73	0
165	437	×	×	×	×	×	✓	–	×	–	×	×	×	×	✓	×	46.78	0	0.46	40.54	0.06	80	17
166	438	×	×	✓	×	×	✓	–	✓	–	✓	×	×	×	✓	×	47.84	0	2.47	42.75	0.47	80	42
167	439	×	✓	✓	×	×	✓	×	✓	–	✓	×	✓	×	✓	✓	52.07	1.68	5.21	41.6	1.66	87	54
168	440	–	–	×	–	×	✓	–	×	–	×	×	×	×	✓	×	49.9	0	1.06	45.98	0	60	22
169	441	–	–	✓	–	×	✓	–	✓	–	×	×	×	×	✓	×	53.43	0.02	7.27	44.87	0.07	60	44
170	442	–	–	✓	–	×	✓	×	✓	–	✓	✓	✓	✓	✓	✓	57.17	1.2	11.81	40.62	0.79	67	80
171	443	–	–	✓	–	×	✓	×	✓	–	✓	✓	✓	✓	✓	✓	60.3	3.01	18.41	37.34	1.9	67	80

Eb09 ID	Sim. ID	VdM91	Ger93a	Bur95	VdM98	Say07	Baa08	Ebb09	Mut13	VGe14	Mut14	Izb30	Ran68a	Des04	Ste14	Pet14	Izb30 [%]	Ran68a [%]	Des04 [%]	Ste14 [%]	Pet14 [%]	% valid	% motion if valid
172	444	–	–	×	–	×	✓	–	×	–	×	✓	×	×	✓	×	58.61	0	2.34	49.64	0.04	60	33
173	448	–	–	✓	–	✓	✓	✓	✓	–	×	✓	×	✓	✓	✓	59.27	0.64	15.33	39.29	0.69	67	80
174	449	–	–	✓	–	✓	✓	×	✓	–	✓	✓	✓	✓	×	✓	57.57	3.7	17.96	29.81	3.95	67	80
175	450	–	–	×	–	×	✓	×	×	–	×	×	×	×	✓	–	39.36	0	7.98	44.46	–	67	20
176	451	–	–	×	–	×	✓	×	×	–	×	×	×	✓	✓	–	32.85	0.59	16.8	37.91	–	67	30
177	452	–	–	✓	–	×	✓	×	✓	–	×	×	×	✓	✓	–	41.45	0.18	18.3	39.42	–	67	50
178	453	–	–	✓	–	✓	✓	×	✓	–	✓	×	✓	✓	×	–	38.6	2.58	18.55	28.11	–	67	70
179	455	–	–	✓	–	✓	✓	×	✓	–	✓	×	✓	✓	×	–	43.77	2.93	19.96	24.19	–	67	70
180	456	–	–	✓	–	×	✓	×	✓	–	×	–	×	✓	×	–	–	0.03	13.38	34.09	–	60	44
181	458	–	–	✓	–	✓	✓	×	✓	–	×	–	×	✓	×	–	–	0.1	18.2	23.4	–	60	56
182	460	–	–	✓	–	✓	✓	✓	✓	–	✓	–	×	✓	×	–	–	0.45	22.28	23.04	–	60	78
183	461	–	–	✓	–	✓	✓	×	✓	–	✓	–	×	✓	×	–	–	0.42	17.93	7.93	–	60	67
184	462	–	–	✓	–	✓	–	×	✓	–	×	–	–	✓	–	–	–	–	13.3	–	–	40	67
185	466	–	–	✓	–	✓	–	✓	✓	–	✓	–	–	✓	–	–	–	–	13.76	–	–	40	100
186	467	–	–	✓	–	✓	–	×	✓	–	✓	–	–	✓	–	–	–	–	16.66	–	–	40	83
	% valid	29	41	100	41	100	76	66	96	3	100	81	92	100	92	65							
	% motion if valid	11	51	79	36	44	77	10	77	33	63	38	28	51	64	46							

G.2. Motion table with ignored validity ranges

Eb09 ID	Sim. ID	VdM91	Ger93a	Bur95	VdM98	Say07	Baa08	Ebb09	Mut13	VGe14	Mut14	Izb30	Ran68a	Des04	Ste14	Pet14	Izb30 [%]	Ran68a [%]	Des04 [%]	Ste14 [%]	Pet14 [%]	% valid	% motion if valid
1	172	×	×	✓	×	×	×	×	×	×	×	×	×	×	×	0	46.32	0	0	35.35	0	93	7
2	173	×	×	×	×	×	×	×	×	×	×	×	×	×	✓	0	47.03	0	0.03	43.65	0.01	93	7
3	174	×	✓	✓	✓	×	×	×	✓	✓	×	×	×	×	✓	1	53.03	0.64	1.31	48.01	0.86	93	43
4	175	×	✓	✓	✓	×	×	×	✓	✓	✓	×	✓	×	✓	1	54.33	1.21	2.31	49.02	1.78	93	57
5	176	×	×	×	×	×	×	×	×	×	×	×	×	×	✓	0	46.27	0	0.01	65.74	0	93	7
6	179	✓	✓	✓	✓	×	×	×	✓	✓	✓	✓	×	×	✓	1	59.34	0.76	5.13	40.75	3.33	93	64
7	183	✓	✓	✓	✓	×	×	×	✓	✓	✓	✓	✓	✓	×	1	65.42	2.65	13.22	35.69	2.4	93	71
8	185	×	✓	✓	×	×	×	×	✓	✓	×	✓	×	✓	✓	0	56.69	0	8.51	40.6	0.38	93	50
9	190	✓	✓	✓	✓	×	×	×	✓	✓	✓	✓	✓	✓	×	1	67.9	1.62	15.87	32.42	3	93	71
10	191	✓	✓	✓	✓	✓	×	×	✓	✓	✓	✓	✓	✓	×	1	74.14	3.95	9.22	26.1	3.56	93	79
11	195	✓	✓	✓	✓	✓	×	×	✓	✓	✓	×	✓	✓	×	–	47.24	1.13	13.77	28.68	–	93	71
12	198	✓	✓	✓	✓	×	×	×	✓	✓	✓	✓	✓	✓	×	–	67.76	1.34	16.43	26.35	–	93	71
13	199	✓	✓	✓	✓	✓	×	×	✓	✓	✓	✓	✓	✓	×	–	69.87	2.29	11.29	22.28	–	93	79
14	206	✓	✓	✓	✓	✓	×	×	✓	✓	✓	–	×	✓	×	–	–	0.54	10.66	9.52	–	87	69
15	210	✓	✓	✓	✓	✓	✓	×	✓	✓	✓	–	–	✓	–	–	–	–	9.43	–	–	73	91
16	211	✓	✓	✓	×	✓	×	×	✓	✓	✓	–	–	×	–	–	–	–	7.58	–	–	73	64
17	213	✓	✓	✓	×	✓	×	×	✓	✓	✓	–	–	×	–	–	–	–	6.73	–	–	73	64
18	214	✓	✓	✓	×	✓	×	×	✓	✓	✓	–	–	×	–	–	–	–	4.65	–	–	73	64
19	215	✓	✓	✓	×	✓	×	×	✓	✓	✓	–	–	×	–	–	–	–	4.47	–	–	73	64
20	216	×	×	✓	×	×	×	×	×	×	×	×	×	×	×	0	46.39	0	0	27.83	0	93	7
21	223	×	✓	✓	✓	×	×	×	✓	✓	✓	✓	×	×	✓	1	56.22	0.39	4.2	40.29	1.86	93	57
22	224	×	×	×	×	×	×	×	×	×	×	×	×	×	✓	0	46.93	0	0.8	43.56	0	93	7
23	225	×	×	×	×	×	×	×	×	×	×	×	×	×	✓	0	52.1	0	6.24	43.4	0.19	93	7
24	226	×	✓	✓	×	×	×	×	✓	✓	×	✓	×	×	✓	1	55.54	0.8	6.93	40.49	0.88	93	43
25	227	×	✓	✓	✓	×	×	×	✓	✓	✓	✓	✓	✓	×	1	63.48	1.46	13.57	34.74	1.65	93	64
26	228	✓	✓	✓	✓	✓	✓	✓	✓	✓	✓	×	×	×	✓	0	51.04	0	3.12	46.41	0	93	79
27	232	✓	✓	✓	✓	×	×	×	✓	✓	×	✓	✓	✓	×	1	57.46	1.66	12.3	36.52	1.14	93	64
28	233	✓	✓	✓	✓	×	×	×	✓	✓	✓	✓	✓	✓	×	1	60.34	4.1	9.41	28.79	3.16	93	71
29	234	✓	✓	✓	✓	×	×	×	✓	✓	✓	✓	✓	✓	×	1	64.19	1.72	15.08	32.83	2.13	93	71
30	235	✓	✓	✓	✓	×	×	×	✓	✓	✓	✓	✓	✓	×	1	68.18	2.33	9.2	26.28	2.91	93	71
31	238	✓	✓	✓	×	×	×	×	✓	✓	×	×	×	✓	✓	–	50.12	0.5	14.68	37.79	–	93	50
32	239	✓	✓	✓	✓	×	×	×	✓	✓	✓	×	×	✓	×	–	47.06	0.93	13.92	28.73	–	93	57
33	241	✓	✓	✓	✓	×	×	×	✓	✓	✓	×	✓	✓	×	–	40.01	3.05	11.99	24.91	–	93	64

Eb09 ID	Sim. ID	VdM91	Ger93a	Bur95	VdM98	Say07	Baa08	Ebb09	Mut13	VGe14	Mut14	Izb30	Ran68a	Des04	Ste14	Pet14	Izb30 [%]	Ran68a [%]	Des04 [%]	Ste14 [%]	Pet14 [%]	% valid	% motion if valid
34	242	✓	✓	✓	✓	×	×	×	✓	✓	✓	×	✓	✓	×	–	53.25	1.13	16.07	26.79	–	93	64
35	243	✓	✓	✓	✓	✓	×	×	✓	✓	✓	×	✓	✓	×	–	49.52	1.99	11.27	22.09	–	93	71
36	246	✓	✓	✓	✓	✓	✓	✓	✓	✓	✓	–	×	✓	×	–	–	0.09	12.46	23.88	–	87	85
37	247	✓	✓	✓	×	✓	×	×	✓	✓	×	–	×	✓	×	–	–	0.72	13.91	19.7	–	87	54
38	250	✓	✓	✓	✓	✓	×	×	✓	✓	✓	–	×	✓	×	–	–	0.39	10.29	9.02	–	87	69
39	251	✓	✓	✓	×	✓	×	×	✓	✓	✓	–	×	✓	×	–	–	0.52	8.79	9.97	–	87	62
40	252	✓	✓	✓	✓	✓	✓	×	✓	✓	✓	–	–	✓	–	–	–	–	9.89	–	–	73	91
41	256	✓	✓	✓	×	✓	×	×	×	✓	×	–	–	×	–	–	–	–	6.87	–	–	73	45
42	257	✓	✓	✓	×	✓	×	×	×	✓	×	–	–	×	–	–	–	–	6.62	–	–	73	45
43	258	✓	✓	✓	×	✓	×	×	×	✓	✓	–	–	×	–	–	–	–	5	–	–	73	55
44	261	×	×	✓	×	×	×	×	✓	×	×	×	×	×	✓	0	47.44	0	0	75.68	0	93	21
45	262	✓	✓	✓	✓	✓	✓	✓	✓	×	×	×	×	×	✓	0	45.96	0	0	66.93	0	93	64
46	263	×	×	×	×	×	✓	×	×	✓	✓	×	×	×	✓	0	48.69	0	0.06	89.69	0.03	93	29
47	264	×	×	✓	×	×	×	×	×	×	×	×	×	×	✓	0	48.12	0	0	81.11	0	93	14
48	265	×	✓	✓	✓	×	✓	×	✓	✓	✓	×	×	×	✓	0	51.04	0	0.13	94.8	0.54	93	57
49	266	×	×	×	×	×	✓	×	×	×	✓	×	×	×	✓	0	47.88	0	0.01	88.65	0	93	21
50	268	×	×	×	×	×	×	×	×	×	×	×	×	×	✓	0	44.81	0	0	49.24	0	93	7
51	269	×	×	×	×	×	✓	×	×	×	×	×	×	×	✓	0	47.78	0	0.01	76.32	0	93	14
52	270	×	×	×	×	×	×	×	×	×	×	×	×	×	✓	0	45.95	0	0.04	73.77	0	93	7
53	271	×	✓	✓	✓	×	✓	×	✓	✓	✓	×	×	×	✓	1	51.74	0.67	1.23	85.84	0.98	93	57
54	272	×	✓	✓	×	×	✓	×	✓	✓	✓	×	×	×	✓	0	47.75	0	0.35	83.88	0.18	93	50
55	273	✓	✓	✓	✓	✓	✓	×	✓	✓	✓	✓	×	×	✓	1	57.92	0.5	2.59	90.08	2.91	93	79
56	274	✓	✓	✓	✓	×	✓	×	✓	✓	✓	×	✓	×	✓	1	51.55	3.5	2.5	89.27	2.17	93	71
57	275	✓	✓	✓	✓	✓	✓	×	✓	✓	✓	✓	✓	×	✓	1	65.4	2.9	4.78	91.35	4.58	93	86
58	276	×	×	×	×	×	×	×	×	×	×	×	×	×	✓	0	45.74	0	0.03	54.54	0	93	7
59	277	×	×	×	×	×	✓	×	×	×	×	×	×	×	✓	0	48.01	0.1	0.71	75.23	0.19	93	14
60	278	×	✓	✓	×	×	✓	×	✓	×	×	×	×	×	✓	0	46.26	0.12	1	73.88	0.15	93	36
61	279	✓	✓	✓	✓	✓	✓	×	✓	✓	✓	✓	✓	×	✓	1	58.59	1.95	5.43	83.71	2.89	93	86
62	280	✓	✓	✓	✓	×	✓	×	✓	✓	×	×	×	×	✓	1	49.62	0.31	3.59	75.66	0.76	93	57
63	281	✓	✓	✓	✓	✓	✓	×	✓	✓	✓	✓	✓	×	✓	1	67.02	5.35	7.35	83.35	4.29	93	86
64	282	✓	✓	✓	✓	✓	✓	×	✓	✓	✓	✓	✓	✓	✓	1	56.19	1.82	9.29	82.5	3.45	93	93
65	283	✓	✓	✓	✓	✓	✓	×	✓	✓	✓	✓	✓	✓	✓	1	70.1	4.97	8.29	81.16	4.96	93	93
66	284	×	×	✓	×	×	✓	×	✓	×	×	×	×	×	×	0	43.49	0	0	22.99	0	93	21
67	285	×	×	✓	×	×	×	×	✓	×	×	×	×	×	✓	0	47.39	0	0	68.46	0	93	21
68	286	✓	✓	✓	✓	✓	✓	✓	✓	×	×	×	×	×	✓	0	46.26	0	0	60.91	0	93	64
69	287	×	×	×	×	×	✓	×	×	×	✓	×	×	×	✓	0	48.96	0	0.06	88.49	0	93	21
70	288	×	×	×	×	×	×	×	×	×	×	×	×	×	✓	0	46.83	0	0	73.97	0	93	7
71	296	×	×	×	×	×	✓	×	✓	×	×	×	×	×	✓	0	46.55	0.16	0.44	79.33	0.19	93	21
72	297	×	✓	✓	✓	×	✓	×	✓	✓	✓	✓	×	×	✓	1	56.84	0.32	2.56	89.18	2.52	93	64
73	304	×	✓	✓	✓	×	✓	×	✓	✓	×	×	×	×	✓	0	48.73	0.05	3.03	76.02	0.35	93	50
74	305	✓	✓	✓	✓	✓	✓	×	✓	✓	✓	✓	✓	×	✓	1	63	2.45	6.43	81.73	3.25	93	86
75	306	✓	✓	✓	✓	×	✓	×	✓	✓	✓	✓	×	✓	✓	1	56.61	0.48	8.77	82.62	2.4	93	79
76	307	✓	✓	✓	✓	✓	✓	×	✓	✓	✓	✓	✓	✓	✓	1	71.25	5.49	8.72	81.09	4.53	93	93
77	308	×	×	✓	×	×	×	×	×	×	×	×	×	×	✓	0	46.62	0	0	53.1	0	93	14
78	309	×	×	×	×	×	×	×	×	×	×	×	×	×	✓	0	46.26	0	0	73.01	0	93	7
79	310	×	✓	✓	×	×	✓	×	✓	×	✓	×	×	×	✓	0	48.5	0.54	0.46	88	0.28	93	43
80	314	×	✓	✓	×	×	✓	×	✓	✓	✓	×	×	×	✓	0	47.6	0	0.94	80.04	0.53	93	50
81	316	×	×	×	×	×	×	×	×	×	×	×	×	×	✓	0	46.22	0	0.12	63.88	0	93	7
82	317	×	✓	✓	×	×	✓	×	✓	×	×	×	×	×	✓	0	47.45	0	2.05	76.86	0.27	93	36
83	320	×	×	×	×	×	×	×	×	×	×	×	×	×	✓	0	47.11	0	0.18	57.93	0	93	7
84	322	×	×	✓	×	×	✓	×	×	×	×	×	×	×	✓	0	49.52	0	3.61	71.31	0.09	93	21
85	325	✓	✓	✓	✓	✓	✓	×	✓	✓	✓	✓	✓	✓	✓	1	64.96	1.5	9.05	75.2	3.4	93	93
86	326	✓	✓	✓	✓	×	✓	×	✓	✓	✓	✓	×	✓	✓	1	58.19	1	13.92	78.22	2.04	93	79
87	327	✓	✓	✓	✓	✓	✓	×	✓	✓	✓	✓	✓	✓	✓	1	71.33	6.47	11.53	71.92	4.54	93	93
88	328	×	×	×	×	×	✓	×	×	×	×	×	×	×	✓	0	47.66	0	2.04	51.3	0	93	14
89	330	✓	✓	✓	✓	×	✓	×	✓	✓	×	×	×	✓	✓	0	52.94	0	8.57	54.57	0.27	93	64
90	331	✓	✓	✓	✓	✓	✓	×	✓	✓	✓	✓	×	✓	✓	1	62.81	0.58	15.09	61.88	2.82	93	86
91	332	✓	✓	✓	✓	×	✓	×	✓	✓	✓	✓	×	✓	✓	1	57.52	0.03	11.17	50.74	0.88	93	79

Eb09 ID	Sim. ID	VdM91	Ger93a	Bur95	VdM98	Say07	Baa08	Ebb09	Mut13	VGe14	Mut14	Izb30	Ran68a	Des04	Ste14	Pet14	Izb30 [%]	Ran68a [%]	Des04 [%]	Ste14 [%]	Pet14 [%]	% valid	% motion if valid
92	333	✓	✓	✓	✓	✓	✓	×	✓	✓	✓	✓	✓	✓	✓	1	61.44	2.11	13.26	52.92	4.35	93	93
93	334	✓	✓	✓	✓	✓	✓	×	✓	✓	✓	✓	×	✓	✓	1	61.73	0.14	16.02	38.35	2.03	93	86
94	335	✓	✓	✓	✓	✓	✓	×	✓	✓	✓	✓	✓	✓	✓	1	69.82	3.03	14.24	47.65	5.34	93	93
95	336	✓	✓	✓	✓	×	✓	×	✓	✓	×	✓	×	×	×	–	57.5	0	5.28	16.69	–	93	57
96	337	✓	✓	✓	×	✓	✓	×	✓	✓	✓	×	×	✓	×	–	54.7	0.03	12.2	16.14	–	93	64
97	338	✓	✓	✓	✓	✓	✓	×	✓	✓	✓	✓	×	✓	×	–	57.98	0	14.55	5.62	–	93	79
98	339	✓	✓	✓	✓	✓	✓	×	✓	✓	✓	×	×	✓	×	–	53.06	0.41	15.28	8.22	–	93	71
99	340	✓	✓	✓	✓	✓	✓	×	✓	✓	✓	✓	×	✓	×	–	55.87	0.02	17.66	6.32	–	93	79
100	341	✓	✓	✓	✓	✓	✓	×	✓	✓	✓	×	✓	✓	×	–	49.64	1.17	14.4	9.47	–	93	79
101	342	✓	✓	✓	✓	✓	✓	×	✓	✓	✓	✓	×	✓	×	–	64.66	0.1	19.62	2.64	–	93	79
102	343	✓	✓	✓	✓	✓	✓	×	✓	✓	✓	✓	✓	✓	×	–	59.59	1.58	19.01	5	–	93	86
103	352	×	×	✓	×	×	×	×	×	×	×	×	×	×	×	0	46.64	0	0	32.51	0	93	7
104	353	×	×	×	×	×	×	×	×	×	×	×	×	×	✓	0	46.35	0	0.01	58.19	0	93	7
105	354	×	×	×	×	×	✓	×	✓	×	×	×	×	×	✓	0	47.72	0	0.38	80.92	0.07	93	21
106	355	×	✓	✓	×	×	✓	×	✓	×	✓	×	×	×	✓	0	47.01	0.16	0.68	85.55	0.32	93	43
107	356	×	×	×	×	×	×	×	×	×	×	×	×	×	✓	0	46.06	0	0.03	45.87	0	93	7
108	357	×	×	×	×	×	×	×	×	×	×	×	×	×	✓	0	47.29	0	0.13	70.06	0.01	93	7
109	361	×	×	×	×	×	✓	×	✓	×	×	×	×	×	✓	0	48.29	0.12	2.24	76.21	0.16	93	21
110	362	×	✓	✓	×	×	✓	×	✓	×	✓	×	×	×	✓	1	52.26	0	6.81	82.94	0.61	93	43
111	363	×	✓	✓	×	×	✓	×	✓	✓	✓	×	×	×	✓	1	54.82	0.74	7.17	80.2	1.2	93	50
112	370	✓	✓	✓	✓	×	✓	×	✓	✓	✓	✓	×	✓	✓	1	56.76	0.5	13.11	77.54	0.85	93	79
113	371	✓	✓	✓	✓	✓	✓	×	✓	✓	✓	✓	✓	✓	✓	1	62.35	4.9	11.62	71.99	3.52	93	93
114	372	×	×	×	×	×	×	×	×	×	×	×	×	×	✓	0	53.64	0	2.28	52.92	0	93	7
115	376	✓	✓	✓	×	×	✓	×	✓	✓	✓	✓	×	✓	✓	0	57.94	0.03	11.55	52.83	0.49	93	71
116	377	✓	✓	✓	✓	✓	✓	×	✓	✓	✓	✓	✓	✓	✓	1	61.54	1.53	12.81	52.66	3.27	93	93
117	378	✓	✓	✓	✓	×	✓	×	✓	✓	✓	✓	×	✓	✓	1	58.15	0.11	15.93	37.79	0.95	93	79
118	379	✓	✓	✓	✓	✓	✓	×	✓	✓	✓	✓	✓	✓	✓	1	55.47	1.75	13.58	47.66	3.84	93	93
119	380	✓	×	×	×	×	✓	×	×	×	×	✓	×	×	×	–	56.53	0	5.29	16.88	–	93	21
120	385	✓	✓	✓	✓	✓	✓	×	✓	✓	✓	×	×	✓	×	–	49.94	0.36	13.2	9.22	–	93	71
121	386	✓	✓	✓	✓	✓	✓	×	✓	✓	✓	×	×	✓	×	–	45.99	0.05	18.67	2.57	–	93	71
122	387	✓	✓	✓	✓	✓	✓	×	✓	✓	✓	×	×	✓	×	–	41.2	0.98	18.2	4.63	–	93	71
123	388	✓	✓	✓	×	✓	✓	×	✓	✓	✓	–	×	✓	✓	–	–	0	13.77	41.99	–	87	77
124	389	✓	✓	✓	×	✓	✓	×	✓	✓	×	–	×	✓	×	–	–	0.05	19.49	32.06	–	87	62
125	390	✓	✓	✓	✓	✓	✓	✓	✓	✓	✓	–	×	✓	×	–	–	0	14.34	35.41	–	87	85
126	391	✓	✓	✓	×	✓	✓	×	✓	✓	✓	–	×	✓	×	–	–	0	17.66	27.37	–	87	69
127	392	✓	✓	✓	×	✓	✓	×	✓	✓	✓	–	×	✓	×	–	–	0	14.94	27.49	–	87	69
128	393	✓	✓	✓	✓	✓	✓	×	✓	✓	✓	–	×	✓	×	–	–	0.02	16.65	20.67	–	87	77
129	394	✓	✓	✓	✓	✓	✓	×	✓	✓	✓	–	×	✓	×	–	–	0.03	16.26	24.7	–	87	77
130	395	✓	✓	✓	✓	✓	✓	×	✓	✓	✓	–	×	✓	×	–	–	0.1	14.82	19.58	–	87	77
131	396	×	×	✓	×	×	×	×	×	×	×	×	×	×	×	0	45.95	0	0	30.37	0	93	7
132	397	×	×	×	×	×	✓	×	×	×	✓	×	×	×	✓	0	46.89	0	0.18	41.67	0	93	21
133	398	×	✓	✓	×	×	✓	×	✓	×	✓	×	×	×	✓	0	47.43	0.33	0.72	45.8	0.46	93	43
134	399	×	✓	✓	✓	×	✓	✓	✓	✓	✓	×	✓	×	✓	1	51.03	3.49	3.32	46.13	1.9	93	71
135	400	×	×	×	×	×	✓	×	×	×	×	×	×	×	×	0	46.01	0	0.01	33.99	0	93	7
136	401	×	×	×	×	×	✓	×	×	×	✓	×	×	×	✓	0	47.06	0	0.6	41.1	0.16	93	21
137	402	×	✓	✓	×	×	✓	×	✓	✓	✓	×	✓	×	✓	1	48.22	1.21	2.66	43.26	1.06	93	57
138	403	×	✓	✓	✓	×	✓	✓	✓	✓	✓	×	✓	×	✓	1	54.35	3.01	5.25	43.15	2.78	93	71
139	404	×	×	×	×	×	✓	×	×	×	×	×	×	×	✓	0	48	0	1.22	45.99	0.01	93	14
140	405	×	✓	✓	✓	×	✓	×	✓	✓	×	×	×	×	✓	0	51.33	0.5	7.58	44.53	0.41	93	50
141	406	✓	✓	✓	✓	×	✓	×	✓	✓	✓	✓	✓	✓	✓	1	57.99	2.2	13.14	40.55	1.59	93	86
142	407	✓	✓	✓	✓	✓	✓	✓	✓	✓	✓	✓	✓	✓	✓	1	61.01	5.13	19.17	37.16	3.07	93	100
143	408	×	×	×	×	×	✓	✓	×	×	×	×	×	×	✓	0	50.66	0.06	2.01	49.52	0.07	93	21
144	409	×	×	✓	×	×	✓	×	×	×	✓	✓	×	✓	✓	0	55	0.44	9.61	44.25	0.33	93	43
145	410	×	✓	✓	✓	×	✓	×	✓	×	×	×	×	✓	✓	0	54.91	0.26	10.23	44.68	0.31	93	50
146	411	✓	✓	✓	✓	✓	✓	×	✓	✓	✓	✓	✓	✓	×	1	62.13	1.13	14.83	34.65	2.16	93	86
147	412	✓	✓	✓	✓	✓	✓	✓	✓	✓	✓	✓	×	✓	✓	1	58.98	0.5	15.92	39.07	1.19	93	93
148	413	✓	✓	✓	✓	✓	✓	×	✓	✓	✓	✓	✓	✓	×	1	57.48	5.14	18.45	29.83	4.94	93	86
149	414	✓	×	×	×	×	✓	×	×	×	×	✓	×	×	✓	–	61.44	0.08	7.54	46.15	–	93	29

Eb09 ID	Sim. ID	VdM91	Ger93a	Bur95	VdM98	Say07	Baa08	Ebb09	Mut13	VGe14	Mut14	Izb30	Ran68a	Des04	Ste14	Pet14	Izb30 [%]	Ran68a [%]	Des04 [%]	Ste14 [%]	Pet14 [%]	% valid	% motion if valid
150	415	✓	✓	✓	✓	✓	✓	×	✓	✓	✓	×	×	✓	✓	–	46.73	0.27	17.54	39.05	–	93	79
151	416	✓	✓	✓	✓	✓	✓	✓	✓	✓	✓	✓	×	✓	✓	–	55.11	0.23	18.12	40.48	–	93	93
152	417	✓	✓	✓	✓	✓	✓	×	✓	✓	✓	×	✓	✓	×	–	51.02	5.59	18.55	28.86	–	93	79
153	418	✓	✓	✓	✓	✓	✓	✓	✓	✓	✓	×	×	✓	×	–	51.56	0.63	21.61	33.5	–	93	79
154	419	✓	✓	✓	✓	✓	✓	×	✓	✓	✓	×	✓	✓	×	–	43.97	5.87	20.71	25.07	–	93	79
155	422	✓	✓	✓	✓	✓	✓	×	✓	✓	✓	–	×	✓	×	–	–	0.5	18.88	24.64	–	87	77
156	424	✓	✓	✓	✓	✓	✓	✓	✓	✓	✓	–	×	✓	×	–	–	0.95	22.88	23.2	–	87	85
157	425	✓	✓	✓	✓	✓	✓	×	✓	✓	✓	–	✓	✓	×	–	–	1.12	18.73	8.59	–	87	85
158	426	✓	✓	✓	×	✓	✓	×	✓	✓	✓	–	–	✓	–	–	–	–	13.66	–	–	73	82
159	428	✓	✓	✓	✓	✓	✓	✓	✓	✓	✓	–	–	✓	–	–	–	–	12.01	–	–	73	100
160	429	✓	✓	✓	✓	✓	✓	×	✓	✓	✓	–	–	✓	–	–	–	–	18.53	–	–	73	91
161	433	×	×	×	×	×	✓	×	×	×	×	×	×	×	×	0	45.91	0	0.19	34.99	0	93	7
162	434	×	×	×	×	×	✓	×	✓	×	✓	×	×	×	✓	0	47.03	0	0.74	41.98	0.23	93	29
163	435	×	✓	✓	×	×	✓	×	✓	✓	✓	×	×	×	✓	1	49.56	0.06	2.45	43.19	0.84	93	50
164	436	×	×	×	×	×	×	×	×	×	×	×	×	×	×	0	46.91	0	0.02	33.09	0	93	0
165	437	×	×	×	×	×	✓	×	×	×	×	×	×	×	✓	0	46.78	0	0.46	40.54	0.06	93	14
166	438	×	×	✓	×	×	✓	×	✓	×	✓	×	×	×	✓	0	47.84	0	2.47	42.75	0.47	93	36
167	439	×	✓	✓	×	×	✓	×	✓	✓	✓	×	✓	×	✓	1	52.07	1.68	5.21	41.6	1.66	93	57
168	440	×	×	×	×	×	✓	×	×	×	×	×	×	×	✓	0	49.9	0	1.06	45.98	0	93	14
169	441	×	✓	✓	✓	×	✓	×	✓	×	×	×	×	×	✓	0	53.43	0.02	7.27	44.87	0.07	93	43
170	442	×	✓	✓	×	×	✓	×	✓	✓	✓	✓	✓	✓	✓	1	57.17	1.2	11.81	40.62	0.79	93	71
171	443	✓	✓	✓	✓	×	✓	×	✓	✓	✓	✓	✓	✓	✓	1	60.3	3.01	18.41	37.34	1.9	93	86
172	444	×	×	×	×	×	✓	✓	×	×	×	✓	×	×	✓	0	58.61	0	2.34	49.64	0.04	93	29
173	448	✓	✓	✓	✓	✓	✓	✓	✓	✓	×	✓	×	✓	✓	1	59.27	0.64	15.33	39.29	0.69	93	86
174	449	✓	✓	✓	✓	✓	✓	×	✓	✓	✓	✓	✓	✓	×	1	57.57	3.7	17.96	29.81	3.95	93	86
175	450	×	×	×	×	×	✓	×	×	×	×	×	×	×	✓	–	39.36	0	7.98	44.46	–	93	14
176	451	✓	×	×	×	×	✓	×	×	×	×	×	×	✓	✓	–	32.85	0.59	16.8	37.91	–	93	29
177	452	✓	✓	✓	✓	×	✓	×	✓	×	×	×	×	✓	✓	–	41.45	0.18	18.3	39.42	–	93	57
178	453	✓	✓	✓	✓	✓	✓	×	✓	✓	✓	×	✓	✓	×	–	38.6	2.58	18.55	28.11	–	93	79
179	455	✓	✓	✓	✓	✓	✓	×	✓	✓	✓	×	✓	✓	×	–	43.77	2.93	19.96	24.19	–	93	79
180	456	✓	✓	✓	✓	×	✓	×	✓	✓	×	–	×	✓	×	–	–	0.03	13.38	34.09	–	87	62
181	458	✓	✓	✓	✓	✓	✓	×	✓	✓	×	–	×	✓	×	–	–	0.1	18.2	23.4	–	87	69
182	460	✓	✓	✓	✓	✓	✓	✓	✓	✓	✓	–	×	✓	×	–	–	0.45	22.28	23.04	–	87	85
183	461	✓	✓	✓	✓	✓	✓	×	✓	✓	✓	–	×	✓	×	–	–	0.42	17.93	7.93	–	87	77
184	462	✓	✓	✓	×	✓	✓	×	✓	✓	×	–	–	✓	–	–	–	–	13.3	–	–	73	73
185	466	✓	✓	✓	✓	✓	✓	✓	✓	✓	✓	–	–	✓	–	–	–	–	13.76	–	–	73	100
186	467	✓	✓	✓	✓	✓	✓	×	✓	✓	✓	–	–	✓	–	–	–	–	16.66	–	–	73	91
	% valid	100	100	100	100	100	100	100	100	100	100	81	92	100	92	65							
	% motion if valid	59	73	79	55	44	69	10	75	67	63	38	28	51	64	46							

H

Outline Matlab-routines

For clarification on the methodology followed or for further research it might be of use to know how post-processing was performed. MATLAB was used for this purpose. This appendix contains the outline of the most important routines.

H.1. Convergence tests

The convergence tests are described in section 3.3 and appendix D. Similar approaches were used for the three types, i.e. convergence test on flume length, cell width and cell height.

Settings and initialization
For each case:
    For each common gauge:
        Read and parse the velocity data
        Resample data on time steps of the longest flume length
        Time shift so that all records start at the 5^{th} peak
For each case except reference:
    For each common gauge:
        Per y-level:
            Calculate maximal peak difference compared with the base case
            Determine relative error
Plot maximal differences over a flume (profiles)
Plot relative error per gauge-case-couple over a flume
Plot mean relative error per case against convergence parameter

H.2. NK09 tests

The NK09 tests are used for the evaluation of IH-2VOF, see chapter 4. Target is to compare numerical data (via IH-2VOF), physical data (from the Nammuni-Krohn (2009) dataset) and analytical solutions (according to linear wave theory and shoaling, and according to Van Gent and Van der Werf (2014)). The scripts for regular and irregular wave tests are almost identical, though for the latter the 2% value of the peaks is used rather than the average.

Settings and initialization
Load case properties
For each calculated case:
    Initialize output storage
    Load gauge data (u, η, x and y) either by parsing the IH-2VOF output files or by loading previously parsed data
    Couple numerical and physical gauge positions

Determine mean peak velocities at each gauge:
Split the records at their downcrossings using WAFO
Find minima and maxima of each single wave
Get mean and standard deviation
Determine spectral properties, reflection and the VG14-velocity:
Obtain the offshore η records and normalize them in time
Decompose them by Zelt and Skjelbreia (1992)
Calculate spectrum of incoming, reflected and total η using WAFO
Get wave properties using WAFO
Find the reflection coefficient from the spectra
Calculate the reflection coefficient by Zanuttigh and Van der Meer (2007)
Obtain the orbital flow velocity according to Van Gent and Van der Werf (2014)
(Irregular:) Draw the wave spectrum at certain gauges
Obtain the orbital flow velocity with linear wave theory and shoaling using $H/2$
Estimate the error range of u using a_r
Obtain and plot the velocity envelope profiles
Plot certain wave records
Draw production plots (H, T, ...)
Draw comparison plots (K_r, H, ...)
Draw bulk peak velocity plots

H.3. Eb09 tests

In the Eb09 tests all stability methods and motion formulae are applied on the numerical data produced by IH-2VOF. Considerable effort is made to reduce computation time by optimizing loops, using matrix evaluations and by using temporary storage of data. Each case is analysed multiple times for the sensitivity analysis.

Settings and initialization
Define situations
Load case properties
For each calculated case:
Load gauge data (u, η, k, x and y) either by parsing the IH-2VOF output files or by loading previously parsed data
If not stored previously (otherwise loaded):
Determine additional case properties (y_t, n, ...)
Derive wave properties:
Obtain offshore η records and normalize them in time
Decompose them by Zelt and Skjelbreia (1992)
Calculate spectrum of incoming η using WAFO
Get necessary wave properties using WAFO and the dispersion relation
Do the above once again for the onshore η records
Store case- and wave properties
For each situation:
For each stability method and motion formula:
Check whether the situation has been calculated previously. If so, copy the result to this situation and continue with the next method/formula
Find stability according to the method/formula
For motion formulae: also obtain the motion percentage
For motion formulae: use temporary storage files with values for Ψ, to be used in other situations
Compose the motion table
Compose the prediction table
Compose the sensitivity table

I

IH-2VOF LOGBOOK

This appendix contains a brief logbook of the work with model IH-2VOF. During the Master's thesis project some problems and drawbacks were encountered, which are described here. The source code of the model has been adapted to fulfil the project needs.

I.1. INVESTIGATING PARALLEL COMPUTING POSSIBILITIES

The latest version of IH-2VOF was downloaded (distributed on July 28th 2014). It contained the MATLAB-GUI and the compiled IH_2VOF.exe with original source code. The IH_2VOF.exe-calculation program is written in Fortran 90 and C++.

From some test runs and by observing the code it appeared that the software is not designed to work on parallel computing systems: a simple test case was up to 30% slower on an Intel Core i5 processor with all four cores enabled, than when the program was run on a single core. Running the program on a single core on a Windows 7 computer is achieved by changing the processor affinity for the IH_2VOF.exe-process in the Windows Task Manager. This observation was also confirmed by running three simulations simultaneously: letting them run together on four cores did not increase total processor power used compared by letting them run on a single core each. It is quite logical that the program does not lend itself to parallel computing, since every new time or iteration step is dependent on the previous.

Setting priority for this process to 'high' (also in the Windows Task Manager) improved calculation power as well. Running four separate instances on four dedicated cores simultaneously would likely be most efficient, though this was not the case. Windows needs some CPU power for maintaining its basic functionality.

I.2. COMPILING SOURCE CODE

Since the source code was also distributed, it was possible to make adaptations to the program. For this an appropriate compiler was needed. According to the *makefile* the free GNU Fortran compiler (gfortran[1]) can be used. The compiler was obtained via the TDM-GCC-C64 compiler suite[2] for 64-bit Windows. The suite also contains the required C++ compiler.

The *makefile* was changed slightly by adapting Linux bash commands to Windows batch commands. The compiler is typically called as follows:

- `mingw32-make clean` (deletes all compiled files for a fresh compilation)
- `mingw32-make mode=opt compiler=gfortran IH2VOF` (normal compilation)

In `makedirectory.cpp` the following adaptation was required:

```
if (!(*status = mkdir(path, S_IRWXU | S_IRGRP | S_IXGRP | S_IROTH | S_IXOTH)))
return;
```

becomes

[1] `https://gcc.gnu.org/wiki/GFortran`
[2] `http://tdm-gcc.tdragon.net/`, uses MinGW

```
//if (!(*status = mkdir(path, S_IRWXU | S_IRGRP | S_IXGRP | S_IROTH | S_IXOTH)))
return;
if (!(*status = mkdir(path))) return;
```

Unfortunately the gfortran compiler produces a slower program than the original program distributed by IH Cantabria. The latter was probably compiled with the commercial Intel Fortran compiler, which logically produces faster code for Intel processors[1]. It was tried to add additional compiler options, though this did not make a large improvement. The final set of options is the following: `-O3 -fno-range-check -ffast-math -flto -funroll-loops`.

It appeared that the compiler makes use of some external shared libraries (libgcc_s_seh64-1.dll, libgfortran_64-3.dll, libquadmath_64-0.dll and libstdc++_64-6.dll) which should be added to the Windows\System32 folder to let IH_2VOF.exe run properly. This can be overcome by compiling the IH_2VOF.exe file with the `-static` option. A single, transferable file is then obtained.

I.3. Improving model performance

Some small changes to the IH-2VOF calculation program were made to make it more efficient for this research. First of all an estimation of remaining computation time was implemented. For this CPU (real) time and model time are stored over the last 200 calculation steps. Remaining CPU time is then estimated by multiplying remaining model time with the ratio of averaged CPU and model time passed over the last 200 steps. Since Δt of each step changes during simulation, this may be a rude approximation. Some tests show however that the approximation seems to be working quite fine, as it is a linearly declining function of the simulation step, see figure I.1. For irregular waves more variation is present, but a trend line can be obtained by using simple linear regression. From figure I.1 it can be observed that time estimation raises in the beginning of the simulation. This coincides with the time required for the first wave to travel through the full numerical flume. Afterwards fluctuations of the estimation around the linear mean are visible, which is indeed result of changes in Δt.

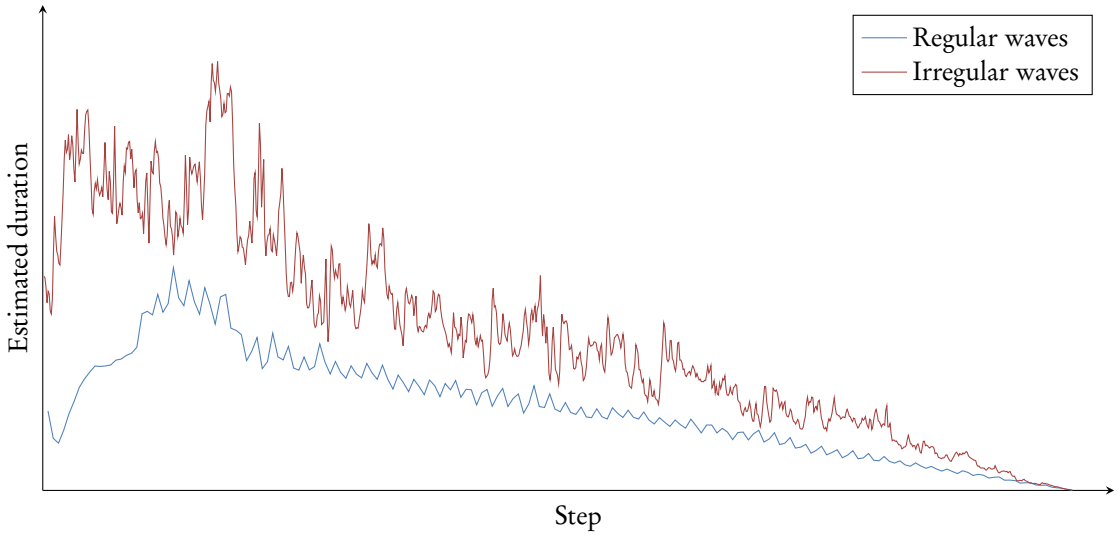

Figure I.1: Estimation of the simulation durations in two cases (scaled)

The next change was to let the executable accept command line arguments. This is not of use when only the GUI is used for running simulations, but it is a very practical tool when running simulations from the command line. The syntax on a Windows computer is as follows:

```
IH_2VOF.exe help
IH_2VOF.exe inputfile [option1] [option2] [...]
```

[1] http://www.polyhedron.com/fortran-compiler-comparisons

With the `help` argument a list with possible options is displayed. The order is not important, except for the position of `inputfile`.

A trial to reduce computation time was to hide screen output after each calculation step, which requires some CPU power. With the `reduceOutput` option output is show nonly every 100 steps. It appeared that computation time in a benchmark was reduced with less than 5%, so it is no major improvement, though it improves readability.

It was observed that every 0.1 s of simulation time the calculation halted for a short period. This coincides with the setting that VOF, u, v and p data over the whole domain should be written at 10 Hz. Writing such large matrices to a hard drive requires a lot of time and should be avoided if they are not of interest. Using a solid state disk seems to be no major improvement. By code analysis it was found that nearly all output files were opened, written to and closed every calculation step. The gfortran compiler uses a small write buffer (which should reduce the number of times data are written to the hard disk), but this buffer is flushed every time a file is closed. A major improvement was thus to take the open and close commands for output files out of the calculation loop, to the front (readinput.f90) and back (IH_2VOF.f90) of it. This improved computation time with nearly 50% in a benchmark.

In light of previous observations option `noEnvelope` was added, which inhibits writing out these data. This can eventually also be achieved by adjusting the input file.

When (broken) turbulence calculation was switched on, the program would write out two sets of k matrices. In Turbulence/info_k.out the k-matrix is written at each time step. When also `write_k = true` the same matrix is written to filesK/k#.txt at 10 Hz. The first was considered to be of no use and was programmatically inhibited.

Ruben Peters was interested in the pressure data at certain locations. This was only possible by writing out p matrices of the whole domain and by applying post-processing. As described above this lowers calculation efficiency. With option `sensorPressure` pressure data at wave gauges are also stored, in a similar fashion as velocities at these gauges. This option requires that one or more gauges are installed and that velocities are calculated at these gauges, which is standard with the GUI. The same effect is obtained by adding `sensor_pressureON = .true.` in the input file, after `sensor_velocityON = .true.`

Exactly the same output was also made available for the turbulence intensity k. The option `sensorK` and input configuration `sensor_kON = .true.` were made available.

I.4. TURBULENCE ISSUES

During research it was discovered that turbulence calculation in IH-2VOF did not work properly. See §3.5 in this report for a detailed explanation. The essential defects are the following:

- In IHC_2VOF.F90 the flags representing the turbulence models are set before the input file is read
- In IHC_2VOF.F90 the call to `CSTRESS()` is passed argument `KEModel` instead of `kemodelAux`
- The GUI configures the (isotropic) k-ε model, but this is not supported by CStress.cpp

When turbulence is switched 'on' one obtains instantaneous production of turbulence based on the 'seed' described in IH Cantabria (2012). Also note that output in the filesK-folder is not value k, but value $\sqrt{2k}$.

I.5. ADDITIONAL ADAPTATIONS AND OBSERVATIONS

During model runs, some observations and adaptations were made, which could be interesting for model use in subsequent research. They will be shortly discussed here.

Time estimation storage Program option `saveEstimation` was created, which stores estimations per time step shown in file timeEst.out. One can read this file with e.g. Excel to perform linear regression while the model is running.

Option 'endtime' Since it can happen that a simulation takes too much time, a special option `endtime` was added to the IH-2VOF command options. When system time reaches the time specified with this option, the

model will stop its calculations as if model end time is reached. This is useful when running the model in batch mode on computers which should be available again at a certain time.

Lock file When the model starts, it will create a lock file called `lock.lock`. The file contains the start time of the model and it will be deleted automatically when the model exists normally. It can be used as an indicator of whether the model is still running. Note that the file is not deleted when the program crashes.

Sensor positions in the input file By accident it was discovered that sensor x-positions in the input file should be in *ascending* order. If not, the parameter will be zero over all time steps. x-positions are defined at the `xout_fs` and `xout_v` definitions. Additionally it was discovered that the minimal sensor distance should be larger than the local Δx. If not, also zero-values were stored. All NK09-simulations had to be redone due to these unreported issues.

It was decided to rewrite this part of the code. Now for each gauge position the nearest cell border is taken. No ascending order is required anymore.

Calculation speed With the optimized model performance as described above, an average of 0.5 – 1.0 milliseconds per grid cell and per model second are required for computation, if the domain is filled with water for about 50%. So if a run with 50 000 cells should simulate 90 seconds, it requires about 2250 – 4500 seconds of computation time. The graph in figure I.2 shows this value for 166 runs. The high peaks are result of non-converging runs or occupied computers. Of course this speed is highly dependent on the CPU. Most of the simulations were done with quad-core Intel Core i5 processors. The speed is also depending strongly on how much water is present in the domain: water-filled cells require more calculations than air-filled cells and porous cells more than air-filled.

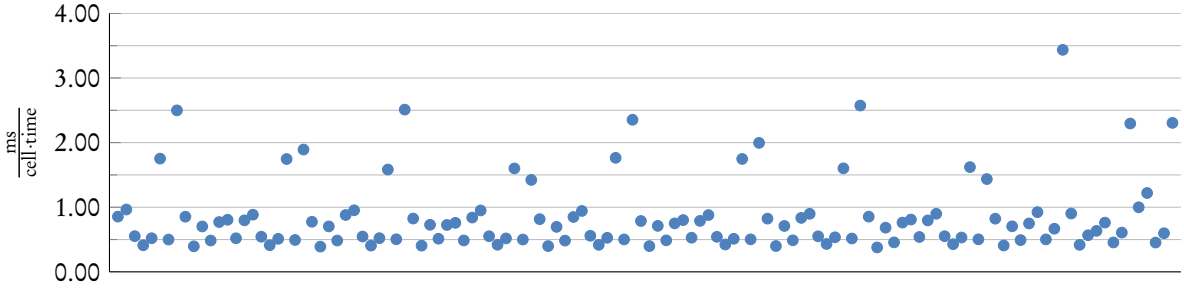

Figure I.2: Typical simulation speeds with both regular and irregular waves. About 50% of the domain filled with water.

Non-converging simulations Some simulations did not run properly. A first problem was a non-converging iteration. This is observed very quickly, as in the first steps `dt` diminished until it reached its minimum value. An error message is shown and calculation stops. The error occurred when the right boundary was put directly at the end of the breakwater, i.e. there was no gap with water behind the breakwater. By adding some space (a couple of centimetres) behind the breakwater, the problem was solved. Probably the model is not capable of having a porous boundary at flume edges, since solid boundaries gave no problem.

A second problem arose with the model runs NK09ir_707, 727, 747 and 767. They all had the same grid configuration and wave parameters. For an unknown reason the took a very long time and did not seem to get solved properly. In figure I.3 the time estimations can be seen. There appear to be phases in which the calculation returns in some kind of a loop, seen at flat regions. The large number of cells was not a problem, since runs with even more grid cells did finish normally. By adapting cell configuration (i.e. $L/\Delta x$ and $H/\Delta y$ values) cases could run properly.

Additional turbulence parameters With option `addTurbOutput` matrix values for ε and ν_t are also written to the filesK-folder. They can be used for additional post-processing.

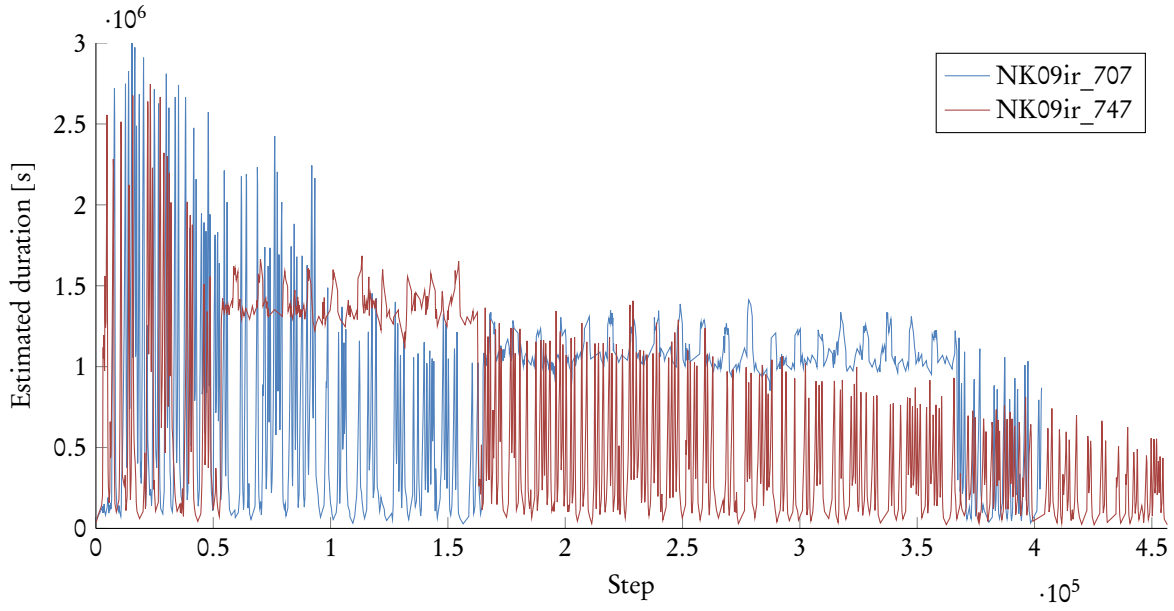

Figure I.3: Estimation of simulation durations with non-converging cases

Paddle definition Similar problems as with the turbulence calculation are present for the paddle definition. Flag `ncenterAux` is defined by paddle type, but the flag is also set before the input file is read. Also a typographic error is present, by which the flag for a static paddle will never be set.

J

Short manual for batch runs

For this research a lot of simulations had to be made. Computational performance of IH-2VOF is best when it runs on a single computer. With Windows batch files one can easily set up a lot of simulations on multiple computers. This appendix gives a short guide to running the simulations in batches. Extensive information on batch files can be found on `http://ss64.com/nt/` and `http://en.wikibooks.org/wiki/Windows_Batch_Scripting`.

J.1. Overview

With help from Kevin Geboers, IT manager at the faculty of Civil Engineering, a batch run system was set up. All case input files were stored on a server in folders, together with a launch script. A single batch script was then started on all computers in a computer room, at a defined date and time, by means of a client management system. The script is run from an administrator account. The computer has a certain name (hostname) which is read by the batch script. It chooses a set of cases assigned to that very computer via a large selection tree. For each case in this set the launch script is run. This script copies all necessary files from the server to a local work folder and starts the IH-2VOF model. During model calculations the time estimation file `timeEst.out` is copied to the server every 10 seconds for monitoring purposes. When the model finishes, all necessary files are compressed and copied back to the server. The local work folder is deleted and the originating batch script is informed that the case has finished. When all cases on that particular computer have finished, the batch scripts finalizes. Figure J.1 gives an overview of the configuration.

In the code hereafter some comments are given. They start with :: and are coloured in purple. Where the line continues, a → mark is placed. When testing scripts it can be useful to disable the line `echo off`. Directories should be chosen according to the system used. Compression is done using the command line version of program 7-Zip[1], called `7za.exe`. Logging by IH-2VOF to the command window is captured and stored in `log.txt` with the utility Wintee[2], called `wtee.exe`.

J.2. Batch script

```
echo off
set workfolder=C:\work\folder
set serverfolder=\\server.nl\path\to\folder\with\cases

:: Go to the work folder
echo Creating work folder...
if exist %workfolder% rmdir /Q /S %workfolder%
mkdir %workfolder%
cd /D %workfolder%
```

[1] `http://www.7-zip.org/`
[2] `https://code.google.com/p/wintee/`

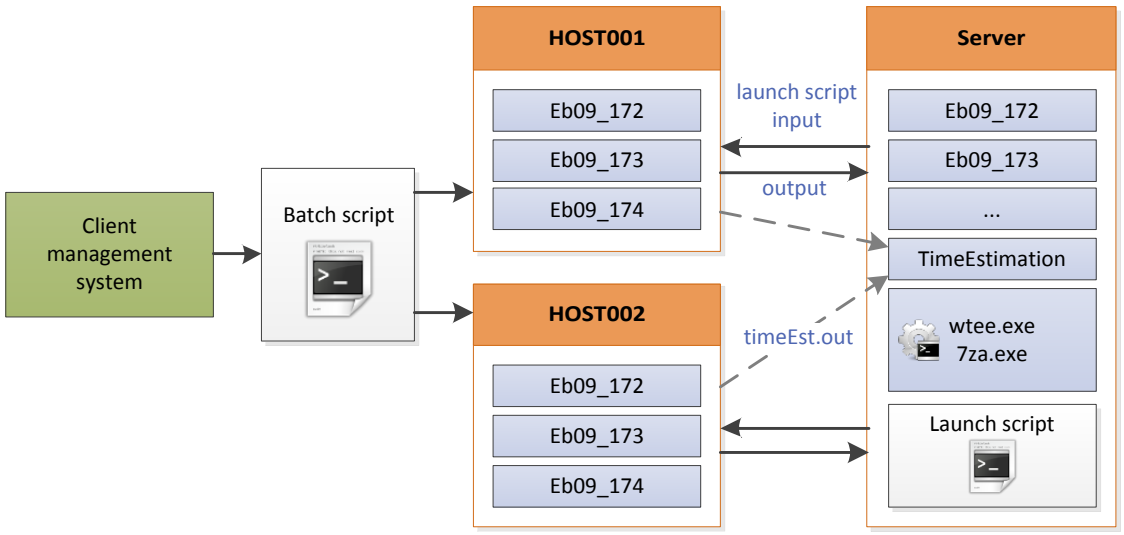

Figure J.1: Batch run configuration

```
:: Read the computer's hostname
echo Reading hostname...
hostname > hostname.txt
set /p hostname=< hostname.txt

echo Hostname of this computer: %hostname%

:: Filter out the correct cases for this computer
if /I "%hostname%" == "HOST001" (
  set _case1=Eb09_172
  set _case2=Eb09_173
  set _case3=Eb09_174
  goto runit )
if /I "%hostname%" == "HOST002" (
  set _case1=Eb09_175
  set _case2=Eb09_176
  set _case3=Eb09_177
  goto runit )
:: Additional cases can be set up by adding blocks similar to these above

:: When no case is assigned to this computer: end the script
goto stop

:runit

:: Transfer the launch script, wtee.exe and 7za.exe to the work folder
echo Initialize work folder...
copy %serverfolder%\launchscript.bat %workfolder%
copy %serverfolder%\wtee.exe %workfolder%
copy %serverfolder%\7za.exe %workfolder%

:: Create monitoring folder
if not exist "%serverfolder%\TimeEstimation" mkdir "%serverfolder%\TimeEstimation"

:: Start the launch scripts for each case
```

```
:: For debugging: replace /C by /K
:: The 4 arguments are passed to the launch script (see its description)
echo Start cases...
start "%_case1%" cmd /C launchscript "%_case1%" "%serverfolder%" "%workfolder%" 1
if defined _case2 start "%_case2%" cmd /C launchscript "%_case2%" "%serverfolder%" →
    "%workfolder%" 2
if defined _case3 start "%_case3%" cmd /C launchscript "%_case3%" "%serverfolder%" →
    "%workfolder%" 4

:: Wait until all cases are finished (all case folders deleted)
:: Transfer the timeEst.out file every 10 seconds
:wait
set stillrunning=0
timeout 10
  if exist "%workfolder%\%_case1%" (
    copy "%workfolder%\%_case1%\timeEst.out" "%serverfolder%\TimeEstimation →
       \%_case1%_timeEst.out"
    set stillrunning=1
  ) else (
    del "%serverfolder%\TimeEstimation\%_case1%_timeEst.out"
  )
if defined _case2 (
  if exist "%workfolder%\%_case2%" (
    copy "%workfolder%\%_case2%\timeEst.out" "%serverfolder%\TimeEstimation →
       \%_case2%_timeEst.out"
    set stillrunning=1
  ) else (
    del "%serverfolder%\TimeEstimation\%_case2%_timeEst.out"
  )
)
if defined _case3 (
  if exist "%workfolder%\%_case3%" (
    copy "%workfolder%\%_case3%\timeEst.out" "%serverfolder%\TimeEstimation →
       \%_case3%_timeEst.out"
    set stillrunning=1
  ) else (
    del "%serverfolder%\TimeEstimation\%_case3%_timeEst.out"
  )
)
if "%stillrunning%" == "1" goto wait

:: All cases are finished and output is transferred
:stop
echo Remove work folder...
cd..
rmdir /Q /S %workfolder%

echo Done!

exit
```

J.3. LAUNCH SCRIPT

```
:: %1 is the case name (and folder)
:: %2 is the server folder (source)
:: %3 is the work folder (target)
:: %4 is the CPU affinity

echo off
```

```
set casename=%1
set workfolder=%3
set casefolder="%~3\%~1"
set serverfolder="%~2\%~1"
set aff=%4

:: Create case folder within work folder
mkdir %casefolder%
cd /D %casefolder%

:: Transfer input files from server to case folder
echo Copying files to case folder...
copy %serverfolder%\*.in %casefolder%
copy %serverfolder%\IH_2VOF.exe %casefolder%
copy %serverfolder%\input %casefolder%
copy %serverfolder%\Mesh.mes %casefolder%
del /Q lock.lock

:: Start IH-2VOF with high priority
echo Starting IH_2VOF...
start /b /high /affinity %aff% IH_2VOF.exe input endtime 2014-10-25-12:15:00 reduceOutput →
    noEnvelope saveEstimation sensorK | "%~3\wtee.exe" log.txt

:: IH-2VOF finished. Compress required output with 7-Zip (7za.exe) to a .zip file
%workfolder%\7za.exe a %casename%.zip -tzip timeEst.out log.txt xc_info.out yc_info.out →
    Sensor_freeSurface Sensor_uHorizontal Sensor_K

:: Copy the required output files back to the server
copy %casefolder%\%casename%.zip %serverfolder%
copy %casefolder%\log.txt %serverfolder%

:: Delete case folder
cd..
rmdir /Q /S %casefolder%

echo Done!

:: This file is exited automatically
```